Establishing an in vitro model for X chromosome reactivation in the germline

Antonio Tarruell Pellegrin

TESI DOCTORAL UPF / 2019

THESIS SUPERVISOR

Dr. Bernhard Payer

Gene Regulation, Stem Cells and Cancer Programme,

Center for Genomic Regulation

DEPARTAMENT OF EXPERIMENTAL AND HEALTH SCIENCE

Acknowledgments

To my family, lab and friends, who brought me here, against all odds.

To the CRG facilities, personnel, management & IT crew, for managing the madness.

To my parents, for showing the way. I hope to reach half of what you achieved one day.

And to my mother, to who I owe purpose.

Abstract

The X-Chromosome dosage compensation is a prime model for the study of epigenetic regulation. In female mammals, one of the X chromosomes is inactivated through X chromosome Inactivation (XCI) during the epiblast differentiation for dosage compensation between sexes. However, XCI is later specifically reversed in female germ cells by reactivation of the inactive X chromosome (XCR) via diffusible signaling molecules produced by female gonadal cells.

The XCR observed in female germ cells is an attractive epigenetic phenomenon, but its mechanistic study is impeded by the low cell numbers present *in vivo* and the need for scalable readouts of X chromosome activity at allelic and single-cell resolution.

To implement a model for the study of germ cell XCR and its signaling effectors, we characterized the XCI and XCR kinetics of a new cell differentiation protocol that differentiates embryonic stem cells (ESCs) into X-inactive epiblast-like cells (Epi-LCs), from which *in vitro* germ cell (PGC-LCs) differentiation is stimulated through a set of cytokines. The goal was to obtain a source of X-inactive PGC-LCs that could be characterized while exposed to XCR-inducing cues.

We discovered that, contrarily to what was believed in the field, PGC-LCs could undergo XCR mediated by the cytokines present in the PGC-LC differentiation media without exposure to female gonadal cells, providing a working hypothesis for ulterior testing of the role of those cytokines in germ cell XCR.

In the search for scalable readouts of X chromosome activity, we tested several oligo-FISH methodologies based on oligonucleotide labeling and hairpin chain reaction.

Of all methodologies tested, we discovered that the signal intensity of hairpin chain reaction coupled with the split-paired probe design of V3.0 smHCR provided a scalable platform to monitor the X activity at allelic resolution.

In summary, this thesis allowed the implementation of an *in vitro* model for XCR characterization in the germline and provided the conceptual foundation for a scalable readout to monitor the X activity at allelic and single-cell resolution.

Resumen

La compensación de dosis en el cromosoma X es un modelo tradicional de regulación epigenética. En mamíferos, la diferencia de dosis génica entre sexos es compensada en las hembras por inactivación de uno de los cromosomas X (XCI) durante la diferenciación del epiblasto. No obstante, en las células germinales de las hembras, el cromosoma X es específicamente reactivado (XCR) en respuesta a la difusión de moléculas de señalización generadas por las células de la gónada femenina.

La XCR de las células germinales femeninas posee interés epigenético, pero su estudio se ve obstaculizado por el escaso número de células en el embrión, así como la escasez de técnicas escalables para estudiar la actividad del cromosoma X con resolución alélica y a escala de célula única. Para implementar un modelo para el estudio de la XCR en línea germinal y sus moléculas de señalización, caracterizamos las cinéticas de XCI y XCR de un nuevo protocolo de diferenciación celular que diferencia células pluripotentes embrionarias (ESCs) en epiblast-like cells con el cromosoma X inactivo (Epi-LCs), a partir de las cuales se estimula la diferenciación *in vitro* de células germinales (PGC-LCs) mediante un conjunto de citoquinas. El objetivo era obtener una fuente de PGC-LCs con un cromosoma X inactivo para caracterizar el fenómeno de XCR tras su exposición controlada a efectores de la XCR, como moléculas de señalización gonadales. Contrariamente a las expectativas del campo, las citoquinas presentes en el medio de diferenciación de PGC-LCs eran capaces de inducir XCR sin precisar exposición directa a células de la gónada femenina, proveyendo un paradigma para la exploración del papel de esas citoquinas en la XCR de células germinales femeninas. Con el objetivo de implementar una técnica analítica escalable para monitorizar la actividad del X, probamos varias técnicas de oligo-FISH basadas en el marcaje fluorescente de oligonucleótidos y la hairpin chain reaction. De entre todos los métodos, descubrimos que combinar la intensidad de señal de la hairpin chain reaction con el diseño bipartito de sondas de la V3.0 smHCR provee una plataforma escalable para el análisis de la actividad del X con resolución alélica. En conclusión, esta tesis permitió implementar un modelo *in vitro* para el estudio de la XCR en la línea germinal femenina y una base conceptual para un análisis escalable de la actividad del X con resolución alélica a nivel de una única célula.

Introduction:

Introduction 1:An *in vitro* model for X chromosome reactivation in the germline

The starting goal of the lab was to set experimental models that would allow us to characterize the kinetics of X-reactivation, the signaling input behind it, and its epigenetic and transcriptional effectors.

There are only three instances of X-reactivation described in the *in vivo* mouse model: In the inner cell mass (ICM) of the blastocyst at **E3.5-4.5** (Mak, Tatyana B Nesterova, et al. 2004; Okamoto, Arie P Otte, et al. 2004; Williams et al. 2011; Deng et al. 2014; Borensztein, Okamoto, et al. 2017; Mohammed et al. 2017), in the primordial germ cells (PGCs) after contact with the developing female gonad **(E11.5-Oocytes)**(Sugimoto & Abe 2007; Chuva De Sousa Lopes et al. 2008; Sangrithi et al. 2017), and partially in the naïve lymphocytes prior to immune activation (Wang et al. 2016; Syrett et al. 2017).

With the latter being undescribed at the time of project design and limited in its scope, the work in the laboratory focused in modeling the ICM and PGC X-reactivation *in vitro*.

The ICM X-reactivation has been modeled in the past with induced pluripotent stem cell (iPSC) reprogramming (Pasque et al. 2014), which, performed in appropriate circumstances, leads to X-reactivation and a naïve pluripotency endpoint state. This model, however, has the disadvantages of being an *in vitro* process stemming from differentiated somatic cells, and a process that does not happen physiologically *in vivo*. The PGC X-reactivation, on the other hand, is a physiologic process that takes place *in vivo*. The germ cell lineage is first specified around **E6.5** as a cluster of Primordial Germ cells (PGCs)(Ohinata et al. 2005) that start their life cycle as X-inactive cells, according to *Xist* RNA-FISH staining and allele-specific PCR data(Sugimoto & Abe 2007). As they migrate and approach the gonad, they are subject to a genome-wide epigenetic reprogramming, resulting in genome-wide erasure of DNA methylation, downregulation of H3k9me2 and upregulation of H3K27me3 histone marks(Sakashita et al. 2015; Kurimoto et al. 2015)**.** On the inactive X-chromosome, the characteristic *Xist* cloud starts eroding and disappears during PGC migration. But it is only when they

reach and invade the female embryonic gonad that X-linked gene reactivation occurs (Sugimoto & Abe 2007). It has been experimentally demonstrated that X-reactivation in PGCs depends on a diffusible signaling ligands produced by female somatic gonadal cells (Chuva De Sousa Lopes et al. 2008). This X-reactivation coincides with imprint erasure, making X-reactivated PGCs the cells that undergo the most drastic epigenetic reprogramming observed *in vivo*. This epigenetic reprogramming step is credited to be a essential step for development of the germ cell lineage **(QUOTE).**

The fact that PGC X-reactivation is a physiologic process and that signaling ligands regulate it makes it a very attractive topic. It has remained unexplored, in virtue of the very low numbers of available *in vivo* PGCs: with only **40** PGCs at **E7.0** and **2.000** PGCs at **E11.5**, the time of gonad invasion (Kagiwada et al. 2012), it is difficult to perform functional or epigenetic analysis of *in vivo* PGCs.

Because of this low cell number, prior studies have been frequently restricted to low-resolution analysis, such as H3K27me3 immunofluorescence (Chuva De Sousa Lopes et al. 2008), *Xist* RNA-FISH (de Napoles et al. 2007; Sugimoto & Abe 2007) and, allele-specific RT-PCR (Sugimoto & Abe 2007). However, the most pressing questions, such as the global kinetics of X-reactivation across the X chromosome, its epigenetic drivers and the transcription factors driving the process cannot be elucidated by those approaches.

Our goal was to implement in the laboratory a new *in vitro* PGC induction model developed by the research group of our collaborator, professor Mitinori Saitou (Kyoto University, Japan). By differentiation of naïve X-active ESCs or iPSCs into X-inactivating epiblast like-cells (Epi-LCs), the differentiation of the ICM into the X-inactivating Epiblast can be modeled *in vitro.* The differentiating Epi-LCs can then be induced into primordial germ cell-like cells (PGC-LCs) by the addition of cytokines or the overexpression of transgenes for the master germ cell fate regulator genes, reproducing the specification of the germline *in vivo* (Hayashi et al. 2011a). In a previous report using cytokine-based PGC-LC differentiation, X-inactive PGC-LCs could be obtained *in vitro*, and the onset of meiosis and subsequent X-reactivation reproduced by the aggregation and culture of female PGC-LCs with *in vivo* E12.5

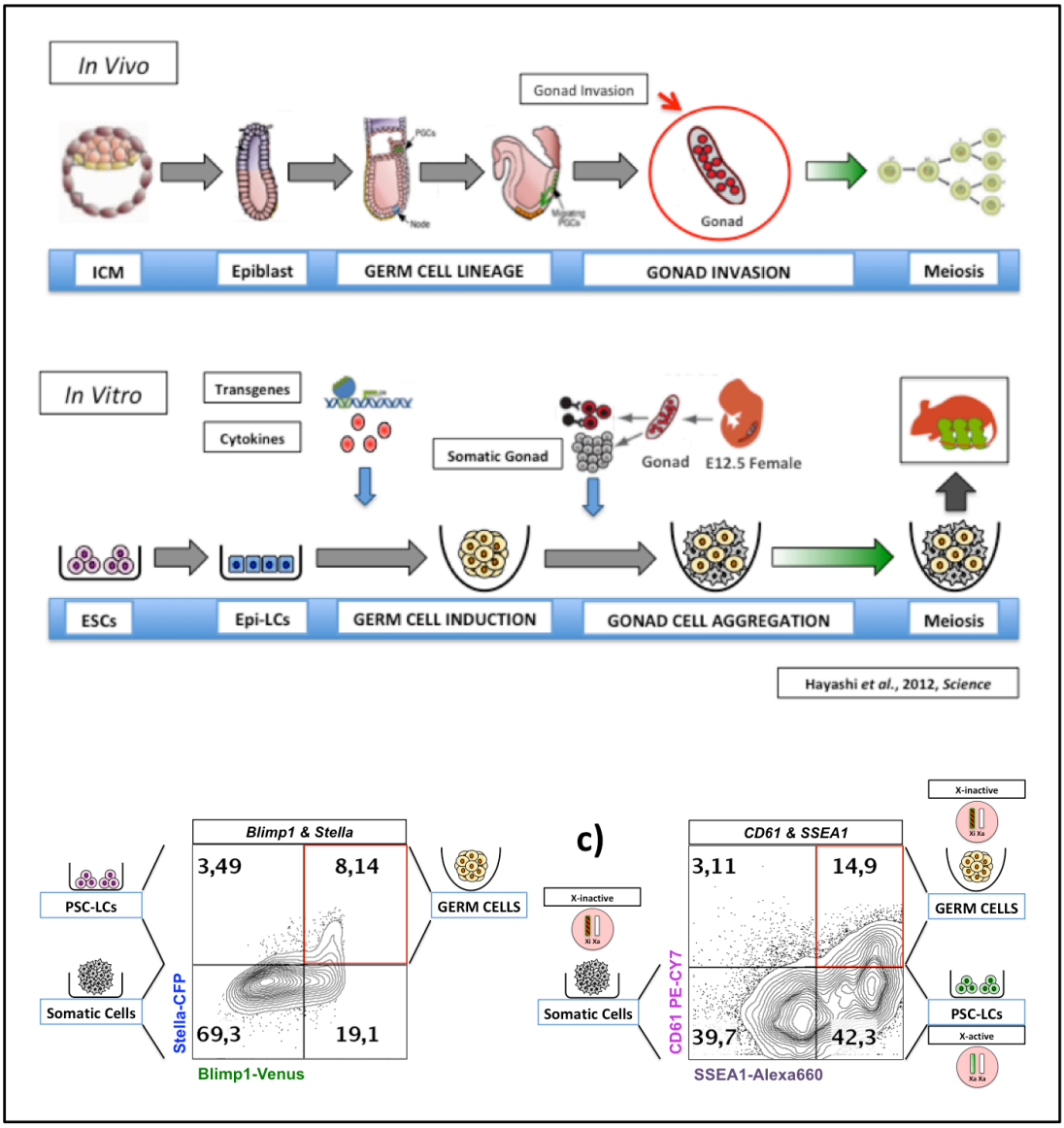

Figure 1: Features of the *in vitro* PGC-LC induction model:

a) .

b) .

female somatic gonadal cells. These meiotic female germ cells, when transplanted into female mice ovaries, develop into mature oocytes and give rise to fertile offspring (Katsuhiko Hayashi et al. 2012), reproducing the *in vivo* X-inactivation and reactivation dynamics **(Fig.1a)**.

This *in vitro* system offers several advantages. It reproduces the life cycle of the *in vivo* X chromosome, as well as yields 10^5 PGC-LCs per experiment, a sufficient amount for

transcriptomic and epigenomic approaches. This range could also provide sufficient material for signaling screening and functional testing experiments. Those PGC-LCs can be induced from a variety of cell lines with different reporter and transgene tools, expanding the versatility of the model. In addition, female PGC-LCs are reported to stay X-inactive unless they are exposed to female somatic gonadal cells (Katsuhiko Hayashi et al. 2012). This is a major advantage over germ cells obtained *in vivo*, where embryonic development heterogeneity and early gonad invasion from as early as E10.5 resulting in a significant fraction of PGCs, which have already contacted the gonad (Hu, Peter K. Nicholls, et al. 2015). For those reasons, *in vitro*-derived PGC-LCs might present a more homogenous cell population, which would be superior to *in vivo*-derived PGCs for studying epigenetic reprograming kinetics or gonadal signal dependency,

The *in vitro* PGC-LC induction does not generate the intended germ cells alone, so a critical step of the protocol is the purification of the PGC-LCs from other byproduct cell lineages. Two main avenues of PGC-LC isolation have been used so far: endogenous fluorescent reporters for the germ cell fate marker genes *Blimp1* and *Stella*, and the antibody staining against the surface pluripotency marker *SSEA1* and the differentiation marker *CD61* (Hayashi et al. 2011b; Hayashi & Saitou 2013a; Hayashi & Saitou 2013c). *Blimp1* and *CD61* are markers of the differentiated germ cell lineage and are not expressed in the naïve, uncommitted pluripotency of the ICM, while the *Stella* and *SSEA1* are markers of the core pluripotent substrate shared between primordial germ cells and the ICM.

Three main defined cell populations arise from an induction: The somatic lineages, the pluripotent stem cell-like cells (PSC-LCs), and the PGC-LCs.

The somatic lineages can be traced by the absence of *Blimp1* and *Stella* expression **(Fig.1b)**, as well as by the absence of the pluripotency surface marker *SSEA1* **(Fig.1c)**. We expected these cells to commit to full X-inactivation as they undergo random differentiation towards different somatic lineages.

The pluripotent stem-cell-like cells (PSC-LCs) can be traced by the absence of *Blimp1*

but presence of *Stella* expression **(Fig.1b)**, as well as by exclusively expressing the pluripotency surface marker *SSEA1* **(Fig.1c)**. They most likely are byproducts of the presence of naïve pluripotency cues amongst the cytokines and germ cell fate master regulator transgenes used for PGC-LC induction.

A fraction of the cells will not be able to follow them to acquire germ cell fate, but will only retain a mixture of pluripotent characteristics and fail to differentiate. We expected those cells to retain or transiently regain an X-active state as they receive pluripotency cues, but fail to acquire germ cell fate.

The primordial germ cell-like cells (PGC-LCs) can be traced by the presence of both *Blimp1* and *Stella* expression **(Fig.1b)**, and the expression of both pluripotency surface marker *SSEA1* and the differentiation surface marker *CD61* **(Fig.1c)**. This reflects the status of the *in vivo* primordial germ cells as cells that express the core pluripotency factors, but have also undergone cell differentiation to the germ cell lineage, instead of remaining at the undifferentiated, naïve pluripotent state represented by the ICM. Based on the characterization of female PGC-LCs in the seminal report as being X-inactive (Katsuhiko Hayashi et al. 2012), this offers a supply of cells for PGC X-reactivation research.

As such, the *in vitro* PGC-LC induction system offers a chance of reproducing the dynamics of *in vivo* PGC X-inactivation and reactivation in a controlled environment, as well as a validated technical toolkit to monitor and purify the *in vitro* PGC-LCs.

With this in mind, we wished to adapt the *in vitro* PGC-LC induction model in order to explore the kinetics, signaling cues and the epigenetic substrate driving X chromosome reactivation in PGCs.

We intended to use the *in vitro* PGC system to obtain a supply of X-inactive PGC-LCs that could be used to track X-reactivation kinetics and its determinants. Three main reports were the basis of the project: The first was a single-cell analysis of *in vivo* primordial germ cells from their specification at E7.0 as X-inactive cells, to their X-reactivation after invading the female gonad at E12.5-14.5, with its peak defined at the

oocyte stage (Sugimoto & Abe 2007). The *in vivo* PGCs were considered to be largely X-inactive until the start of meiosis and female sexual differentiation, even if some genes in the X chromosome started showing mild expression beforehand. The analytic techniques used were RNA-FISH staining against master X-inactivator *Xist* lncRNA and allele-specific RT-PCR from single cells.

The second was a report on an *ex vivo* PGC culture system (Chuva De Sousa Lopes et al. 2008). The researchers isolated X-inactive *in vivo* PGCs and showed that the cells could only undergo X-reactivation if exposed to a diffusible ligand produced exclusively by female, but not male or sex-reversed female gonads. The status of the X chromosome was tracked both by immunostaining against the X-inactivation marker spot H3K27me3 and an X-linked fluorescent transgene.

The third was the seminal report on *in vitro* cytokine female PGC-LC induction and development till early meiosis. By tracking the status of the X chromosome by immunostaining against H3K27me3, which is enriched in th inactive –chromosome forming a distinct spot within the nucleus, the authors conclude that female PGC-LCs are X-inactive until they are aggregated and co-cultured with female somatic gonadal cells, resulting in meiosis onset and X-reactivation (K. Hayashi et al. 2012).

Those combined reports were the foundation that gave us confidence that the *in vitro* PGC-LC induction model could be adapted as a suitable model for PGC X-reactivation research. The combination of X-inactive PGC-LCs in a controlled environment and the knowledge of the gonadal aggregation as a deterministic driver of X-reactivation promised a ready source material for the transcriptomic and epigenomic exploration of PGC X-reactivation, our first primary goal. Our second goal was to optimize this system so that it could be used in a screening approach to discover which were the signaling ligands from the female gonad responsible for the PGC X-reactivation phenotype.

Introduction 2: Oligo-FISH assays: scaling up the allelic & single-cell resolution

One of the main concerns for any laboratory in the X-inactivation and reactivation research field is which assays to choose in order to monitor the expression of X-linked genes in an allele-specific fashion, so that any transcriptional, structural and epigenetic

changes between the X-inactivating or reactivating chromosome may be distinguished from its active neighbor. An additional consideration is that this assay should not only be amenable to *in* vitro cell culture models, with their greater sample sizes and defined conditions, but talso for the *in vivo* model as well.

This is an additional challenge, because the activity of the X-chromosome fluctuates at great speeds during the early mouse embryo development (transcriptionally, as few as 24H for ICM XCR (Patrat et al. 2009; Borensztein, Okamoto, et al. 2017) and Epiblast random XCI (Mohammed et al. 2017) in the mouse), shows significant divergences depending on cell fate, and in many cases the cell populations undergoing this change are minute (<1.000 cell size) and only undergo expand to greater population sizes after the processes dictating the changes in X-activity are mostly complete.

At last, the complex nature and resilience of the X-inactivation process means that often much work needs to be devoted to craft multiple transgenic or knockout procedures into the research model. This is already labor-intensive process when done on *in vitro* models, and a grievous investment if new mouse lines need to be established for *in vivo* analysis. As such, it is a convenient strategy to shy away from assays that require the introduction of additional transgenes to work as much as possible, and work as much as possible with genotype-independent strategies.

From technical specs, an ideal workhorse assay in such a laboratory should meet five requirements: It needs to grant allele specificity; work with low sample sizes; have high temporal resolution; determine heterogeneity of the sampled population; low cost for intensive sampling, and do not require the presence of any transgenes.

From the X chromosome biology, it should yield information about which of the two X-chromosomes is committed for X-inactivation or reactivation; what are the transcriptional changes of the different X-linked genes and non-coding RNAs (ncRNAs) depending on their location across the X chromosome; and which are the enforcers of this X-inactivation process, be it epigenetic chromatin modifications or structural changes in 3D organization of the X chromosome.

Across the story of the X-inactivation and reactivation research field, two major approaches have been used to meet those requirements.

The first approach used microscopic analysis of immunofluorescence against X-inactivating epigenetic marks, such as H3k27me3, followed by RNA *In situ* fluorescence hybridization (RNA-FISH) against the X-activity regulator LncRNAs, *Tsix* & *Xist*, and culminated by nascent intron RNA-FISH against X-linked genes. In some cases, DNA-FISH imaging is also performed.

In traditional RNA-FISH methods, both for X-linked genes and non-coding RNAs, bacterial artificial chromosomes (BAC) or phosmids containing the cloned double-stranded genomic DNA sequence corresponding to the locus of interest were ordered or cloned. This sequence region was then amplified, either by plasmid expansion in bacterial cultures, *in vitro* RNA transcription, or PCR amplification, and finally fragmented and labeled with modified nucleotides, either fluorescently-marked or containing haptens such as digoxigenin **(QUOTES)**.

The labeled probe was applied onto the sample, hybridizing complementarily to the endogenous RNA of interest. Probe binding was restricted through the parameters of the hybridization, which include competitor sequences, salt contents, formamide and temperature, and a series of stringent washes ensuring that only the desired target RNA may be bound by the probe **(QUOTES)**. Either by the binding of fluorescent imagers to the haptens, or direct imaging in case of fluorescent nucleotide labeling, the desired RNA target could be visualized *in situ*.

This approach can track all relevant questions in X chromosome biology: Commitment, transcriptional changes & kinetics for X-linked genes, and epigenetic & structural enforcement of the X-inactivation process.

The X-chromosome committed to inactivation or reactivation is identified by a combination of immunofluorescence and LncRNA-FISH.

The *Xist* LncRNA coats the X chromosome committed to inactivate, followed by deposition of heterochromatic histone marks such as MacroH2A, H2K119ub and H3k27me3, forming a recognizable heterochromatic spot in the nucleus once the X-inactivation process is underway **(QUOTES)**. Conversely, described instances of X-

reactivation in the ICM and PGCs of the embryo and *in vitro* iPSC reprogramming are always preceded by the loss of *Xist* inactivator LncRNA coating and the heterochromatic epigenetic marks such as H3k27me3, resulting in the disappearance of the inactivated X spot **(QUOTES)**. In the ICM of the embryo and *in vitro* iPSCs, it coincides with *Tsix* expression over the reactivated X chromosomes **(QUOTES)**.

Because at least one marker is available to distinguish X-active (*Tsix*) and X-inactive state (*Xist* & H3k27me3 spot), the number and activity of X chromosomes in any single cell of interest can be queried, as well as identifying if the cell is undergoing X-inactivation or reactivation.

The kinetics and transcription of the X-linked genes can be interrogated at allelic resolution with nascent intron RNA-FISH against target X-linked genes. Because the intron sequences are spliced out of the mature mRNA as it is being transcribed and then degraded, the intron RNA sequence is short-lived and present only in close proximity to its DNA Locus. When imaged by nascent intron RNA-FISH in a microscope, this manifests as a spot-like nascent transcription next to any transcriptionally active X-linked allele.

In cells that have undergone X-inactivation, only one X chromosome is active, and consequently, only one X-linked gene nascent transcription site will be visible.

In female cells having undergone X-reactivation, two nascent transcription sites are visible, one for each allele. As long as detection efficiencies of nascent transcription are above **85%**, going as high as **95%**, this guarantees allelic and single-cell resolution readout of the corresponding X-linked gene activity.

By querying multiple X-linked genes in the same staining, the transcriptional kinetics of genic of X-inactivation and reactivation can be followed. In addition, the presence of genes that escape the X-inactivation or reactivation process can be ascertained.

At last, the epigenetic and structural enforcement of the X-chromosome inactive or reactivated status can also be interrogated. Performing X-chromosome paint or targeted

DNA-FISH from BAC or Fosmid-cloned sequences of genes of interest, either the whole X or specific genes of interest DNA sequence can be visualized.

The combination of immunofluorescence and DNA-FISH, when imaged with super-resolution microscopy, can ascertain which epigenetic marks are enriched in a particular X-linked gene of interest or the whole chromosome, either to transcriptionally silence or activate it.

DNA-FISH super-resolution imaging of the entire X-chromosome, or particular loci, when combined with immunofluorescence or RNA-FISH allows to see the relationship between structural changes, such as compaction, formation of distinct silenced or transcribed domains, or locus-to-locus contacts, and the epigenetic modifications or LncRNA presence (Sunwoo et al. 2015); **(QUOTES)**.

The traditional Immunofluorescence & FISH approach has multiple advantages.

First, it fulfills all the X-inactivation/reactivation commitment, transcriptional kinetics and epigenetic & structural enforcer readout requirements.

In addition it fulfills 4 out of the five technical specs.

It grants allelic resolution, since 1 X-linked nascent RNA-FISH spot marks X-inactive status for the gene, while 2 spots marks this gene as reactivated.

It has single-cell resolution, the lowest possible sample size, as long as nascent X-linked gene detection efficiency is above 85%.

In addition, it has high temporal resolution. Previous reports with this technique have successfully tracked every cell division from the early zygote from single-cell to blastocyst stage while interrogating X-linked gene expression (Patrat et al. 2009; Namekawa et al. 2010)**.**

The power of those two features is manifest when we remember that those reports determined the *de novo* origin of imprinted X-inactivation from analysis of Oocyte and pre-morula stage zygote, two of the most challenging biological samples in a developing embryo.

Because it preserves the original structure of the fixed tissue or embryo, this technique has histological and subcellular resolution. Combined with its single-cell resolution, this makes it the perfect tool to ascertain if any individual cell shows a different X-activity status than its neighbors, and associate it to different cell fate and tisular markers to discover the reasons for it. This feature, when used in early embryos, was key to distinguish the extraembryonic membranes, which undergo stable imprinted X-inactivation, against the ICM, which undergoes X-reactivation and later random X-inactivation in the epiblast (Mak, Tatyana B. Nesterova, et al. 2004; Okamoto, Arie P. Otte, et al. 2004). It also possesses the advantage that in under-explored fields or biological phenomena, such as PGC biology, most previous reports are knockout analysis with immunofluorescence and other *in situ* techniques with histologic resolution, helping extrapolation and comparation of phenotypes.

It also is justifiably mid cost, with labeling of an X-linked gene incurring in a typical expense of 1.500€ for 20 FISH labeling reactions. This is key into allowing enough samplings to track processes on *in vivo* or *in vitro* models at high temporal resolution. The current record is 2H timepoints (Syrett et al. 2017), but the use of fixed samples can still drive it further down.

It is also independent of the presence of any transgenes to yield conclusive results.

There are still two great drawbacks to this approach. The first is that traditional FISH probe labeling methods are dependent on a complicated set of cloning, amplification and labeling reactions that yield highly variable results per labeling attempt. Even with the existence of commercial labeling kits, only a fraction of synthesis reactions will meet the fluorescent labeling inclusion necessary for >85% X-linked gene detection efficiency, increasing the cost and man-hours expense. In addition, successful synthesis batches will yield sample for a very limited amount of reactions. This problem draws diminishing returns, ensuring that any attempt to probe multiple genes needs increasing expertise and specialization from the researcher.

The second drawback is that, since genes must be assayed one by one, or in limited multiplexing pools, the method can only assay a limited fraction of the X-linked genes

and has very limited throughput.

The combination of those factors limits most reports to assay a maximum of 2-4 X-linked genes or ncRNAs per publication, highly limiting the throughput and scope of publications based on traditional FISH methods. Even in a specialized laboratory, the current limit ranges between 12 (Patrat et al. 2009) and 16 (Namekawa et al. 2010) X-linked genes, against the more than the 1.000 genes of the murine X chromosome **(QUOTE)**.

To conclude, the two major drawbacks of traditional FISH-based approaches have are low reproducibility between synthesis batches and exploding high cost past a certain threshold number of target genes. Taken together, the result is a low throughput and lack of scalability, even if the technique is a conceptually simple and relatively user-friendly introductory readout to the X-activity. It is mainly used to describe kinetics of the phenomena of interest and by newcomers to the field.

In order to increase the throughput and obtain X chromosome wide-resolution, an alternative approach was devised. It exploits the discovery of distinctive X-linked stable single-nucleotide polymorphisms (SNPs) footprints specific to the different mouse strains (Babak et al. 2008).

When the full extent of the strain-specific SNPs was catalogued (Keane et al. 2011), controlled crosses between different mouse strains could be devised, yielding hybrid embryos and pluripotent stem cell lines with one X chromosome from each parental (Babak et al. 2008). The fact that each X chromosome had a specific SNP signature could be exploited for allele-specific DNA and RNA-sequencing. Applied to RNA-sequencing, it allowed to extensively catalog the kinetics of gene silencing during X-inactivation, including which genes escaped X-inactivation (Pinter et al. 2015; Berletch et al. 2015; Yang, Babak, Shendure, Yang, et al. 2010). It yielded complimentary insight in the epigenetic marks regulating X-inactivation when applied to allele-specific bisulfite sequencing **(QUOTE)** and ChIP-SEQ **(QUOTE)**, elucidating the contributions of DNA methylation and repressive histone marks in X-inactivation, respectively.

It also became possible to avoid the cost associated to sequencing approaches.

Exploiting the sensitivity of amplification kinetics to SNPs in standard RT-PCR primer sets with un-expensive SYBR-Green chemistry (Wangkumhang et al. 2007), it was possible to craft allele-specific RT-PCR primer sets to monitor X-linked genes. This however needs extensive optimization until an adequate primer set is found (Yang et al. 2016).

For a long time, this approach was restricted to *in vitro* cell culture models due to the need of high sample inputs (10^5-10^6 cells per experiment), but later improvements in single-cell sequencing and Chromatin immunoprecipitation led first to the transcriptomic analysis of *in vivo* ICM X-reactivation (Deng et al. 2014), followed by transcriptomic and chromatin epigenomics of imprinted X-inactivation (Borensztein, Syx, et al. 2017), ICM X-reactivation (Borensztein, Okamoto, et al. 2017) and random X-inactivation (Mohammed et al. 2017) in the early embryo.

While the trend of the field may seem to move towards SNP-based sequencing approaches that address transcriptomics, epigenomics and DNA conformation at the scale of the whole X chromosome, the SNP-based sequencing approach has five crippling disadvantages: First, it is genotype-dependent and mostly restricted to a handful of published pluripotent stem cell line clones; Second, it requires extensive and scarcely available bioinformatics expertise; Third, it is very costly (range of 5.000-20.000€ per workflow); Fourth, it has very limited temporal resolution (typically a maximum of 10 timepoints), consequence of its cost.; Fifth, it is, in practice, transgene-dependent, as X-inactivation and reactivation processes are always heterogeneous to some extent. This forces the creation of transgenes to specifically purify a homogeneous fraction of the population for sequencing, further increasing the labor hours and cost before sequencing can be performed.

In practice, this means that the kinetics of the X-inactivation or reactivation phenotype of interest are always characterized first by Immunofluorescence and RNA-FISH, and the sequencing approach is only deployed afterwards as an auxiliary technique to explore the epigenomics and transcriptomics of an already well-known process. With all

factors above taken into account, typical workflows may take 3-5 years of work before project completion and are restricted to a handful of labs of the X-inactivation and reactivation field.

When we started the project, the determinants, kinetics and extent of female PGC X-reactivation were virtually unknown, and the knowledge available of X-reactivation kinetics definitively too scarce to justify the expenses of allele-specific sequencing.

As such, our goals were twofold:

First, to implement an Immuno & RNA-FISH approach on our *in vitro* PGC-LC model Second, to map the PGC-LC XCR phenomenon kinetics with it before committing to sequencing.

We faced three main challenges.

The first was the absence of a published protocol for simultaneous immunofluorescence & RNA-FISH in single-cell PGC suspensions. While previous attempts for *Xist* LncRNA RNA-FISH analysis of *in vivo* PGCs had been performed, the reports were fractionary, usually performed in cells protected by the inclusion in a whole-mount embryo, and they were not combined with immunofluorescence. (Nesterova et al. 2002; de Napoles et al. 2007; Sugimoto & Abe 2007)**.** All of those reports featured high cell detachment, low cell counts, and, in some cases, morphological damage. Another concern was the need for a common protocol for our 4 cell types of interest: ESCs, Epi-LCs, PGC-LCs and MEFs in order to avoid biases due to different protocols, and that our PGC-LCs needed to be available in cell suspension formats. This provided us motivation to develop and refine our own protocol.

The second was the low reproducibility and high batch effect found on classic BAC-FISH probe labeling protocols. Since we needed to score PGC-LCs X-reactivation kinetics *de novo*, given the absence of any previous reports, the analysis of multiple X-linked genes (6-13x) with high temporal resolution was necessary. This was out of the reach of traditional BAC-FISH based approaches; those can most of the time cover at

most 4 X-linked loci before diminishing returns in labeling effort and cost are felt.

The third was the relatively scarce time and focus we could dedicate to this particular project, and the need to capitalize it in publication terms. Since our main focus was to implement the *in vitro* PGC-LC model in the lab and focus on transcriptomics and epigenomics of their X-reactivation, the protocols and technology used should be simple, scalable, and far less labeling-intensive than the requirements typically seen in traditional FISH approaches. Moreover, they should be novel and publishable, in order to maximize the benefits, and they should be reproducible, with scarce expertize required to obtain results.

In order to fulfill those requirements, the most critical factor to solve it was to improve over the complication and synthesis batch effects associated to traditional FISH probe labeling. For this our best option was to use oligo-FISH instead.

Oligo-FISH approaches hail to the Singer lab **(QUOTE)**, and come from the discovery that a pool of multiple short of 50bps oligonucleotide probes carrying a bundled 5-fluorophore group each could be designed, synthesized and hybridized *in situ* against the target mRNA molecule of interest, allowing to quantify the total number of RNA target molecules within the cell. Later, the Arjun Raj laboratory showed that the pool of oligonucleotides could be shortened to 20bps oligonucleotide probes carrying a single fluorophore group covalently conjugated to its 3´-terminus, with lower cost and improved results. While initially used to target and quantify single mRNA molecules (Raj & Tyagi 2010)**(BETTER QUOTES)**, it was soon adapted to DNA targets in the form of DNA oligo-paints (Beliveau et al. 2015)**(BETTER QUOTES)**, and soon it was discovered, that, by targeting exclusively gene intronic sequences, oligo-FISH could be used to visualize exclusively nascent transcription spots. This later approach, named ICE-FISH (Levesque & Raj 2013), could yield the same readout as traditional FISH methods if applied to X-linked genes.

Using an Oligo-FISH approach presented seven advantages compared against

traditional FISH methods.

First, synthesis batch labeling effect is much lower. Typical synthesis batches allow for two hundred FISH reactions, against the 10-20 in traditional FISH approaches.

In addition, using commercial providers bypasses batch synthesis concerns entirely.

Second, the amount of probe is much larger, making whole mount embryo labeling approaches viable and making routine RNA-FISH experiments much easier.

Third, the specificity and performance of the probeset stems from the bioinformatics design alone, greatly helping multiplexing and scalability. This means that the results can be predicted, instead of relying on a combination of guesswork for the most appropriate genomic regions to be used and the variable results of BAC probe labeling, and accordingly, projects can be accurately budgeted and scaled up for any number of targets of interest with certainty, something not possible with traditional BAC-labeling FISH approaches.

Fourth, it can target strand-specific LncRNAs. This is a special advantage because the X chromosome is a functional hotspot for those, with 9 strand-specific LncRNAs described in roles of functional relevance in X-inactivation alone so far. Since many X-linked candidates remain unexplored for the lack of a quick assay of predicted specificity, the use of oligo-FISH opens the lab many options for future projects.

Fifth, targeting DNA target loci with oligo-FISH becomes increasingly practical and cost-effective, increasingly eliminating the only niche that justified the use of traditional BAC-FISH, which had capitalized that niche in the past.

Sixth, once a probeset is designed and tested, it can be used reproducibly by even inexperienced users and ordered again if the probe supply is exhausted. It meant that advances in this project would be immediately useful to any future fellows in the lab.

At last, an optimized oligo-FISH probeset is a valuable & publishable resource. Since the results of a probeset are perfectly reproducible and only the same 6-10 X-linked genes are targeted by traditional RNA-FISH in the immense majority of the reports, with an absence of published oligo-FISH sets against them, a methods paper would fulfill an unfulfilled demand in the field and reach satisfying metrics.

While initially valuable, there was room for improvement in oligo-FISH. There were two main vulnerabilities and disadvantages of Oligo-FISH approaches that needed to be addressed.

The first was the low signal intensity per oligonucleotide probe. Traditional oligo-FISH probesets included 50-100 probes, for a total of only 50-100 fluorophores per target RNA molecule. This was a far cry from the 10^4 fluorophores per target RNA molecule of traditional BAC-FISH.

The second was the high cost & low documentation of commercial approaches. With traditional commercial nascent oligo-FISH, the cost probeset was 1.000$. This was straight out unaffordable for us. This also acted as a limiter to any attempts to increase signal intensity by increasing the size of the probeset.

If we wished to fulfill our goals, we would need to turn to academic sources. We set us to implement an oligo-FISH probe technology that would fulfill the following criteria:

1. The probeset specificity and performance must be fully predictable at the informatics design step. Design and validation of probesets must be conceptually simple and do not require any programing skills.
2. Is based on DNA Oligonucleotides of less than 100bp length.
3. It cannot come from a commercial provider, nor use enzymatic amplification.
4. The cost of the oligo probeset must be less than 200€ per target gene.
5. Ability to switch fluorophores easily, without purchase of a new probeset.
6. It must recognize nascent transcription sites by performing Intronic RNA-FISH.
7. It must recognize mature mRNAs & LncRNAs by performing Exonic RNA-FISH.
8. Signal is intense enough for scoring & quantification without computer analysis.

Ideally, two other desirable traits should be included:

9. It must recognize genomic DNA loci by performing oligo DNA-FISH.
10. It must be amenable to Flow Cytometry analysis (FACs).

If those additional goals were achieved, the oligo-FISH approach would gain flexibility to perform all FISH experiments needed for X-inactivation research and gain high throughput associated typically associated with systems biology approaches, phasing out traditional FISH approaches, allowing for extensive characterization of all possible X-linked LncRNA candidates and opening the possibility to publish validated probesets developed in the lab as a useful byproduct.

The Arjun Raj laboratory Oligo-FISH approach did not originally have many competitors, but multiple alternatives have started to emerge, with the field undergoing an explosion in the last 2 years. The main drive was an attempt to lower the probeset cost per target gene, increasing the technology throughput to system biology levels, and reducing the financial penalty associated with failed probeset designs. At 1.000$ per design attempt, most laboratories cannot afford the risk of a new probeset not yielding the desired results. This has resulted in a much lower user base for oligo-FISH technology than expected by the advantages of the method.

While the approaches published up to date are too numerous to be explained here, two factors were considered for each of them. Those were the nature of the primary probe binding the target nucleic acid, and the fluorescent signal deposition.

For the primary probe design, there are two main factors. The first is if the primary probe is a single oligo, or split probe pairs which need to bind closely to the same target to trigger fluorescent signal deposition, increasing specificity.

The second is the length target nucleic acid sequence bound complementarily by the primary probe. In order to save on costs, the minimal, and most often used length to target mRNA & LncRNA sequences, which usually have fairly specific sequences, is 20bps. However, this puts quite stringent requirements on bioinformatics design, as specificity of the probe and lack of off-target binding go in hand with increasing primary probe length. With 35bps of length, DNA loci with lesser evolutionary conservation may be bound safely, with 50bps being the usual maximal length used.

For the fluorophore deposition, roughly four main strategies are apparent:

The first approach is to use a single imager Fluorescent oligo-tag hybridized to an unlabeled primary oligonucleotide probe pool. Examples of this philosophy include the MER-FISH (Chen et al. 2015) & smiFISH (Tsanov et al. 2017) approaches.

The second approach is branched DNA, in which successive imager fluorescent oligonucleotides hybridize to the primary probes binding the target nucleic acid and amplify the signal (Player et al. 2001). Sadly, most examples of them are commercial secrets, under the commercial names RNAscope (Wang et al. 2012) & ViewRNA (Battich et al. 2013). The sole exceptions to this are the recently published FISH-STICT (Sinnamon & Czaplinski 2014) and SABER approaches (Kishi et al. 2018).

The third approach is enzymatic signal amplification. On it, the primary probes binding the target nucleic acid serve as a guide for an enzymatic activity that accumulate fluorescent molecules. These include padlock probes **(QUOTES)** and the alkaline phosphatase miRNA detection module of the commercial RNAscope (Wang et al. 2012) & ViewRNA (Battich et al. 2013) technologies, and the recently published CLAMP-FISH approach from the Arjun Raj lab **(QUOTE)**.

The fourth approach is In-house fluorescent labeling of unmarked oligonucleotide probes. On it, a set of unlabeled oligonucleotide probes of minimal length (20bps) is purchased to minimize cost, and the desired fluorescent label is added to an aliquot of the oligonucleotide pool. While initially restricted to the commercial Stellaris approach spearheaded by the Arjun raj lab **(QUOTE)**, some academic published approaches also exist (Sunwoo et al. 2015; Gaspar et al. 2017).

The fifth and last approach is sequence-dependent signal amplification by hairpin chain reaction (HCR). On it, a primary probe binds the target RNA molecule. After primary probe hybridization and washes, two fluorescently labeled hairpin oligos are presented to the sample. In absence of probes, the fluorescent oligonucleotides self-hybridize with themselves and cannot bind any cellular nucleic acid sequence, being washed away. However, if the primary probe sequence is present, it displays an initiation site that the hairpin oligos can bind. Upon recognition of the initiation site, the hairpin oligos hybridize with it and gain an open conformation. This drives a chain reaction in which

each hairpin generates a hybridization site for its complementary neighbor, extending in a self-assembled polymer of 100 copies of maximal length per primary probe initiation site. This means that a single primary probe can surpass the entire signal intensity of a Stellaris commercial oligo probeset and allow single-molecule quantification. While initially based on RNA probes **(QUOTE)**, it soon jumped to 100bps long DNA oligo probes (Choi et al. 2014), which were shortened to affordable 35bps long DNA oligos (Shah, Lubeck, Schwarzkopf, T.-F. He, et al. 2016) and later adapted to split-paired 50bps DNA oligo probes to reduce noise and increase probe specificity (Choi et al. 2018). In addition, branched HCR was developed, in which a Hairpin polymer assembles 100 initiation sites, which can be recognized by additional hairpins, netting 10^4 potential fluorescent labels per primary probe (Liu et al. 2018)**.** While it was developed after writing this thesis, the potential of such a development being published, as well as the adaptation of a split-paired probe system for HCR was apparent from the start of the project.

Results:

Chapter 1: Adapting the *In Vitro* PGC-LC model for X-inactivation research

Introduction:

While the *in vitro* PGC-LC induction model provided a starting point, additional features need to be added to it. The protocol needed to be optimized for a hybrid cell line, in order to be able to distinguish the transcripts and epigenetic marks pertaining to each of the two X chromosomes. Hybrid cell lines result from a cross between different domestic mouse subspecies, leading to female mice that carry one X chromosome from each parent. Each of them carries a specific single nucleotide polymorphism (SNP) footprint, which can be used to specifically recognize their alleles at their DNA and RNA sequence (Keane et al. 2011; Yang, Babak, Shendure & Disteche 2010; Babak et al. 2008; Deng et al. 2014). Including such a cell line would allow to perform transcriptomic and epigenomic analysis of the X-reactivation process.

In addition, an X-linked fluorescent reporter was necessary to distinguish and purify any PGC-LCs that underwent X-reactivation. Moreover, in order to create an assay that can be easily monitored, it is helpful to pick which of the X chromosomes is going to be inactivated. By using skewed cell lines, the X chromosome that is to be inactivated can be chosen, instead of the random X-inactivation pattern observed *in vivo* (Lee & Lu 1999; . This last part is critical in generating an easy to monitor assay, in which the same X-chromosome is deterministically pushed into an X-inactive state in PGC-LCs. With the addition of an X-linked fluorescent reporter and a hybrid cell line background, the X-inactive PGC-LCs would be dark, and upon the addition of X-reactivation cues, become fluorescent. The hybrid background would allow to specifically track the transcripts of the reactivating X chromosome to find the kinetics and pattern of X reactivation **(Fig.2)**.

This combination of features would be critical not only for the description of the Kinetics of X-reactivation and its epigenetic substrate, but also to enable a screening approach against the signaling ligands involved in the X-reactivation process.

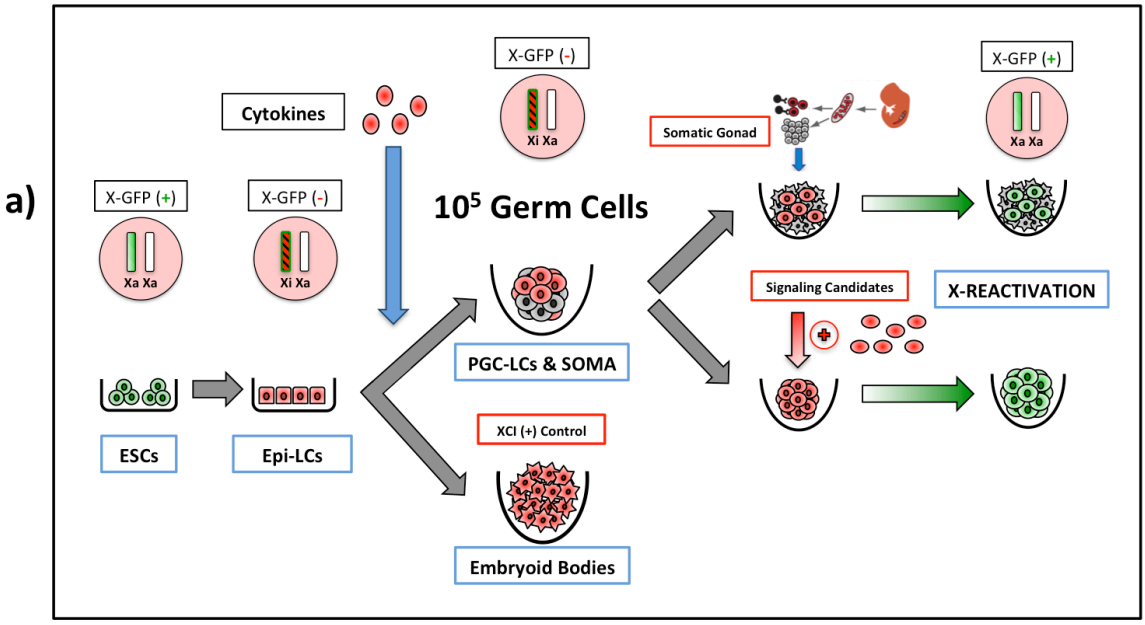

Figure 2: Features of an *in vitro* model for X-reactivation in PGCs:

In addition, internal positive controls for full, stable X-inactivation were necessary. The X-inactivation process has been divided into **three stages: initiation, spreading and early gene silencing and locked X-inactivation** (Payer et al. 2011). The initiation and early gene silencing would be represented in the *in vitro* model by the differentiation of naïve pluripotent ESCs and iPSCs to Epi-LCs. However, it has been shown that even *in vitro* Epiblast Stem Cells (EpiSCs)(Pasque et al. 2012; Pasque et al. 2011; Costanzi & Pehrson 1998), which represent a more differentiated epiblast state than the Epi-LCs, lack some of the features of the locked X-inactivation state. As such, there was a need to provide a positive internal control for the locked X-inactivation status and X-linked gene silencing, in order to prove that any X-reactivation phenotype arose from specific signaling input, and not the artifactual erosion of an incomplete X-inactivation phenotype.

Our solution was to differentiate in parallel the same starting Epi-LC cells as PGC-LCs and Embryoid bodies. The embryoid body protocol differentiates the same starting Epi-LCs in the same low-binding plate and base cell culture media as PGC-LC induction, but in the absence of the Germ cell-inducing signaling cues or transgenes. These culture conditions model the differentiation of the three germ layers, and the stable locked X-

inactivation that appears at this stage and is irreversibly inherited in most somatic cell lineages of the individual (Yang, Babak, Shendure & Disteche 2010; Ahn & Lee 2010). By differentiating embryoid bodies in parallel, the ability to perform locked X-inactivation and a negative control for germ cell induction are provided for each and every *in* vitro PGC induction.

In this chapter, we show the implementation of the cytokine and transgene PGC-LC induction methods, and screen previously existing cell lines to consider their viability as tools for an X-reactivation model.

We next optimized the cytokine *in vitro* PGC-LC induction protocol to work on a hybrid cell line, and did preliminary analysis of its ability to match previous X-inactivation and reactivation results on female *in vitro* PGC-LCs. After checking the quality and proper differentiation of all cell fates involved in the protocol, we screened additional hybrid cell lines with X-linked fluorescent reporters for suitability.

After characterization, we observed a discrepancy between our results and the expected X-inactivation kinetics. In order to explore this discrepancy, we selected the most promising cell line, analyzed the classic *Tsix*, *Xist* and H3K27me3 X-activity markers and explored their relationship with gene activity on the inactivating X chromosome. This led us to the discovery that classic X-inactivation markers such as *Xist* and H3K27me3 overestimated the degree of X-inactivation compared to actual X-linked gene inactivation, while X-linked *eGFP* reporter fluorescent protein levels underestimated it. Further analysis allowed us to refine the earliest Epi-LC differentiation timespan in which cells committed for genic X-inactivation could be obtained. We next proceeded to explore the relationship between Epi-LC, embryoid body differentiation time, and cytokine media composition. We found out that the cytokine media composition could drive spurious X-reactivation in our model, and defined the differentiation conditions that would minimize its impact the most on the protocol.

Optimization of the *in vitro* PGC Induction procedure in BVSC reporter cell lines

Motivation:

Our first objective was to implement the *in vitro* PGC induction protocols in the lab.

Because the *in vitro* PGC induction protocol is reported to be very sensitive to the cell line and differentiation approach used, we wished to establish it in the lab by testing it on 4 published cell lines and endogenous reporters used in the original method development (Hayashi et al. 2011b). We chose them because all of them have fluorescent PGC fate reporters (BVSC) whose efficiency is proven both *in vivo* (Ohinata et al. 2008) and *in vitro* (Hayashi et al. 2011b), and in one case, also harbor the transcription factor cassette (BP14A) for transgene-based PGC Induction (Nakaki et al. 2013a). Because transcription factor-based PGC induction has very high efficiency, we used it as a positive control compared to the less efficient cytokine-based PGC induction method.

Our second objective was to implement cytokine-based PGC induction and sorting without the need for the *Blimp1*-Venus and *Stella*-CFP (BVSC) transgenes. Those

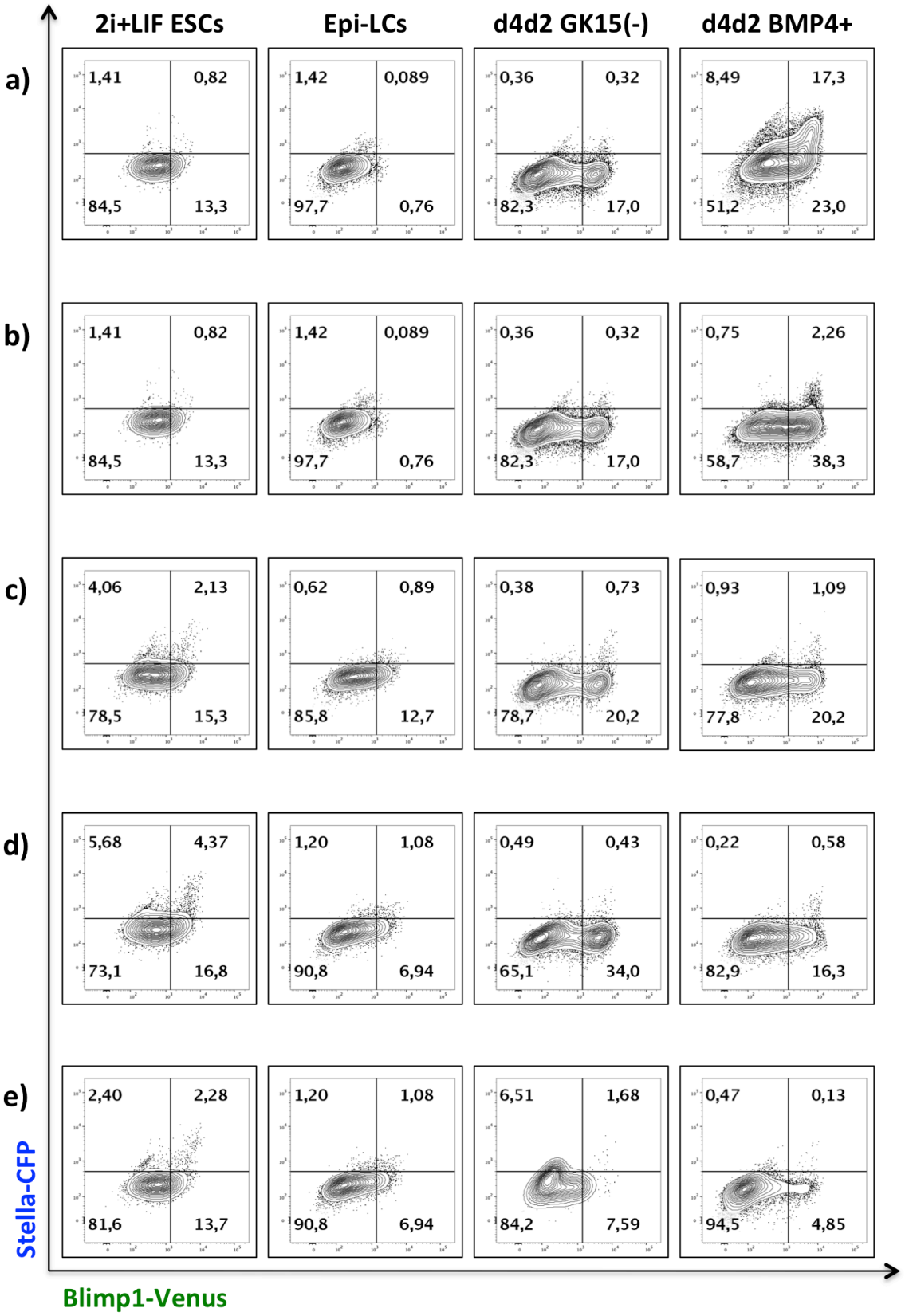
2i+LIF ESCs
Epi-LCs
d4d2 GK15(-)
d4d2 BMP4+
a)
1,41 0,82 84,5 13,3
1,42 0,089 97,7 0,76
0,36 0,32 82,3 17,0
8,49 17,3 51,2 23,0
b)
1,41 0,82 84,5 13,3
1,42 0,089 97,7 0,76
0,36 0,32 82,3 17,0
0,75 2,26 58,7 38,3
c)
4,06 2,13 78,5 15,3
0,62 0,89 85,8 12,7
0,38 0,73 78,7 20,2
0,93 1,09 77,8 20,2
d)
5,68 4,37 73,1 16,8
1,20 1,08 90,8 6,94
0,49 0,43 65,1 34,0
0,22 0,58 82,9 16,3
e)
2,40 2,28 81,6 13,7
1,20 1,08 90,8 6,94
6,51 1,68 84,2 7,59
0,47 0,13 94,5 4,85
Stella-CFP
Blimp1-Venus

Figure 3: BVSC *In vitro* PGC-induction shows worse yields than published literature and requires transgene induction for consistent yields:

a) Male BP14A transgene-induced *in vitro* PGC-LCs alongside parent ESCs, Epi-LCs and negative control embryoid bodies.
b) Male BP14A cytokine-induced *in vitro* PGC-LCs alongside parent ESCs, Epi-LCs and negative control embryoid bodies.
c) Female BVSC6 cytokine-induced *in vitro* PGC-LCs alongside parent ESCs, Epi-LCs and negative control embryoid bodies.
d) Female BVSC1 cytokine-induced *in vitro* PGC-LCs alongside parent ESCs, Epi-LCs and negative control embryoid bodies.
e) Male BVSC2 negative control cell line transgene-induced *in vitro* PGC-LCs alongside parent ESCs, Epi-LCs and negative control embryoid bodies.

transgenes make PGC induction and sorting easier, but were absent in the hybrid female cell lines we wanted to use for X-chromosome research. We aimed to obtain similar results in PGC-purification by FACS-sorting using the surface marker antibodies *CD61* and *SSEA1* as we did with the BVSC PGC reporter transgenes.

Female mouse pluripotent stem cell lines tend to lose one of their X chromosomes during culture and expansion, presumably due to selection against the hypomethylated state of XX ESCs . The resulting X0 cells are unable undergo X-inactivation, and consequently, reactivation. Our third objective was therefore to test if one of the 2 female BVSC cell lines was suitable for cytokine-based PGC induction and had a stable XX karyotype. If this was the case, the cell line could have been directly used to study X chromosome reactivation.

Results:

To achieve our goals, we induced in parallel 4 different BVSC cell lines, using both cytokine- as well as transcription factor cassette-based PGC-LC induction, whenever possible. We performed FACs analysis of PGC Inductions 4 days after cytokine or transgene PGC induction. Embryoid body differentiation conditions without cytokines from the same material were used as negative controls.

The male BP14A transgene cell line was subject to transgene **(Fig.3a and 4a)** and

cytokine **(Fig.3b and 4b)** PGC induction.

The male BVSC2 line, which lacks the PGC induction transgene cassette, was used as a negative control for transgene induction conditions **(Fig. 4e).**

The female BVSC6 **(Fig.3c and 4c)** and BVSC1 **(Fig.3d and 4d)** cell lines were only subject to cytokine PGC Induction, as they lacked the PGC induction transgene cassette.

We were able to induce *in vitro* PGCs using transgene cassette inductions, as evident by BVSC reporter transgene readout **(Fig.3a and 4a)**, even if our cytokine PGC induction efficiency was quite low, particularly in the BP14A male cell line **(Fig3b and 4b)**. This led us to conclude that, while we were able to reliably induce *in vitro* transgene PGC induction, cytokine PGC induction needed substantial improvement before this PGC induction approach could be implemented as the lab model system.

The female BVSC lines also showed low cytokine PGC induction efficiency **(Fig3b and c; Fig3c and d)**. However, our main concern was the fact that the *CD61* and *SSEA1* surface marker pattern was not yielding the same results as the BVSC reporter transgenes, and failed to show a distinct subpopulation as the BVSC reporters allowed **(data not shown)**. This led us to conclude that the FACs-sorting & analysis procedure needed to improve substantially before female cell lines lacking the BVSC reporters could be used as a model system.

In addition, the female BVSC lines, while diploid and having a mostly normal karyotype, had already underwent X-loss. Most of the cells were X0 karyotype, with only 35% cells conserving XX karyotype, in the best of cases **(data not shown)**. As X0 cells do not undergo X-inactivation, this led us to conclude that those cell lines would not be a suitable model for X-inactivation and reactivation studies.

Discussion and Conclusions

Our initial experiments showed several obstacles:

First, only transgene cassette-based PGC-LC Induction was able to support robust efficiencies at yields supporting its regular use as *in vitro* model for XCR research.

The success of cytokine *in vitro* PGC-LC induction seemed cell line-dependent and suffered low efficiency.

Only a modest 2% PGC-LC yield was reached in the male BP14A cell line, while in female BVSC cell lines, the PGC-LC yields were close to the trace PGC amounts shown by negative Embryoid body controls without cytokine addition. It is a well-reported fact that Embryoid body formation results in the spontaneous differentiation of trace amounts of PGCs (typically **<1%** in our hands), but those PGCs are unable to yield viable and fertile offspring (Geijsen et al. 2004). This stands in contrast to cytokine- (Hayashi et al. 2011a) and transgene-based (Nakaki et al. 2013a) PGC-LC induction, and precludes us the use of randomly differentiated *in vitro* PGCs from Embryoid bodies.

Our reasoning is that only *bona fide* PGC-LCs, and not randomly differentiated PGCs, could be trusted to accurately model the XCI & XCR processes happening *in vivo*.

While transgene-based PGC-LC induction seemed a better alternative, with yields in the **8-17%** range, two considerations held us from its use. First, it required the insertion of two separate transgenes, the rttA doxycycline responder and the transgene PGC induction cassette, besides the systematic validation & testing of multiple clones for PGC specification. The second was the fear that the overexpression of the *Prdm14* transgene included in the cassette would antagonize the master X-inactivator *Xist* (Payer et al. 2013) and eventually prevent X-inactivation from taking place in the PGC-LCs.

Second, the *CD61* & *SSEA1* surface markers failed to discriminate the PGC-LC population as accurately as the BVSC reporters did. The use of those markers has been described to be able to discriminate PGC-LCs differentiated from a variety of iPSC & ESC cell lines (Hayashi et al. 2011b; Nakaki et al. 2013b; Hayashi & Saitou 2013c), and, besides cytokine PGC-LC induction method, is a key component required to render

in vitro PGC-LC induction a versatile and widely accessible model. As such, troubleshooting the problems found with the staining procedure was an absolute priority, as in-depth research in X-inactivation/reactivation requires the use of specific legacy cell lines adapted for chromosome & allele specific sequencing. The use of those cell lines is essential, and the insertion of the BVSC transgenes in them and the associated lengthy validation procedures *in vivo* (Ohinata et al. 2008) were considered too time consuming to be practical, so the optimization & use of *CD61* and *SSEA1* surface markers was essential.

Third, the female BVSC cell lines we had access to did not conserve the XX karyotype, but did quickly lose one X chromosome to reach an X0 karyotype. In our experience, standard female pluripotent stem cell lines lose their X chromosomes so quickly that individual clone selection and expansion are not a viable strategy to recover stable XX populations, unless this is coupled with a continuous selection, such as X-linked fluorescent reporters or drug selection markers.

Fourth, the PGC-LC yield from the cytokine induction needed to be dramatically upscaled to be a useful model. For the differentiation of 1 million input Epi-LCs, published typical cytokine PGC-LC differentiation efficiencies were in the range of **5-10%** (Hayashi et al. 2011b; Hayashi et al. 2011a; Hayashi & Saitou 2013b), this means a theoretical maximum of 50.000 to 100.000 PGC-LCs per experiment, for a projected cost of 600€ per experiment in cytokines alone. As such, upscaling the experiment beyond these limits to obtain more PGC-LCs was not considered acceptable, and the project needed to be executed within these constraints, reaching a minimal PGC-LC efficiency of 5%. It also meant that all *in vitro* PGC-LCs needed to be in an X-inactive state to study their reactivation afterwards.

In view of all the above, multiple improvements were necessary. We decided that using the existing BVSC cell lines or focusing on the derivation of new female cell lines of

stable karyotype for transgene PGC-LC induction was not a time-effective approach.

Instead, we focused on optimizing Cytokine-based PGC-LC induction in the karyotypically stable female hybrid cell line EL16.7 TST and using effectively the *CD61* and *SSEA1* surface markers for FACs purification of the resulting PGC-LCs.

The state of X-activity of those PGC-LCs would then be interrogated, and the readout techniques would be optimized to function in PGC-LC cells when necessary, focusing on techniques that required low cell numbers to offset the low yields of the model.

In vitro cytokine PGC induction and X-reactivation in the EL16.7 cell line

Motivation

As the female BVSC cell lines were unsuitable for X-reactivation research due to their karyotype, we focused on optimizing the cytokine PGC-LC induction and *CD61* and *SSEA1* purification on karyotypically stable female cell lines. We had three goals:

First, we wished to optimize the cytokine PGC-LC induction and *CD61* and *SSEA1* staining so that we could obtain PGC-LC yields above **5%** of input cells, and FACs-sort them for further culture and analysis.

Second, we wished to address the state of X-inactivation in our *in vitro* female PGC-LCs, and see if they reproduce the X-inactive state that is seen *in vivo*, and their posterior X-reactivation only when they are exposed to the female gonadal cells, as has been described previously (Katsuhiko Hayashi et al. 2012). Reproducing these results was key; otherwise, the cytokine-based *in vitro* PGC-LC system would not be amenable as a research model for our purpose.

Third, we wished to verify that cell differentiation had proceeded correctly at all stages: Naïve pluripotent stem cells, Epi-LCs, PGC-LCs and meiotic GC-LCs after their aggregation with the female gonadal cells.

Results

To achieve our goals, we chose the EL16.7 TST hybrid ESC cell line . This cell line was derived in the past from a hybrid *Mus musculus/castaneus* hybrid offspring, and has one X chromosome derived from *mus musculus* subspecies, while the other is derived from *mus castaneus* subspecies (Lee & Lu 1999). Furthermore, the *Mus musculus* X chromosome harbors a truncation of *Tsix* (TST allele), therefore leading to skewed X-inactivation with always the *Mus musculus* X being chosen for inactivation, while the *Mus castaneus* X would remain active. This setup offers three advantages: The first is that the resulting hybrid cell line is very resistant to X chromosome loss over extended periods of cell culture, avoiding the danger of an X0 karyotype. The second is that the cell line as a distinct subspecies-specific footprint of single-nucleotide polymorphisms (SNPs) that allows to discriminate RNA and DNA sequence from each X Chromosome, using published allele-specific sequencing pipelines and RT-PCR sets (Deng et al. 2014; Babak et al. 2008; Keane et al. 2011; Yang, Babak, Shendure & Disteche 2010). The third advantage is the skewing, therefore allowing to assign transcripts of *Mus musculus* background to the inactive X-chromosome, which is reactivated during X-reactivation, thereby enabling the allele-specific study of X-inactivation and X-reactivation in bulk-experiments (without skewing single-cell assays would be necessary).

Optimization of the *CD61* and *SSEA1* surface marker stainings on PGCs

We differentiated EL16.7 TST ESCs to Epi-LCs for 2 days, then induced PGC-LCs with cytokines and cultured the PGC-induction bodies for 4 days, which is the minimum timeframe for the *CD61* and *SSEA1* PGC markers to build up to detectable levels in FACs analysis. The PGC-LCs were stained for the *CD61* and *SSEA1* surface markers and FACs-sorted in parallel to *in vivo* E11.5 female mouse gonads. The resulting *in vivo* PGCs were used as a positive control for *CD61* and *SSEA1* PGC staining (**Fig.5a**), while the female somatic gonadal cells and the EL16.7 TST PGC-LCs were aggregated together to form reconstituted ovaries, to promote X-reactivation and meiotic progression in the PGC-LCs.

SSEA1 is a marker for cells that have pluripotent status, while *CD61* marks cells with a differentiated status. As expected, the naïve pluripotent ESCs (**81%)** and the Epi-LCs

(**82,4%)** predominantly expressed *SSEA1*, but lacked *CD61* expression. In contrast, both *in vivo* E11.5 PGCs and *in vitro* PGC-LCs (**14.9%)** showed co-expression of *CD61* and *SSEA1* markers, a trait specific to the germ cell lineage.

As *CD61* is a marker of differentiated cells, it was also expressed by a subset of the cells produced in the PGC-LC induction body that have differentiated to a somatic fate (**42.8%**). The cells that expressed *SSEA1* only (**42,3%**) were supposed to be pluripotent stem cell-like cells (PSC-LCs), cells which have escaped proper differentiation and retained pluripotent characteristics, without being germ cells (Hayashi et al. 2011b; Nakaki et al. 2013b; Hayashi & Saitou 2013c). These were an un-desired byproduct of the protocol and not used for further study.

The fact that *in vivo* PGCs and *in vitro* PGC-LCs share similar *SSEA1* and *CD61*(+) staining patterns led us to conclude that our cytokine *in vitro* PGC-LC induction has been successful.

Initial characterization of X-reactivation in PGC-LCs after gonadal aggregation

Our next goal was to verify if the X chromosome activity status matched in our PGC-LC induction above matched described reports. We sampled the experiment described in (**Fig.5a**) for immunostaining analysis. We included the starting ESCs and day 2 Epi-LCs used for cytokine PGC-LC induction, as well as PGC induction bodies after 1 and 3 days of culture. The *in vitro* PGC-LCs were sorted after 4 days of culture with the gating settings seen in (**Fig.5a**) and aggregated with the female somatic gonadal cells to form reconstituted ovaries. After 3 days of co-culture, the reconstituted ovaries were sampled for immunostaining.

The only published report at that time studying X-reactivation in the in vitro PGC-LC system used the H3K27me3 immunostaining spot over an X-inactive chromosome to track the activity of the X chromosome status across the female PGC differentiation procedure (Katsuhiko Hayashi et al. 2012). In their study, the first X-inactive cells were seen at day 2 of Epi-LC differentiation (**20%**). X-inactivation spreads after 24H of cytokine *in vitro* PGC induction, with the majority of cells being X-inactive (**85%**), and this extends to the *in vitro* PGC-LCs after 3 days of culture. After 3 days of PGC body

culture, the researchers purified the PGC-LCs and aggregated them with female somatic gonadal cells. After 3 days of co-culture, more than **90%** of the PGC-LCs were X-active and lacked the H3K27me3 spot.

Their results roughly match our observations (**Fig.5b)**. We did not observe any H3K27me3 spots in naïve ESCs, coincident with their fully X-active status. At day 2 of Epi-LC differentiation, **39%** of Epi-LCs harbored an X-inactivation H3K27me3 spot. This percentage increased drastically 24H after cytokine PGC-LC induction, with **68%** of cells displaying an X-inactivation spot.

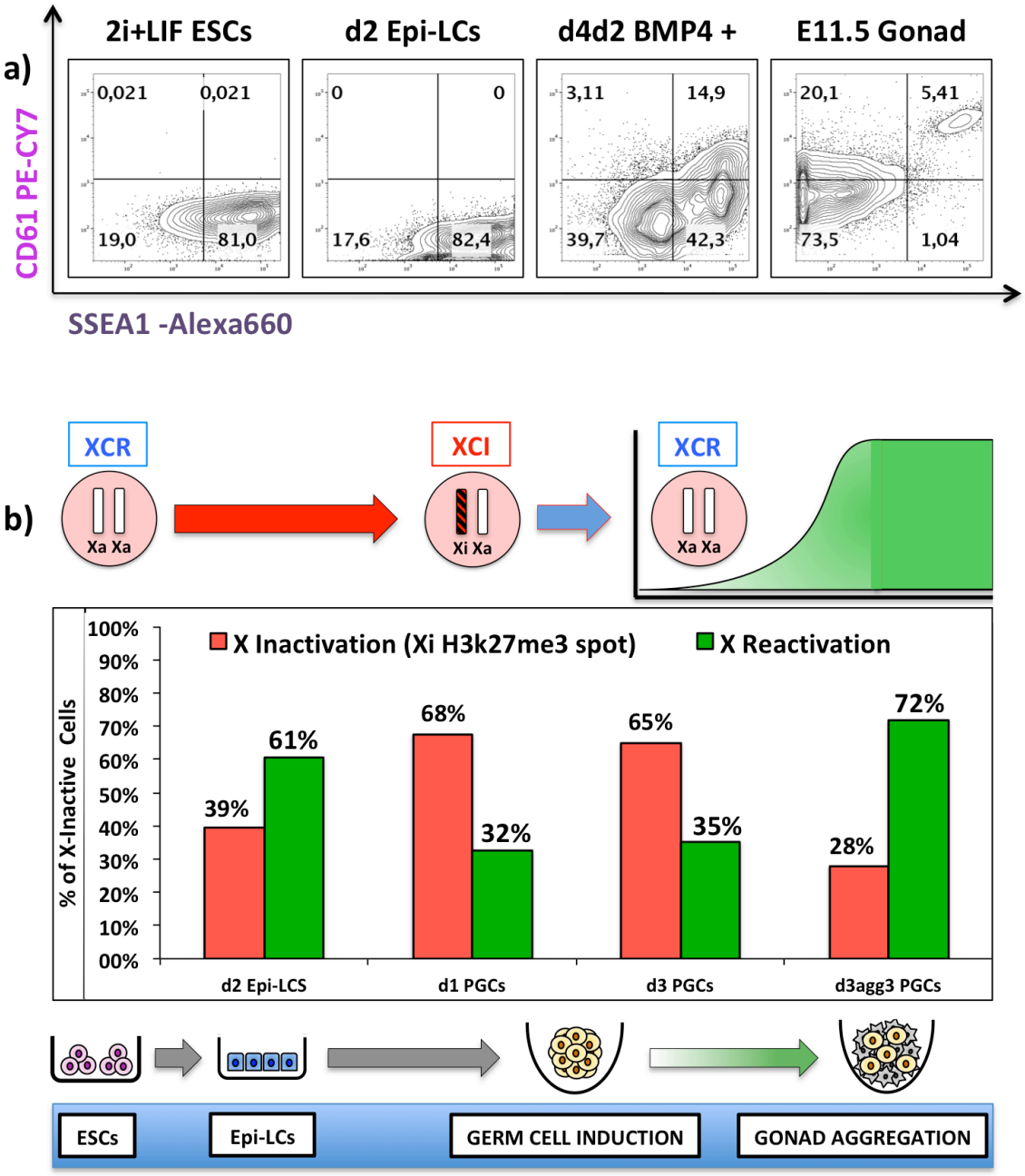

Figure 4: Cytokine *In vitro* PGC-induction and gonadal aggregation allow to track XCI on PGC-LCs:

a) Female EL16.7 cytokine-induced *in vitro* PGC-LCs alongside parent ESCs, Epi-LCs and the E11.5 gonadal cell suspension. PGCs in the upper right quadrant.

b) Scoring the Female EL16.7 cells X-inactivation state through H3K27me3 and *Nanog* immunofluorescence in Epi-LCs, day1 body cells, day3 PGC-LCs and day4 PGC-LCs after 3 days of gonadal aggregation.

The first observable timepoint in which *in vitro* PGC-LCs can be sorted from their neighbors is after 48H of culture (Kurimoto et al. 2015). In order to identify PGC-LCs, cells were co-stained with a *Nanog* antibody staining to discriminate the PGC-LCs from their somatic neighbors.

While on day 3 PGC-LCs have **65%** of cells displayed an X-inactivation spot, and were thus majorly X-inactive, after 3 days of co-culture with somatic gonadal cells the situation flipped, with **72%** of PGC-LCs becoming X-active and lacking an X-inactivation spot.

This led us to conclude that *in vitro* PGC-LCs reproduce the characteristics of *in vivo* PGCs, including their X-inactive state before reaching the female gonad and their X-reactivation after exposure to female somatic gonadal cells.

But there were also discrepancies between our data and the published results by Hayashi et al. The starting day2 Epi-LCs were showing **39%** X-inactive cells, against the **20%** observed in the original report. We credited this to the fact that we differentiated our starting Epi-LCs for 12 hours longer than in the original report, to boost the X-inactivation of the starting materials. We did also notice that the X-inactivation and X-reactivation observed in our PGC-LCs were less drastic than in the original report. We credited this to two factors.

The first was that *Nanog* could also be expressed from PSC-LCs that retained some pluripotent features, but were not properly differentiated. Those cells would be expected to not have undergone full X-inactivation, due to their pluripotent stem cell characteristics.

The second was that our standard immunostaining protocols were suboptimal for PGC-LCs, and to a lesser degree, to Epi-LCs. Standard cytospinning protocols destroy nuclear morphology of PGC-LCs and Epi-LCs, as well as standard permeabilization procedure with CSK buffer and most antibody permeabilization buffers (Satoshi H Namekawa & Lee 2011). While we did partly circumvent the problem by depositing the PGC-LCs on adsorbent-treated microscope slides, this method resulted in the selective loss of PGCs from the substrate (**data not shown)**. We also were unable to find an

antibody for immunostaining that could distinguish PGC-LCs from the undifferentiated pluripotent stem cell-like cells (PSC-LCs) contaminants that *in vitro* cytokine PGC-LCs produces.

Our conclusions are therefore twofold. H3K27me3 immunostaining indicated that our *in vitro* cytokine PGC-LCs follow the X-inactivation and reactivation dynamics expected from *in vivo* PGCs. On the other hand, we decided that the problems in immunostaining and PGC markers for immunofluorescence, as well as its lower throughput, precluded further use of immunostaining as a reliable readout technique until the protocol was optimized.

Real-time PCR analysis of cell differentiation across the cytokine PGC-LC induction

We next wished to check that our results were stemming from properly differentiated cells.

In order to determine proper cell differentiation at all stages of the protocol, precursor naïve pluripotent stem cells, Epi-LCs, PGC bodies cultured for 3 days after PGC-LC induction, and the reconstituted ovaries after 3 and 6 days of gonadal somatic cell co-culture were harvested. Their gene expression for multiple markers of proper differentiation and cell fate for each stage was compared by RT-PCR against *in vivo* E11.5 PGCs and somatic gonadal cells as a control **(Fig.6)**.

Nanog is a marker of pluripotent ESCs and iPSCs, but its expression is shared with PGCs and PGC-LCs **(Fig.6a)**. As expected, it was downregulated as ESCs were differentiated into Epi-LCs, and it was later upregulated in PGC-LCs and in meiotic PGC-LCs of reconstituted ovaries. The expression of *in vitro* PGC-LCs at all stages was the same of *in vivo* E11.5 PGC-LCs (in green). As expected, its expression was completely absent in somatic gonadal cells (in blue).

The *de novo* DNA methyltransferase Dnmt3b is a marker of the differentiating epiblast,

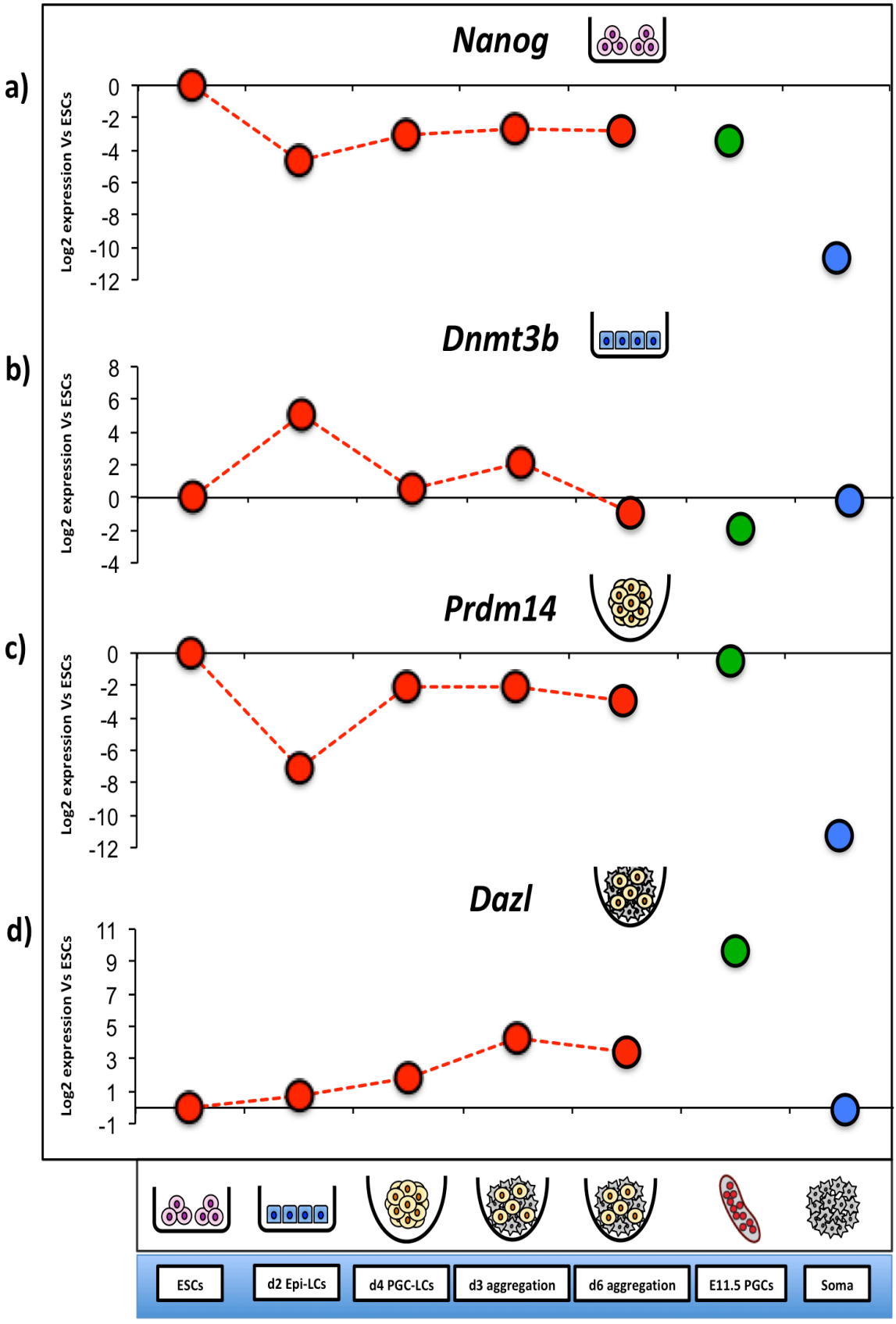
a)
Nanog
Log2 expression Vs ESCs
0
-2
-4
-6
-8
-10
-12
b)
Dnmt3b
Log2 expression Vs ESCs
8
6
4
2
0
-2
-4
c)
Prdm14
Log2 expression Vs ESCs
0
-2
-4
-6
-8
-10
-12
d)
Dazl
Log2 expression Vs ESCs
11
9
7
5
3
1
-1
ESCs
d2 Epi-LCs
d4 PGC-LCs
d3 aggregation
d6 aggregation
E11.5 PGCs
Soma

Figure 5: Cytokine *In vitro* PGC-induction and gonadal aggregation allow to track XCI on PGC-LCs:

a) ESCs marker *Nanog* expression across cytokine PGC-LC induction (in red), compared versus sorted E11.5 *in vivo* PGCs and somatic gonadal cells.
b) Epi-LCs marker *Dnmt3b* expression across cytokine PGC-LC induction (in red), compared versus sorted E11.5 *in vivo* PGCs and somatic gonadal cells.
c) PGC-LCs marker *Prdm14* expression across cytokine PGC-LC induction (in red), compared versus sorted E11.5 *in vivo* PGCs and somatic gonadal cells.
d) Meiotic PGC-LCs marker *Dazl* expression across cytokine PGC-LC induction (in red), compared versus sorted E11.5 *in vivo* PGCs and somatic gonadal cells.

(Fig.6b). and was nearly absent in the starting pluripotent ESCs and drastically upregulated in Epi-LCs. It was again downregulated after PGC-LC differentiation, at similar levels as *in vivo* PGCs. This fits expectations, as PGCs are known to undergo a genome-wide DNA demethylation as part of their epigenetic reprogramming, and downregulate all DNA-methyltransferases (Kagiwada et al. 2012; Hayashi et al. 2011b; Katsuhiko Hayashi et al. 2012)**.** *Dnmt3b* expression was also very low in somatic gonadal cells (in blue).

Prdm14 was expressed in the starting pluripotent cells (both in ESCs and iPSCs), as well as in PGCs **(Fig.6c)**. Together with BLIMP1 and TFAP2C, PRDM14 is one of the three major transcription factors that confer PGC fate and is a component of the PGC-LC transgene specification cassette (Nakaki et al. 2013b). In our experiments, Prdm14 was downregulated as ESCs were differentiated into Epi-LCs and then was upregulated at all PGC-LC stages. The expression of *in vitro* PGC-LCs was close to *in vivo* E11.5 PGC-LCs (in green). As expected, Prdm14 expression was completely absent in the somatic gonadal cells (in blue), in a similar fashion to *Nanog*.

DAZL has long been used as a marker of meiotic onset and progression of PGCs into meiotic germ cells **(Fig.6d)**, and has been used to detect meiotic maturation of *in vitro* germ cells as they are co-cultured in reconstituted ovaries (Katsuhiko Hayashi et al. 2012). We observed that Dazl RNA starts its mild expression after PGC-LC specification, and is upregulated after aggregation with somatic gonadal cells, indicating the onset of the meiotic program.

The fact that Dazl did not reach the expression levels of the *in vivo* PGCs (in green) in our hands can be explained as the PGC-LC RNA being diluted by the RNA of the accompanying somatic gonadal cells. Alternatively, it could also point out that our reconstituted ovary co-culture conditions were suboptimal.

Our data led us to conclude that we could specify *in vitro* PGC-LCs with the cytokine-based induction protocol, and reproduce the *in vivo* X-inactive state. We were also able to reproduce their X-reactivation when in contact with the female somatic gonad, as previously described *in vivo* (Hu, Peter K Nicholls, et al. 2015), *ex vivo* (Chuva de Sousa Lopes & Roelen 2008) and *in vitro* (Katsuhiko Hayashi et al. 2012). The *CD61* and *SSEA1* surface marker FACs-sorting was also considered to be a viable approach.

The expression of the RT-PCR markers led us to consider that our *in vitro* results accurately reproduced *in vivo* PGC biology.

Discussion and conclusions

Our analysis of *in vitro* cytokine–induced PGC-LCs led us to the following conclusions:

First was that the surface markers *CD61* and *SSEA1* could be used to sort the *in vitro* cytokine PGC-LCs, precluding the need to develop a cell line with germ cell reporter transgenes, and allowing a greater flexibility in cell lines used.

Second was that *in vitro* PGC-LCs could accurately model the X-inactivation and reactivation dynamics previously observed *in vivo* (Hu, Peter K Nicholls, et al. 2015), *ex vivo* (Chuva de Sousa Lopes & Roelen 2008) and *in vitro* (Katsuhiko Hayashi et al. 2012). Moreover, the RT-PCR analysis supported this being a result of proper *in vitro* PGC-LC specification and not an artifact of aberrant or failed cell differentiation. This led us to consider *in vitro* PGC-LCs as a suitable model of X-reactivation research.

Third was the fact that better technical readouts and a more detailed investigation of X chromosome activity across the protocol were necessary. Initially, our RNA extraction protocols was unable to yield enough material from the scarce amount of purified *in vitro* PGC-LCs, and we had to resort to extract the RNA of whole aggregates including

the accompanying undifferentiated and somatic cells. While this was tolerable for the detection of very distinctive markers, it introduced a measure of uncertainty. It also rendered impossible the assessment of X-inactivation and reactivation at the transcriptional level, as the surrounding somatic cells (X-inactive) and undifferentiated pluripotent contaminant cells (presumably X-active) would render the measurements inaccurate.

In addition, while immunostaining with H3K27me3 allowed us to track the XCI and XCR across the protocol, we decided that it was not a suitable long-term approach. We were interested in the transcriptomics of X-reactivation, and the H3K27me3 immunostaining has been mostly suitable as a proxy for X status in contexts where few cells are available, as the early embryo. Given its low throughput and the difficulties in preserving PGC attachment and morphology during the protocol, we preferred to abandon this approach until the immunostaining protocol was optimized in PGC-LCs.

Of more concern was the fact that only **65%** of PGC-LCs displayed X-inactivation prior to FACs sorting.

While we attributed the lower percentage compared to the previous *in vitro* report (Katsuhiko Hayashi et al. 2012) to the shortcomings observed with NANOG as a marker and our immunostaining protocol, it was also possible that fractions of PGC-LCs could remain X-active.

In reaction to all the above, we decided to focus on optimizing the protocol on cell lines carrying X-linked fluorescent reporters, and move on to characterizing the transcriptional status of the X. We would use the fluorescent reporters to track the extent and state of X-inactivation across the differentiation procedure, and we would use allele-specific RT-PCR to assess the extent of X-inactivation. The relationship between the transcriptional status of the X chromosome and other X-linked classic markers of X activity, such as *Xist* and *Tsix* RNA-FISH staining, as well as H3K27me3 spot immunofluorescence, would be ellucidated.

The goal was to validate the starting X-inactive status of the Epi-LCs and PGC-LCs, and find a starting Epi-LC differentiation timepoint that guaranteed full X-inactivation

without compromising PGC-LC induction.

Timelines of X-inactivation of *In vitro* induced Epi-LCs from different cell lines

Motivation

Our ultimate goal was to be able to accurately track X-inactivation and reactivation dynamics at the transcriptional and epigenomic level. For this, we needed a hybrid cell line that had a SNP composition amenable to allele-specific sequencing and RT-PCR. In addition, this cell line had to have an X-linked fluorescent reporter to track which cells

had undergone X-inactivation or reactivation. Finally, this cell line needed skewed X-inactivation (Lee & Lu 1999); this meant that we needed for the X chromosome of our choice to be the only one which could be inactivated and reactivated, instead of allowing random X-inactivation, as it happens *in vivo* (Wutz 2011).

If cell lines with these characteristics were available, they still needed to undergo the fastest X-inactivation possible. The success of *in vitro* PGC-LC induction was described to require very short Epi-LC differentiation times, 2 days at most (Hayashi & Saitou 2013b; Hayashi & Saitou 2013c), before the Epi-LCs were reported to lose competence for PGC fate and start dying (Hayashi et al. 2011b).

Methods and results

We screened five hybrid ESC & iPSC cell lines for suitability, two of them subject to random X-inactivation, and three of them subject to skewed X-inactivation. All of them had an X-linked *eGFP* reporter in the *mus musculus* chromosome (a K. Hadjantonakis et al. 2001; Wu et al. Neuron 2014, Moritz Bauer unpublished). In order to track their X-inactivation kinetics, we differentiated them to Epi-LCs and tracked their *X-eGFP* signal until stable X-inactivation could be observed **(Fig.7)**.

X-inactivation kinetics of hybrid *musculus/castaneus* cell lines

We first tested the X-inactivation kinetics of three *mus musculus/castaneus* hybrid iPSC

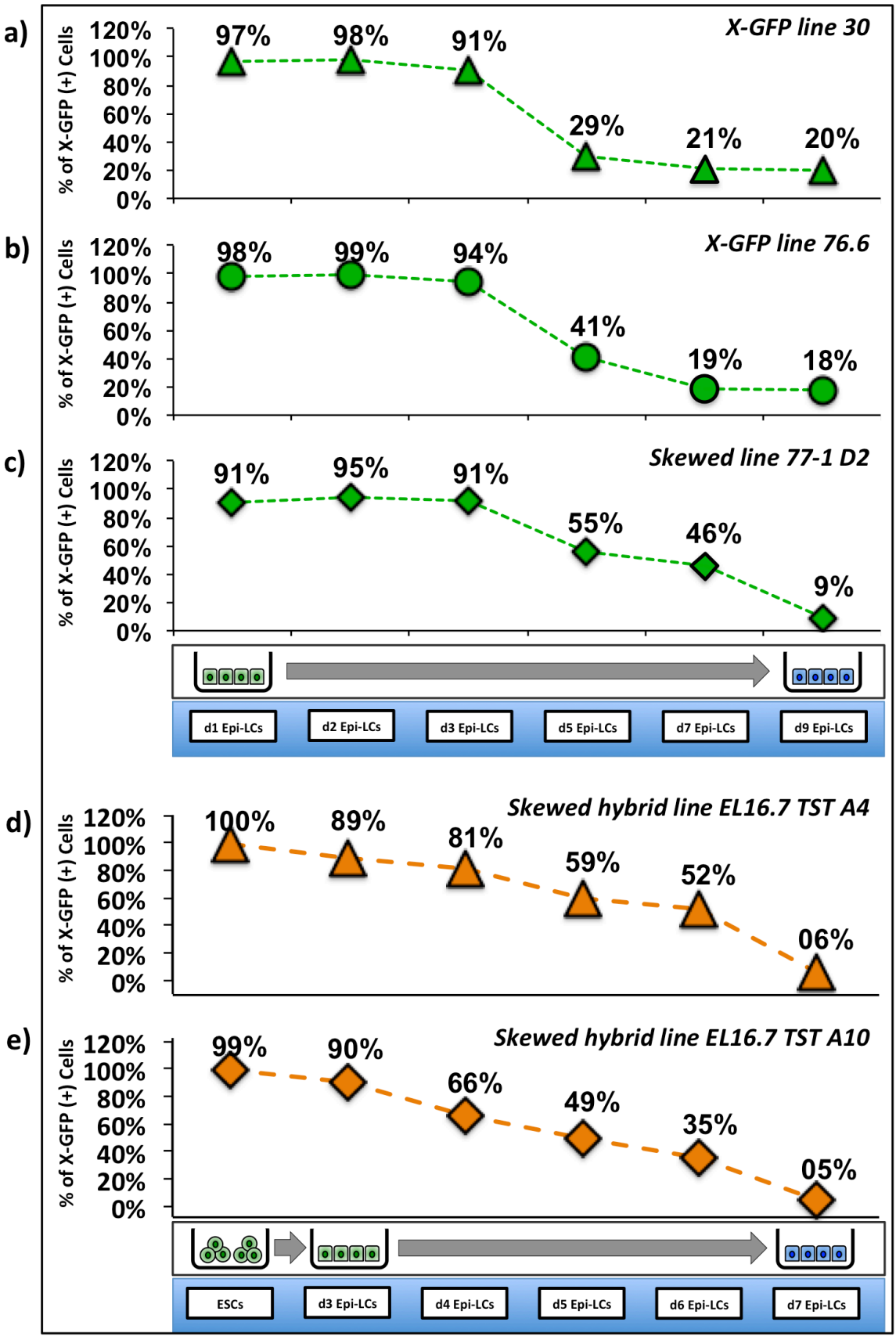
a)
X-GFP line 30
% of X-GFP (+) Cells
120%
100%
80%
60%
40%
20%
0%
97%
98%
91%
29%
21%
20%
b)
X-GFP line 76.6
98%
99%
94%
41%
19%
18%
c)
Skewed line 77-1 D2
91%
95%
91%
55%
46%
9%
d1 Epi-LCs
d2 Epi-LCs
d3 Epi-LCs
d5 Epi-LCs
d7 Epi-LCs
d9 Epi-LCs
d)
Skewed hybrid line EL16.7 TST A4
100%
89%
81%
59%
52%
06%
e)
Skewed hybrid line EL16.7 TST A10
99%
90%
66%
49%
35%
05%
ESCs
d3 Epi-LCs
d4 Epi-LCs
d5 Epi-LCs
d6 Epi-LCs
d7 Epi-LCs

Figure 6: Timelines for X-inactivation onset during Epi-LC differentiation:

a) naïve iPSCs from line 30 are induced to Epi-LCs for 9 days, and the cells are FACs-analyzed daily for their X-inactivation kynetics across the protocol.
b) naïve iPSCs from line 76.6 are induced to Epi-LCs for 9 days, and the cells are FACs-analyzed daily for their X-inactivation kynetics across the protocol.
c) naïve iPSCs from skewed line 77-1D2 are induced to Epi-LCs for 9 days, and the cells are FACs-analyzed daily for their X-inactivation kynetics.
d) naïve ESCs from skewed line EL16.7 TST A4 are induced to Epi-LCs for 9 days, and the cells are FACs-analyzed daily for their X-inactivation kynetics.
e) naïve ESCs from skewed line EL16.7 TST A10 are induced to Epi-LCs for 9 days, and the cells are FACs-analyzed daily for their X-inactivation kynetics.

lines, iPSC 30, 76-6 and 77-1D2. We differentiated them to Epi-LCs and cultured them for 9 days.

The hybrid iPSC cell lines 30 **(Fig.7a)** & 76-6 (**Fig.7b)** are subject to random X-inactivation. This means that not all cells will inactivate the *musculus* X-chromosome and its X-linked *X-eGFP* transgene at the end of the X-inactivation process, but will inactivate the *castaneus* chromosome instead.

The hybrid iPSC cell line 77-1D2 **(Fig.7c)** has skewed X-inactivation, due to a CPG island deletion in the *Tsix* gene of the *musculus* chromosome (Lee & Lu 1999). The consequence is that the *musculus* chromosome will be inactivated in all the cells of the population, becoming *X-eGFP*-negative at X-inactivation endpoint.

All cell lines showed virtually no X-inactivation until 3 days of Epi-LC differentiation, where virtually all cells still displayed X-active status **(Fig.7a, b and c)**. After 5 days of Epi-LC differentiation, a first sharp onset of X-inactivation could be seen.

For the non-skewed cell lines 30 **(Fig.7a)** & 76.6 **(Fig.7b)**, a stable state was reached after 7 days of Epi-LC differentiation. About **80%** of the population inactivated the *mus musculus* X chromosome while **20%** of the population inactivated the *castaneus* X chromosome instead.

This ratio is different from the expected **50%** chance that would be expected from *in vivo* observations in pure *musculus* animals (Wutz 2011). This is explained because in

crosses between different mouse subspecies, the X-inactivation choice between the two X-chromosomes is non-random. Indeed, it has been reported that in hybrids, some natural skewing occurs, with the *musculus* X chromosome having a higher chance of being inactivated due to the so-called Xce-effect (Cattanach & Papworth 1981; Thorvaldsen et al. 2012, Payer 2016).

For the skewed cell line 77-1D2 **(Fig.7c)**, the X-inactivation rates were slower, reaching their X-inactivation endpoint at day 9, instead of day 7 of differentiation. At day 9, only **9%** of cells still had detectable *musculus* X-active chromosomes.

Our conclusion was that the rates of X-inactivation were too slow for us to wait for the Epi-LCs to X-inactivate. If the optimal timepoint for X-inactivation was day 9, those Epi-LCs were unlikely to be competent for cytokine *in vitro* PGC-LC induction. In addition, the above-mentioned cell lines were karyotypically unstable, requiring frequent FACs sorting and verification to avoid losing their X chromosome and becoming X0 cells. This led us to conclude that we would need to choose alternative cell lines.

Selection of skewed hybrid *musculus/castaneus* lines with deterministic X-inactivation and stable karyotype

In order to overcome these limitations, we needed a karyotypically stable hybrid cell line, in addition to its fluorescent X-linked reporter. Another Phd student in our laboratory, Moritz Bauer, derived two additional EL16.7 TST hybrid ESC cell lines (Ogawa et al. 2008; Lee & Lu 1999) by adding X-linked reporters to them, the EL16.7 TST A4 single color & A10 dual color lines (unpublished). This hybrid cell line had increased karyotypic stability and a hybrid *castaneus/musculus* X chromosome composition. It also had two chief advantages over the previous cell lines.

The first feature of this cell line was the TST truncation. The *TST* allele truncates the *Tsix* transcript in the *musculus* X-chromosome (Luikenhuis et al. 2001, Ogawa et al. 2008), guaranteeing deterministic X-inactivation of the *musculus* chromosome during Epi-LC differentiation.

The second feature was the inclusion of a *X-eGFP* reporter in the *musculus* X chromosome. In addition, the EL16.7 TST A10 dual color line has a second *X-tdTomato* reporter in the *castaneus* X chromosome. This allowed us to sort out cells that have lost their X chromosome and have acquired an X0 karyotype.

We decided to test EL16.7 TST A4 single color **(Fig.7d)** and A10 dual color **(Fig.7e)** X-inactivation kinetics and see whether we could get faster X-inactivation and increased karyotypic stability. We optimized Epi-LC culture conditions and differentiated them for 7 days.

We observed the first X-eGFP inactivated cells after 3 days of differentiation, but the most noticeable shift could be observed after 4 days of differentiation. The earliest X-eGFP inactivation endpoint observable was day 7 of differentiation, where only **5%** of the population remained X-active.

Analysis of the EL16.7 TST dual color cell line could not detect any significant X chromosome loss, with X0 cells below **0.5%** at all times.

Our analysis of multiple X-inactivation timelines leads us to conclude four things.

First, the Epi-LC X-inactivation kinetics were fairly homogeneous across different cell lines, with the first observable X-eGFP downregulation visible after 3 days of differentiation. The first sharp increase of X-eGFP inactive cells could only be observed after 5 days of differentiation, and this was a trait shared amongst all cell lines.

Second, we chose the EL16.7 TST A10 dual color line for future work, as it combined the faster X-inactivation speed observed with fluorescent reporters for X-inactivation and XX karyotype. In addition, it had compatibility with known allele-specific RT-PCR and sequencing pipelines due to the hybrid *Mus musculus/Mus castaneus* strain background (Pinter et al. 2015).

Third, the excessively slow X-eGFP inactivation kinetics observed for all Epi-LC lines (**Fig.7a-e)** did not match the X-inactivation speed observed with H3K27me3 immunostaining in previous experiments with the EL16.7 line **(Fig.5a-b).** This made us wonder how accurately the X-eGFP and the H3K27me3 reflect the actual status of the

X chromosome at the transcriptional level.

At last, the number of days needed to completely inactivate the X chromosome of Epi-LCs is incompatible with successful PGC-LC induction. Epi-LCs are at their prime after 2 days at most (Hayashi & Saitou 2013b; Hayashi & Saitou 2013c), and they start losing competence for PGC fate and start dying shortly afterwards (Hayashi et al. 2011b). Therefore, differentiating them for 7 days before inducing PGC-LCs seemed a losing proposition.

FACs-sorting X-inactive Epi-LCs was also not an option, as those cells lose their viability and PGC-LC competence (Nakaki 2017).

Analysis of *Tsix, Xist* and H3K27me3 markers during Epiblast-like cell differentiation

There were two remaining possibilities to make cytokine *in vitro* PGC-LCs a workable model. The first was to hope that the cytokine-based *in vitro* PGC-LC induction was able to stimulate X-inactivation in all cells as they differentiated. This has some support

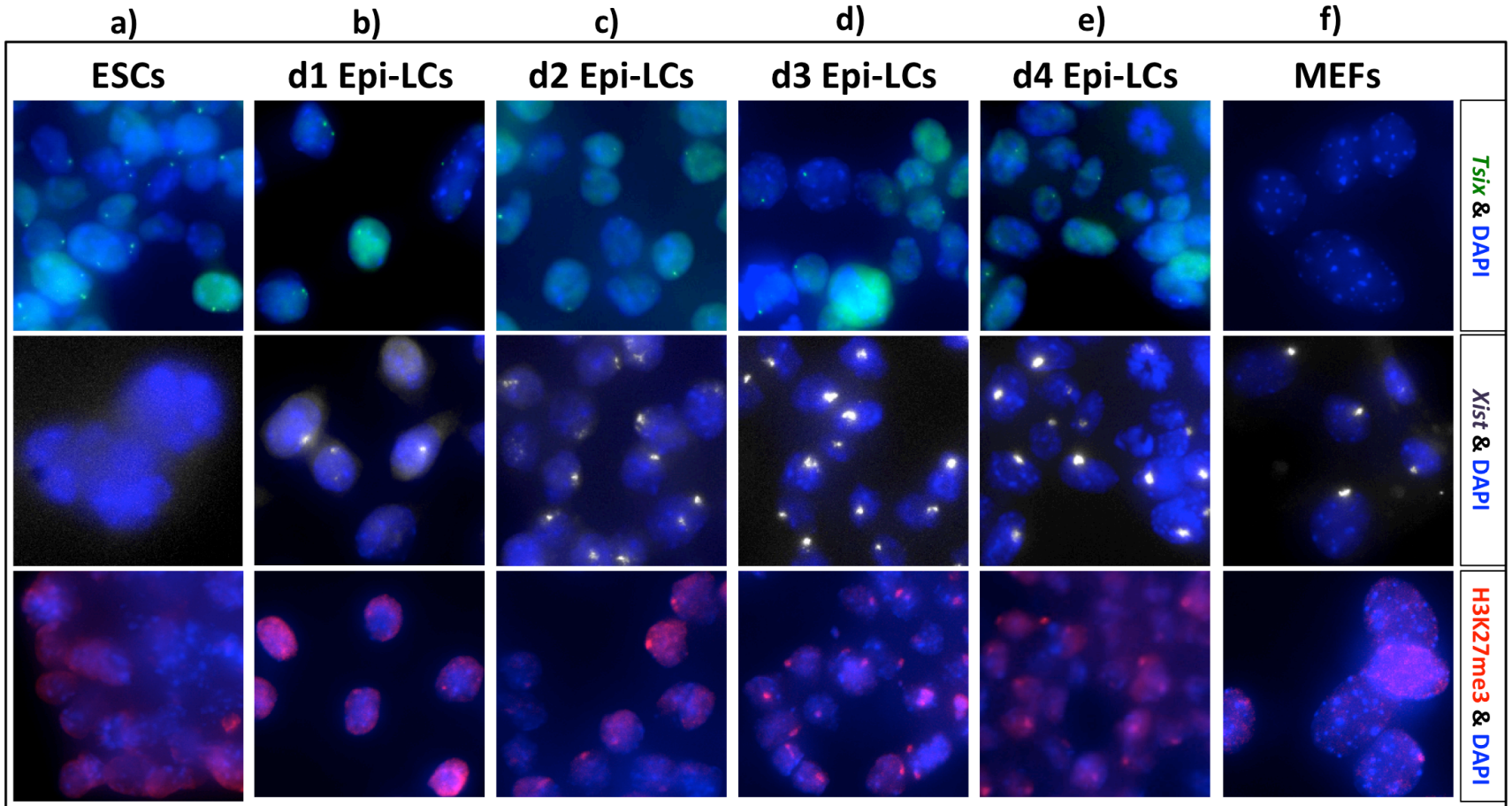

Figure 7: Timelines for X-inactivation onset during Epi-LC differentiation:

a) naïve ESCs from EL16.7 TST A10 line staining for *Tsix (*green), *Xist (*white) and H3K27me3 (red).
b) day1 Epi-LCs from EL16.7 TST A10 line staining for *Tsix (*green), *Xist (*white) and H3K27me3 (red).
c) day2 Epi-LCs from EL16.7 TST A10 line staining for *Tsix (*green), *Xist (*white) and H3K27me3 (red).
d) day3 Epi-LCs from EL16.7 TST A10 line staining for *Tsix (*green), *Xist (*white) and H3K27me3 (red).
e) day4 Epi-LCs from EL16.7 TST A10 line staining for *Tsix (*green), *Xist (*white) and H3K27me3 (red).
f) Stably X-inactivated female MEFs staining for *Tsix (*green), *Xist (*white) and H3K27me3 (red).

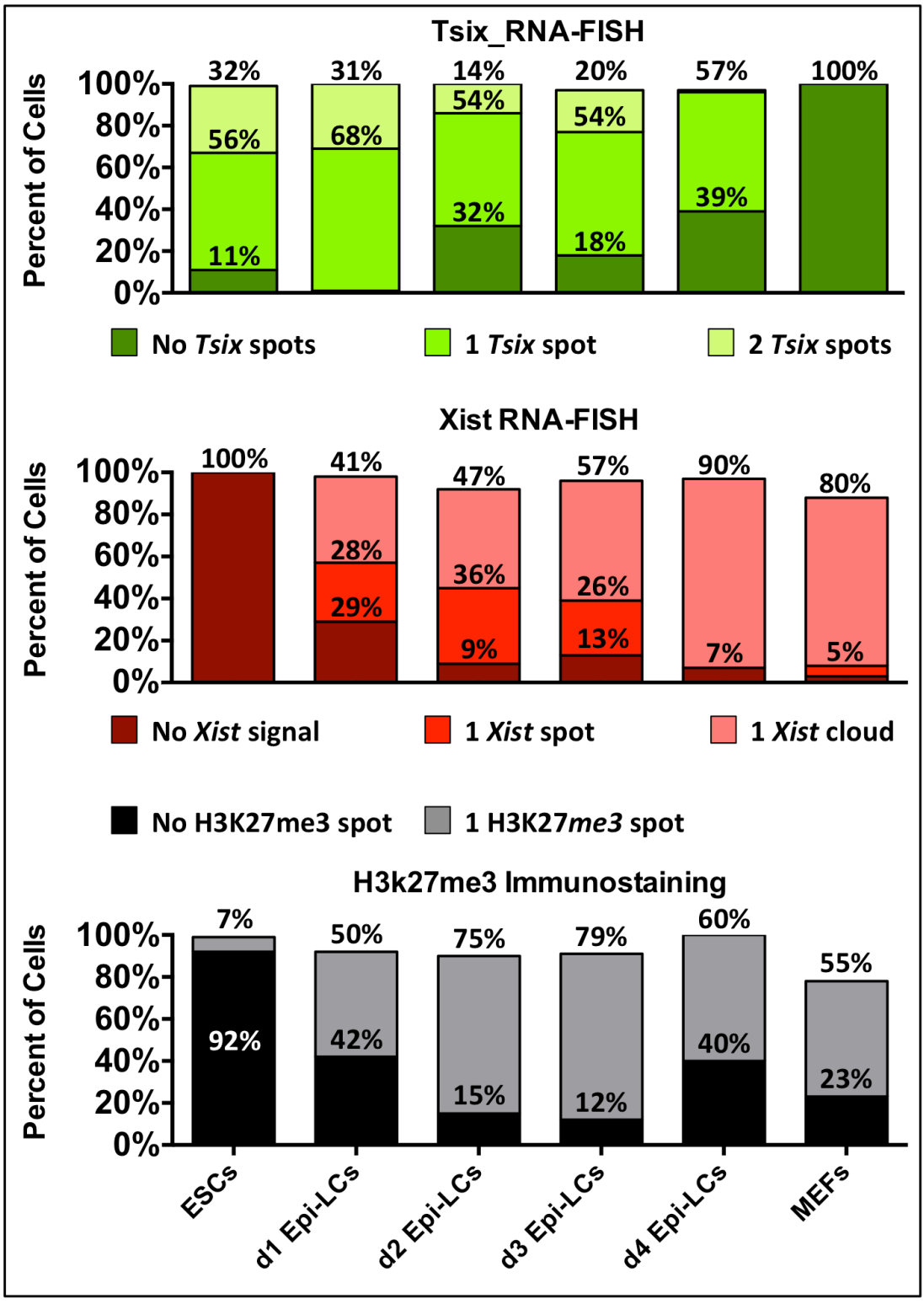
a)
Tsix_RNA-FISH
Percent of Cells
100%
80%
60%
40%
20%
0%
32%
56%
11%
31%
68%
14%
54%
32%
20%
54%
18%
57%
39%
100%
No Tsix spots
1 Tsix spot
2 Tsix spots
b)
Xist RNA-FISH
Percent of Cells
100%
41%
28%
29%
47%
36%
9%
57%
26%
13%
90%
7%
80%
5%
No Xist signal
1 Xist spot
1 Xist cloud
No H3K27me3 spot
1 H3K27me3 spot
c)
H3k27me3 Immunostaining
Percent of Cells
7%
92%
50%
42%
75%
15%
79%
12%
60%
40%
55%
23%
ESCs
d1 Epi-LCs
d2 Epi-LCs
d3 Epi-LCs
d4 Epi-LCs
MEFs

Figure 8: Quantification of X-inactivation onset during Epi-LC differentiation:
a) *Tsix* RNA-FISH quantification for ESCs, day1-4 Epi-LCs, and X-inactive MEFs.
b) *Xist* RNA-FISH quantification for ESCs, day1-4 Epi-LCs, and X-inactive MEFs.
c) H3K27me3 spot quantification for ESCs, day1-4 Epi-LCs, and X-inactive MEFs.

in a previous report, as all cells seem to X-inactivate 24H after cytokine PGC-LC induction based on H3K27me3 staining (Katsuhiko Hayashi et al. 2012). The second

was if the *X-eGFP* reporter drastically underestimated the speed of X-inactivation due to the stability of X-eGFP mRNA or protein in Epi-LCs. If earlier than day 7 Epi-LCs undergo X-inactivation, the chances of successful PGC-LC induction would rise dramatically.

We sampled EL16.7 TST A10 dual color cells from the previous experiment during the first 4 days of Epi-LC differentiation for RNA-FISH and immunofluorescence analysis. In order to see if the *X-eGFP* reporter underestimates the speed of X-inactivation, we compared it against the expression of the master X-inactivator *Xist* lncRNA and its counter regulator *Tsix* by RNA-FISH. We also tracked the progression of X-inactivation H3K27me3 spot by immunofluorescence. **(Fig.8)** After this, the percentages of cells in the population for each of the three markers were quantitated **(Fig.9)**.

The *Tsix* lncRNA is expressed from the active X chromosomes and has biallelic expression in female naïve pluripotent cells, forming two nascent transcription spots. When naïve pluripotent cells undergo differentiation, *Tsix* expression is downregulated leading to *Xist* expression on the X chromosome that is to be inactivated (Lee & Lu 1999)**.**

Indeed, we observed biallelic *Tsix* RNA expression in the starting ESCs, forming two nascent transcription spots, antagonizing the *Xist* lncRNA (**Fig.8a and 9a**). As the Epi-LCs differentiated up to day 3, the *Tsix* signal became dimmer (**Fig.8b-d**), but there was always a fraction of the population that expressed it biallelically (**Fig.9a**). This changed at day 4 of differentiation, in which *Tsix* RNA became monoallelically expressed from

the remaining active X chromosome in the whole population (**Fig.8e and 9a)**.

In somatic cells such as mouse embryonic fibroblasts (MEFs), *Tsix* was not expressed (**Fig.8f and 9a)**.

The *Xist* lncRNA is only highly expressed from the X chromosome chosen for X-inactivation after pluripotent stem cell differentiation. It starts expression as a *Xist* nascent pinpoint, after which the *Xist* RNA expands into a cloud that coats the entire inactivating X chromosome and silences it. At the *Xist* cloud stage, the *Xist*-coated X chromosome is targeted for stable and inheritable X-inactivation in all daughter cells (Payer et al. 2011).

We observed *Xist* lncRNA only at trace levels in naïve ESCs **(Fig. 8a and 9b)**. As the Epi-LCs differentiated, *Xist* transcription increased dramatically. At day 2 of Epi-LC differentiation, virtually all cells showed *Xist* transcription (**Fig.8b-c** and **Fig.9b**). The Epi-LCs still showed sizable fractions of the population with nascent *Xist* transcription spots until day 4 of differentiation (**Fig.8d-e** and **Fig.9b**). However most Epi-LCs at day 4 (**Fig.8e** and **Fig.9b**) displayed *Xist* clouds like stably X-inactivated cells such as MEFs (**Fig.8f** and **Fig.9b**).

The H3K27me3 histone mark is one of the most well known epigenetic signs associated with X-inactivation. It forms a conspicuous spot over the inactivating X chromosome, which can be tracked by immunofluorescence. It is absent in the starting ESCs, but already appears as soon as day 1 of Epi-LC differentiation **(Fig.8b and 9c).** At day 2 of Epi-LC differentiation, virtually all cells display a H3K27me3 X-inactivation spot, and it only becomes more intense until it peaks at day 4 of Epi-LC differentiation **(Fig.8c-e and 9c)**. The MEFs show less conspicuous X-inactivation spots **(Fig.8f and 9c).** The reason is that stably inactivated somatic cells usually display less prominent spots, as other epigenetic marks take over to ensuring an X-inactive state (Payer et al. 2011).

The combined results of *Xist* and H3K27me3 stainings would lead to the conclusion that

day 2 Epi-LCs should be considered fully inactivated. This finding is puzzling. It does not match the results of downregulation of the *X-eGFP* fluorescent reporter, which shows X-inactivation onset at day 4, and its endpoint at day 7.

The X-inactivation in day 2 Epi-LCs is also much higher than the previous *in vitro* report (Katsuhiko Hayashi et al. 2012): **75%** H3K27me3 X-inactive cells **(Fig.9c)** versus the previously reported **20%**.

We concluded that actual X-inactivation likely happened in day 4 Epi-LCs. In day 4 Epi-LCs, biallelic expression of *Tsix* disappears, all cells display a mature *Xist* cloud, and the H3K27me3 spot reaches maximal intensity **(Fig.9a-c)**. This pattern is much

closer to X-inactive somatic cells such as MEFs.

In addition, repetitions of the same experiment by a fellow PhD student in the lab gave the same results (Jacqueline Severino, personal communication).

Further deliberation led us to two major conclusions.

First, we concluded that full X-inactivation in Epi-LCs was more likely to happen after 4 days of Epi-LC differentiation, even if some markers pointed to day 2 X-inactivation.

Second, the relationship between X-linked gene inactivation and the *X-eGFP*, *Xist* and H3K27me3 markers needed to be elucidated. We considered otherwise hard to conclude if the Epi-LCs we used for PGC-LC induction were X-inactive or not.

Benchmarking X-eGFP reporter against the allele-specific expression of X-linked genes

We wished to locate the timepoint during Epi-LC differentiation in which the X-linked genes are inactivated. Our motivations were twofold. First, we wished to perform future cytokine PGC inductions from Epi-LCs that had undergone full genic X-inactivation. This would guarantee inactive PGC-LCs that, after being exposed to somatic gonadal cells or the appropriate signaling candidates, would enable us to study X-reactivation.

Second, we wished to reconcile the diverging results between the X-linked *X-eGFP*

reporter and the *Tsix, Xist* and H3K27me3 reporters. Allele-specific analysis of X-linked genes would allow us to know how genic silencing relates to each of the X-inactivation markers described above.

We decided to probe the allele-specific expression of X-linked genes during the Epi-LC differentiation timeline. We got a set of allele-specific RT-PCR primers tailored to our EL16.7 hybrid cell line SNPs, courtesy from our collaborators in the Jeannie T. Lee lab (Pinter et al. 2015).

We differentiated the EL16.7 TST A10 dual color ESC line into Epi-LCs, and sampled their RNA expression until day 5 of differentiation. We compared their X-linked gene

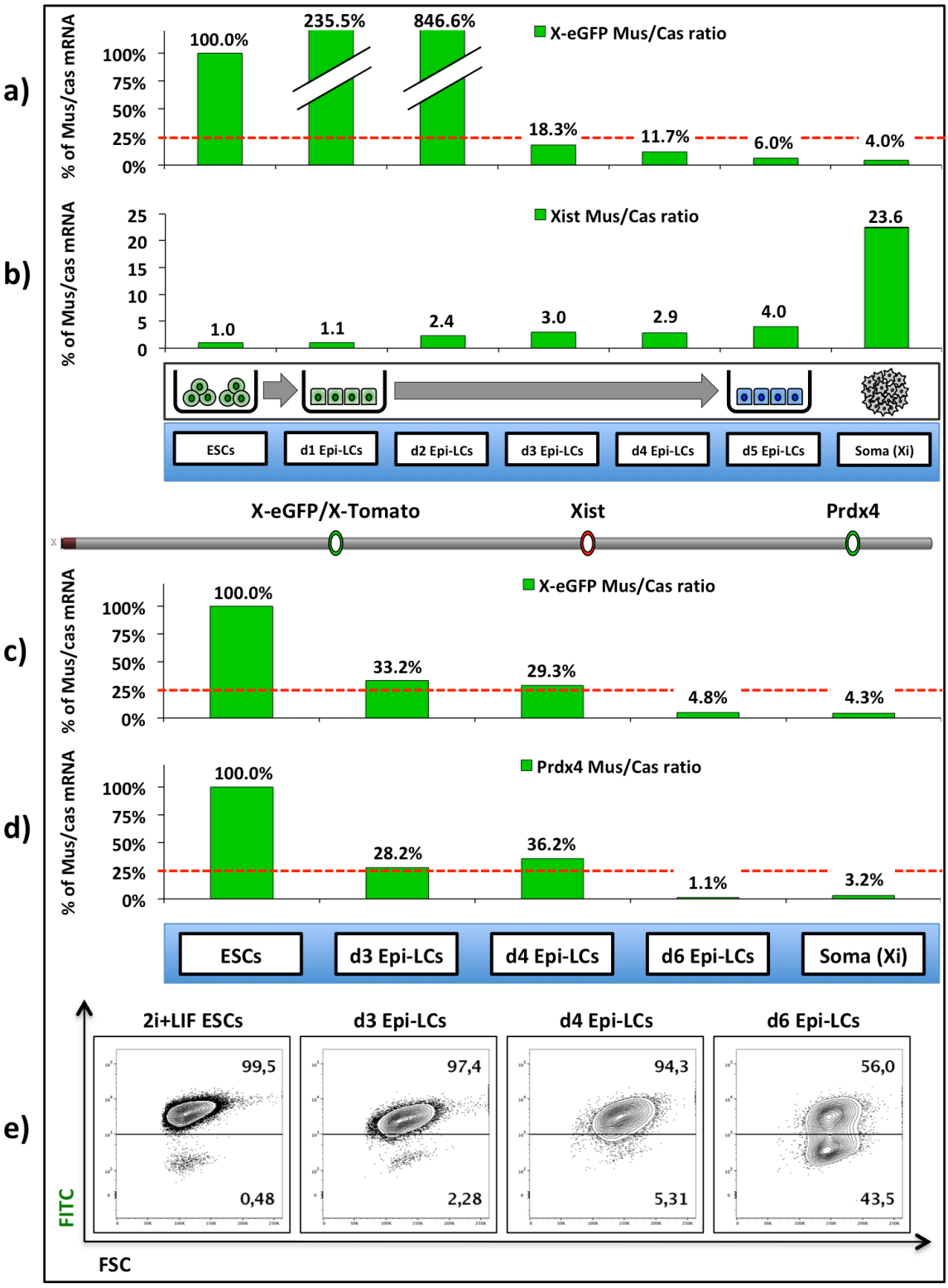
a)
% of Mus/cas mRNA
X-eGFP Mus/Cas ratio
100.0%
235.5%
846.6%
18.3%
11.7%
6.0%
4.0%
b)
Xist Mus/Cas ratio
1.0
1.1
2.4
3.0
2.9
4.0
23.6
ESCs
d1 Epi-LCs
d2 Epi-LCs
d3 Epi-LCs
d4 Epi-LCs
d5 Epi-LCs
Soma (Xi)
X-eGFP/X-Tomato
Xist
Prdx4
c)
X-eGFP Mus/Cas ratio
100.0%
33.2%
29.3%
4.8%
4.3%
d)
Prdx4 Mus/Cas ratio
100.0%
28.2%
36.2%
1.1%
3.2%
ESCs
d3 Epi-LCs
d4 Epi-LCs
d6 Epi-LCs
Soma (Xi)
e)
2i+LIF ESCs
d3 Epi-LCs
d4 Epi-LCs
d6 Epi-LCs
99,5
0,48
97,4
2,28
94,3
5,31
56,0
43,5
FITC
FSC

Figure 9: Allele-specific RT-PCR of X-inactivation during Epi-LC differentiation:

a) Allele-specific expression of the *X-eGFP* reporter by RT-PCR. Naïve ESCs are differentiated to day1-5 Epi-LCs and NPCs. If the value is below 25% (Red bar), the locus is monoallelically expressed and subject to X-inactivation.
b) Allele-specific expression of the *Xist* reporter by RT-PCR. Naïve ESCs are differentiated to day1-5 Epi-LCs and NPCs. If the value is below 25% (Red bar), the locus is monoallelically expressed and subject to X-inactivation.
c) Allele-specific expression of the *X-eGFP* reporter by RT-PCR. Naïve ESCs are differentiated to day3-6 Epi-LCs and NPCs. If the value is below 25% (Red bar), the locus is monoallelically expressed and subject to X-inactivation.
d) Allele-specific expression of the *Prdx4* reporter by RT-PCR. Naïve ESCs are differentiated to day3-6 Epi-LCs and NPCs. If the value is below 25% (Red bar), the locus is monoallelically expressed and subject to X-inactivation.
e) FACs-analysis of the *X-eGFP* reporter protein levels. Naïve ESCs are differentiated to day3-6 Epi-LCs..

expression to their progenitor ESCs and *in vitro* differentiated neuron precursor cells (NPCs) from the same parent ESC line, courtesy of fellow PhD student Moritz Bauer.

The parent naïve ESCs fully express the two alleles for the genes located on their *musculus* and *castaneus* X chromosomes. On the other hand, the *in vitro* NPCs are known to engage in stable X-inactivation (Marks et al. 2015) and only express the allele for the *castaneus* X chromosome, while the *musculus* alleles are silent. This sample also had been checked to be fully X-inactive.

In order to know the state of X-linked gene activity during Epi-LC differentiation, we calculated the fold change expression of the *musculus* alleles for *Xist* and the *X-eGFP* reporter, and divided it by the fold-change expression of the *castaneus*-linked *Xist* and its *X-Tomato* reporter.

The resulting *musculus*/*castaneus* gene expression ratio (*Mus/Cas* ratio) was normalized to the parent naïve ESCs and plotted across the Epi-LC differentiation. We decided to use the *Mus/Cas* expression ratio of NPCs as a positive control for full genic X-inactivation **(Fig.10a and b)**.

The last question was, which *musculus*/*castaneus* ratio should be considered as a sign of genic X-inactivation. Previous reports showed that cells with less than **25%**

musculus/*castaneus* expression ratio **(Fig.10, in red)** to be committed to stable X-inactivation (Deng et al. 2014), and we decided to follow this convention.

The *X-eGFP* transgene was not downregulated during the two first days of Epi-LC differentiation, and was only downregulated at day 3 **(Fig.10a)**. Surprisingly, the X-eGFP transgene was showing genic X-inactivation in day 3 Epi-LCs, and reached comparable levels to X-inactivation NPC control in day 5 Epi-LCs. The X-inactivating *Xist* lncRNA was continuously upregulated, and became conspicuous from day 3 Epi-LCs onwards, even if it did not reach the levels of the NPC X-inactivation controls **(Fig.10b)**.

Our conclusion was that the *X-eGFP* reporter mRNA and protein levels were in severe disagreement. By the *X-eGFP* mRNA expression alone, day 3 Epi-LCs would be considered to undergo genic X-inactivation, which is a sharp contrast to *X-eGFP* fluorescent protein readouts, which would suggest X-inactivation to occur from day 5 onwards.

It was possible that the previous results were particular to the *X-eGFP* reporter locus, and the relationship between *X-eGFP* mRNA levels and its fluorescent protein levels needed to be addressed.

We differentiated again Epi-LCs from the same cell line, and analyzed the allele-specific expression of the X-linked *X-eGFP* **(Fig.10c)** and *Prdx4* **(Fig.10d)** genes. The fluorescent protein levels were monitored by FACs analysis for the same timepoints during Epi-LC differentiation **(Fig.10e).**

The day 3 and 4 Epi-LCs were very close to commit to genic X-inactivation for both *X-eGFP* **(Fig.10c)** and *Prdx4* **(Fig.10d)** genes, but full genic silencing only came at day 6 of Epi-LC differentiation.

While the allele-specific RT-PCR pointed to genic X-inactivation from as early as day 3 Epi-LCs and full silencing at day 6, the *X-eGFP* FACs analysis displayed different results. Even if the *X-eGFP* locus underwent genic inactivation in day 3 and 4 Epi-LCs,

the only display was a mild downregulation of *eGFP* protein levels. When the *X-eGFP* locus had been fully silenced in day 6 Epi-LCs, the FACs analysis inaccurately displayed **56%** of the population as still being X-active **(Fig.10e)**.

Discussion and conclusions

The data above led us to several conclusions.

First, the *X-eGFP* reporter fluorescent protein levels were not an accurate readout of genic X-inactivation, but that its mRNA expression was. The *X-eGFP* behavior is mirrored in the *Prdx4* gene, which is located far away from the *X-eGFP* locus on the X chromosome. This makes the results of allele-specific RT-PCR kinetics very unlikely to be an artifact or an oddity in the genic X-inactivation process. As such, the *X-eGFP* reporter fluorescent protein level is an accurate tool to track the X-active state or X-reactivation process, but has a sizable lag when it comes to track X-inactivation.

Second, the day 3 and 4 Epi-LCs were appropriate timepoints for our main goal: to use gene-inactivated Epi-LCs as the starting material to induce our *in vitro* PGC-LCs. While day 6 Epi-LCs show full X-linked gene silencing, they are far from the optimal timepoint for Epi-LC induction as PGC-LC induction efficiency decreases substantially after day of Epi-LC differentiation (Hayashi & Saitou 2013b; Hayashi et al. 2011b; Hayashi & Saitou 2013c).

Third, the *Xist* and H3K27me3 markers significantly overestimate the degree of X-inactivation in Epi-LCs, and did not provide an accurate reflection on the genic X-inactivation process. In general, relying on H3K27me3 spot alone at the onset of X-inactivation process will lead to an overestimation of the degree of genic X-inactivation. It may be more useful as a marker of the cells who have committed to X-inactivation, but not how far the gene silencing has set in. This was concerning, as previous experimental reports of the X-reactivation phenotype of *ex viv*o PGCs (Chuva De Sousa Lopes et al. 2008) and *in vitro* PGC-LCs (Katsuhiko Hayashi et al. 2012) relied predominantly on the H3K27me3 staining marker. Only few reports so far have directly assessed the expression of X-linked genes, and were performed on *in vivo* PGCs (Sugimoto & Abe 2007; Hu, Peter K. Nicholls, et al. 2015). This was compounded by

the fact that both *ex vivo* (Chuva De Sousa Lopes et al. 2008) and *in vitro* PGC (Katsuhiko Hayashi et al. 2012) reports admitted that the H3K27me3 spot disappearance during X-reactivation experiments hinged on being indistinguishable from the increased H3K27me3 nuclear background staining, and not erasure *per se*. Therefore, we needed to define our own criteria to score Epi-LCs and the resulting *in vitro* PGC-LCs as sufficiently X-inactive before they were used in X-reactivation experiments.

In consideration of all the above, we decided to interpret cells as being committed to genic X-inactivation when the entire population displayed monoallelic or no *Tsix* expression, transition to full *Xist* cloud expression and displayed H3K27me3 spots. For the topic of genic X-inactivation itself, the *musculus/castaneus* ratio needed to be lower than 25% value, as in previous reports (Deng et al. 2014)**.** Multiple X-linked genes needed to display the same result to be taken in consideration. The *X-eGFP* protein levels were considered reliable only as an X-reactivation marker, and any X-inactivation data needed to be confirmed by *X-eGFP* RT-PCR. The *X-eGFP* mRNA levels, on the other hand, were considered a reliable marker of genic X-inactivation.

We suspect that the lag of the *X-eGFP* reporter to track X-inactivation has one main factor The *eGFP* protein has a half-life parameter **(QUOTE)**, and we concluded that it therfore is not a good proxy for the current *X-eGFP* locus transcriptional status for a rough 48H span. Also, even the minute transcription from the *X-eGFP* locus that cells committed for genic X-inactivation still experience might be enough to sustain high enough *eGFP* protein levels, making it underestimate the actual degree of X-linked gene silencing beyond terminal, stable genic X-inactivation.

To conclude, we decided to use X-linked gene inactivation by allele-specific RT-PCR as the benchmark of reliable X-inactivation phenotype. *Xist* or H3K27me3 markers would then be used to confirm any results obtained.

The Epi-LC X-inactivation kinetics showed us that differentiating Epi-LCs for longer times to promote X-inactivation was limited up to day4 Epi-LC culture before

diminishing returns were felt.

In order to maximize the X-inactivation state of our starting *in vitro* PGC-LCs, we decided to explore the second X-inactivation parameter open to us: the relationship between Epi-LC differentiation time and *in vitro* PGC-LC X-inactivation.

Subpopulations of *In vitro* Embryoid body & PGC-LC Inductions avoid X-inactivation in a cytokine-dependent fashion

Motivation

An important feature of the *in vitro* PGC-LC induction protocol is that the input cells are differentiated in a 3D organoid culture system, instead of cultured as a 2D monolayer. The organoid culture system offers an environment closer to the *in vivo* E6.25 to E7.5 epiblast from which PGC-LCs specify. The cells are given a network of cell-to-cell contacts that mimics the tightly packaged epiblast found *in vivo*.

This protocol is remarkably close to one of the main models of the X-inactivation field, the embryoid body differentiation system. In typical embryoid body differentiation protocols, naïve pluripotent stem cells are aggregated in hanging droplets or low-binding cell culture plates without any pluripotency signaling cues to form 3D spheroids (Marks et al. 2015; Ahn & Lee 2010). This instructs the cells to mimic the epiblast differentiation and the formation of the 3 germ layers, reproducing the random X-inactivation dynamics of an *in vivo* epiblast. This process is purportedly fast and a staple protocol to obtain stably X-inactivated cells.

The cytokine-based *in vitro* PGC-LCs system introduces instead Epi-LCs as starting material, and exposes them to BMP4 cytokine to induce PGC-LC fate. In addition, it introduces them to a set of "non-essential cytokines" as Leukemia inhibitory factor (LIF), Stem cell factor (SCF) and epidermal growth factor (EGF), which provide survival and proliferation cues for the newly specified PGC-LCs (Hayashi et al. 2011b; Hayashi & Saitou 2013b; Hayashi & Saitou 2013c).

This cytokine composition posed a potential problem. as BMP4 and LIF have been found to stimulate pluripotent ESC and iPSC lines to a naïve X-active state **(QUOTES)**, and are routinely used to maintain naïve pluripotency in culture (Nichols & Ying 2006a) **(QUOTES)**. In addition, Epiblast Stem cells (EpiSCs), pluripotent stem cell lines that recapitulate the fully X-inactive, differentiated epiblast prior to the specification of the three germ layers, undergo X-reactivation when exposed to BMP4 and LIF signaling molecules (Kime et al. 2016). The LIF and SCF signaling molecules are also key components of EGC derivation, a protocol that converts *in vivo* PGCs to naïve pluripotent Embryonic Germ cells, or EGCs (Durcova-Hills G 2006) **(MORE QUOTES)**. The EGCs have been shown to undergo X-reactivation from X-inactive E8.5 *in vivo* PGC-LCs in one of the two experimental reports on PGC XCR available at that time (Chuva De Sousa Lopes et al. 2008).

Our concern was that the starting Epi-LCs, which are not as locked in their X-inactivation as EpiSCs, could be X-reactivated by LIF and SCF before they could commit to PGC-LC fate. Given the previous report of *in vitro* PGC-LC X-inactivation (K. Hayashi et al. 2012), we assumed that any X-active cells would stem from defects in cell differentiation, and BMP4 to be less likely to produce artifactual X-reactivation. So our goal was to locate a Epi-LC and embryoid body differentiation setup that would ensure a stable X-inactivation on all cells, independently of the cytokines supplied.

Results

In order to test the embryoid body differentiation kinetics and address the impact of cytokines in X-inactivation, we differentiated day 2, 3 and 4 Epi-LCs into embryoid bodies in presence of the LIF, SCF and EGF cytokines. We reasoned that LIF and SCF posed the major threat to induce X-reactivation.

The resulting embryoid bodies were stained for the SSEA1 surface marker after 4 and 6 days of differentiation, allowing us to distinguish between somatic and pluripotent stem cells. The *X-eGFP* reporter would allow us to monitor the progression of X-inactivation and its differences between the two populations. The days 4 and 6 account for the earliest possible timepoint for CD61 and SSEA1 FACs-sorting and the timepoint that

has the higher levels of surface marker for FACs-sorting, respectively (Hayashi et al. 2011b; Hayashi & Saitou 2013b; Hayashi & Saitou 2013c) **(Fig.11)**.

In addition, we sampled the RNA of the starting naïve ESCs, parent Epi-LCs, day 6 embryoid bodies and terminally X-inactivated NPC controls, and queried the allele-specific expression of *X-eGFP* and *Prdx4* X-linked loci. This allowed us to validate any results obtained from X-eGFP FACs analysis.

We presumed that the most likely mechanism in which ectopic X-reactivation or absence of X-inactivation to arise was the appearance of undifferentiated pluripotent stem cells contaminants. (PSC-LCs). If the PSC-LCs are an effect of failed differentiation or lingering pluripotency, it should be expected for them to retain or gain naïve X-active status. In the absence of BMP4 to drive cell differentiation, we assumed this to be the most stringent setup to detect eventual failures in cell differentiation and

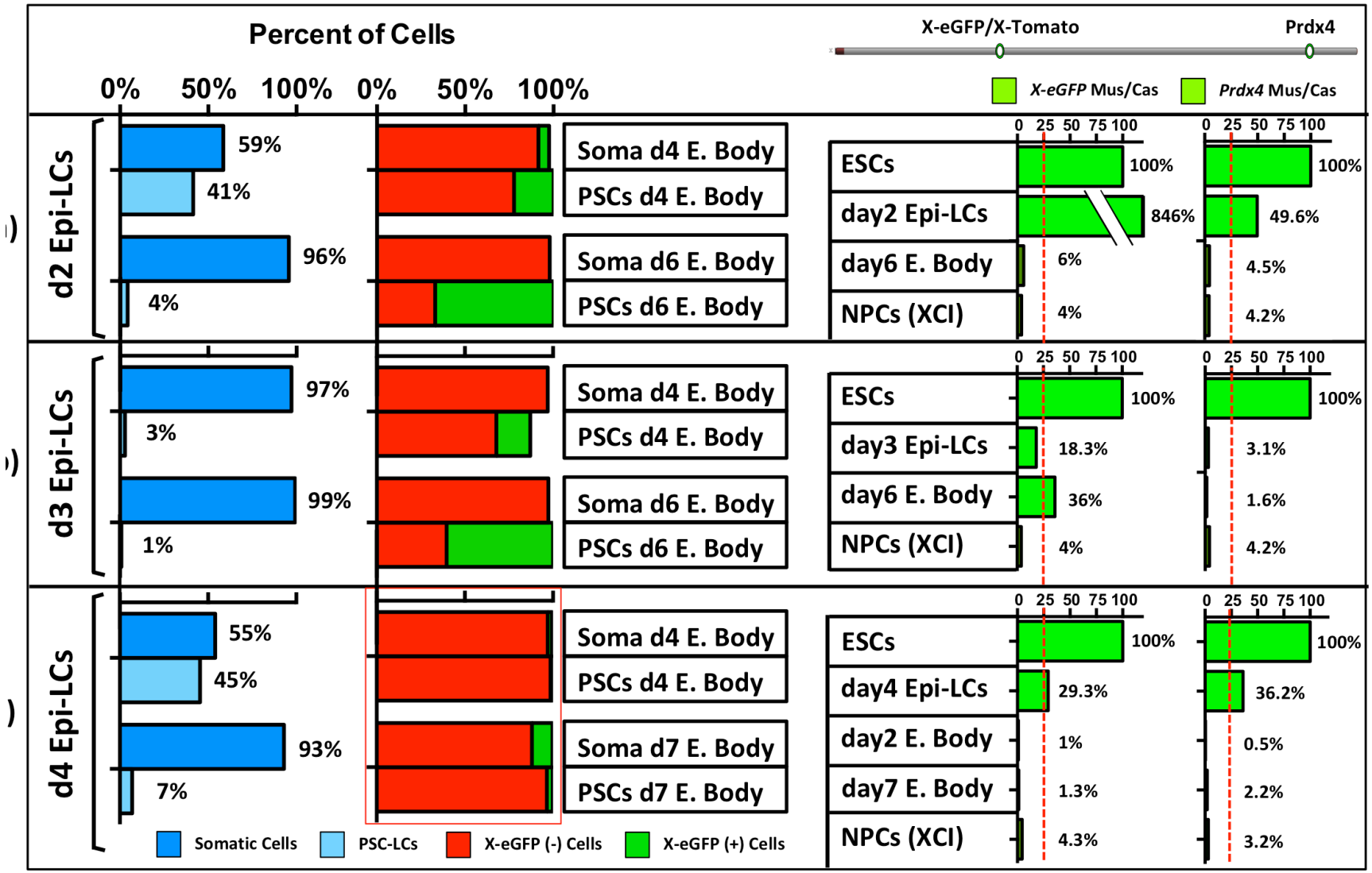
Percent of Cells
0% 50% 100% 0% 50% 100%
X-eGFP/X-Tomato
Prdx4
X-eGFP Mus/Cas
Prdx4 Mus/Cas
d2 Epi-LCs
59%
41%
96%
4%
Soma d4 E. Body
PSCs d4 E. Body
Soma d6 E. Body
PSCs d6 E. Body
ESCs
day2 Epi-LCs
day6 E. Body
NPCs (XCI)
100%
846%
6%
4%
49.6%
4.5%
4.2%
d3 Epi-LCs
97%
3%
99%
1%
Soma d4 E. Body
PSCs d4 E. Body
Soma d6 E. Body
PSCs d6 E. Body
ESCs
day3 Epi-LCs
day6 E. Body
NPCs (XCI)
100%
18.3%
36%
4%
3.1%
1.6%
4.2%
d4 Epi-LCs
55%
45%
93%
7%
Soma d4 E. Body
PSCs d4 E. Body
Soma d7 E. Body
PSCs d7 E. Body
ESCs
day4 Epi-LCs
day2 E. Body
day7 E. Body
NPCs (XCI)
100%
29.3%
1%
1.3%
4.3%
36.2%
0.5%
2.2%
3.2%
Somatic Cells
PSC-LCs
X-eGFP (-) Cells
X-eGFP (+) Cells

Figure 11: Allele-specific RT-PCR of XCI during embryoid Body differentiation:
a) FACs analysis of day 4 and 6 embryoid bodies from day2 Epi-LCs and allele-specific RT-PCR for *X-eGFP* and *Prdx4*.
b) FACs analysis of day 4 and 6 embryoid bodies from day3 Epi-LCs and allele-specific RT-PCR for *X-eGFP* and *Prdx4*.
c) FACs analysis of day 4 and 6 embryoid bodies from day4 Epi-LCs and allele-specific RT-PCR for *X-eGFP* and *Prdx4*.

X-inactivation. If we managed to suppress X-activity and PSC-LC cells in this setup, they should guarantee X-inactive PGC-LCs after cytokine *in vitro* PGC-LC induction.

Effect of non-essential cytokines on a population of X-reactivating PSC-LCs

We did first induce embryoid body from day 2 Epi-LCs, the optimal timepoint for PGC-LC induction (Hayashi & Saitou 2013b; Hayashi & Saitou 2013c) **(Fig.11a)**. After 4 days of embryoid body differentiation, we observed that **59%** of cells had differentiated to somatic fate, while a **41%** of PSC-LCs had not differentiated yet and retained pluripotent characteristics, as evidenced by the SSEA1 surface marker staining.

Out of those populations, somatic cells had **6%** of X-eGFP(+) cells, while the PSC-LCs had **22.3%**.

After 6 days of embryoid body differentiation, most of the PSC-LCs had disappeared, with only a **4%** remaining. When looking at the X-eGFP behavior of somatic cells, the only X-eGFP(+) somatic cells were X0 karyotypic aberrations, below **3%**. The remaining PSC-LCs, on the other hand, showed **67%** of X-eGFP(+) cells, a higher fraction than at day 4.

As we did induce embryoid bodies from day 3 Epi-LCs, we observed a decrease in the number of PSC-LCs, with only **3%** at day 4 and **1%** at day 6 of differentiation **(Fig.11b)**. In addition, virtually all somatic cells were X-eGFP(-) since day 4. The PSC-LCs, however, displayed a similar behavior to the day2 Epi-LC induction, with a **19.3%** of X-eGFP(+) cells at day 4, and **60.3%** at day 6 of embryoid body differentiation.

When we analyzed the allele-specific expression of *X-eGFP* and *Prdx4* loci, we observed that the day 2 and 3 Epi-LCs still maintained X-active state; however, day 6 embryoid bodies scored X-inactivation levels similar to X-inactive NPC controls. We interpreted that 6 days of embryoid body differentiation were sufficient for the immense majority of the cells to reach terminal X-inactivation, regardless of the differentiation time of the starting Epi-LCs. However, this also meant that the bulk of the embryoid body masked the signal of the X-eGFP(+) subpopulations. In order to analyze accurately the allele-specific gene expression during *in vitro* differentiation protocols, the subpopulations would need to be FACs-sorted prior to RNA extraction and interrogated separately.

The observation that PSC-LCs became increasingly X-active from day 4 to 6 of embryoid body differentiation was of particular concern. We concluded that the LIF and SCF cytokines acted to slow down cell differentiation, generating a fraction of cells with pluripotent characteristics, the SSEA1(+) cells (PSC-LCs). This influence could be counteracted to some extent by the differentiation protocol, as the PSC-LCs diminished significantly from day 4 to 6 of embryoid bodies. This would represent that the majority of PSC-LCs were in the process of differentiation and X-inactivation, a fate they will follow with increased differentiation time. However, a minority fraction of those PSC-LCs would not be fated to differentiate or X-inactivate, but to retain and regain naïve pluripotency characteristics, including X-reactivation. This would explain why this fraction of PSC-LCs would increase their X-eGFP(+) cell fraction from day 4 to 6 of embryoid body differentiation.

Effect of day 4 Epiblast-like cells on X-reactivation and early genic X-inactivation

With this in mind, we wished to ask two questions: whether the day 4 Epi-LCs were differentiated enough to preclude the PSC-LC X-reactivation phenomena, and how soon the X-inactivation phenotype arose in the bulk population of the embryoid body. In order to address this, we performed the same experimental setup, but also sampled the day 2 bodies for allele-specific gene expression **(Fig.11c)**.

After 4 days of embryoid body differentiation, we observed a **55%** of somatic and a **45%** of PSC-LCs, as evidenced by the SSEA1 surface marker staining. At day 6 of embryoid body differentiation, only **7%** PSC-LCs remained. The FACs analysis showed that both PSC-LCs and somatic cells had trace X-eGFP expression at day 4, with less than **3%** X-eGFP(+) PSC-LCs. At day 6 of embryoid body differentiation, the PSC-LCs showed an **11.7%** of *X-eGFP*(+) cells, a lower percentage than the ones obtained from day 2 or 3 Epi-LCs differentiation.

When analyzing the allele-specific expression of *X-eGFP* and *Prdx4* loci, we observed that genic X-inactivation happened as early as day 2 of embryoid differentiation, with comparable expression to fully X-inactive NPC controls. This feature was preserved at day 7 of differentiation.

Discussion and conclusions

The above data led us to several conclusions.

First, cytokines in the *in vitro* PGC-LC induction media could prevent or revert the differentiation of a fraction of the starting Epi-LCs, resulting in the formation of PSC-LCs. The majority of the PSC-LCs would eventually differentiate and engage in X-inactivation, albeit after two additional days of embryoid body differentiation. The exception would be a subpopulation of PSC-LCs, which would either keep their starting X-active state, escaping the cell differentiation cues of the protocol, or undergo X-reactivation after suffering exposure to the cytokine signaling. This process happened independently of the starting Epi-LC differentiation day, but was mitigated with increasing Epi-LC differentiation times, with day4 Epi-LCs offering the best results. While we tested the combination of the three "non-essential" cytokines (LIF, SCF and EGF), based on previous reports and literature on Epi-SCs (Kime et al. 2016) and EGCs (Durcova-Hills G 2006; Chuva De Sousa Lopes et al. 2008), we credited the X-activation phenotype to the LIF and SCF cytokines.

Second, the embryoid body differentiation protocol suffices to drive the X-inactivation of the vast majority of cells in similar timespans and conditions to the cytokine *in vitro* PGC-LC differentiation protocol. While some subpopulations may escape X-

inactivation by X-eGFP FACs analysis, the vast majority of the cells in the embryoid body can be driven to full X-inactivation as early as day 2 in the proper conditions.

Third, the embryoid body enhances genic X-inactivation and can drive it even when the starting Epi-LCs have not reached that state. As such, embryoid body differentiation acts as a separate parameter, besides cytokine composition in cell culture media and Epi-LC differentiation time, in determining whether cells will reach genic X-inactivation in embryoid body formation.

Fourth, the genic X-inactivation proceeds faster than indicated by the X-eGFP reporter during FACs analysis, presumably due to the eGFP protein half-life. In the right conditions, genic X-inactivation can happen as early as day2 in embryoid body differentiation.

At last, there are subpopulations in the embryoid body that have a different X-inactivation state that are of critical interest, but too few in numbers to be detected by allele-specific gene expression analysis in the whole embryoid body. The next stages of the project would need to sort the different subpopulations and analyze allele-specific gene expression of as few as 10^3 to 10^4 cells, be it to check proper PGC-LC cell differentiation or to analyze their X-inactivation status prior to experiments.

All of the above lead into a multifactorial model, in which the fraction of PSC-LCs that escapes the differentiation cues and undergoes X-reactivation relies on four factors: cytokine media composition, Epi-LC differentiation days and embryoid body differentiation time. When playing with the two parameters available to us (Epi-LC and embryoid body differentiation time), we identified day 2 to 4 Epi-LCs and days 4 to 7 of embryoid differentiation as the experimental window in which viable embryoid bodies could be produced and the somatic and pluripotent subpopulations distinguished.

While the X-active PSC-LC cells could not be fully eliminated, we identified the use of day 4 Epi-LCs and 7 days embryoid body differentiation time as the optimal setup within those constraints that could reduce them the most.

One of the major problems was to prove whether the progressing X-activity found in the PSC-LCs was X-reactivation from X-inactive Epi-LCs, or a small core of X-active PSC-LCs that resist the Epi-LC, then the embryoid body differentiation and X-inactivation cues that most of their brethren wind up following. The second scenario is partially ruled out by the differentiation of day 2 Epi-LCs. The remaining PSC-LCs after 6 days of differentiation were **60.3%** X-eGFP(+), but accounted only for **4%** of the total cells. This amount of cells is too low to cause the scenario observed after 4 days of differentiation, with a **41%** of PSC-LCs and **19.3%** of them being X-eGFP(+).

The most likely case is that a fraction of PSC-LCs winds up undergoing X-reactivation due to LIF and SCF influence. Proving this with absolute certitude would require to certify that all cells at the onset of embryoid body differentiation were X-inactive, univocally identify the precursors of the PSC-LC lineage, and then track their X chromosome activity across the entire protocol. Given that the SSEA1 FACs analysis marker only becomes distinctive for those PSC-LCs at day 6 of differentiation, and that the X-eGFP marker has a lag of approximately 48H in reporting genic X-inactivation, we did lack the means to perform this experiment. The scope of the analysis (single-cell resolution, distinguishing between PGC-LC and PSC-LC lineage, even when they share the same pluripotency core factors) required excessive development for the benefits it would yield.

We concluded that the only X-active cells identified were PSC-LCs meant that cytokine *in vitro* PGC-LC induction was safe to use, as the PSC-LCs were going to be SSEA1(+), but CD61(-). This meant they could be distinguished from PGC-LCs which are double-positive for SSEA1 and CD61. In addition to the pro-differentiation effects we expected from BMP4 cytokine and extended Epi-LC differentiation time, besides X-eGFP marker sorting, we expected to be able to ensure X-inactive PGC-LCs and overcome the X-reactivation cytokine influence we had observed.

To summarize, we identified with SCF and LIF an X-reactivating signaling influence in the cytokine *in vitro* PGC-LC induction protocol, and found the optimum in the parameters we could manipulate to mitigate it. This X-reactivating signaling matched expectations from literature from *ex vivo* (Chuva De Sousa Lopes et al. 2008) and *in*

vitro (Kime et al. 2016) models. We identified that the different subpopulations in the embryoid body display different behaviors towards X-inactivation or reactivation, and concluded that allele-specific gene expression needs to be assessed separately from each of those separate subpopulations.

With this in mind, we focused on applying RNA extraction protocols that could assess expression from populations as low as 10^3 to 10^4 ranges of cells, which we had obtained for PGC-LC yields and X-active PSC-LCs. We decide to test the range of Epi-LCs and embryoid body differentiation times we identified in the previous experiments, with the intent of identifying the conditions that afforded the best possible yield of X-inactive PGC-LCs for our experiments.

Global Discussion & Conclusions

In this chapter, we set up to adapt the *in vitro* PGC model for X-reactivation research. In order to do so, we first explored the options available in the published literature, both for PGC-LC induction and X-reactivation research. We then focused on finding the setup that allowed us to obtain consistent PGC-LC isolation and X-reactivation readouts with the least need for transgenic cell line generation. This was done in order to cut down on the time investment on crafting cell lines before having a clear answer of the model ability to reproduce *in vivo* dynamics and previous reports. This led us to settle that the use of cytokine PGC-LC induction and the use of CD61 and SSEA1 surface markers was sufficient to obtain and isolate *in vitro* PGC-LCs. While this required significant optimization and had relatively low PGC-LC efficiencies and a high cost per experiment for cytokines, we reasoned that the benefit of being able to use existing female hybrid cell lines with a proven track record for allele-specific X-reactivation research compensated the drawbacks. In addition, our first results with H3K27me3 showed that this approach yielded significant amounts of X-inactive PGC-LCs **(69%)** that efficiently reactivated upon exposure to somatic gonad, and RT-PCR analysis supported that cell differentiation was proceeding adequately across all stages of the protocol. We reasoned that if we could obtain consistently similar amounts of starting

X-inactive PGC-LCs, the cytokine PGC-LC induction system and sorting for CD61 and SSEA1 would be a sufficient setup.

We consequently focused our efforts on hybrid cell lines, TST alleles and X-linked *eGFP* reporters to be able to monitor the X-inactivation and reactivation process at single cell resolution.

When we evaluated the ability of multiple cell lines to track Epiblast-like cell X-inactivation at single-cell resolution with *X-eGFP* reporters, we discovered that the X-inactivation kinetics obtained with the *X-eGFP* reporter were too slow to match known *in vivo* epiblast differentiation, and out of the range in which *in vitro* PGC-LCs could be induced. This led us to compare Epiblast-like cell X-inactivation process with classic markers such as *Tsix, Xist* and H3K27me3 staining against the *X-eGFP* reporter and allele-specific expression of X-linked genes. Surprisingly, all of them diverged from X-linked gene expression in some capacity, with the *Tsix, Xist* and H3K27me3 markers overestimating the degree of X-inactivation, while the X-eGFP reporter fluorescent protein levels underestimating it. We concluded that allele-specific gene expression was the only way to assess complete X-inactivation or reactivation during *in vitro* PGC-LC differentiation. This also meant that the X-inactivation results on *in vitro* PGC-LCs, both in our lab and in the previous report, needed to be reevaluated.

We next wished to know which were the parameters governing X-inactivation during *in vitro* PGC-LC induction, in order to ensure full X-inactivation in all cells. By monitoring the *X-eGFP* reporter and allele-specific expression of X-linked genes during embryoid body differentiation, we saw that the Epiblast-like cells and embryoid body differentiation times interplayed with the cytokines used in PGC-LC induction to control the X-inactivation process. In particular, the non-essential cytokines (LIF, SCF and EGF) used to drive proliferation of *in vitro* PGC-LCs sustained a population of pluripotent-stem-cell like cells (PSC-LCs) that underwent or maintained X-reactivation, even if the vast majority of cells underwent genic X-inactivation as early as two days of

embryoid body differentiation.

While the effect of non-essential cytokines could not be fully denied, it was mitigated with increasing amounts of Epiblast-like cell differentiation time, with day 4 Epi-LCs reducing the X-reactivation phenomena to a minimum, and within PGC induction-compatible boundaries.

We interpreted these results on X-reactivation of PSC-LCs as an artifact caused by properly un-differentiated Epi-LCs reverting to a pluripotent state. Indeed, this population is reported to appear during cytokine PGC-LC differentiation (Hayashi et al. 2011b; Hayashi & Saitou 2013a; Hayashi & Saitou 2013c), but no analysis of its X-activity state has been performed to date. Still, the fact that it was X-active coincided with our expectations of a pluripotent stem cell regaining a naïve state. At this stage, we interpreted that PGC-LCs, having undergone a differentiation procedure, should be exempt from this dynamic. We also expected that the BMP4 cytokine, the master signaling activity behind PGC specification *in vivo* and *in vitro,* would shift the signaling balance of the media towards cell differentiation and X-inactivation in future cytokine *in vitro* PGC-LC differentiations.

With the experiments of this chapter, we concluded that we had established a sufficient pool of readout techniques to accurately monitor the X-inactivation and reactivation during *in vitro* PGC-LC differentiation. In addition, our setup used a hybrid cell line with a TST allele and an *X-eGFP* reporter linked to it, including all the optimal resources currently available to monitor X-reactivation.

With our ability to achieve cytokine PGC-LC induction on hybrid cell lines and the CD61 and SSEA1 sorting of PGC-LCs, we thought that we had established a viable *in vitro* model for PGC X-reactivation research.

At this stage, there still remained a couple of pressing concerns.

The existence of different subpopulations with heterogeneous X-activity meant that it was necessary to sort the separate soma, PSC-LCs and germ cell populations, separate

the X-inactive and X-active subpopulations through the live X-eGFP reporter, and then perform allele-specific gene expression analysis for each of them. Given the relatively minute size of those populations, we needed to be able to extract sizable amounts of RNA from populations as small as 10^4 cells. Our RNA extraction protocols at the time were not able to perform satisfactorily in those circumstances to allow gene expression analysis without amplification-based methods.

The second limitation was the relatively low yield that we would obtain per PGC induction, with an estimated maximum of 10^5 PGC-LCs per cytokine induction at a sustainable budget. This, combined with the requirements for signaling molecule testing, meant that we needed to guarantee PGC-LC sorting efficiencies of **10%**, while ensuring the entirety of PGC-LCs were X-inactive. This was also very likely to constrain us to *X-eGFP* and allele-specific gene expression analysis, with occasional upscaling of the experiments when a particular analytic technique warranted it.

While the insertion of the transcription-factor based PGC-LC induction cassette and the rTTa transgene would have allowed us to increase the PGC induction efficiency, we chose to focus on exploiting the current model as it was, as we had not gathered enough data yet about *in vitro* PGC-LC X-inactivation and reactivation state.

The third issue we encountered was that the kinetics of X-inactivation of *in vitro* Epi-LCs was very different from the reports from *in vivo* Epiblasts (Deng et al. 2014; Mohammed et al. 2017; Borensztein, Syx, et al. 2017; Borensztein, Okamoto, et al. 2017). The original reports of *in vivo* epiblast differentiation were based on H3K27me3 and *Xist* markers, and they reported X-inactivation in 48H, from E4.5 to the E6.5 epiblast **(QUOTE)**. Later reports performed allele-specific analysis reported gene X-inactivation in an even shorter span of a single day, from E5.5-E6.5 (Mohammed et al. 2017). The fact that *in vitro* Epi-LC X-inactivation kinetics were delayed in respect to this, forced us to define experimentally the optimal span of Epi-LC differentiation as the minimal amount able to yield *bona fide* PGCs and full X-inactivation during embryoid body differentiation without compromising PGC-LC differentiation efficiency.

With these constraints in mind, we focused on using cytokine PGC-LC induction with

the EL16.7 TST Dual Color line as a model for X-reactivation in PGCs, optimizing all analytic techniques to perform optimally in PGC-LCs, and to analyze its X-inactivation and reactivation phenotypes.

Chapter 2: XCR of *in Vitro* PGC-LCs from an X-inactive state

Introduction:

By monitoring activity of the X-linked eGFP transgene, we previously found that female Epi-LCs could support full X Chromosome Inactivation (XCI) upon Embryoid body formation from day 2 (48H) of epiblast fate induction, even if Epi-LC cells only acquire full XCI after day 7 (168H) of cell culture.

We also concluded that X-linked gene inactivation is partly unlinked from the classic microscopy markers H3K27me3 X-linked spot & *Xist*-lncRNA cloud, as X-active Epi-LC cells were fully showing presence of those XCI markers. The use of *in vitro* PGCs as a model for X-reactivation requires to identify an Epi-LC induction timepoint that optimizes the yield of PGC-LCs while ensuring the maximal degree of XCI. In order to consider, which timepoints of Epi-LC induction to test, we accounted that previous reports of maximal Epi-LC similarity to *in vivo* epiblast transcriptomes after 48H induction **(QUOTE)** and that *In vitro* PGC induction efficiency decreases after a 36-48H of Epi-LC induction (Hayashi et al. 2011a; Katsuhiko Hayashi et al. 2012).

Given that the *in vitro* PGC induction protocol involves an embryoid body formation step, and that virtually all induced female PGC-LCs bear a H3K27me3 spot (Katsuhiko Hayashi et al. 2012) we concluded that obtaining of fully X-inactivated PGC-LCs from day 2 Epi-LCs was possible.

We decided to screen an interval of 48H (day 2) to 96H (day 4) of Epi-LC Induction,

from the theoretical optimum for PGC-LC induction efficiency (day 2 Epi-LCs) to the first timepoint during Epi-LC induction in which we observed genic inactivation (day 4 Epi-LCs).

Results:

Screening of Epi-LCs & Sorted PGC-LCs XCI points to cytokine-driven XCR

We performed a screening by inducing PGC-LCs from 48H (day 2)**(FIG.1a)**, 72H (day 3)(**FIG.2b)** & 96H (day 4)**(FIG.2c)**, and culturing them for 7 days, before FACs-sorting

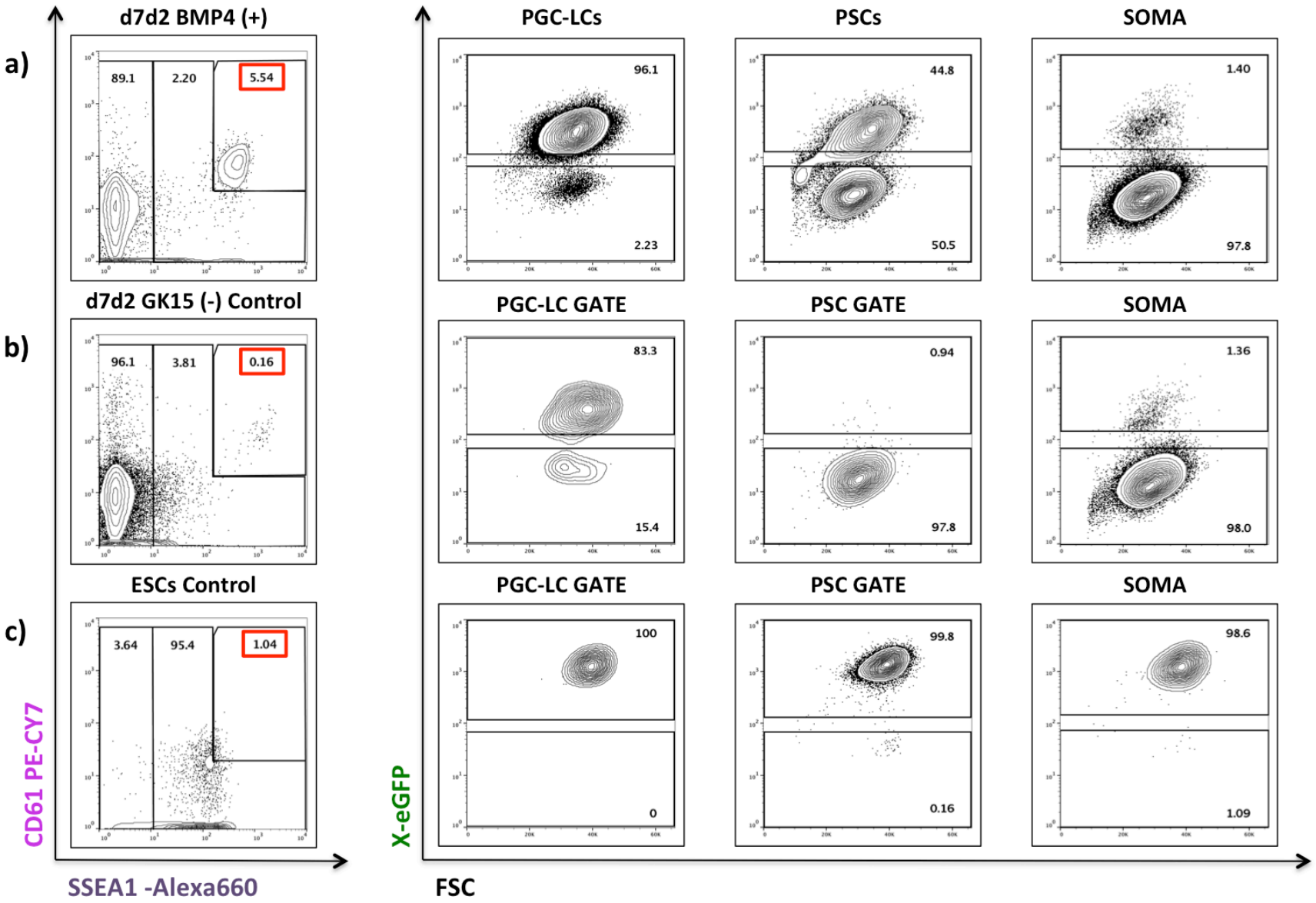
a)
b)
c)
d7d2 BMP4 (+)
d7d2 GK15 (-) Control
ESCs Control
89.1
2.20
5.54
96.1
3.81
0.16
3.64
95.4
1.04
PGC-LCs
PSCs
SOMA
96.1
2.23
44.8
50.5
1.40
97.8
PGC-LC GATE
PSC GATE
SOMA
83.3
15.4
0.94
97.8
1.36
98.0
PGC-LC GATE
PSC GATE
SOMA
100
0
99.8
0.16
98.6
1.09
CD61 PE-CY7
SSEA1 -Alexa660
X-eGFP
FSC

Figure 1: Female *In vitro* PGC-LC-specific X-activity after 7 days of Culture in cytokine PGC Induction media:

a) *In vitro* PGC-LCs are induced from day 2 Epi-LCs, and the induction FACs-analyzed after 7 days of culture in PGC Induction media for the X-activity status of cells depending on their cell fate.
b) Embryoid bodies are formed from the same day 2 Epi-LC precursors, in GK15 base media without PGC induction cytokines, and FACs-analyzed after 7 days of culture in PGC Induction media for the X-activity status of cells depending on their cell fate.
c) The original ES progenitor cells used for Epi-Lc induction are expanded, an analyzed simultaneously to PGC Inductions and Embryoid bodies to exclude ES-like undifferentiated cells and as a X-active control.

the different subpopulations for RT-PCR analysis. For comparison, embryoid bodies from the same Epi-LC precursor cells, but lacking the cytokines required for PGC induction in their media (GK15 embryoid bodies), were induced simultaneously for each timepoint assayed, in order to act as a negative control **(FIG.2b, FIG.3c)**.

A sample of naïve pluripotent stem cells of the same clone used for the *in vitro* PGC induction were run in parallel, to compare against a naïve X-active control and discriminate against any escaped undifferentiated cells, so that there is no possible confusion of PGC-LCs and escaped PSCs **(FIG.1c).**

We started by assessing the PGC-LC X Chromosome status from day 2 Epi-LCs, the optimal PGC induction timepoint **(FIG.1a)**. After sorting, we observed that for all Epi-LCs conditions tested, we would obtain a sizable majority of X-eGFP(+), X-active PGC-LCs. Notably, only the PGC-LCs, as defined by the population defined both by CD61(+) & SSEA1(+) surface markers, showed sizable X-activity (98% of the PGC-LC population). Both the somatic cells (Soma), defined by their absence of SSEA1 surface marker signal (SSEA1(-)) and undifferentiated remnants of Pluripotent Stem Cells (PSCs), defined by the presence of single surface marker SSEA1 (SSEA1(+)), showed only trace percentages of X-active cells. Somatic lineages (SSEA1(-)) are expected to proceed with their X-inactivation towards locked X-inactivation, as *in vivo* **(QUOTE)**.

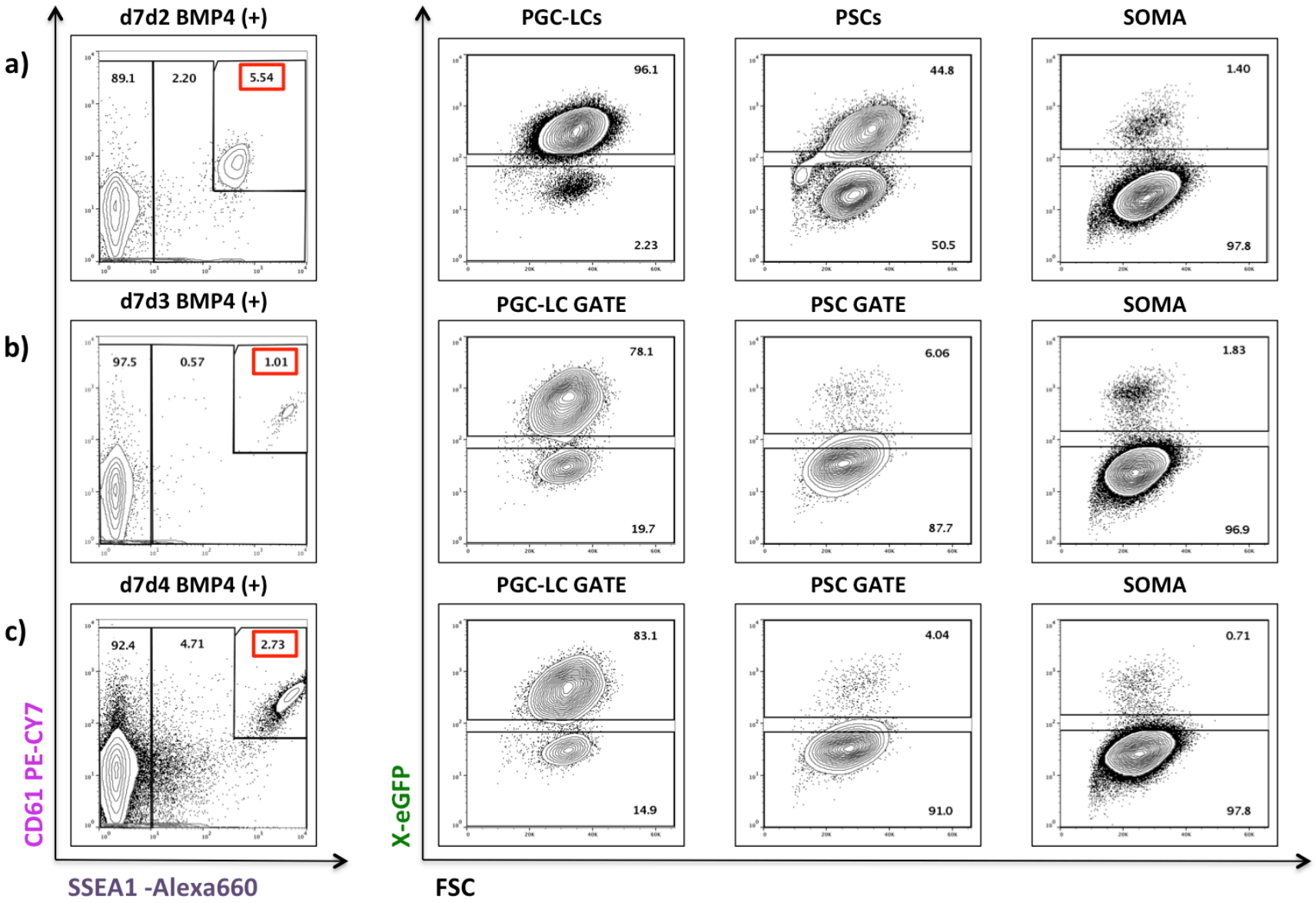
a)
b)
c)
d7d2 BMP4 (+)
d7d3 BMP4 (+)
d7d4 BMP4 (+)
89.1
2.20
5.54
97.5
0.57
1.01
92.4
4.71
2.73
PGC-LCs
PSCs
SOMA
96.1
2.23
44.8
50.5
1.40
97.8
PGC-LC GATE
PSC GATE
SOMA
78.1
19.7
6.06
87.7
1.83
96.9
PGC-LC GATE
PSC GATE
SOMA
83.1
14.9
4.04
91.0
0.71
97.8
CD61 PE-CY7
SSEA1 -Alexa660
X-eGFP
FSC

Figure 2: Longer Epi-LC differentiation mitigates partially *In vitro* PGC-LC X-active phenotype at expense of yield:

a) *In vitro* PGC-LCs are induced from day 2 Epi-LCs, and the induction FACs-analyzed after 7 days of culture in PGC Induction media for the X-activity status of cells depending on their cell fate.

b) *In vitro* PGC-LCs are induced from day 3 Epi-LCs, and the induction FACs-analyzed after 7 days of culture in PGC Induction media for the X-activity status of cells depending on their cell fate. X-activity and PGC-LC yield drop.

c) *In vitro* PGC-LCs are induced from day 4 Epi-LCs, and the induction FACs-analyzed after 7 days of culture in PGC Induction media for the X-activity status of cells depending on their cell fate. X-activity and PGC-LC yield drop.

In the meantime, the fact that PSC contaminants were a small fraction of the population and mostly X-inactive confirms that the *in vitro* PGC induction protocol supplies the adequate cues for all cells within the embryoid body to complete cell differentiation, and that the X-active phenotype was not an artifact due to incomplete differentiation, but was specific to the PGC-LC fate.

It is of note that the aggregation into embryoid bodies without PGC-induction cues resulted in the induction of trace amounts of CD61(+), SSEA1(+) cells with a surface marker signature congruent with PGC-LCs for all timepoints assayed **(FIG.1b)**.

As such, the germ cell induction efficiency with BMP4 can be measured as multiples of the random germ cell differentiation rate from the negative control.

This is expected given previous reports on how random embryoid body differentiation protocols can give yield to trace amounts of germ cells, but those cells are known to be unable to give rise to fertile offspring (Geijsen et al. 2004). In the negative control, randomly-differentiated germ cells are characterized by having lower X-EGFP(+) fraction than in the *in vitro* PGC-LCs, suggesting the cytokine *in vitro* PGC induction protocol might be linked to a PGC-specific X-activity phenotype.

A previous report had shown that virtually all cytokine-induced *in vitro* female PGC-LCs showed a H3K27me3 X-linked spot, and supposedly X-inactivation status, unless

they were exposed to female gonadal somatic cells (Katsuhiko Hayashi et al. 2012). As such, the fact that our *in vitro* PGC-LCs were predominantly X-active **(FIG.1b)**, as indicated by our X-linked eGFP marker, we interpreted as an artifact, one that required optimization of PGC induction parameters.

We considered that the lack of PGC-LC X-inactive cells was caused by insufficient X-inactivation marks on the starting Epi-LC material. We had previously observed that the levels of the inactivation markers H3K27me3 X-linked spot & *Xist*-lncRNA cloud were drastically enriched during day 3 of Epi-LC culture, peaking with gene inactivation at day 4. This led us to assume that PGC induction from day 3 or 4 Epi-LC precursor cell material would lead to X-inactive PGC-LCs.

When we increased the Epi-LC differentiation time to 72H (day 3)(**FIG.2b)** & 96H (day4)**(Fig.2c)**, we observed a decrease of PGC-LC induction efficiency from its day 2 optimum of 5.77%**(Fig.2a)**. However, we observed that the PGC-LCs derived from both day 3 & day 4 Epi-LCs had a similar percentage of X-active cells (87-73%). While the increase of X-inactive cells from 2% to a 19.5% is an improvement, this comes with a concomitant decrease of PGC-LC induction efficiency from 5.44% to a meager 0.7% **(Fig.2b&c)**, close to the spontaneous germ cell induction rates found in negative controls **(Fig.3)**. The lowered PGC induction efficiency at those later timepoints (10^3 cells range) only opens the possibility of descriptive insights on the process of X-reactivation (XCR) by RNA-seq, but not analysis of its epigenetic determinants by

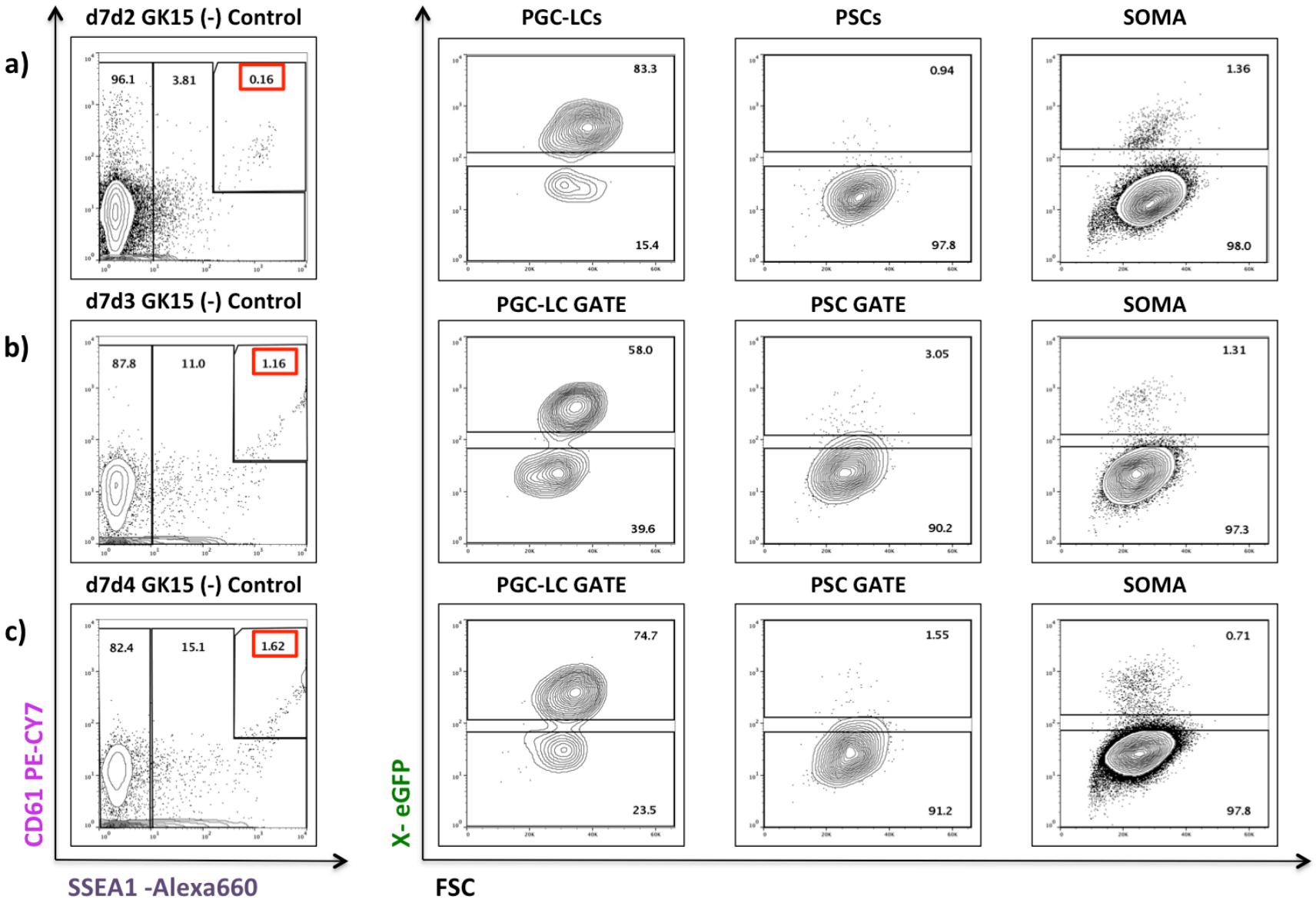
a)
b)
c)
d7d2 GK15 (-) Control
d7d3 GK15 (-) Control
d7d4 GK15 (-) Control
96.1
3.81
0.16
87.8
11.0
1.16
82.4
15.1
1.62
CD61 PE-CY7
SSEA1 -Alexa660
PGC-LCs
PSCs
SOMA
PGC-LC GATE
PSC GATE
SOMA
PGC-LC GATE
PSC GATE
SOMA
83.3
15.4
0.94
97.8
1.36
98.0
58.0
39.6
3.05
90.2
1.31
97.3
74.7
23.5
1.55
91.2
0.71
97.8
X- eGFP
FSC

Figure 3: Embryoid body negative controls show low random PGC-LC specification and different X-activity status after 7 days of Culture in in base GK15 cell culture media :

a) Embryoid bodies are induced from day 2 Epi-LCs, and the induction FACs-analyzed after 7 days of culture in base GK15 cell culture media for the X-activity status of cells depending on their cell fate.
b) Embryoid bodies are induced from day 3 Epi-LCs, and the induction FACs-analyzed after 7 days of culture in base GK15 cell culture media for the X-activity status of cells depending on their cell fate.
c) Embryoid bodies are induced from day 4 Epi-LCs, and the induction FACs-analyzed after 7 days of culture in base GK15 cell culture media for the X-activity status of cells depending on their cell fate.

ChIP-Seq, or its mechanistic analysis by experimental perturbation of the system, which require far larger amount of cells (10^5-10^6 cells).

The presence of X-active PGC-LCs was surprising, and seemingly conflicted with previous reports of X-inactivation marks in PGC-LCs (Katsuhiko Hayashi et al. 2012), as well as multiple reports on the X-reactivation of PGCs *in vivo* entirely relying on contact with a soluble ligand produced by the E10.5-11.5 sexually differentiating gonad in order to reactivate the X Chromosome (Chuva De Sousa Lopes et al. 2008; Hu, Peter K. Nicholls, et al. 2015; Sugimoto & Abe 2007)**.** Such a contradiction to previous reports demanded an explanation.

One possibility was that the sorted PGC-LCs were actually pluripotent stem cells, which underwent only partial differentiation, and reverted to a naïve (X-active) pluripotent status upon the addition of the cytokines used for PGC-LC induction. As we Showed in the previous chapter, the non-essential cytokines (SCF, EGF & LIF) intended to drive the proliferation of PGC-LCs are able to promote an X-active population during embryoid body differentiation, and both main cytokines used during PGC-LC induction (BMP4 & LIF) have been previously reported to be able to drive efficiently X chromosome reactivation by converting primed pluripotent Epiblast Stem Cells to naïve pluripotent ESCs at concentrations 10-fold times lower than the ones used for PGC-LC induction, and in similar timeframes (Kime et al. 2016).

In order to interrogate this possibility, precursor ESCs, Epi-LCs, somatic cells and PGC-LCs both X-eGFP(+) & (-) were sorted and gene expression assayed by RT-PCR **(Fig.4)**. While it is complex to discriminate naïve pluripotent stem cells from primordial germ cells, as both are defined by the expression of a largely overlapping core of naïve pluripotency factors, the PGC-LCs should show expression of differentiation factors such as *Blimp1* & *AP2-gamma,* which are absent in the un-differentiated ESCs, a reduction of the *Klf4* naïve pluripotency factor, hallmark of the inner cell mass (ICM)(Hayashi et al. 2011a), and the expression of novel characterized differential markers as *Dnd1* **(QUOTE)**. The soma population of the embryoid body would show absence of expression of all those genes.

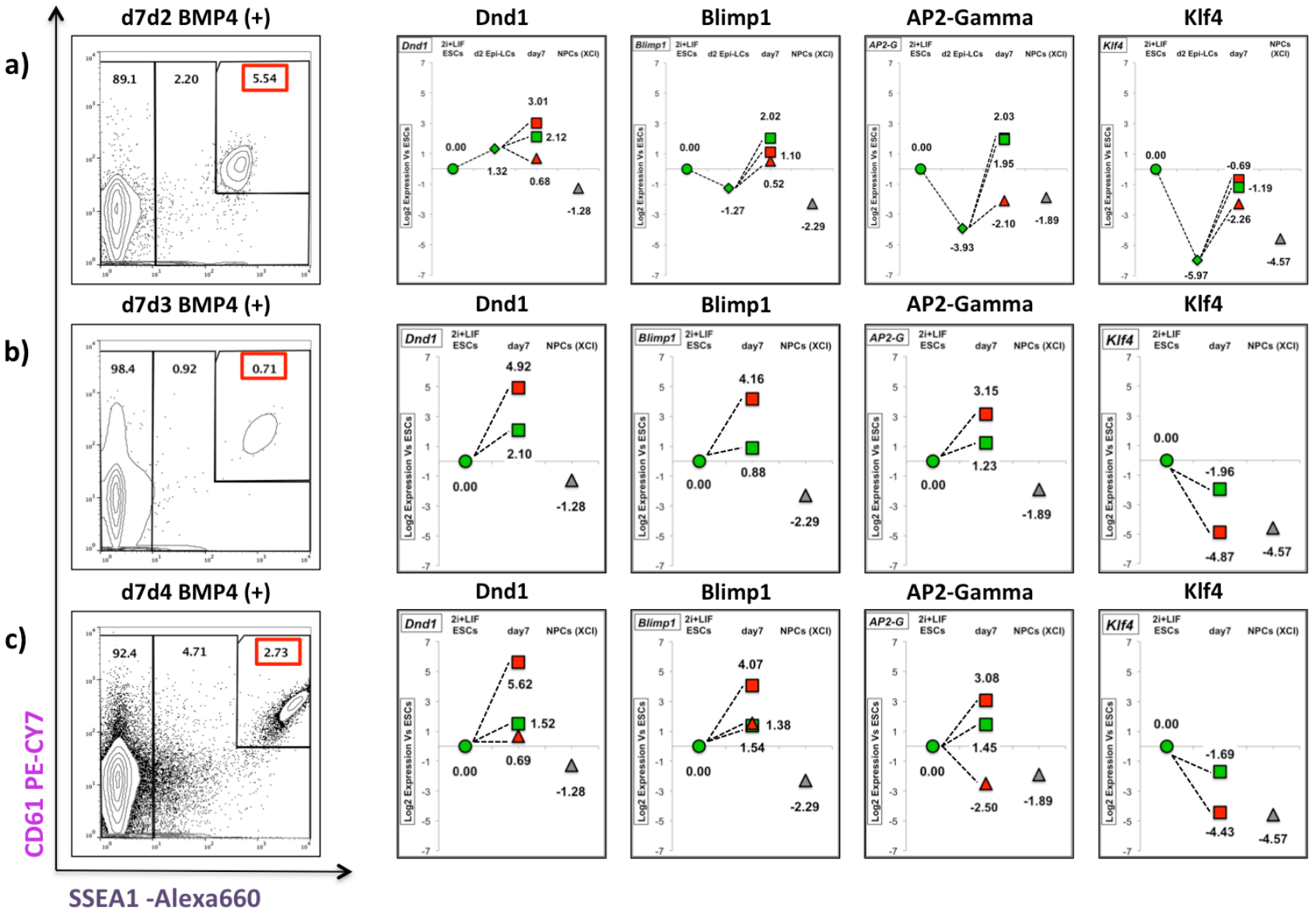
a)
b)
c)
d7d2 BMP4 (+)
d7d3 BMP4 (+)
d7d4 BMP4 (+)
89.1
2.20
5.54
98.4
0.92
0.71
92.4
4.71
2.73
CD61 PE-CY7
SSEA1 -Alexa660
Dnd1
Blimp1
AP2-Gamma
Klf4
2i+LIF ESCs
d2 Epi-LCs
day7
NPCs (XCI)
Log2 Expression Vs ESCs
0.00
3.01
2.12
1.32
0.68
-1.28
2.02
1.10
0.52
-1.27
-2.29
2.03
1.95
-2.10
-1.89
-3.93
-0.69
-1.19
-2.26
-5.97
-4.57
4.92
2.10
4.16
0.88
3.15
1.23
-1.96
-4.87
5.62
1.52
0.69
4.07
1.38
1.54
3.08
1.45
-2.50
-1.69
-4.43

Figure 4: Female *In vitro* PGC-LC inductions are analyzed for PGC-fate gene expression based on X-activity status and cell type subpopulation after 7 days of Culture in cytokine PGC Induction media:

a) *In vitro* PGC-LCs are induced from day 2 Epi-LCs, and the ESCs, Epi-LC, as well as the PGC & Soma cell populations are FACs-sorted after 7 days of culture in PGC Induction media. The impact of X-activity and cell population in PGC-marker and cell-differentiation marker gene expression are assayed by RT-PCR.

b) *In vitro* PGC-LCs are induced from day 3 Epi-LCs, and the ESCs, as well as the PGC & Soma cell populations are FACs-sorted after 7 days of culture in PGC Induction media. The impact of X-activity and cell population in PGC-marker and cell-differentiation marker gene expression are assayed by RT-PCR.

c) *In vitro* PGC-LCs are induced from day 4 Epi-LCs, and the ESCs, as well as the PGC & Soma cell populations are FACs-sorted after 7 days of culture in PGC Induction media. The impact of X-activity and cell population in PGC-marker and cell-differentiation marker gene expression are assayed by RT-PCR.

We tracked the gene expression from ES cells to Epi-LC and PGC-LC stages, and compared the behavior of germ cell differentiation markers (*Blimp1* & *AP2-Gamma*), naïve differentiation markers (*Klf4*) & pre-meiotic germ cell enriched genes (*Dnd1*) in PGC inductions from day 2, 3 & 4 Epi-LCs. The gene expression levels were normalized to the levels of the starting ES cells used for the PGC Induction protocol.

The gene expression of *in vitro*-derived neural precursor cells (NPCs) differentiated from the same ES cell line was monitored as negative control for germ cell marker genes and positive control for full X-chromosome inactivation **(QUOTE)**.**(FIG.4)**

We observed that PGC-LCs induced from day 2 Epi-LCs displayed mild upregulation of the differentiation factors *Blimp1* & *AP2-Gamma*, a poor downregulation of naïve pluripotency factor *Klf4* in comparison from the precursor ESC levels, and upregulation of the pre-meiotic *Dnd1* gene marker. The Epi-LC differentiation was deemed adequate, as shown by the steep downregulation of naïve pluripotency marker *Klf4* from its ESCs precursors, but the PGC-LCs regained *Klf4* expression levels closer to naïve ESCs after induction **(FIG.4a)**.

The moderate up-regulation of differentiation and pre-meiotic genes, in conjunction

with the moderate up-regulation of the surface markers CD61 & SSEA1, led us to conclude a legitimate, but suboptimal differentiation towards PGC fate.

When induced from day 3 **(FIG.4b)** & 4 Epi-LCs **(FIG.4c)**, the PGC induction efficiency dropped. We noticed however a concomitant increase in CD61 & SSEA1 surface marker signal intensity, more similar to *in vivo* PGC levels. The combination of higher expression of differentiation & pre-meiotic genes alongside the higher downregulation of naïve pluripotency marker *Klf4* made us conclude that a higher degree of germ cell differentiation and quality happened from the differentiation of PGC-LCs from day 3 & 4 Epi-LC materials.

Another observation was that systematically, eGFP(-), X-inactive PGC-LC cells showed more pre-meiotic & germ cell differentiation gene expression, as well as naïve ESC cell marker expression, than their X-active counterparts **(FIG.4b-c)**.

While a sizable proportion (11-19.5%) of X-inactive germ cells could be established, the question of why X-active cells could arise from Epi-LC populations at timepoints suggested to be X-inactive remained. Moreover, given the low yield of X-inactive PGC-LCs (range of 10^3 cells), it was important to understand this phenomenon in order to improve the X-inactive PGC-LC yield, as approaches to study X-reactivation needed at least 10-100 fold higher supply of X-inactive PGC-LCs.

The first possibility was for the actual X-activity to be an artifact of the *X-eGFP* reporter transgene, an effect of the eGFP protein long half-life, or for the X-activity to be an artifact circumscribed to a single genic locus. Another possibility was selective loss of the X-tomato marked *castaneus* chromosome in all cells. This would lead to a X0 phenotype, and the only cells able of survive would be those able to undo their X-inactivation on the *eGFP*-marked *musculus* X-chromosome. High X-loss during *in vitro* PGC-LC derivation has been previously reported **(QUOTE)**.

In order to assess the possibility of X-chromosome loss, we analyzed by FACs and RT-PCR the expression of the *eGFP* fluorescent reporter located on the X-inactivation primed *musculus* X-chromosome, as well as the expression of its *td-tomato* counterpart

on the X-active *castaneus* counterpart, in all previous PGC-LC inductions from day 2, 3 & 4 Epi-LCs **(FIG.5)**. We observed that virtually all somatic and PGC-LC cells had X-tomato signal, both at the protein level (as assessed by FACs) and at the RNA level (as assessed by RT-PCR). Moreover, we observed that the expression balance between *eGFP* & *td-tomato* reporters, which have a targeted insertion within the same region at the *Hprt* gene locus in the two different chromosomes, is exactly the same in PGC-LCs as the one found in the starting naïve ESCs – the prototypical cells known for having naïve X-activity **(FIG.5b)**. Moreover, we observed that, no matter the starting Epi-LC differentiation time (including *bona fide* gene-silenced day 4 Epi-LCs), we would always obtain ES cell-like levels of naïve, complete X-activity. The X-eGFP(-) cells, on the other hand, would remain fully X-inactive. While this observation speaks strongly against an X0 phenotype scenario, the X-activity of the *eGFP* reporter could be a localized event, which may not be representative of all genes located in the span of the X-chromosome.

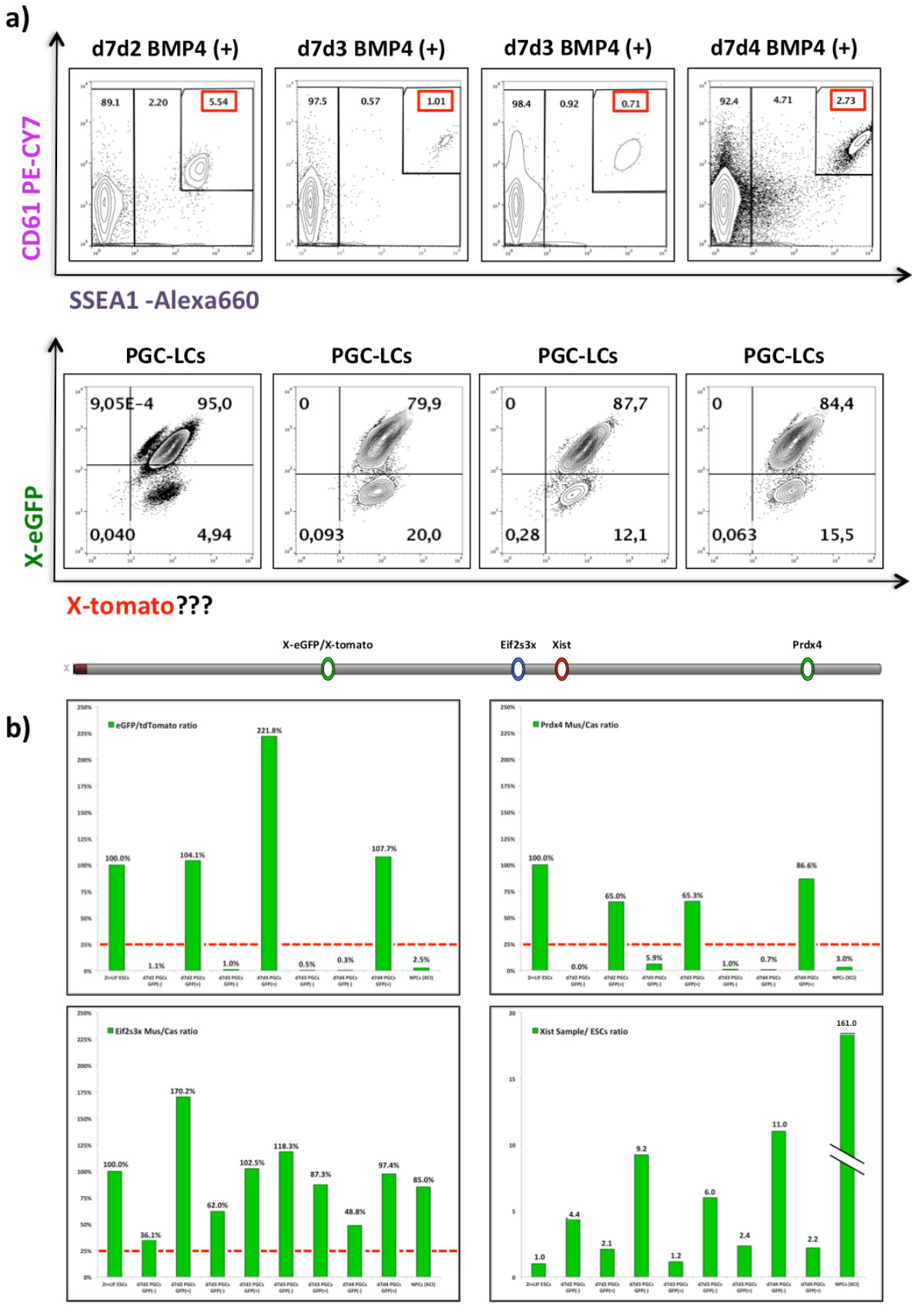
a)
d7d2 BMP4 (+)
d7d3 BMP4 (+)
d7d3 BMP4 (+)
d7d4 BMP4 (+)
89.1
2.20
5.54
97.5
0.57
1.01
98.4
0.92
0.71
92.4
4.71
2.73
CD61 PE-CY7
SSEA1 -Alexa660
PGC-LCs
PGC-LCs
PGC-LCs
PGC-LCs
9,05E-4
95,0
0,040
4,94
0
79,9
0,093
20,0
0
87,7
0,28
12,1
0
84,4
0,063
15,5
X-eGFP
X-tomato???
X-eGFP/X-tomato
Eif2s3x
Xist
Prdx4
b)
eGFP/tdTomato ratio
100.0%
1.1%
104.1%
1.0%
221.8%
0.5%
0.3%
107.7%
2.5%
Prdx4 Mus/Cas ratio
100.0%
0.0%
65.0%
5.9%
65.3%
1.0%
0.7%
86.6%
3.0%
Eif2s3x Mus/Cas ratio
100.0%
36.1%
170.2%
62.0%
102.5%
118.3%
87.3%
48.8%
97.4%
85.0%
Xist Sample/ ESCs ratio
1.0
4.4
2.1
9.2
1.2
6.0
2.4
11.0
2.2
161.0

Figure 5: Female *In vitro* PGC-LCs conserve XX karyotype and show *bona fide* X-activity on multiple X-linked loci:

a) *In vitro* PGC-LCs are induced from day 2 (d7d2) to day 3 (d7d3) and day 4 Epi-LCs (d7d4 PGC-LCs), and the *X-tomato*(+); *X-eGFP*(+) & (-) PGC cell populations are FACs-sorted after 7 days of culture in PGC Induction media.

b) Allele-specific expression of the *X-eGFP/X-tomato, Prdx4*, *Eif2s3x* & *Xist* X-linked loci is assayed by RT-PCR. The expression from each allele is normalized to X-active ESCs levels, then the ratio between *musculus* and *castaneus*-linked expression is calculated. If a cell *musculus/castaneus*-linked ratio value is below 25% (Red bar), the locus is monoallelically expressed and subject to X-inactivation.

In order to test this possibility, we needed to test other genic loci. We examined the allele-specific expression of the X-linked *Prdx4* gene locus, which is known to be subject to X-inactivation, the X-linked *Eif2s3x* escapee gene locus, which is reported to be completely impervious to the X-inactivation process, and the expression of the *Xist* lncRNA, the master regulator and initiator of X-Inactivation. The loci that respond the X-inactivation or reactivation process are shown in green, while the X-linked escapee genic loci are shown in blue. While we observed *Eif2s3x* locus allelic expression experience some fluctuations across the different cell types, it was always sizably expressed from the 2 X-chromosomes (biallelically) during differentiation, confirming its status as an escapee of X-inactivation **(FIG.5b)**. The *Prdx4* locus, on the other hand, showed the same biallelic expression levels as the parent ESCs in X-eGFP(+) cells, while in the X-eGFP(-) PGC-LC cells, as well as in positive controls for X-inactivation, Soma and NPCs, the *Prdx4* locus had its *musculus*, eGFP-linked counterpart fully silenced, while the *castaneus*-linked allele was fully expressed (monoallelic expression). This phenotype was reproducible regardless of how many days the starting Epi-LCs were differentiated **(FIG.5b)**.

When we addressed the *Xist* lncRNA expression, we observed that, while there was a sizable downregulation from the high levels of expression reached in Epi-LCs, the X-eGFP(-) PGC-LCs still had a 10-fold increase in *Xist* expression compared to the X-active ESCs they were descended from, and a 5-10 fold higher *Xist* expression versus their X-eGFP(+) PGC-LC counterparts. It is worth noting that X-eGFP(+) PGC-LCs

have virtually the same residual expression levels as the starting X-active ESCs.

Note that the expression levels of *Xist* are the highest in stably X-inactivated cells such as NPCs, but far lower *Xist* expression levels support stable X-inactivation, as seen in Epi-LCs and X-eGFP(-) PGC-LCs **(FIG.5b)**. In combination with the silencing of the *musculus*-linked *Prdx4* and *eGFP* loci, this led us to conclude that proper X-inactivation took place in X-eGFP(-) PGC-LC cells, instead of being a fluorescent reporter artifact. However, we also observed that in X-eGFP(-) PGC-LCs, the *Xist* expression levels are lower than in their starting Epi-LC progenitors. This is counter-intuitive, as cells are expected to steadily increase their *Xist* expression levels as they differentiate and enforce X-inactivation, till other epigenetic enforcers stably lock in place the X-inactivation phenotype **(QUOTE)**, and this can readily observed upon analysis of the NPCs control differentiated from the same ESC line.

This suggests that the X-eGFP(+) PGC-LCs arise through a process of gradual downregulation of *Xist* signal from their starting Epi-LC starting point. We previously chose to culture *in vitro* induced PGC-LCs for 7 days, as germ cell surface markers CD61 & SSEA1 were nearly undetectable till day 4-5 of culture (Hayashi & Saitou 2013b; Hayashi & Saitou 2013c). Also longer embryoid body differentiation times let cells acquire and stabilize X-inactivation as time goes on, both as described in our own results as well as in previous reports **(QUOTE)**. However, *Xist* expression suggested that a process of X-reactivation was taking place – and that an early sorting of PGC-LCs at the earliest timepoint possible (day 4 of culture) could actually increase the yield of X-inactive PGC-LCs. In order to test this hypothesis, we induced PGC-LCs from day 2 Epi-LCs and cultured them for 4 days. We monitored X-eGFP expression every single day by FACs analysis **(FIG.6a & FIG.7a)** and took RNA samples from unsorted bodies, before FACs sorting X-eGFP(-) & (+) PGC-LC populations and analyzing their gene expression at day 4 of culture **(FIG.6b & FIG.7b)**. We chose to use day 2 Epi-LCs as starting material for the PGC Induction for two reasons:

The first is that it increased the PGC-LC yield per induction. As harvesting the PGC-LCs after 4 days of culture (the technical known limit to early PGC-LC sorting) results in very low levels of CD61 surface marker up-regulation (Hayashi et al. 2011a), this would lead to underreporting the number of PGC-LCs induced. An increased yield was

also required to accumulate enough sample for analysis. The second reason is that day 2 Epi-LCs have had time to accumulate X-inactivation marks, but did only start the process of gene inactivation. If we could obtain an enrichment in X-eGFP(-) PGC-LCs in these circumstances, this would support that the cells first fully differentiated and X-inactivated as expected from an embryoid body, and only then underwent X-reactivation in a PGC-specific fashion.

By FACs analysis, we observed a general downregulation of X-eGFP fluorescent protein marker after 12 hours of PGC Induction, but only a 2% of the total cell population could be considered X-eGFP(-). The general X-eGFP(-) fraction of the population was of 33.4% after 48H (day 2), and 72.0% after 72H (day 3). By day 4, at the time of FACs-sorting, 97% of the cells of the Body were X-inactive **(FIG.6a & 7a)**.

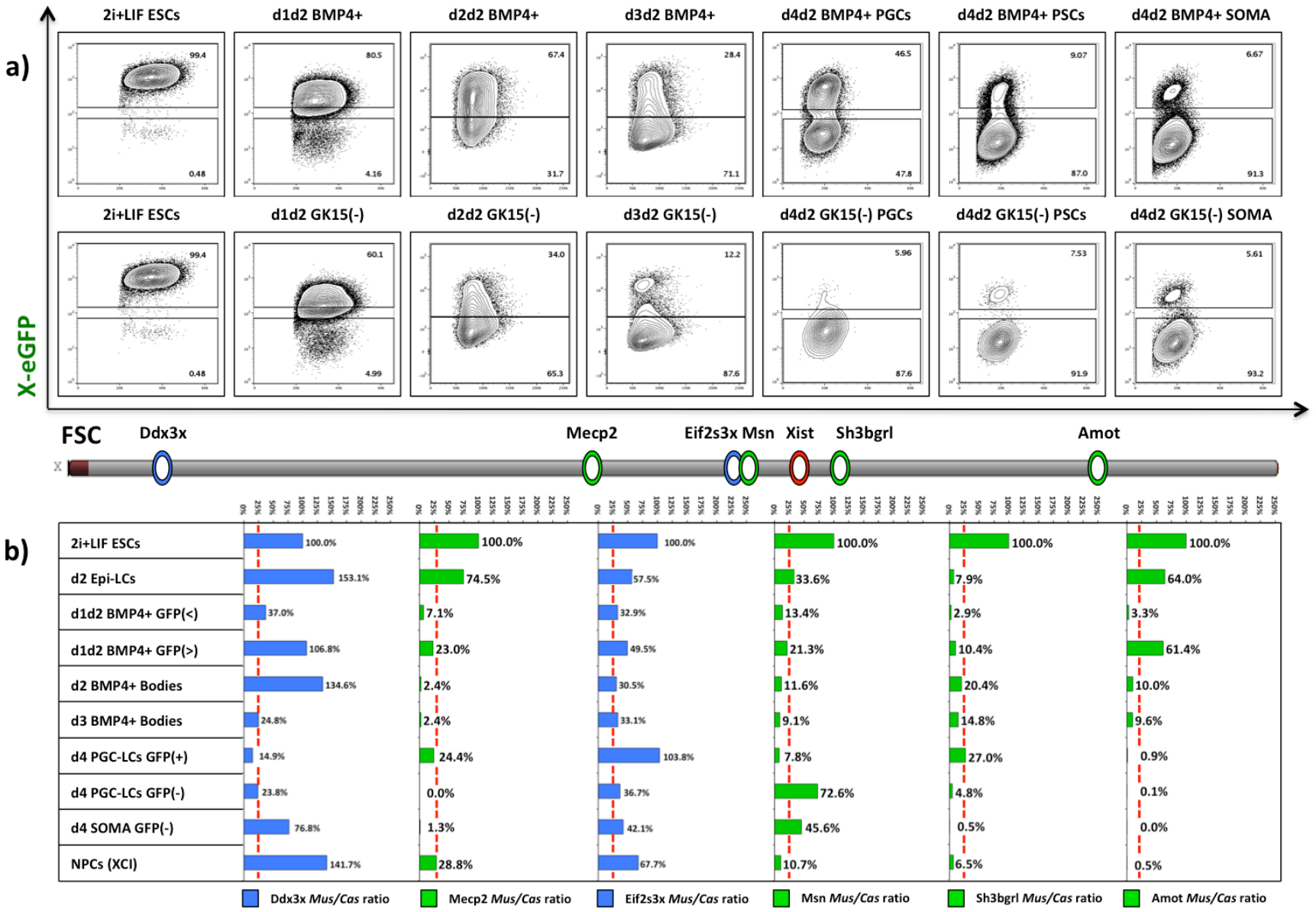
a)
2i+LIF ESCs
d1d2 BMP4+
d2d2 BMP4+
d3d2 BMP4+
d4d2 BMP4+ PGCs
d4d2 BMP4+ PSCs
d4d2 BMP4+ SOMA
99.4
0.48
80.5
4.16
67.4
31.7
28.4
71.1
46.5
47.8
9.07
87.0
6.67
91.3
2i+LIF ESCs
d1d2 GK15(-)
d2d2 GK15(-)
d3d2 GK15(-)
d4d2 GK15(-) PGCs
d4d2 GK15(-) PSCs
d4d2 GK15(-) SOMA
99.4
0.48
60.1
4.99
34.0
65.3
12.2
87.6
5.96
87.6
7.53
91.9
5.61
93.2
X-eGFP
FSC
Ddx3x
Mecp2
Eif2s3x
Msn
Xist
Sh3bgrl
Amot
b)
2i+LIF ESCs
d2 Epi-LCs
d1d2 BMP4+ GFP(<)
d1d2 BMP4+ GFP(>)
d2 BMP4+ Bodies
d3 BMP4+ Bodies
d4 PGC-LCs GFP(+)
d4 PGC-LCs GFP(-)
d4 SOMA GFP(-)
NPCs (XCI)
100.0%
153.1%
37.0%
106.8%
134.6%
24.8%
14.9%
23.8%
76.8%
141.7%
100.0%
74.5%
7.1%
23.0%
2.4%
2.4%
24.4%
0.0%
1.3%
28.8%
100.0%
57.5%
32.9%
49.5%
30.5%
33.1%
103.8%
36.7%
42.1%
67.7%
100.0%
33.6%
13.4%
21.3%
11.6%
9.1%
7.8%
72.6%
45.6%
10.7%
100.0%
7.9%
2.9%
10.4%
20.4%
14.8%
27.0%
4.8%
0.5%
6.5%
100.0%
64.0%
3.3%
61.4%
10.0%
9.6%
0.9%
0.1%
0.0%
0.5%
Ddx3x Mus/Cas ratio
Mecp2 Mus/Cas ratio
Eif2s3x Mus/Cas ratio
Msn Mus/Cas ratio
Sh3bgrl Mus/Cas ratio
Amot Mus/Cas ratio

Figure 6: Female *In vitro* PGC-LCs undergo initial genic X-inactivation and posteriorly gain X-reactivation in a time-dependent fashion:

a) *In vitro* PGC-LCs are induced from day 2 Epi-LCs, and the *X-eGFP*(+) & (-) PGC cell populations are FACs-analyzed daily from 1 to 4 days of culture in cytokine PGC Induction media.

b) Allele-specific expression of the X-inactivation marker genes, *Mecp2*, *Msn, Sh3bgrl & Amot* (in green) and X-inactivation Escapee genes *Ddx3x* & *Eif2s3x* (in blue) is assayed by RT-PCR. The expression from each allele is normalized to X-active ESCs levels, then the ratio between *musculus* and *castaneus*-linked expression is calculated. If a cell *musculus/castaneus*-linked ratio value is below 25% (red dashed line), the locus is monoallelically expressed and subject to X-inactivation.

The dynamics of X-eGFP silencing in the (-) control of Embryoid body formation were faster still. This observation confirms our previous results on the negative effect of the PGC induction media on X-eGFP reporter silencing **(FIG.6a & 7a)**. Upon FACs sorting, we observed that the levels of CD61 up-regulation were mild versus the negative control. We were however had confident that the gating represented PGC-LCs, as the population had a vastly different X-eGFP reporter behavior when compared against any possible PSC contaminants and its negative control counterpart. We observed a 47% of X-eGFP(-) PGC-LCs after 4 days of culture **(FIG.6a & 7a)**, in contrast to the scarce 2% X-eGFP(-) PGC-LCs observed after 7 days of culture in the previous experiment **(FIG.2a)**.

We then wished to confirm the results obtained by eGFP FACs analysis at the gene expression level. In order to assess the spread of the X-inactivation phenotype, we queried the allelic expression of a number of loci spread across the X chromosome: the X-inactivation escapee loci *Ddx3x* & *Eif2s3x*, the X-inactivation marker loci *Prdx4*, *Gpc4*, *Mecp2*, *Amot*, *Sh3bgrl* & *Msn*, and the expression of the master X-inactivator *Xist* lncRNA, as well as *eGFP* reporter transcription **(FIG.6b & 7b)**.

While the expression of the escapee genes *Eif2s3x* & *Ddx3x* fluctuated during the differentiation procedure, showing in some cases preferential expression from the *castaneus* allele on the X-active chromosome, it remained expressed biallelically. The

Eif2s3x locus was robustly expressed in all cell types across the differentiation procedure, and along with the differentiated (+) control for XCI that NPCs offer, it is a good guideline on the levels of preferential *castaneus* expression below which the locus should be considered inactivated **(FIG.6b)**.

We observe that while a sizable proportion of the body remained X-eGFP(+) after 2 and 3 days of PGC induction **(FIG.6a & 7a)**, the allele-specific expression rates for *eGFP* reporter and all X-inactivation responder genes were below 20%, a threshold we chose for monoallelic expression and X-inactivation. The X-inactivation escapee genes *Eif2s3x* & *Ddx3x*, on the other hand, remained biallelically expressed **(FIG.6b & 7b)**.

When we address the expression of X-eGFP(-) & (+) PGC-LCs, we observe that in X-eGFP(+) PGC-LCs, all loci except *Amot* & *Sh3bgrl* show X-reactivation. In addition, the expression from the X-active *castaneus* allele in all X-reactivated genes is still predominant, which, in addition to raised, but mostly monoallelic expression from the *Amot* & *Sh3bgrl* loci, points to a still nascent and ongoing process of X-reactivation in *X-eGFP*(+) PGC-LCs **(FIG.6b & FIG.7b)**.

In the other hand, the X-eGFP(-) PGC-LCs show full X-inactivation across all inactivation marker loci assessed, with the exception of *Msn*, in a way that matches or surpasses the locked X-inactivation seen in NPCs and in the own somatic population of the embryoid bodies. The conclusions from the *Msn* gene, however, should be viewed with caution, as this gene has a particularly low expression in PGC-LCs.

The genes *Prdx4* & *Gpc4*, early responders to X-inactivation, are the ones to show the earliest and largest X-inactivation effect **(FIG.7b)**.

The expression of the X-linked *eGFP* reporter is entirely in line with X-inactivation marker genes mentioned above, further supporting the suitability of the X-linked *eGFP* reporter as a marker of X-reactivation **(FIG.7b)**. However, the fact that eGFP protein signal in day 2 and 3 bodies during PGC-LC differentiation protocol is far higher than its expression at mRNA level would suggest, points out that, while the X-eGFP reporter is very apt at monitoring naïve X-activity & the X-reactivation phenotype, it´s levels of fluorescent protein are less fit to monitor accurately the kinetics of X-inactivation, presumably due to the long half-life of the fluorescent protein **(QUOTE)**.

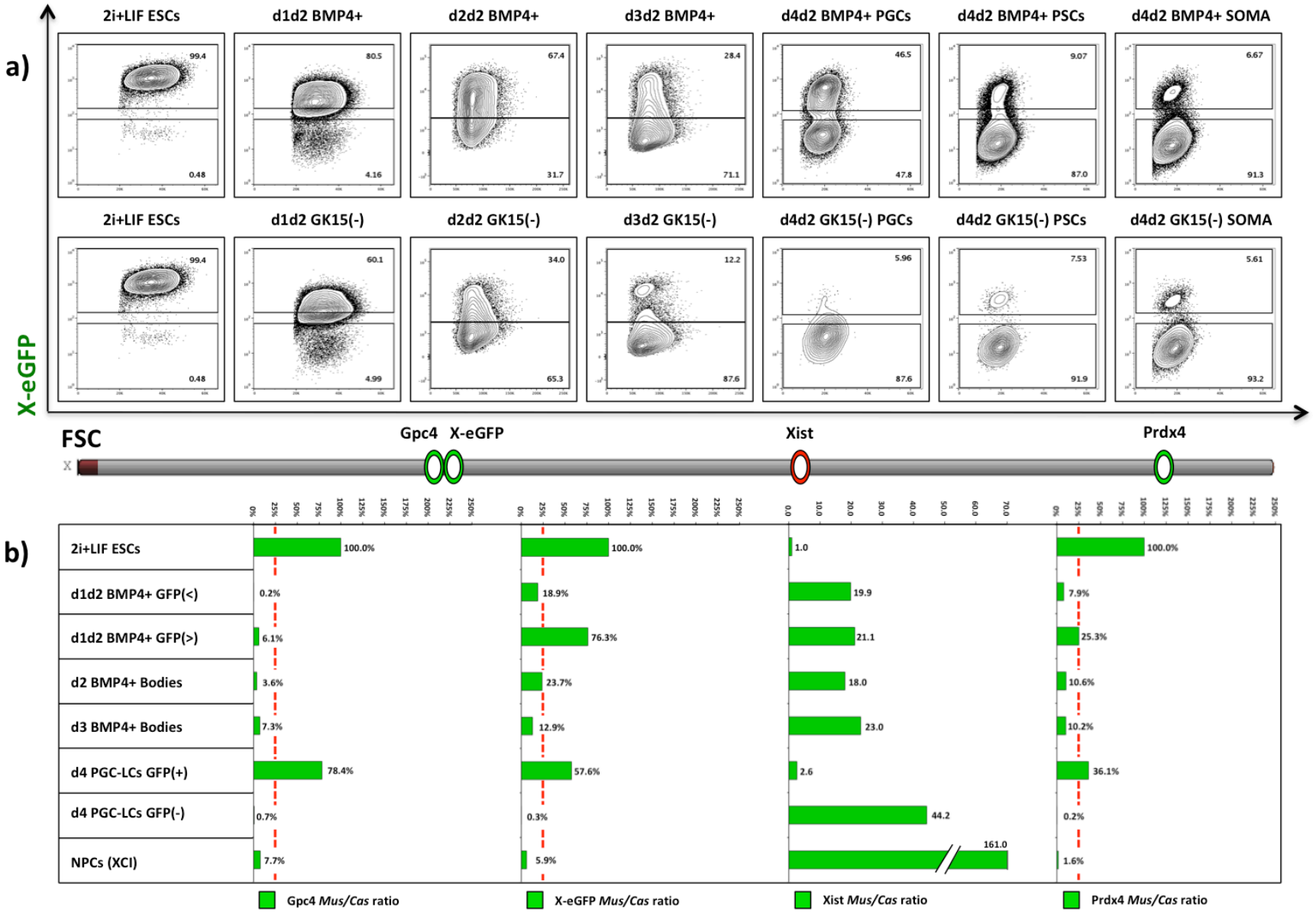
a)
2i+LIF ESCs
d1d2 BMP4+
d2d2 BMP4+
d3d2 BMP4+
d4d2 BMP4+ PGCs
d4d2 BMP4+ PSCs
d4d2 BMP4+ SOMA
99.4
0.48
80.5
4.16
67.4
31.7
28.4
71.1
46.5
47.8
9.07
87.0
6.67
91.3
2i+LIF ESCs
d1d2 GK15(-)
d2d2 GK15(-)
d3d2 GK15(-)
d4d2 GK15(-) PGCs
d4d2 GK15(-) PSCs
d4d2 GK15(-) SOMA
99.4
0.48
60.1
4.99
34.0
65.3
12.2
87.6
5.96
87.6
7.53
91.9
5.61
93.2
X-eGFP
FSC
X
Gpc4
X-eGFP
Xist
Prdx4
b)
2i+LIF ESCs
d1d2 BMP4+ GFP(<)
d1d2 BMP4+ GFP(>)
d2 BMP4+ Bodies
d3 BMP4+ Bodies
d4 PGC-LCs GFP(+)
d4 PGC-LCs GFP(-)
NPCs (XCI)
100.0%
0.2%
6.1%
3.6%
7.3%
78.4%
0.7%
7.7%
100.0%
18.9%
76.3%
23.7%
12.9%
57.6%
0.3%
5.9%
1.0
19.9
21.1
18.0
23.0
2.6
44.2
161.0
100.0%
7.9%
25.3%
10.6%
10.2%
36.1%
0.2%
1.6%
Gpc4 Mus/Cas ratio
X-eGFP Mus/Cas ratio
Xist Mus/Cas ratio
Prdx4 Mus/Cas ratio

Figure 7: Female *In vitro* PGC-LCs undergo initial genic X-inactivation and posteriorly gain X-reactivation in a time-dependent fashion:

a) In vitro PGC-LCs are induced from day 2 Epi-LCs, and the *X-eGFP*(+) & (-) PGC cell populations are FACs-analyzed daily from 1 to 4 days of culture in cytokine PGC Induction media.

b) Allele-specific expression of the X-inactivation marker genes*, Gpc4*, *X-eGFP,* & *Prdx4* (in green) and the X-inactivation LncRNA master regulator *Xist* is assayed by RT-PCR. The expression from each allele is normalized to X-active ESCs levels, then the ratio between *musculus* and *castaneus*-linked expression is calculated. If a cell *musculus/castaneus*-linked ratio value is below 25% (red dashed line), the locus is monoallelically expressed and subject to X-inactivation.

Perhaps more interestingly, even when induced PGC-LCs from the same day 2 Epi-LCs timepoint, all the X-eGFP(-) cells derived from this PGC induction showed much greater expression of *Xist* lncRNA after only 12H and 4 days of PGC culture, respectively, than in X-eGFP(-) PGC-LCs after 7 days of culture **(FIG.7b)**. This supports a scenario in which extended PGC culture promotes *Xist* lncRNA downregulation, which, if sustained across time, should eventually lead into X-reactivation **(FIG.6 & FIG.7)**. The most surprising aspect however was , the discovery that regardless of the eGFP fluorescent protein readouts, all X-eGFP(<) *poor* cells were X-inactive after only 12H of embryoid body differentiation. Even the X-eGFP(>) rich cells were X-inactive across all loci excepting *Amot* & the X-eGFP reporter transgene **(FIG.6b & 7b)**. This meant that, after only 12H of PGC induction, a high proportion of cells in the embryoid body must have undergone X-inactivation, which was not observed in the progenitor Epi-LCs, nor reached afterwards, if we judge the low levels of *Xist* lncRNA found in the X-eGFP(-) PGC_LCs induced from day 2 Epi-LCs after 7 days of culture in PGC induction media **(FIG.7b)**.

The sum of all previous results supported the scenario of an X-reactivation phenotype specifically appearing in the PGC-LC population across the PGC-LC induction protocol, as the comparison of this last experiment with the previously screened PGC-

LC inductions for 7 days of cell culture has shown. In addition, the fact that PGC-LC culture, and not the degree of starting Epi-LC inactivation, is the defining factor governing X-inactivation in PGC-LCs, further supports that the X-activity found in female *in vitro* PGC-LCs is a X-reactivation phenotype from an initial X-inactive state. Moreover, the ability of the *X-eGFP* reporter transcription to monitor the active or inactive status of the X-chromosome is fully supported, even if its fluorescent activity should be interpreted carefully when trying to infer X-inactivation kinetics under 24-48H timeframes, due to the long protein half-life.

However, there is still an alternative interpretation to our results: The X-active, X-eGFP(+) PGC-LCs do not arise through a process of X-reactivation from inactive cells, but were instead a naïve, X-active subset of Epi-LCs which became PGC-LCs through germ cell fate specification or competitive advantage over X-inactive PGC-LCs. While the Soma and the PSC escapees would have undergone X-inactivation as they differentiated during the embryoid body culture, most PGC-LCs would have kept their initial X-active state. Therefore we can only be certain about X-reactivation in our PGC-LCs, if the entirety of the cells of the embryoid body were X-inactive before PGC fate specification happened. One of the ways for a constitutively X-active PGC-LC population (the X-loss phenotype hypothesis) was previously discussed and evidence provided against it, as our cells were of XX karyotype also after PGC-LC differentiation. As such, the only remaining task to ensure that X-reactivation in our PGCLCs truly occured from a previously inactive state and was not purely due to a failure of X-inactivation, was to monitor X-activity of the starting embryoid body population.

For that we had to choose the starting embryoid body timepoint to monitor. Given previous reports that embryoid body formation was able to boost the H3K27me3 X-inactivation spot from a 20% of the starting day 2 female Epi-LCs to virtually all cells after 24H of embryoid body formation (Katsuhiko Hayashi et al. 2012), 24H after PGC induction offered a timepoint in which a strong X-inactivating cue took place and germ cell fate could still have not been acquired. Our own observation that at this timepoint eGFP fluorescence was strongly downregulated and X-eGFP(-) cell population presence first appeared also supported this choice. Due to the lag in X-eGFP signal downregulation during X-inactivion, we sampled RNA after 24H of PGC induction

from days 3 & 4 Epi-LCs. In order to use the most stringent testing scenario, we also took samples from day 2 Epi-LC induced PGC-LCs and aimed for a shorter embryoid body differentiation timing - 12H only – and FACs-sorted the GFP-highest and lowest portions of the embryoid body **(FIG.8)**.

In essence, we added an additional timepoint for early X-inactivation for all previously monitored PGC inductions, allowing us to see how the starting X-inactivation status on the differentiating embryoid body impacts subsequent X-activity on day 4 & day 7 PGC-LCs **(FIG.9)**. When we interrogated the X-eGFP reporter protein expression by FACs, we observed that for PGC-induction embryoid bodies differentiated from day 3 & 4 Epi-LCs, 24H of differentiation were enough to give rise to a substantial X-eGFP(-) population (over 40% of cells) **(FIG.8a)**. This was not the case in the PGC-induction embryoid bodies from day 2 Epi-LCs; after 12H, where only 4% of the population could be considered X-inactive based on X-eGF*P* reporter expression **(FIG.8a)**.

We then analyzed the allelic expression of a number of loci spread across the X chromosome: the X-inactivation escapee loci *Ddx3x* & *Eif2s3x*, the X-inactivation marker loci *Prdx4*, *Gpc4*, *Mecp2*, *Amot*, *Sh3bgrl* & *Msn*, and the expression of the master X-inactivator *Xist* lncRNA, as well as *eGFP* reporter transcription **(FIG.8b & FIG.9b)**. We observed that all loci except *Sh3bgrl* showed clear signs of X-inactivation and displayed monoallelic expression in X-eGFP-poor cells differentiated from day 2 Epi-LCs and the bodies from day 3 & 4 Epi-LCs. Only the X-eGFP-enriched cells differentiated from day 2 Epi-LCs showed X-active loci as *Amot* & the *eGFP* reporter locus, while the remaining loci were X-inactivated **(FIG.8b)**. The master X-inactivator lncRNA *Xist* was expressed across embryoid bodies, regardless of the starting Epi-LC differentiation timespan, and showed a downregulation across the different days of PGC culture. The X-inactive PGC-LCs sorted after 7 days of culture typically showed a 5-

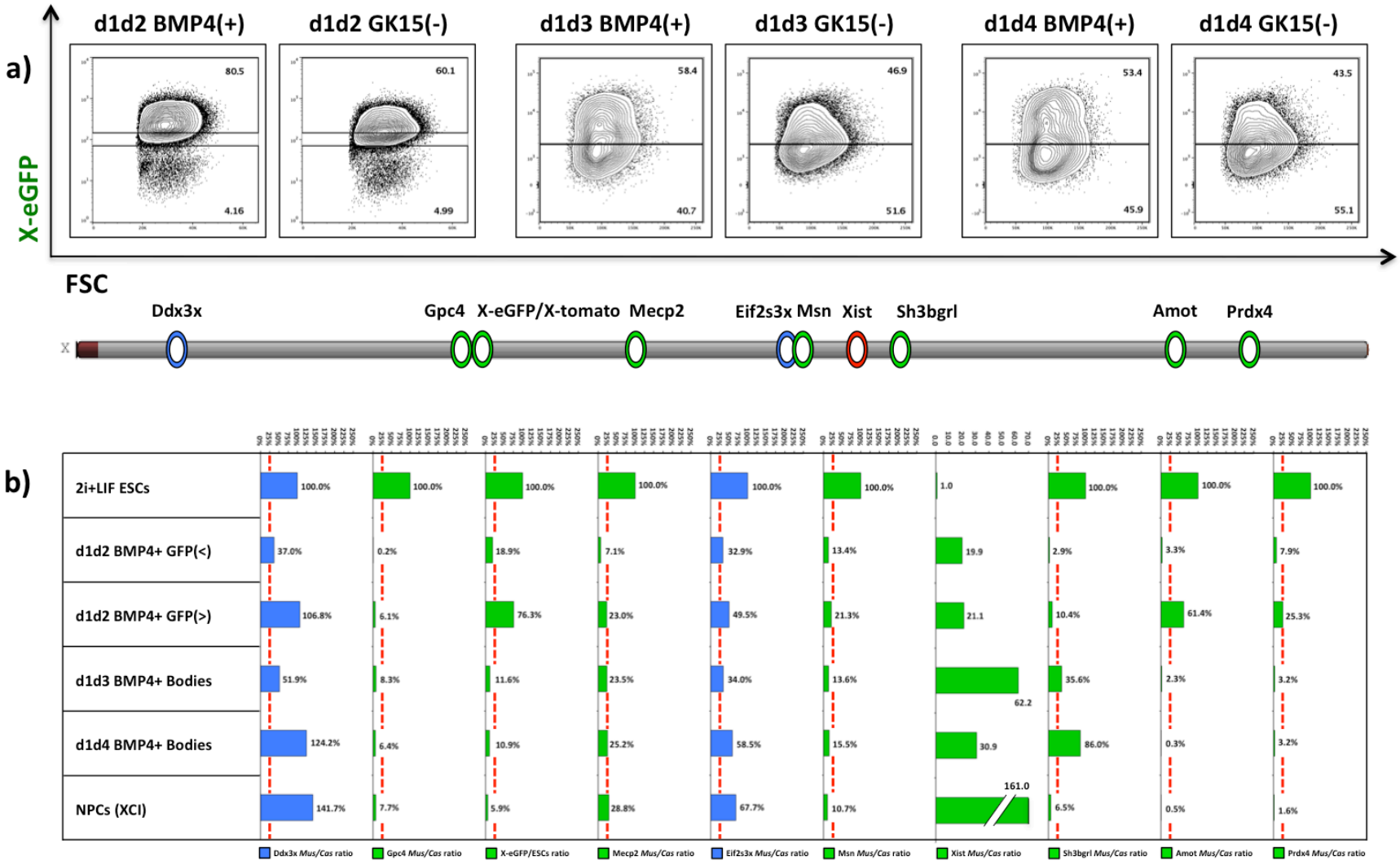
a)
d1d2 BMP4(+)
d1d2 GK15(-)
d1d3 BMP4(+)
d1d3 GK15(-)
d1d4 BMP4(+)
d1d4 GK15(-)
80.5
4.16
60.1
4.99
58.4
40.7
46.9
51.6
53.4
45.9
43.5
55.1
X-eGFP
FSC
Ddx3x
Gpc4
X-eGFP/X-tomato
Mecp2
Eif2s3x
Msn
Xist
Sh3bgrl
Amot
Prdx4
X
b)
2i+LIF ESCs
d1d2 BMP4+ GFP(<)
d1d2 BMP4+ GFP(>)
d1d3 BMP4+ Bodies
d1d4 BMP4+ Bodies
NPCs (XCI)
Ddx3x Mus/Cas ratio
Gpc4 Mus/Cas ratio
X-eGFP/ESCs ratio
Mecp2 Mus/Cas ratio
Eif2s3x Mus/Cas ratio
Msn Mus/Cas ratio
Xist Mus/Cas ratio
Sh3bgrl Mus/Cas ratio
Amot Mus/Cas ratio
Prdx4 Mus/Cas ratio

Figure 8: All *In vitro* PGC-LC induction bodies undergo full genic X-inactivation in the first 12-24H of culture, independently of the days of Epi-LC differentiation and the *X-eGFP* protein signal readout:

a) *In vitro* PGC-LCs are induced from day 2 (d1d2), 3 (d1d3) & 4 (d1d4) Epi-LCs for 12-24H from induction onset, and the *X-eGFP*(+) & (-) PGC cell populations are FACs-analyzed.

b) Allele-specific expression of the X-inactivation marker genes*, Gpc4, X-eGFP, Mecp2*, *Msn, Sh3bgrl*, *Amot & Prdx4* (in green), the X-inactivation Escapee genes *Ddx3x* & *Eif2s3x* (in blue) and the X-inactivation LncRNA master regulator *Xist* is assayed by RT-PCR. The expression from each allele is normalized to X-active ESCs levels, then the ratio between *musculus* and *castaneus*-linked expression is calculated. If a cell *musculus/castaneus*-linked ratio value is below 25% (Red bar), the locus is monoallelically expressed and subject to X-inactivation.

fold downregulation of their *Xist* expression from their day 1 counterparts, leading us to suspect that even those cells would eventually undergo X-reactivation after prolonged PGC-LC culture **(FIG.8b & FIG9b)**. Our interpretation is that, regardless of the starting Epi-LC material differentiation days, the starting cells during PGC-induction protocol undergo rapid genic X-inactivation in the first 24H of induction, prior to PGC-LC cell fate acquisition. Taken together, our data suggest that some regulatory mechanism is able to drive fast X-inactivation in the first 24H of embryoid body differentiation, and that only PGC-LCs undergo X-reactivation in a regulated fashion across the days of PGC-LC culture. As the cells from the embryoid body are in an X-inactive state, the X-activity of the PGC-LCs should be considered a *bona fide* X-reactivation phenotype. When considering the kinetics of X-inactivation and aiming for good PGC induction efficiency, we therefore recommend the use of day 3 Epi-LCs as the starting material when inducing female *in vitro* PGC-LCs to study X-reactivation.

One could consider that, while the average precursor population after 24H of PGC-LC induction was showing consistent X-inactivation, there could have existed naïve X-active subpopulations which could be clonally expanded and gave rise to the X-active PGC-LCs without the need of a X-reactivation process. As such, the X-inactivation status needed to be confirmed at the single-cell resolution level. In order to rule the former scenario out, we took the eGFP-enriched subset of cells from day 2 Epi-LCs

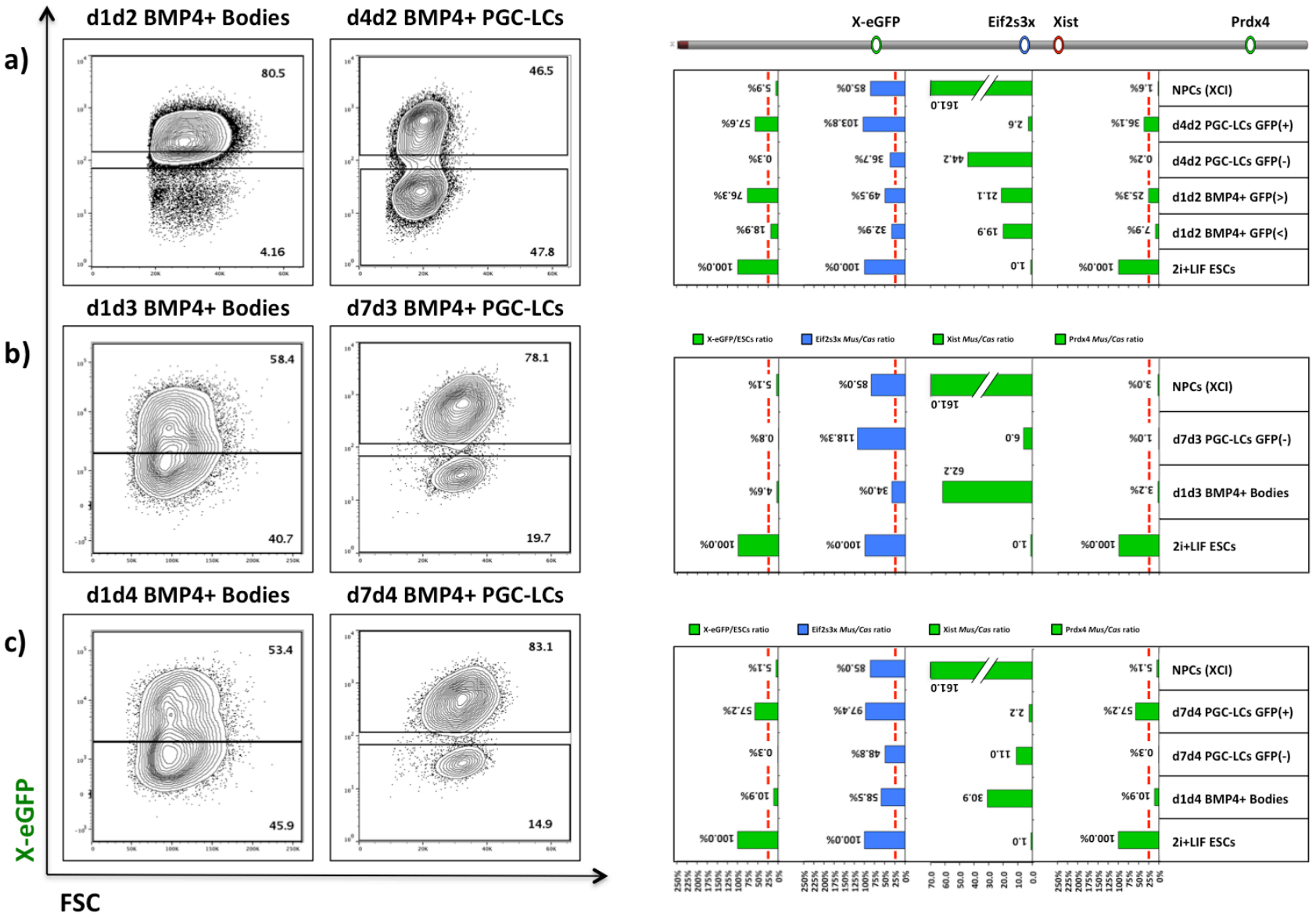
a)
d1d2 BMP4+ Bodies
d4d2 BMP4+ PGC-LCs
80.5
4.16
46.5
47.8
b)
d1d3 BMP4+ Bodies
d7d3 BMP4+ PGC-LCs
58.4
40.7
78.1
19.7
c)
d1d4 BMP4+ Bodies
d7d4 BMP4+ PGC-LCs
53.4
45.9
83.1
14.9
X-eGFP
FSC
X-eGFP
Eif2s3x
Xist
Prdx4
NPCs (XCI)
d4d2 PGC-LCs GFP(+)
d4d2 PGC-LCs GFP(-)
d1d2 BMP4+ GFP(>)
d1d2 BMP4+ GFP(<)
2i+LIF ESCs
X-eGFP/ESCs ratio
Eif2s3x Mus/Cas ratio
Xist Mus/Cas ratio
Prdx4 Mus/Cas ratio
d7d3 PGC-LCs GFP(-)
d1d3 BMP4+ Bodies
d7d4 PGC-LCs GFP(+)
d7d4 PGC-LCs GFP(-)
d1d4 BMP4+ Bodies

Figure 9: All *In vitro* PGC-LC induction bodies suffer full genic X-inactivation in the first 24H of culture, after which PGC-LCs undergo a time-dependent X-reactivation phenotype:

a) In vitro PGC-LCs are induced from day 2 (d1d2), 3 (d1d3) & 4 (d1d4) Epi-LCs for 12-24H from induction onset, and the *X-eGFP*(+) & (-) PGC cell populations are FACs-analyzed. After 4 or 7 days of cell culture, X-eGFP(+) & (-) PGC-LCs are FACs-sorted and their genic X-inactivation status assayed by allele-specific RT-PCR.

b) Allele-specific expression of the X-inactivation marker genes *X-eGFP & Prdx4* (in green) ,the X-inactivation Escapee gene *Eif2s3x* (in blue) and the X-inactivation LncRNA master regulator *Xist* is assayed by RT-PCR. The expression from each allele is normalized to X-active ESCs levels, then the ratio between *musculus* and *castaneus*-linked expression is calculated. If a cell *musculus/castaneus*-linked ratio value is below 25% (Red bar), the locus is monoallelically expressed and subject to X-inactivation.

after 12H of embryoid body differentiation and performed RNA-FISH staining against the mature *Xist* lncRNA, comparing their *Xist* signal **(FIG.10b)** against mouse embryonic fibroblasts (MEFs) which are stably X-inactivated **(FIG.10c)**, and naïve X-active ESCs, which are *Xist*-negative **(FIG.10a)**. If the cells were properly X-inactivated, they would have displayed a cloud-like *Xist* signal across the entire span of the X chromosome, similar to MEFs **(FIG.10c).** We adapted previous oligo RNA-FISH probe designs against *Xist* (Del Rosario 2016) using V2.0 smHCR technology (see chapter 3), in order to increase signal and sensitivity (Choi et al. 2014; Shah, Lubeck, Schwarzkopf, T. He, et al. 2016). We observed that a high proportion of the cells within differentiation bodies displayed *Xist* clouds similar to the MEF cells, and scored similar percentages of *Xist* signal. It should be noted that the percentages of *Xist* cloud (+) cells are never 100%, even in stably X-inactivated MEF cell populations due to detection limits of the RNA-FISH method **(QUOTE)**. The combination of an even *Xist* X-inactivating signal across most cells of the population, and the confirmed ongoing genic X-inactivation at the RT-PCR level lead us to conclude that the biallelic expression of X-linked genes in PGC-LCs likely arose by germ cell-specific X-reactivation. Although we cannot completely rule it out without extensive single-cell analysis of X-linked gene expression, we do not believe that a substantial *naïve*, X-active subpopulation remains

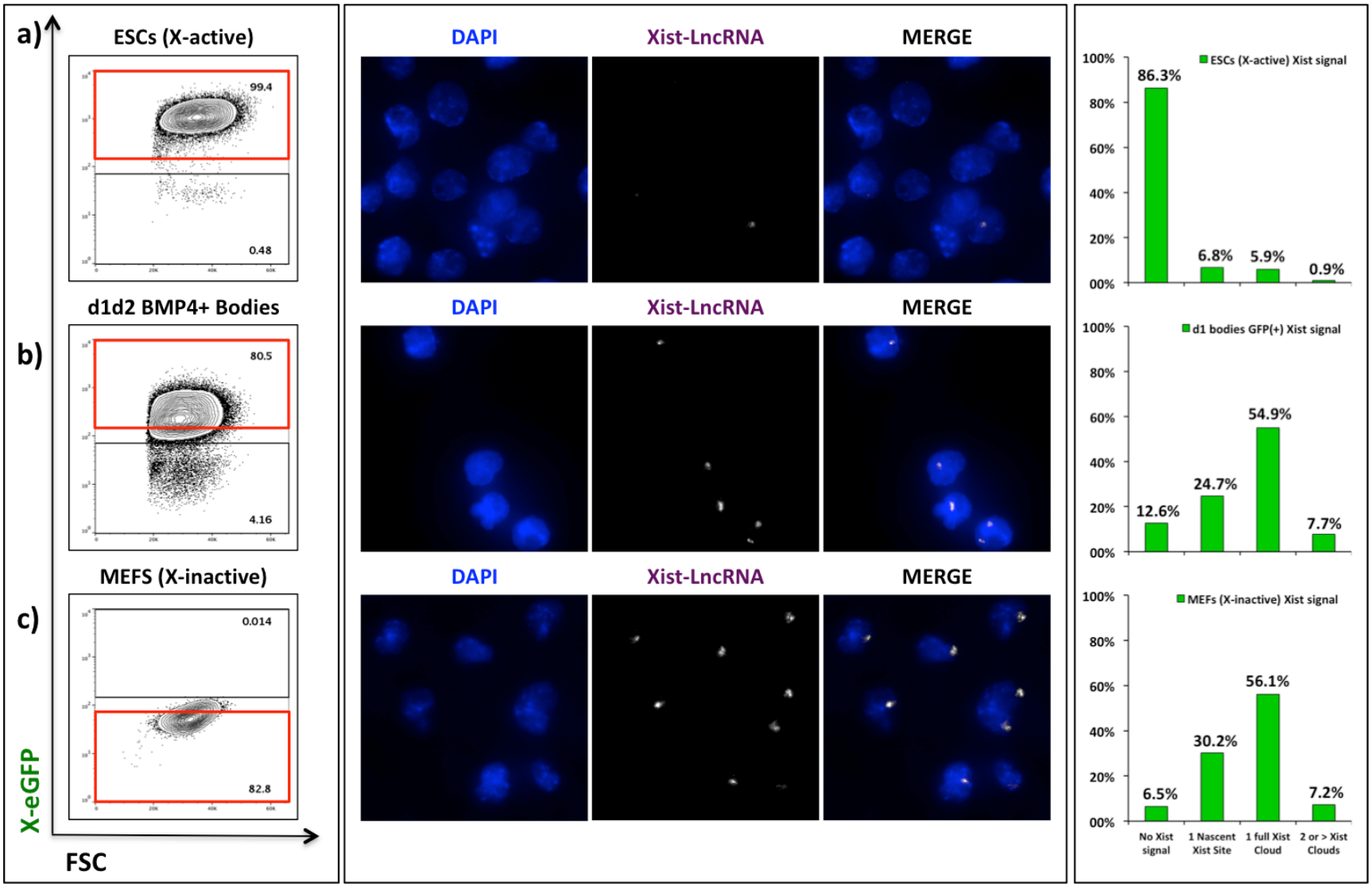
a)
ESCs (X-active)
99.4
0.48
b)
d1d2 BMP4+ Bodies
80.5
4.16
c)
MEFS (X-inactive)
0.014
82.8
X-eGFP
FSC
DAPI
Xist-LncRNA
MERGE
DAPI
Xist-LncRNA
MERGE
DAPI
Xist-LncRNA
MERGE
100%
80%
60%
40%
20%
00%
ESCs (X-active) Xist signal
86.3%
6.8%
5.9%
0.9%
d1 bodies GFP(+) Xist signal
12.6%
24.7%
54.9%
7.7%
MEFs (X-inactive) Xist signal
6.5%
30.2%
56.1%
7.2%
No Xist signal
1 Nascent Xist Site
1 full Xist Cloud
2 or > Xist Clouds

Figure 10: Cells of *In vitro* PGC-LC induction bodies show X-inactivation after 12H of culture, as monitored at single-cell resolution by *Xist* RNA-FISH staining:

a) X-active, Naïve pluripotent, *X-eGFP(+)* ESCs are stained as a negative control for the master X-inactivator LncRNA *Xist*. Cells showing nascent transcription or a full cloud of *Xist* signal have undergone X-inactivation.
b) The most intense *X-eGFP(+)* cells from a PGC-LC induction from day2 Epi-LCs are sorted after 12H of culture and stained for the master X-inactivator LncRNA *Xist*. Cells showing nascent transcription or a full cloud of *Xist* signal have undergone X-inactivation.
c) Fully X-inactive, differentiated, *X-eGFP(-)* MEFs are stained as a positive control for the master X-inactivator LncRNA *Xist*. Cells showing nascent transcription or a full cloud of *Xist* signal have undergone X-inactivation.

within the cells before being subjected to the PGC-LC differentiation protocol.

All the former results lead us to conclude that *in vitro* PGC induction with cytokines produces *bona fide* X chromosome reactivation of female PGC-LCs, in a time-dependent fashion. This can be readily observed when the X-inactivation status is monitored, from the naïve pluripotency X-active status present in the starting ESCs, to their genic X-inactivation after 1 day of embryoid body differentiation, and the X-specifc reactivation in PGC-LCs, from the partial genic reactivation of day 4 PGC-LCs, to the full genic reactivation at day 7 of culture **(FIG.11a&b)**. We infer that this process is probably driven by PGC induction cytokines, as the germ cells spontaneously differentiated in the negative control embryoid bodies are more X-inactivated, and is specific to PGC-LCs, as the remainder cells arising from PGC induction (Soma) are X-inactive **(FIGs.1-3).**

We have demonstrated that this reactivation phenotype is not inhibited by prolonged Epi-LC differentiation (**FIG.11a** & **FIG.11b**), and that it starts from a homogeneously inactivated population. We confirmed this both for the span of the X chromosome (FACs analysis and allele-specific expression of multiple loci) as well at the single cell resolution level (*Xist* RNA-FISH).

With our optimization of the *in vitro* PGC-LC-system for the investigation of X-inactivation and X-reactivation, we provided here the ground work enabling further studies on the detailed assessment of the kinetics and spread of X-chromosome reactivation in the germ cell lineage using high throughput technologies such as allele-specific RNA-SEQ & ChIP-SEQ.

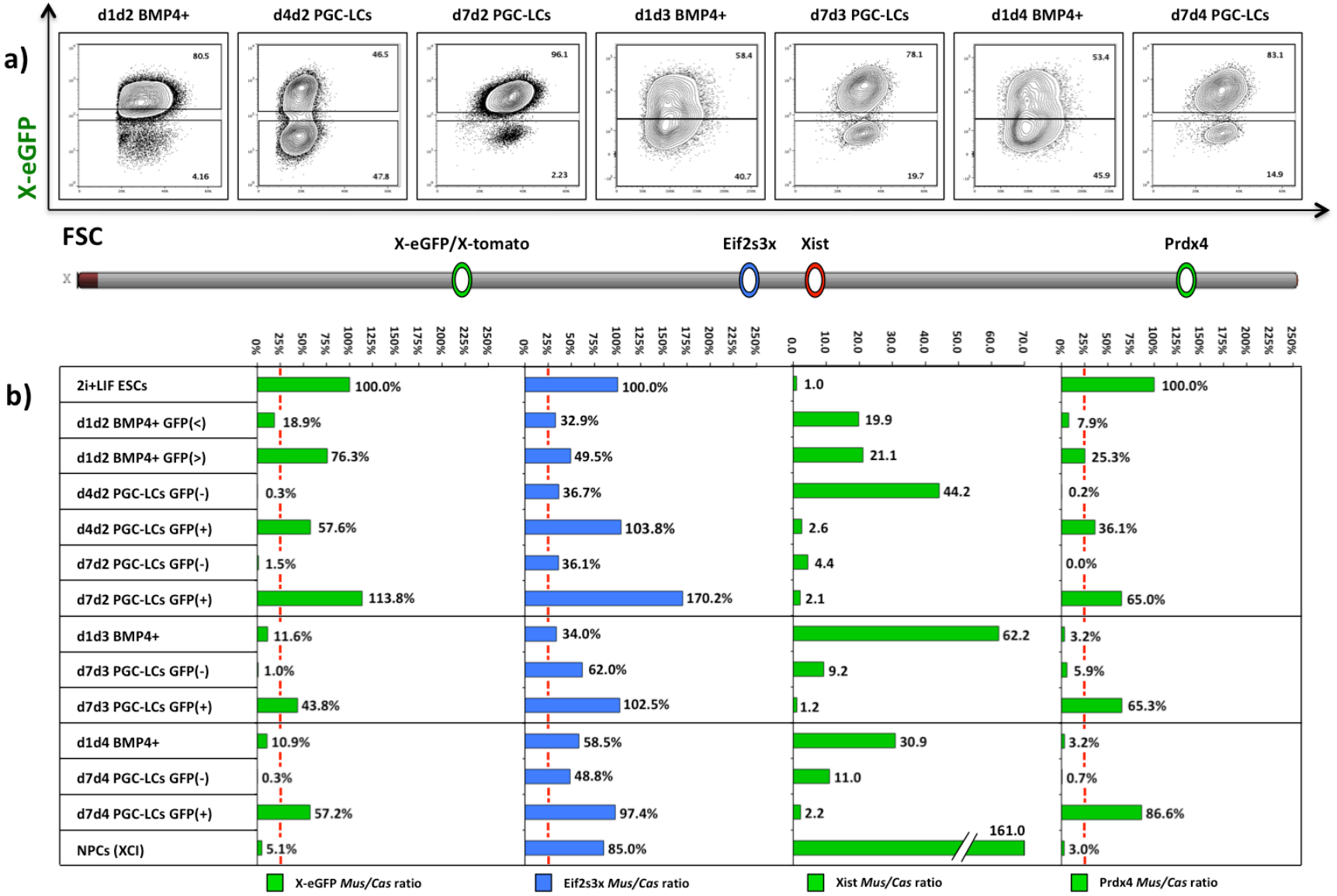
a)
d1d2 BMP4+
d4d2 PGC-LCs
d7d2 PGC-LCs
d1d3 BMP4+
d7d3 PGC-LCs
d1d4 BMP4+
d7d4 PGC-LCs
X-eGFP
80.5
4.16
46.5
47.8
96.1
2.23
58.4
40.7
78.1
19.7
53.4
45.9
83.1
14.9
FSC
X-eGFP/X-tomato
Eif2s3x
Xist
Prdx4
b)
2i+LIF ESCs
d1d2 BMP4+ GFP(<)
d1d2 BMP4+ GFP(>)
d4d2 PGC-LCs GFP(-)
d4d2 PGC-LCs GFP(+)
d7d2 PGC-LCs GFP(-)
d7d2 PGC-LCs GFP(+)
d1d3 BMP4+
d7d3 PGC-LCs GFP(-)
d7d3 PGC-LCs GFP(+)
d1d4 BMP4+
d7d4 PGC-LCs GFP(-)
d7d4 PGC-LCs GFP(+)
NPCs (XCI)
100.0%
18.9%
76.3%
0.3%
57.6%
1.5%
113.8%
11.6%
1.0%
43.8%
10.9%
0.3%
57.2%
5.1%
100.0%
32.9%
49.5%
36.7%
103.8%
36.1%
170.2%
34.0%
62.0%
102.5%
58.5%
48.8%
97.4%
85.0%
1.0
19.9
21.1
44.2
2.6
4.4
2.1
62.2
9.2
1.2
30.9
11.0
2.2
161.0
100.0%
7.9%
25.3%
0.2%
36.1%
0.0%
65.0%
3.2%
5.9%
65.3%
3.2%
0.7%
86.6%
3.0%
X-eGFP Mus/Cas ratio
Eif2s3x Mus/Cas ratio
Xist Mus/Cas ratio
Prdx4 Mus/Cas ratio

Figure 11: *In vitro* PGC-LCs undergo X-reactivation from an initial X-inactivation state, dependent on the time of cell culture in cytokine PGC induction media:

a) *In vitro* PGC-LCs are induced from day 2 (d1-7d2), 3 (d1-7d3) & 4 (d1-7d4) Epi-LCs. After 1, 4 or 7 days of cell culture, *X-eGFP*(+) & (-) PGC-LCs are FACs-sorted when appropriate and their genic X-inactivation status assayed by allele-specific RT-PCR.

b) Allele-specific expression of the X-inactivation marker genes *X-eGFP & Prdx4* (in green) ,the X-inactivation Escapee gene *Eif2s3x* (in blue) and the X-inactivation LncRNA master regulator *Xist* is assayed by RT-PCR. The expression from each allele is normalized to X-active ESCs levels, then the ratio between *musculus* and *castaneus*-linked expression is calculated. If a cell *musculus/castaneus*-linked ratio value is below 25% (Red bar), the locus is monoallelically expressed and subject to X-inactivation.

Discussion & Global Conclusions:

The question is why *in vitro* female PGC induction with cytokines always resulted in X chromosome reactivation in our hands? Seemingly, this contradicts all preexisting reports, both *in vivo* (Hu, Peter K. Nicholls, et al. 2015; Chuva De Sousa Lopes et al. 2008; Sugimoto & Abe 2007) and *in vitro* (Katsuhiko Hayashi et al. 2012), in which PGCs are specified in a fully X-inactive fashion, start some measure of slow X-reactivation as they close in with the developing gonad (Sugimoto & Abe 2007), and only undergo X-reactivation as they invade the sexually differentiating gonad. The gonadal somatic cells, which drive germ cell X-reactivation through a diffusible ligand (Chuva De Sousa Lopes et al. 2008) also need to be of XX female sex, as both male and feminized *sry* knockout male gonads fail to elicit the X-reactivation phenotype. Reactivation of the bulk of X-linked genes coincides with the onset of female germ cell meiosis, and reaches its zenith in the early stages of oogenesis (Sugimoto & Abe 2007; Deuve et al. 2015) While there is evidence for incipient, and apparently cell autonomous initial phase of X-chromosome reactivation in PGCs, which involves downregulation of Xist, loss of the H3K27me3 spot and reactivation of some X-linked genes (Sugimoto & Abe 2007). completion of the X-reactivation process is dependent on somatic signals, once PGCs enter into the female gonads.

Also, the first characterization of *in vitro* female PGC-LCs able to yield offspring

seemed to support this view. In this study, the Epi-LCs were differentiated for 2 days, and then the X-activity of the PGC-LCs was interrogated through H3K27me3 spot analysis. This showed that the virtual entirety of the population showed H3K27me3 spot after 24h of differentiation, which was slightly reduced in PGC-LCs after day 3 of culture. The cells were then immediately sorted according to their expression of *Blimp1-eGFP* reporter for this germ cell differentiation gene, and aggregated with somatic cells from the female E11.5 gonad in new embryonic bodies. The germ cells then lost their H3K27me3 spot signal after 4 days of gonad co-culture, at the same time they started to undergo the first steps of meiotic prophase. (Katsuhiko Hayashi et al. 2012).

While these observations seemingly state in a clean-cut fashion that *in vitro* PGC-LC induction cannot support X-reactivation on PGC-LCs on its own, our own results show that H3K27me3 spot and transcriptional activity of X-linked genes can be unlinked, as our results on day 2, 3 & 4 Epi-LCs X-inactivation kinetics has shown. Moreover, the use of *Blimp1-eGFP* reporter allowed for an earlier PGC-LC sorting than we were able, due to the limitations of CD61 surface marker to 4 days of culture as the earliest timepoint available, and we already have shown that as much as 50% of the PGC-LCs are X-inactive after 4 days of culture, and the remainder was midway through their gene reactivation process.

Taking into account these observations, we predict that culture of the same PGC-LCs for 7 days, as we do, would result in H3K27me3 spot erasure.

We thus consider that, in fact, the seemingly complete X-chromosome inactivation seen during PGC-LC culture is in fact an artifact of the readout method, and that H3K27me3 spot signal alone cannot be used as a proxy for X-linked gene inactivation, particularly at the early stages of the process.

We speculate that the PGC-LCs described by Hayashi *et al.* might have been equally X-reactivated as ours, and that the conclusions from the H3K27me3 spot could be misleading in this context.

Historically, both H3K27me3 spot & *Xist* RNA-FISH analysis have often been used as a main proxy readout for X-inactivation as allele-specific analysis of gene inactivation

is technically more challenging and either involves gene-specific RNA-FISH or requires the availability of *musculus/castaneus* mixed strain backgrounds when using sequencing-based methods. In order to get a more defined view of the different aspects of X-inactivation and X-reactivation during early embryo and germ cell development, more and more studies involving allelic analysis of X-activity are recently emerging .

What is the driving force behind X-chromosome reactivation? We propose that the cytokines used in the induction media (LIF, BMP4, SCF & EGF) might play a direct or indirect role in X-chromosome reactivation. There are 2 known instances of X chromosome reactivation *in vivo*: the epiblast of the blastocyst embryo and the germ cells upon gonad entry. In the epiblast, X-reactivation takes place presumably to allow random X-chromosome inactivation upon differentiation, and in germ cells to allow meiotic recombination and proper segregation of the X during meiosis. It is not implausible then to think that the signaling molecules enforcing epiblast and germ cell X-reactivation may be the same. The LIF, SCF & BMP4 signaling molecules are well known to activate signaling pathways enforcing naïve, X-active pluripotency in ESCs & iPSCs (**QUOTE)**, which correspond to the *in vivo* E4.5 epiblast.

These very same molecules are diffused across the whole ICM, but so do other signaling axis as Wnt3, ActivinA & FGF family ligands, which promote cell differentiation and X-chromosome inactivation (Schulz 2017), and Retinoic Acid (RA), with the same differentiation effects, is also present in high concentrations **(QUOTE)**. It is the formation of a local zone in the posterior postimplantation epiblast, in which LIF & BMP4 signaling is protected from the aforementioned differentiation pathways by BMP8, secreted from the extraembryonic ectoderm (ExE) and stimulated by Wnt signaling (specifically, Wnt3) that leads to *in vivo* PGC specification between E6.5 & E7.5 (Ohinata et al. 2009).

The *in vitro* PGC-LC induction protocol (Hayashi et al. 2011a) actually resulted from this analysis & characterization of the *in vivo* signaling context, then reduced to the absolute minimum number of factors necessary. The authors of the original report were well aware that the signaling molecules characterized *in vivo* were not enough to fully account for the speed of specification and proliferation of *in vivo* PGC-LCs (Ohinata et

al. 2009), and the *in vitro* PGC-LC induction protocol cytokines were an even more restricted subset (Hayashi et al. 2011a). Further development of the protocol showed that even BMP8 was dispensable for *in vitro* cytokine PGC-LC induction as the visceral endoderm is absent (Nakaki et al. 2013b), and it is this variant that we have used for all PGC inductions.

Suspiciously enough, the Retinoic Acid, a major meiotic inducer produced by the female gonad, has been repeatedly discussed and put forward as the major missing signaling factor to raise the cytokine-driven *in vitro* PGC induction efficiency and proliferation rates to those seen *in vivo* **(QUOTE)**.

This is further supported by the fact that a recent report has shown that Epiblast Stem Cells (EpiSCs), which model the differentiating epiblast and underwent the first stages of X-Chromosome inactivation, undergo X-reactivation when exposed to the same core cytokines of PGC induction media (LIF & BMP4)

, after exactly 7 days of exposure and at a 10-fold lower concentration than in the *in vitro* PGC induction protocol (Kime et al. 2016).

The signaling molecules of *in vitro* PGC induction protocol are functionally divided in two classes: the core cytokines (LIF & BMP4) that are necessary for PGC fate acquisition, and the accessory cytokines (SCF, EGF) that are necessary for robust proliferation and expansion of PGC-LCs. These same signaling molecules are also expressed in the migration path of the PGCs *in vivo* as guiding morphogens and into the sexually differentiating female gonad at E10.5-11.5. The LIF soluble ligand is expressed in the entire migration path alongside the SCF ligand, which in both its membrane-bound and soluble forms is responsible for the survival and migration of *in vivo* PGCs . It is of note that those ligands are used as a checkpoint to ensure proper PGC migration – a wave of downregulation of those ligands expression sweeps the migration path, and all PGCs that are not invading the developing gonad die. This phenomenon is interpreted as a safeguard against carcinogenic processes, as PGCs which mis-localize and don´t invade the gonad invariably give rise to teratomas (Leitch et al. 2013). Suspiciously enough, these ligands expression coincides with the first

stages of *in vivo* X-chromosome reactivation in migrating PGCs, as described in (Sugimoto & Abe 2007).

In addition to LIF & SCF, the developing female gonads also express high levels of BMP morphogens, Wnt ligands and Retinoic Acid. The BMP2, 4, 5, 7 & 15 ligands are expressed at high levels in the developing gonad, and have been proposed as major drivers of late female meiotic progression and follicle growth, which has been described as the stage in which X-reactivation peaks (Deuve et al. 2015). Meanwhile, Retinoic acid is the most well known factor triggering female sexual differentiation, by its critical role in the female Vs male *Sry/Sox9* differentiation pathway, as well as being the most well-known meiosis inducer up to date (Windley & Wilhelm 2016)

Both Retinoic Acid & BMP15 are key signaling molecules that have enabled the first mature *in vitro* oogenesis protocol (Hayashi et al. 2017a). Those oocytes can give rise to offspring and show all features of *in vivo* oocytes…. and necessarily, X-reactivation, as otherwise those cells wouldn´t be viable, lacking X-linked gene dosage. This would be in accordance with recent research showing that *in vivo* female mouse Oocytes undergo X-reactivation at those stages. (Sugimoto & Abe 2007; Deuve et al. 2015)

Wnt4, in addition to IGF1, has been recently characterized to be differentially expressed in female gonads, in which it cooperates with Retinoic acid at E11.5-12.5 in order to drive the female sexual differentiation of the gonad vs. the male pathway (Windley & Wilhelm 2016) - the exact timing at which the female XX somatic gonad has been shown to produce molecules, which promote X-chromosome reactivation in PGCs (Chuva De Sousa Lopes et al. 2008). The interesting part is that the male gonad sexual differentiation at the same developmental stage is controlled by the expression of ActivinA & bFGF ligands, conspicuous drivers of X-inactivation (Schulz 2017), as well as the exhaustive suppression of Retinoic Acid production (Windley & Wilhelm 2016). It becomes more interesting when considering that coincident Retinoic Acid & Wnt4 signals in the adult testis have been recently shown to be the driving force in the start of male meiosis and spermatogenetic differentiation, their oscillatory patterns explaining the cause of the wave-like pattern of spermatogenesis across the male seminiferous tubules (Mark et al. 2014)

Another ligand family involved in sexual differentiation in the E10.5-12.5 gonad is

Hedgehog (Windley & Wilhelm 2016). Interestingly, a recent report has shown how Sonic & Indian hedgehog ligands (HH) are produced in the E4.5 ICM, ESCs & iPSCs, where they upregulate the expression of the X-activator *Tsix* lncRNA through a signaling cascade, resulting on *Tsix* expression and *Xist* silencing through GLI transcription factors(Del Rosario et al. 2017). The structure generating HH signals is the visceral endoderm .The similarity between the visceral endoderm & the gonad specification is not limited to the fact that they produce many of the same signaling molecules; both of them are specified by the same master transcriptional regulator, GATA4 **(QUOTE)**(Windley & Wilhelm 2016).

We have shown supporting evidence for a shared signaling substrate driving X-reactivation in E4.5 epiblast & in PGCs as they invade the female meiotic gonad at E10.5-12.5, and we suggest that those signaling ligands will yield verifiable X-reactivation phenotypes when supplied to the X-Inactive transgene-induced *in vitro* PGC-LCs system. But if the recipe for *in vitro* PGC-LC cytokine induction does induce reproducibly X-reactivation, what are the signaling molecules that ensure that *in vivo* PGCs are X-inactivated from their specification at E7.25 until they reach the female meiotic gonad, and block X-reactivation in male and *Sry*-knockout feminized male gonads? I propose that the reason is that *in vivo* PGCs are exposed to a cocktail of X-inactivating and differentiating cytokines, which are absent in the *in vitro* cytokine induction protocol. Moreover, the expression of these same X-inactivating cytokines is shared with the male gonad sexual differentiation, were they drive male germ cell fate and inhibit meiotic progression. It might be the specific effect of this male-specific expression of the X-inactivating cytokines that inhibits the expression of meiosis-related cohesin complexes, transcription factors and other effectors that drive X-reactivation in both female epiblast and meiotic E12.5 germ cells.

In the gastrulating embryo, the *in vivo* PGCs are specified in the posterior epiblast. As the *in vivo* PGCs are exposed to the PGC-enhancing signaling of LIF, BMP2, BMP4, SCF & EGF, they do so in an environment in which the signaling cytokine balance has shifted towards cell differentiation and X-inactivation. The whole epiblast is subject to Wnt3 signaling, which enhances PGC differentiation competence, but is also a main

driver of X-inactivation. The Wnt & FGF paracrine pro-differentiating ligands, previously overcome in the epiblast by naïve pluripotency enhancing signaling, becomes predominant during differentiation, helped by Activin A signaling(Schulz 2017). The combined Wnt, FGF & ActivinA signaling drives downregulation of the core naïve pluripotency transcription factors, while Patched transmembrane signaling directly impacts the X-inactivation locus by downregulating the Hedgehog-driven transcription of X-activator *Tsix* (Del Rosario et al. 2017), allowing expression of the master X-inactivator *Xist* lncRNA(Tan et al. 2016)⁹³**(Tan et al. 2016)³⁷**. This X-inactivation process is helped by the generalized down-regulation of core naïve pluripotency factors, while additional signaling molecules like Nodal & Lefty become expressed. The combination of BMP8, Nodal & Lefty at E6.5 in the posterior epiblast would negate the differentiation effect of Wnt, FGF and Activin A and allows LIF, BMP2, BMP4, SCF & EGF to induce enough expression of core naïve pluripotency and germ cell transcription factors to drive germ cell specification and proliferation (Ohinata et al. 2009). However, the Wnt, FGF, and Activin A signaling, in combination with Nodal & Lefty, might be enough to ensure X-inactivation of *in vivo* PGCs. The X-inactivation is further compounded and enforced by the action of Integrins and other cell-to-cell contact pathways as Patched; as the naïve-supporting ligand expression disappears and the PGC-LCs move from the specification site, only differentiating cues are available and they are exposed to the mechanical stresses of gastrulation and migration, which are known to be transmitted through Integrin signaling. Integrin signaling is known to promote cell polarization, which is directly at odds with pluripotency **(QUOTE)**. The X-inactivation effect should be far stronger on *in vivo* PGC specification than it is on cytokine *in vitro* PGC-LC induction protocol: While the Epi-LCs in the protocol are differentiated as low-confluence 2D monolayers which lack Wnt3 signaling and the cell-to-cell contacts of Integrin and other mediators, the *in vivo* differentiating Epiblast gets Wnt3 presence, strong-cell-to-cell contacts as in an embryoid body & polarity-enhancing signals as Integrin, as well as being exposed to multiple ligands absent in the *in vitro* protocol, such as Nodal & Lefty. The continued action of Integrin and other cell-to-cell contact cues, in addition to the general pro-differentiation signaling cues is probably enough to keep *in vivo* PGCs X-inactive until they reach the proximity of the developing female gonad.

The proposed effect of cell polarization is crucial to explain my own results; in particular, how the aggregation of embryoid bodies for as few as 24H is able to drive sweeping genic X-Inactivation on all loci probed, regardless of the Epi-LC differentiation time. While the stimulation of X-Inactivation upon embryoid body formation is expected, its speed was surprising to us. One may question how this occurs, as *Xist* spreading upon ectopic overexpression is of the few phenomena of X-inactivation reported to take place in such short amounts of time, and our precursor Epi-LC Cells are already coated with a full *Xist* cloud and H3K27me3 spots in most instances, particularly for day 3 & 4 Epi-LCs, without showing full genic X-inactivation. This may be due to the extended half-life of X-linked mRNAs detected by our qPCR assay even after X-linked gene inactivation. Alternatively, other aspects of X-inactivation could be the main drivers of genic X-inactivation, like changes in 3D-chromatin structure or the acquisition of a specific X-inactivating chromatin configuration like for example histone deacetylation, DNA-methylation or incorporation of macroH2A upon embryoid body formation.

Another possibility is that a similar dynamic as HnRNPu or YY1-mediated *Xist* coating occurs, in which a X-inactivation factor protein has recruited silencing machinery and complexes, ready to enforce X-inactivation, but the localization signal to the inactivating X chromosome has not occurred yet. Upon the addition of proper cues (embryoid body formation), this required signaling cue is met and the pre-assembled silencing complexes are deposited on the inactivating X, where they enforce full genic X-inactivation.

It is interesting to note that a similar phenotype has been described for lymphocytes, in which partial X-reactivation in naïve B & T Lymphocyte progenitors is reversed as they are immunologically activated. This process is mediated by *Xist* cloud re-localization to the inactive X, and takes only 24H (Wang et al. 2016; Syrett et al. 2017). While our situation is very different, as the inactivating X is already coated by a full *Xist* cloud and has a H3K27me3 spot, it should be noted that a series of screenings have identified over 200 proteins binding to the mature *Xist* transcript **(QUOTE)**, and screening for XCI-factors has yielded a number of factors involved in X-inactivation which could produce

such sweeping changes in response to the polarization and mechanical cues of embryoid body formation (Bhatnagar et al. 2014; Sripathy et al. 2017a; Lessing et al. 2016). Besides the expected chromatin modifier enzymes, a great deal of them were factors involved in signaling, DNA replication, chromatin condensation complexes and mitotic kinases. It should be noted that the culmination of X-inactivation process is associated with the late replication of the X chromosome and its shuttling to an inactive, peripheral nuclear compartment **(QUOTE)**. It has been recently shown that DNA replication is a sweet spot in which chromatin gains accessibility, and in which the daughter DNA molecule can be given completely different epigenetic modifications than its parent strand. This observation directly explains how pluripotent stem cell *in vitro* differentiation towards other cell types occurs in "bursts" after transcription factors bind and transcribe differentiation genes immediately after replication, imparting euchromatic marks upon them as a consequence **(QUOTE BARCELONA CONGRESS)**, and how large multicopy transgenes get reactivated or silenced in the *C. elegans* germline in the span of a few cell divisions. In a recent report, K. Reis *et al.* showed how replication timings of DNA could shift the chromatin context to euchromatic (early replication) or heterochromatic (late replication) depending on the timing of DNA replication. Even more interesting was the demonstration that euchromatic context and gene reactivation could be achieved within one single cell division, and the key to it were DNA replication cofactors whose function (and loss of it) directly impacted the speed of DNA replication (Reis 2016)**(REPLACE UPDATED QUOTE)**.

The former screened XCI-factors, biased towards mitotic and signaling Kinases and DNA replication factors, combined with the replication timing provide a possible explanation on how X-inactivation can be completed in the span of only 24 hours. As the embryoid body formation provides polarity cues previously absent, the Integrin and other cell-contact based signaling pathways activate and transduce through the preexisting signaling kinases. Those could activate the translocation to the inactivating X chromosome of already pre-assembled silencing protein complexes, which weren´t having any effect on X-inactivation due to the lack of a localization cue. A series of DNA replication cofactors might also be relocated to the X, where they drive the latter, long replication timings of the inactive X chromosome.

The combination of late replication timing combined with the relocation of additional heterochromatin mark writers to the inactivating X in a coordinated fashion in 3D embryoid bodies allows for a fast, sweeping X-inactivation that the 2D monolayer Epi-LCs cannot match. Cells differentiated in 2 D might only access some of the heterochromatin epigenetic writers and resources, as they lack a significant part of their X-inactivator signaling and cell polarity cues that their *in vivo* counterparts can access. I would like to propose this interpretation as the "replication & combined arms" hypothesis.

As such, its is probable that the Epi-LC differentiation process at 48H, with only 20% of H3K27me3 X-inactivation spots, might reach the X-Inactivation kinetics seen on *in vivo* E6.5 epiblasts, which have 100% H3K27me3 X-inactivation spots, if they were differentiated with additional Wnt3 & Retinoic Acid signals in a 3D embryoid body context.

Our findings on the fast X-inactivation after 24H embryoid body formation opens an excellent platform for exploring the signaling pathways driving X-inactivation, and the ways silencing complexes are recruited to the inactive X. By modulating and comparing the speed of X-inactivation of Epi-LCs differentiated from pluripotent stem cells as a 2D monolayer Vs the 3D embryoid body, the basis of the signaling pathways behind differential X-inactivation speed can be compared. It would be possible to compare embryoid bodies against non-aggregated Epi-LC parent cultures after 24H, and assess which known Epigenetic writers & XCI-factors are differentially present on the inactive X chromosome, as well their differential gene transcription to identify XCI-factors involved. It would also possible to test which are the stockpiled factors that will provide the X-inactivation silencing burst. A timeline of Epi-LC differentiation for increasingly long times can be performed, and then the X-inactivation measured after 24H of embryoid body formation. The RNA-SEQ analysis of transcription from timings that can sustain the accelerated X-inactivation burst from the ones that cannot would allow the identification of the XCI-factors involved. It would also be possible to use small molecule inhibitors against the signal transduction cascades of the candidate XCI pathways, supplied in the media of embryoid body formation. After 24H and 3 days of embryoid body formation, the extent of X-inactivation could be compared against untreated controls. Long-lasting impairments of XCI kinetics, coupled with RNA

expression analysis from X-active-GFP(+) and X-inactive-GFP(-) cells would indicate that the signaling pathway is involved in X-chromosome inactivation, and RT-PCR of genes involved in the differentiation of the 3 germ cell layers against untreated controls could help confirm that it is not a cell differentiation impairment.

The other important question is the relationship between cell cycle stage and genic silencing. By my "replication & combined arms" hypothesis, a burst of deposition of silencing marks and genic X-inactivation should occur immediately after X-linked DNA replication. By monitoring nascent transcription from synchronized cell populations during Epi-LC differentiation immediately after DNA replication vs the interphase, it should be possible to know whether the genic X-inactivation speeds up in a DNA-replication linked fashion, or not. An even speed of genic silencing would indicate that the replication-mediated silencing is untrue, while bursts of inactivation after DNA replication would validate it.

We consider that our results describe, to the best of my knowledge, the speed of this genic X-inactivation burst for the first time. While the aggregation in embryoid bodies has been known to speed up pluripotent stem cell differentiation **(QUOTE)**, their formation from *in vitro*-induced Epiblasts may be the cause of this extremely fast X-inactivation, probably because the cell differentiation starts from a homogenous cell population primed for differentiation into the three germ layers. Our model system with hybrid *castaneus/musculus* pluripotent stem cell lines and the subsequent embryoid body formation from *in vitro*-induced Epi-LCs allows the throughput & affordable cost per assay to screen against the signaling, effectors & dynamics of the X-inactivation burst after embryoid body formation.

The former description may explain how the *in vivo* PGCs reach their X-inactive status after specification, but not how male and *Sry* knockout-feminized male gonads are unable to drive X-inactive *in vivo* germ cell X-reactivation, both on our own results and previous reports (Chuva De Sousa Lopes et al. 2008; Emmanuela Greco 2016; Severino

2018).

In vivo germ cells encounter X-reactivating cues from E10.5-E12.5. This timespan roughly encompasses the separation of the somatic gonad from the adrenocortical primordium to the timing of sexual female vs male differentiation gonad differentiation switch (Hu, Peter K. Nicholls, et al. 2015; Nef et al. 2005; Pitetti et al. 2013). We analyzed the known expression profile of signaling ligands expressed from the gonad, and which signaling ligands are differentially expressed in the male vs female gonad. Analysis of available bibliography showed two interesting facts. The first was that virtually all signaling ligands and pathways expression was shared between both sexes, from the adrenogonadal precursor specification at E9.5, to the E12.5 switch between female and male gonad sexual differentiation programs; the difference is which ligands are differentially expressed between the female and male sex.

The gonads arise from a common precursor, the adrenogonadal primordium, at E9.5. The signaling molecules Wnt4, RSPO1, & IGF family ligands drive the differentiation and proliferation of somatic gonadal cells. At E10.5, in XY gonadal cells, the combined signaling will result in the upregulation of a MAP kinase signaling cascade, and the upregulation of the critical gonad master transcription factor, GATA4. It is at E12.0-12.5 that the sexual differentiation switch, and the change of the signaling balance occurs. In males, GATA4 will bind to the promoter of the Y-linked male sex determining gene, *SRY*. The SRY transcription factor will drive expression of Sox9, which will coordinate the male-specific signaling activities. In addition to initiating the cascade, p38MAPkinase will coordinate the male-specific degradation of Retinoic Acid in the testis by inducing expression of the Retinoic Acid-degrading enzyme CYP26B1 in the male somatic gonadal cells. This enzymatic activity is enough to degrade any external supply of Retinoic Acid, ensuring that male germ cells do not enter meiosis (Windley & Wilhelm 2016). The end result is the male-specific expression of Nodal & Lefty, as well as ActivinA & FGF signaling and the complete absence of Retinoic Acid signaling. Some ligands of the Wnt family will also show a male-biased expression. This male-specific signaling environment serves one main purpose: it specifically suppresses the onset of meiosis on male germ cells and makes them exit the cell cycle, staying quiescent in a mitotic arrest. Moreover, the suppression of meiosis is entirely dependent on the continued signaling input from the male-overexpressed ligands: if the

Activin Receptor type 1B gene or the *SMAD2* gene function is eliminated, the male germ cells enter meiosis precociously. The reason is that Activin Receptor type 1B transduces the Activin & Nodal ligand signals, and SMAD2 associates with SMAD4 to transduce signals from Activin ligands. Moreover, if p38MAPkinase function is lost, so is the male-specific CYP26B1 enzyme activity. The Retinoic Acid signaling ligand is then not degraded, and the male germ cells enter meiosis immediately. In addition, even if the knockouts on female or male signaling activities are performed later in gonad development, the need for a male/female specific signaling remains; if the signaling cues are altered, the female oocyte-supporting granulosa cells can transdifferentiate into sperm-supporting male Sertoli cells, and vice-versa. This is effect is thought to be a relic of the sexual phenotype switches that the teleost ancestors of mammalians were able to perform, and which influenced posterior organogenetic processes. (Windley & Wilhelm 2016).

It is interesting to note that previous screens for XCI-factors identified the Activin receptors Alk2 & 4 and their downstream signal transduction effectors SMAD2 & 4 as key signaling inputs maintaining the X-inactivation status in differentiated cells. If these genes are interfered with, even somatic cells with a strong locked X-inactivation phenotype undergo X-reactivation. Those screens also identified the TGF-Beta signaling superfamily (which includes Activins & BMPs*)*, and specifically, BMP2, as XCI-factors. The PI3K/AKT signaling pathway, involved in such prominent fields as pluripotency or cell polarization, was also involved. In all cases, the downstream signaling of TGF-beta signaling was performed through SMADs 2, 3 & 4*,* which completely overlaps with the male-specific signal transduction cascade (Sripathy et al. 2017a; Bhatnagar et al. 2014; Lessing et al. 2016; Windley & Wilhelm 2016).

On the other hand, the female gonads, in the absence of Y-chromosomal *Sry* male-determining gene, never upregulate the Sox9 transcription factor, and, consequently, are dominated by high levels of Wnt4 & RSPO1 ligand expression. In combination with high levels of FST, which suppresses the Activin signaling effects, those drive the overexpression of BMP family ligands. The fact that female somatic gonadal cells do *not* produce CYP26B1 enzyme allows the Retinoic Acid produced by the mesonephros

to diffuse into the gonad and, in combination with the aforementioned female-determiner cytokines, start meiosis.

The signaling pathways enforcing the meiotic development of female germ cells, and X-reactivation can now be studied directly with since the recent development of *in vitro* protocols for PGC expansion and early meiosis in gonad cell-free cultures (Ohta et al. 2017a; H. Miyauchi et al. 2017). Thanks to the defined quality of this media, it has been possible to learn several interesting facts. With the use of pharmacologic drugs that mimic the effects of LIF & SCF signaling, *in vitro* female PGC-LCs can sustain proliferation up to 7 days in culture, in a DNA-demethylated state similar to E10.5 *in vivo* germ cells. This stage corresponds to gradual H3K27me3 spot erasure, and, presumably, X-reactivation *in vivo* (Ohta et al. 2017a).In a later step, Retinoic Acid upregulates Stra8, and BMPs 2,4 & 7 induces a different subset of meiosis genes and allowing meiosis prophase to take place. Importantly, all BMPs, 2,4, & 7 tested drive their effect by the signaling receptor heterodimer formed by BMPRII & Alk3, and transduce their signals through SMADs 1, 5 & 8. It should then be noted that all the BMPs above can drive meiotic initiation, and that while BMP2 is the most efficient at it, BMP4 can drive it effectively too (H. Miyauchi et al. 2017). This would explain our own results with cytokine *in vitro* PGC-LC induction – we are supplying our cells a demonstrated meiosis inducer with X-reactivator activity without any compensator X-inactivating signaling pathways to counteract it.

As such, I postulate that the male-specific gonad signaling ligands are the same that drive the X-inactivation and differentiation in the early female epiblast and lock X-inactivation in somatic cells, while the female-specific gonad signaling ligands are the same that drive naïve pluripotency & X-reactivation in the ICM, as well as specifying the PGCs in the E6.25-E7.5 posterior epiblast. The shared gonad signaling activities are Wnt4, RSPO1 & IGF family ligands that drive the E9.5 gonad specification. The next critical signaling input is the appearance of LIF & SCF, which drive & guide the PGCs to the gonads at E10.5, which coincides with DNA methylation erasure. It is at this point that dominant signaling activities drive either the male or female fate. The male signaling context arises from the overexpression of ActivinA & FGF, as well as Nodal

& Lefty and the complete absence of Retinoic Acid signaling. Some ligands of the Wnt family are also present, which ties to the Wnt3 pro-differentiating cues present in the Epiblast. In general, the above stated signaling activities mainly rely on p38MAPkinases, and, more importantly, on SMAD2, and less clear contributions of SMADs 3 & 4 in their signal transduction cascade (Windley & Wilhelm 2016). This largely overlaps with the signal transduction cascade of known X-inactivation promoting factors, except from the PI3K/AKT axis (Sripathy et al. 2017a; Bhatnagar et al. 2014; Lessing et al. 2016). The female signaling context arises from the predominant expression of Wnt4 & RSPO1, which are joined by FST to block Activin signaling & other pro-male pathways. As the PGCs invade the female gonad, strong Retinoic Acid signaling and BMP2, 4, 5 & 7 ligands collaborate to drive the meiotic prophase and progression of X-reactivation. Finally, the collaboration of Retinoic Acid, GDF9 & BMP15 drives *in vitro* oogenesis, during which germ cell X-reactivation is completed (Sugimoto & Abe 2007; Deuve et al. 2015).

I propose that the signaling pathways driving naïve X-activity in the blastocyst epiblast, PGC specification & later X-chromosome reactivation are the same, using the same BMP, Retinoic Acid and naïve pluripotency cytokines (LIF, SCF, HH), some of which might have their expression driven by the same master regulator (GATA4) in both visceral endoderm and E10.5-12.5 female meiotic gonad. Critically, the TGF-Beta signaling pathway superfamily would be the determinant of X-activity status, both for X-reactivation & X-inactivation phenotypes, with BMP signaling being the shared core enforcer of X-activity, be it X-reactivation or X-inactivation. The BMP signaling input is transduced into enforcing X-inactive status (concordant to previous XCI-factors research (Bhatnagar et al. 2014; Przanowski et al. 2018)), or X-reactivation, as our own results support, by the use of exclusive sets of receptors and signal transducers and integration of the surrounding signaling pathway activity. When BMP signaling is predominant, and takes place in a naïve pluripotency/pro-meiotic context, BMP ligands act through Alk 3-6 receptors and channel their signal transduction by SMADs 1, 5 & 8. This signaling effect is compounded by the presence of LIF, SCF & HH ligands, as well as per lipidic low-dosage Retinoic Acid & LPA ligands, and the PI3K/AKT signaling pathway. In the meiotic gonad, RSP01 also joins the X-reactivating signaling input,

while Wnt4 & FSH serve auxiliary roles by ensuring the overexpression of BMP receptors & the repression of the X-inactivating ActivinA signaling, respectively. This is how X-reactivation signaling could be enforced. In cases in which cell differentiation and X-inactivation must be predominant, Wnt3, FGF & ActivinA signaling cooperate to drive cell differentiation and X-inactivation. Either due to cell competence or through signaling-induced response, signaling cues from the TGF-beta superfamily are routed by Alk 1-2 receptors, as well as the SMAD 2 & 4 signal transduction cascade. This might ensure that any further BMP signaling input would follow this signaling pathway and won´t trigger ectopic X-reactivation in somatic differentiated cells. The signaling activities of Nodal & Lefty ligands help X-inactivation in the differentiating epiblast and the E10.5-12.5 gonad context, while High levels of Retinoic Acid in there might aid the random X-inactivation process. This model would explain how the BMP signaling pathway has been pointed both as an X-inactivation factor(Bhatnagar et al. 2014; Przanowski et al. 2018; Sripathy et al. 2017b) and an X-reactivator(Kime et al. 2016). I propose that the BMP signaling pathway may be a source for the X-chromosome counting system implied to act before random X-inactivation, and the rewiring of the BMP signaling pathway could act as an excellent opportunity to add a layer to the redundancy and robustness of X-inactivation mechanisms (Schulz 2017). The PI3K/Akt pathway, has equally been involved in both X-inactivation(Przanowski et al. 2018; Bhatnagar et al. 2014; Sripathy et al. 2017b) and reactivation(Kime et al. 2016), and accordingly, may have the same behavior as the BMP signaling pathway.

As a last argument, naïve, un-activated B & T lymphocyte precursors have been recently shown to undergo partial X-reactivation (Wang et al. 2016; Syrett et al. 2017). It is interesting to note that the germ cell fate specifier Blimp1 has been first discovered as a transcription factor involved in lymphocyte fate specification, and that lymphocytes have been recently shown to express some naïve pluripotency-associated factors like c-Myc **(QUOTE)**. While it may seem hard to relate this lymphocyte X-reactivation phenotype within the epiblast and in Germ cells, which happen in a pluripotent-related context, lymphocytes are actually very close in their needs to PGCs: they require a highly motile, migration-capable cell morphology; as highly tissue-invasive cells, they must be protected against tumorigenic processes, which the transcription factors and

control programs that share with germ cells reputedly excel at; and, at last, activated lymphocyte clones must remain dormant, yet ready to undergo fast clonal proliferation from a single cell while avoiding deviations that could compromise their function or result in autoimmunity. Indeed, it has been proposed that naïve B & T lymphocyte X-reactivation also serves the purpose of driving female-specific overexpression of the X-linked hotspot of immunity genes, which has been shown to happen as a consequence of lymphocyte X-reactivation (Wang et al. 2016; Syrett et al. 2017).

As such, all X-reactivation and inactivation phenotypes known may be explained by virtue of shared pluripotency, meiosis-enhancing signaling cues between the epiblast and the PGCs in their specification & gonad invasion, and all X-reactivating cell types (epiblast, PGCs) share a common core transcription factor regulator tied to the X-activity switch, Prdm14. Both the epiblast and the meiotic germ cells must face the same problem: they need to reactivate the inactive X chromosome from an inactive state. In case of the epiblast this might be needed to ensure that the alleles from both X chromosomes have an equal chance to be expressed in the tissues of the embryo in the ensuing random X-inactivation process **(QUOTE)**; the PGCs need an euchromatin environment without repressive epigenetic marks to allow meiotic recombination between the two X-chromosomes to take place **(QUOTE)**; and the lymphocytes greatly benefit for allowing bi-allelic expression of immunity genes from the 2 X chromosomes. In both epiblast and PGCs, an exhaustive erasure of the repressive epigenetic marks is necessary, as well as a highly accessible & decondensed chromatin. It might seem at first alien that naïve pluripotency and meiosis could be mediated by the same signaling, as meiosis is seen as a differentiation process. This view has been recently challenged by the discovery that cohesins and mediators of the synaptonemal bridge, first discovered as meiotic effectors, are actually key factors to sustain the 3D chromatin structure of naïve pluripotent cells **(QUOTE)**. Also, it has been discovered recently that the cells in the epiblast have the ability to initiate meiosis, and exposed to the signaling input to do so in their native niche; they are only prevented to do so by a repressive program held under a master regulator, *Max***.** Loss of function of this transcription factor leads to pluripotent cells spontaneously initiating meiosis, and this process is stimulated by the addition of Retinoic Acid (Suzuki et al. 2016).

In addition, PGC fate could only be considered different from pluripotent stem cell fate

in that PGCs are determined through the re-expression of core pluripotency factors shared with the naïve pluripotency network of the epiblast (and by extension ESCs & iPSCs), but those are carefully steered in PGCs by a set of pro-differentiation factors such as Blimp1, AP2-gamma & T-brachyury to avoid reversion to epiblast fate. A similar pluripotency reversion event can be forced in the laboratory by converting PGCs into Embryonic germ cells (EGCs), which revert to an X-active, naïve pluripotency from an X-inactive state (Chuva De Sousa Lopes et al. 2008; Durcova-Hills et al. 2008). Coincidentally, it is LIF, SCF & FGF-2 combination which drives the X-reactivation from PGCs – and LIF & SCF cytokines are part of our PGC induction media (Hayashi et al. 2011a; Nakaki et al. 2013b). As such, the proposed model may not only explain the *in vivo* ICM and Germ cell X-reactivation phenotypes, as well as their likely transcriptional effectors and their signaling substrate, but also the *in vitro* phenomenon of EGC X-reactivation. It also ties the observation that E10.5-12.5 male gonads are unable to drive X-reactivation and the signaling substrate involved in enforcing and maintaining X-inactivation across differentiated cell types, and is further limited and pinpointed to a series of receptors and signal transducers at a resolution precise enough to enable their experimental testing.

The discovery of the PGC-LC X-reactivation phenotype is an exciting finding, but one that the cytokine *in vitro* PGC induction is badly prepared to handle. As the maximal yield of X-inactive PGC-LCs in the protocol is 10^3 cells in the optimal setting for maximal PGC-LC yield and X-inactivation, it is difficult to obtain a pure X-inactive PGC-LC population of enough size to seed in culture with the candidate X-reactivator signaling molecules without an utterly prohibitive financial cost, given the cost of PGC induction cytokines. And it is not possible to eliminate part of the cytokines, as this would result in negligible PGC-LC yields, as it has been already shown (Hayashi et al. 2011a). What is feasible is to analyze the X-reactivation phenotype as considered from the day 1 X-inactive starting embryoid bodies, up to 4-7 days of germ cell culture. While this is promising and would allow the characterization of the *in vitro* PGC-LC reactivation phenotype, it would be difficult to track the early events involved in days 2 & 3 of germ cell culture, due to our current dependency on the CD61 surface marker. Also, the fact that PGC-LC fate and X-reactivation are dependent on the same molecules would bias conclusions towards a cell-autonomous reactivation phenotype,

instead of a signaling-molecule driven one and would make it difficult to tease apart signaling effects on germ cell fate or XCR directly.

Other coworkers in the lab have been involved in the screening of X-reactivator signaling molecules in PGCs, and in collaboration with them we confirmed the role of Retinoic Acid as an X-reactivator on in vivo X-inactive PGCs (Emanuela Greco and Jaqueline Severino, personal communications). This ongoing work shifted to the attempts into adapting the *in vitro* cytokine PGC induction protocol as a platform for X-reactivator molecule screening, as well as to characterize X-reactivation phenotype of Retinoic Acid in PGCs. The results I obtained showed how this system was unsuitable for this purpose. Upon obtaining them, I actively encouraged the generation of a new *X-eGFP* reporter transgene cell line, which implements the new *in vitro* PGC Induction with a transcription factor cassette (Nakaki et al. 2013b) as a solution. Because it bypasses the requirement of cytokines to induce PGC-LCs through the overexpression of Blimp1, Ap2-Gamma & Prdm14 from a doxycycline-controlled cassette, the PGC induction can be unlinked from signal-dependent X-reactivation phenotypes. I had not followed this avenue of work myself due to time constraints and due to the concerns that the *in vitro* PGC induction with this system could lead to artifacts in PGC quality and X-reactivation due to the overexpression of Prdm14, a naïve pluripotency factor. However, I predicted that the use of Epi-LCs differentiated for 3 days for transgene-driven *in vitro* PGC induction and the sorting of PGC-LCs after 5 days of germ cell culture would yield fully X-inactive PGC-LCs. This transgene-based PGC induction system would allow to experimentally test, if indeed the cytokines drive X-reactivation in PGC-LCs, would be of low cost compared to the cytokine system and could yield up to 10^5-10^6 X-inactive PGC-LC cells. This would be enough to characterize the epigenetic drivers of X-reactivation through allele-specific ChIP-SEQ & RNA-SEQ experiments, as well as allow functional assays to manipulate the underlying pathways, such as candidate X-reactivator ligand molecule co-culture, signal transduction cascade inhibition & activation with small molecule inhibitors, as well as shRNA-knockdown assays.

The use of the transgene cell line and the use of the optimized Epi-LC differentiation

conditions discovered in this work led my coworkers to obtain fully X-inactivated PGC-LCs, with only trace amounts of X-active PGC-LCs. When those X-inactive PGC-LCs were cultured in Retinoic acid, BMP2 and SCF-containing media as part of a recently published *in vitro* PGC culture, expansion and meiosis induction protocol (H. Miyauchi et al. 2017), they underwent X-reactivation, as predicted from the literature and my own results. It should be noted that the same report(H. Miyauchi et al. 2017) also shows that BMP4 can induce the start of meiosis, an effect explained by the fact that in PGC context, BMP2, 4, 5 & 7 have been proven to signal through the same receptor, Alk3, and that this same report also has demonstrated that Wnt4 can synergize with the BMP signaling pathway to drive meiotic progression. The use of LIF & Retinoic Acid also is also able to stimulate the meiotic gene expression program, which was very recently shown to promote erosion of the X-inactivating H3K27me3 spot epigenetic mark (H. Miyauchi et al. 2017; Ohta et al. 2017a).

Chapter3: Implementing a PGC-compatible, modular Oligo-FISH to monitor X chromosome activity at allelic & single-cell resolution:

Introduction:

We focused our efforts on the In house fluorescent probe labeling and hairpin chain reaction approaches alone.

In-house fluorescent labeling techniques offered us the opportunity to re-use published probesets for two X-linked genes, *Med14* and *Msn* (Yang et al. 2016), and the two main X-linked LncRNAs, *Tsix* and *Xist* (Del Rosario et al. 2017), since the exact same un-labeled oligo sequences than in the publications could be ordered and labeled with our chosen fluorophore. This offered the chance to test the approach on good positive controls. Those approaches also used the Stellaris-like 20bps long oligo probes, which gave us two key advantages: we could use a lot of existing published expertise and documentation, since this is the oldest and most reported oligo design strategy, and each oligo order was only 2€. This meant we could afford 100 oligos per target gene, and were less dependent on the success or failure of each individual oligonucleotide, spreading the risk across the pool.

We decided to test two different In-house labeling methods.

The first was what we will term the "N-SH probe labeling method" **(Fig.1a)**, since it lacks a dedicated methods publication (Sunwoo et al. 2015). On it, the unlabeled oligonucleotide primary probes are pooled together and subject to 3´-terminal labeling with di-deoxy UTP nucleotides containing an NH2 amine group. The amine-modified nucleotides are transferred by expedient of terminal-deoxynucleotydil-transferase (abbreviated as "tdt transferase") to the 3´end of the oligonucleotides. The reaction takes advantage of the affinity of the tdt transferase for Uracil nucleotides and its excellent kinetics, and bypasses its major limitation, the tendency to form monopolymeric tracts of a single base, by capping the 3´end of the probe with a dideoxynucleotide. This guarantees that only a single amine-labeled oligo can be transferred per probe.

After this, the oligo pool is carefully purified from amine contaminants, and exposed to a great molar excess of NHS-ester conjugated fluorescent dye. When an NHS-Ester is exposed to an amine, it generates a covalent bond NHS-amine bond, conjugating the fluorophore to the oligo probeset. A single ethanol purification is then reported to get rid of the unbound fluorescent dye.

The second was what we will term the "Enzymatic probe labeling method" **(Fig.1b)**, developed by the Ephrussi lab (Gaspar et al. 2017). The mechanism is very similar. It also uses tdt transferase enzyme, di-deoxy UTP nucleotides containing an NH2 amine group and NHS-ester conjugated fluorescent dye. In this case, however, the NHS-dye is conjugated to the NH2-di-desoxy UTP nucleotide first, and it is then alicuoted and stored for later use. The di-desoxy UTP nucleotide conjugated with the fluorescent dye is then transferred by tdt transferase enzyme action directly to the 3´-terminus of the unlabeled oligonucleotide probe pool.

This presents two key advantages. The first is that, since NHS-dye conjugates react with atmosphere moisture, the entire 150€ vial of reagent must be used at once in the "N-SH labeling Sunwoo method" (Sunwoo et al. 2015). By conjugating it to the amine-modified UTP first, multiple labeling and troubleshooting attempts can be made unexpensively. The second is that it removes a purification step, making the protocol shorter. Its possible catch was that tdt transferase is a capricious enzyme, which does not take well to fluorescent labels, which are hydrophobic and bulky. Since the former "N-SH labeling Sunwoo method" does not incur into this, the two approaches complement each other nicely.

We also decided to focus heavily in hairpin chain reaction-based methods. Three approaches were available to us, and we intend to test a fourth in the future.

In the "Choi V2.0 single-molecule HCR" **(Fig.1c)**, a single 100bps-long probe uses a central 50bps target recognition region to hybridize to the target RNA. It extrudes two 25bps-long HCR initiation sites at the 5´ and 3´ termini, and each of them can trigger the appearance of a 100-copy long fluorescent hairpin polymer, for a total maximum of 200 fluorescent groups per primary probe. We had two main concerns. The first is that

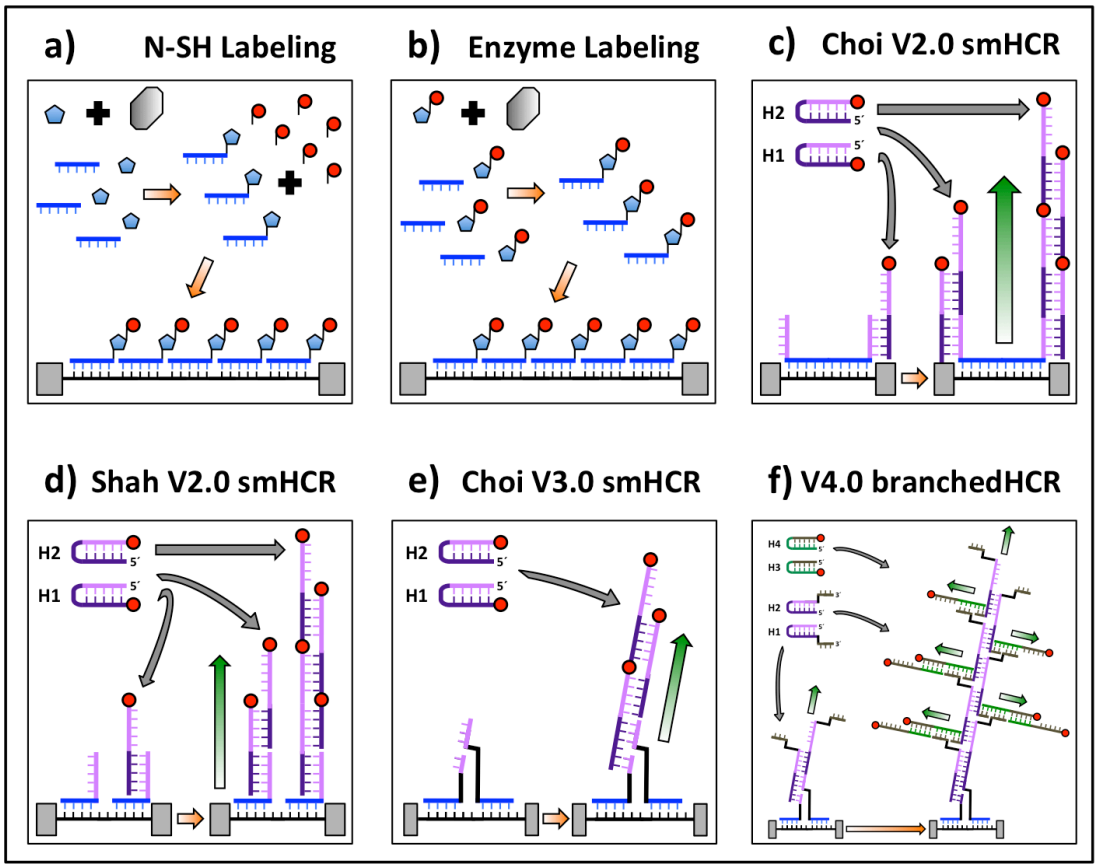

Figure 1: Features of the *Tested* RNA-FISH methods:

a) N-SH chemical labeling method.
b) Enzymatic Labeling method.
c) smHCR V2.0 (Long) Choi et al. 2014
d) smHCR V2.0 (Short) Shah et al. 2016.
e) smHCR V3.0 Choi et al. 2018.
f) smHCR "V4.0" adapted to Chinese Branched smHCR.

each individual primary probe costed 10€, but, since long oligos are prone to truncation, few commercial providers can synthesize them reliably, and only at great additional expenses in probe purification.

The second was that, since the probe design was radically different, it would need to program a specific pipeline to design probes. We lacked that bioinformatic expertise.

In the "Shah V2.0 single-molecule HCR" **(Fig.1d)**, the probes are 45 bps-long oligonucleotides with a single 20bps-long target RNA recognition region and a single terminal 25bps-long HCR initiation site. The initiation site generates a 100-copy long fluorescent hairpin polymer, meaning 100 fluorescent groups per primary probe. Since each individual probe cost 4.5€, and the reduced length of the oligo was less prone to truncation and may be synthesized without great purification, it was advantageous over the former approach. Another interesting feature is that, since it used the standard 20bps-long target RNA recognition module, we could use the resources and design expertise available for this traditional oligo-FISH design.

In the "Choi V3.0 single-molecule HCR" **(Fig.1e)**, the HCR initiator site sequence is physically split between two primary probes. Only when the two primary probes are hybridized to the target, at an exact distance of 2bps between them, can the split HCR initiator trigger the apparition of a 100-copy fluorescent polymer. Since each of the split pair probes has a 25bps hybridization to the target RNA, and a gap of 2 unoccupied bps, this gives the design a total hybridization footprint. This split pair probe feature coincides with the commercial RNAscope & ViewRNA methods, which have the highest signal-to-ratio characteristics so far, and this design philosophy is reputed to make primary probe designs almost off-target proof. While this approach was not yet published at the time of the experiments, I predicted that the HCR development would next include this feature, as it was the logical evolution of the method. Consequently, I managed to obtain and test the method pre-publication.

In the **hypothetical** "V4.0 branched HCR method" **(Fig.1f)**, the HCR initiator site

sequence is physically split between two primary probes, like in the V3.0 smHCR. Only when the two primary probes are hybridized to the target, the initiator site is reconstituted and the 100-copy hairpin chain reaction polymer forms. The key here is that instead of fluorescent groups, each hairpin copy formed a new HCR initiator site. When the HCR initiator site forms, it is recognized by a pair of fluorescently labeled hairpins, forming 100-copy, fluorescently-labeled polymers per site. This would lead to a total of 10^4 fluorophores per primary probe. While this approach does not exist yet, the branched HCR method itself has been published (Liu et al. 2018)**,** but it uses a single primary probe instead split-paired primary probes. However, since the original laboratory behind V3.0 smHCR already explored the possibility of branched HCR in the past, and are interested to increase the fluorescent signal to promote whole-mount embryo FISH approaches (Trivedi et al. 2018), it is very likely that this approach is in development right now. If not, adding an intermediate adaptor oligo that hybridizes the V3.0 smHCR primary probes and contains the initiator site for the published branched HCR method (Liu et al. 2018) should be feasible.

Their most attractive features against In-house labeling methods were threefold. First, since each primary probe could generate a minimum of 100 fluorescent groups on target, it generated much brighter signal intensities than In-house labeling methods, with a concomitant increase in detection efficiency and decrease in cost being expected. Second, since both the primary probe and the fluorescently labeled hairpins can be bought separately for any oligonucleotide synthesis manufacturer with appropriate quality controls and high purity, labeling chemistry was not a concern and the only factor that we needed to optimize would be our probe design quality. The limited amount of fluorescent imager oligos makes purchase viable.

Third, since primary probe and fluorescent imager hairpin are separate, the fluorophore used can easily be changed from one experiment to the next.

Our goals for this chapter were to optimize an Immunostaining & RNA-FISH protocol for all the 4 cell types involved in our *in vitro* germ cell system model: 4 cell types of

interest: ESCs, Epi-LCs, PGC-LCs and the MEFs that act as positive X-inactivation controls. In addition, we wished to implement an oligo-FISH protocol with the traits described above to target X-linked genes and LncRNAs for single-cell, allelic-resolution and affordable readout of the X chromosome transcriptional status.

In this chapter, we first discuss the experimental controls, expected results and strategies necessary to develop oligo-FISH probesets able to track X-chromosome activity via RNA-FISH of XIC locus LncRNA behavior and X-linked gene nascent transcription. We also discuss the scoring requirements and the parameters that need optimization in order to reach our goal.

We later show the implementation of a new Immunostaining & RNA-FISH protocol for ESCs, Epi-LCs, PGC-LCs and MEFs.

We then move to evaluate the "N-SH probe labeling method" and see its ability to perform probe labeling and score X-activity status when applied against published probesets for X-linked genes *Med14* & *Msn*, as well as X-linked LncRNAs *Tsix* & *Xist*.

We later evaluate the "Enzymatic probe labeling method" against the very same probesets for X-linked genes *Med14* & *Msn*, as well as X-linked LncRNAs *Tsix* & *Xist*. We also compare their performance against commercially synthesized probes for the LncRNAs *Tsix* & *Xist*, evaluate the discrepancies in scoring ability based on predicted signal intensities and steps in the probe labeling protocol, and discuss the convenience of our In-house labeling methods in the light of those results.

In response to our experiences with the former methods, we turn to test the "Choi V2.0 single-molecule HCR" on *eGFP* mRNA exonic targets and "Shah V2.0 single-molecule HCR" on *Tsix* and *Xist* LncRNAs, respectively. After exploring the results, we attempt to design intronic probesets against nascent transcription of multiple X-linked genes with the "Shah V2.0 single-molecule HCR" method. A total of 4 X-linked genes (*Atrx*, *Ddx3x*, *Ndufb11* & *Fmr1*) and two *Tsix* LncRNA targets are explored.

Different parameters and hypotheses are explored to increase signal-to-noise ratio to scorable extents, chiefly temperature, and synthesis efficiency via probe design.

We move on to test the "Choi V3.0 single-molecule HCR" method on *eGFP* mRNA exonic targets and nascent transcription of X-linked genes *Eif2s3x* & *Prdx4* via intronic probesets. We discuss the increases in signal-to-noise ratio, point to possible causes and explore the ability of V3.0 single-molecule HCR oligo-FISH to score X-activity at single-cell resolution compared to other methods tested.

At last, the implications of the hairpin-chain reaction based methods are summarized and future directions and new projects opened by the use of this new technique within and outside X-inactivation & reactivation field are proposed and discussed.

Results:

Experimental design & In-house probe labeling method testing:

Motivation & Experimental design:

Our first objective was to implement an experimental design that could give affair evaluation of the ability of different oligo-FISH methods to follow our requirements.

For this, we needed well-characterized readouts in the fields that may give a good perspective on the ability of the method to track all relevant readouts of X-activity that may be tracked by FISH.

There are three elements to consider: the target nucleic acid, the behavior differences between X-linked genes, and the X-activity marker LncRNAs *Tsix* & *Xist*.

In addition, the karyotype of the cell population must be carefully controlled so that all cell types have a normal diploid XX (female) or XY (male) karyotype.

When all of those factors are taken into account, the oligo-FISH staining can acquire a limited number of patterns, as defined in the sketches of **(Fig.2a-g)**. The DNA sequence of the two alleles of X-linked genes is represented by ellipses and the nucleus in blue, while the surrounding space is the cell cytoplasm. The primary oligo probe is represented in blue, with its fluorescent label group in red. **(Fig.2a-c)**.

There are three possible nucleic acid sequences to target, each with its own associated readout.

In exonic RNA-FISH, the primary probes are targeted to hybridize the exons of the spliced mRNA or LncRNA, as represented by grey boxes **(Fig.2a)**. In this scenario, any of the two alleles has a chance to be transcriptionally activated and form a nascent transcription site (NTS), as represented by the orange ellipse. When this happens, a population of nascent transcripts in different states of completion clusters around the nascent transcription site. As transcription of the RNA progresses, the introns are spliced out co-transcriptionally (Levesque & Raj 2013)**(QUOTE)**, and the mature mRNAs are released from the nucleus and exported into the cytoplasm. The end result of a RNA-FISH staining against mRNA targets is a myriad of spots in the cytoplasm and nucleus of the cell, with a brighter spot around the nascent transcription sites. While targeting exons in a mRNA allows to detect nascent transcription, its is not a very reliable way to measure X-linked gene activity. The reason is that you need to have a nascent transcription site with an enormous quantity of transcripts on it to score it with confidence. Otherwise, it is easy to mistake it with a mature spliced mRNA leaving the nucleus. Since not all transcription sites have large transcript populations at that time, this strategy leads to severe underestimation of the transcriptional activity of any given gene.

In intronic RNA-FISH, the primary probes are targeted against the un-spliced introns of the nascent transcript, be it genic mRNA or a LncRNA **(Fig.2b)**. The vast majority of introns are spliced out co-transcriptionally as the nascent transcript is extending. The intron is available for binding once it starts being transcribed, but once the intron sequence transcription is finished and a new exon sequence is reached, the splicing machinery will immediately splice out the intron sequence, without the nascent transcript being released from the nascent transcription site (orange ellipse) (Levesque & Raj 2013)**(QUOTE)**. Only a small fraction of the total intron sequence is available at a given time in any nascent RNA and multiple nascent transcripts can be found in a nascent transcription site, as per the "Christmas Tree" model (Levesque & Raj 2013)**(QUOTE)**. Since mature mRNAs or LncRNAs are released from the nucleus and exported into the cytoplasm only after all the introns have been degraded, an intron

RNA-FISH staining forms a single fluorescent spot per active X-linked allele in the nucleus. This arrangement gives intron RNA-FISH three key properties.

First, it is a real-time readout of the transcriptional activity in that region of the X-chromosome. Second, since only a random fraction of the total Intron sequence is available for each transcript in the nascent transcription site, signal intensity for nascent transcription sites is going to be very variable between cells in a population and even between alleles, and generally fainter than an exonic RNA-FISH would be.

Third, since the number of active transcription sites is constrained by karyotype, any probe un-specificity & off-target binding can be immediately recognized, since it will result in more fluorescence spots that the karyotype of the cell allows.

In DNA-FISH, the primary probes are targeted against the desired DNA locus sequence **(Fig.2c)**. Since the in-depth descriptive reports of the X chromosome structural differences in megadomains between X-inactive and active state, and the reported influence of LncRNAs in keeping this high order structure (Nora et al. 2014; Deng et al. 2015), the X chromosome has seen increasing interest as a model to study maintenance and transition of high-order 3D of the chromosome and its functional impact. In those reports, the key component was the use of oligonucleotide probesets for direct DNA-FISH staining. In oligo-DNA FISH, the DNA sequence for the alleles (white ellipses) is exposed after a salt and temperature-mediated denaturation, offering access to single-stranded DNA that the fluorescently labeled probes can bind (in black). The expected fluorescent signal is a number of pots equal to the number of X chromosomes in the cell. An aspect to take in consideration is that, while the DNA locus is permanently present in all cells and always available for binding, it will be limited to only two copies in any female karyotype. This complicates the difficulty to target it, since primary probe numbers, specificity & binding efficiency must be very high in order to generate signal, when compared against exon or Intron targets, which have a pool of transcript copies to be targeted.

The other point is the expected behavior of the targeted LncRNA or nascent transcript.

There are 4 different types of transcripts typically targeted to monitor the X-activity status.

The XCI marker genes **(Fig.2d, red spots)** are the genes that undergo silencing during the X-inactivation process. Intronic RNA-FISH against an XCI marker gene will typically show 2 nascent transcription spots in X-active cells. Once the X-inactivation progresses, the *Xist* LncRNA and associated repressive chromatin marks will cover the vast majority of the X chromosome. This makes the alleles located in such areas silent, so that in X-inactive cells, a maximum of a single nascent transcription spot may be located (Patrat et al. 2009; Williams et al. 2011; Namekawa et al. 2010).

The XCI escapee genes **(Fig.2e, purple spots)** are the genes that escape silencing during the X-inactivation process. Intronic RNA-FISH against an XCI escapee will show 2 nascent transcription spots both for X-active & X-inactive cells (Patrat et al. 2009; Namekawa et al. 2010). The XCI escapee genes are typically located in areas that escape the repressive heterochromatin spreading wrought during X-inactivation, and their identity can vary depending on tissue or type of X-inactivation process.

The *Tsix* LncRNA **(Fig.2f, red spots)** is expressed from the two X-chromosomes in X-active, naïve pluripotent stem cells and accumulated on top of its transcription site (Lee & Lu 1999). Either exonic or Intronic RNA-FISH will show 2 spots in X-active naïve pluripotent stem cells, show one single spot in cells that have chosen & enforced the inactivation of an X chromosome, and be absent in X-inactive cells **(QUOTES EPIBLAST)**.

The *Xist* LncRNA **(Fig.2g, in orange)** is expressed from the X-chromosomes chosen to undergo X-inactivation. In X-active cells, such as naïve pluripotent stem cells, it only has negligible nascent transcription levels and is virtually undetectable. However, once the cell has started the process of X-inactivation, the *Xist* LncRNA first accumulates as a single spot near its nascent transcription site, then spreads to form a single full cloud covering the X chromosome (Sunwoo et al. 2015)**(QUOTES)**. Once the full cloud is formed, *Xist* silencing influence is felt, while dissipation of the cloud has been reported as a prelude to X-reactivation in all known instances (Pasque et al. 2014; Syrett et al. 2017; Sugimoto & Abe 2007; Mak, Tatyana B Nesterova, et al. 2004; de Napoles et al. 2007; Nesterova et al. 2002).

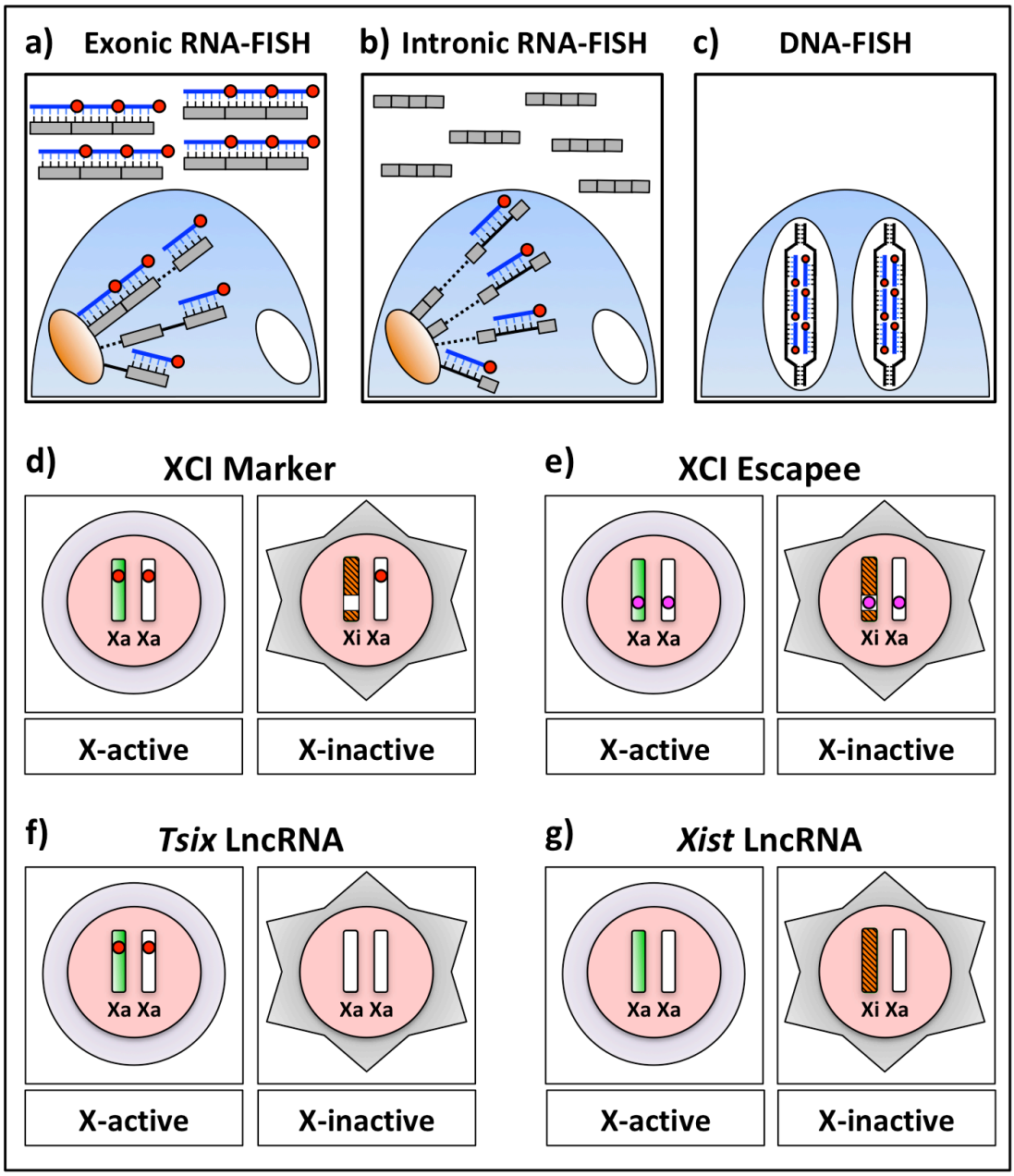

Figure 2: Features of Fluorescent *In situ* Hybridization and expected results:

a) Exonic RNA-FISH.
b) Intronic RNA-FISH.
c) DNA-FISH.
d) X-linked responder gene: ESCs Vs MEFs.
e) X-linked escapee gene: ESCs Vs MEFs.
f) *Tsix* LncRNA Expected behavior.
g) *Xist* LncRNA Expected behavior.

Methods and results:

We monitored the 4 classes of transcripts during our experiments. In order to achieve our goal of a combined Immunostaining & oligo-FISH pipeline in PGC-LCs, all experiments & results in this chapter aimed to reach the following exclusion principles:

Standard Karyotype: the karyotype stability and integrity of female XX cells and male XY cells was internally controlled in each experiment by RNA-FISH staining against *Tsix* in pluripotent diploid stem cells (ESCs & PGC-LCs), or *Xist* in X-inactivated diploid somatic cells (Epi-LCs & MEFs). This was performed to avoid distortion of the results due to anomalous counts of X chromosomes during the tests. All cell types were tested for their expected *Tsix* & *Xist* expression patterns during each experiment as a positive and negative control.

XX X-active female cells should form up to two 2 spots during Intronic RNA-FISH; male XY cells and X-inactive XX female cells should only form up to 1 spot during Intronic RNA-FISH. The presence of any significant percentage of the cell population showing higher counts tan stated that cannot be explained by cell division dynamics is taken as noise and disqualifies the approach for later use.

Detection efficiency: to yield reliable results, the key for the intronic RNA-FISH on X-linked genes or the exonic *Tsix* & *Xist* RNA-FISH is high detection efficiency.

In the case of *Tsix* for pluripotent cells and *Xist* for X-inactivated ones, the LncRNA signal should be detectable in **virtually 100%** of live cells.

For the intronic RNA-FISH on X-linked genes, in X-active female naïve pluripotent stem cells, at least **80%** of X-active cells should display **2 nascent transcription spots** for the X-linked genes. This is considered the lowest detection efficiency to yield results in the early embryo (Williams et al. 2011), which , together with the naïve ESC Vs MEF comparison, is considered the benchmark of the field. Lower detection efficiencies have yielded results later proven misleading (Kalantry et al. 2010)

Signal intensity, noise and visual scoring: All intron nascent transcription RNA-FISH against X-linked genes needs to generate single fluorescence spots, without visible

noise or with confusing signals open to subjective interpretation. No background substraction software can be used to enhance, clear the signals or required to interpret the results in any way. The purpose of this is to make any tool developed straightforward and simple to score, instead of relying on complex custom signal interpretation pipelines that require extensive expertise.

Compatibility between Immunofluorescence & RNA-FISH: Any protocol for Immunostaining & RNA-FISH should support Immunofluorescence followed by an RNA-FISH staining step, and preserve cell morphology and signal intensity for both techniques.

In conclusion, this chapter followed two aims.

The first was to develop a combined Immuno & RNA-FISH protocol for all our 4 cell types of interest.

The second was to implement a convenient oligo-FISH technology to monitor transcriptional status of the X chromosome, by proving its ability to track the 4 traditional functional groups of X-linked transcripts: XCI marker genes, XCI escapees, and the *Tsix* & *Xist* LncRNAs.

In order to translate these goals into experimentally scorable parameters, each experiment in this chapter used intronic RNA-FISH against an X-linked gene, be it XCI marker or Escapee, and exonic RNA-FISH against the LncRNAs *Tsix* & *Xist*. When combined with the 4 exclusion principles discussed above, this allowed us to obtain a conclusive answer about the ability of each oligo-FISH probe technology or Immuno-FISH protocol to meet our needs.

Implementing an Immuno & RNA-FISH protocol for ESCs, Epi-LCs, PGC-LCs & MEFs:

Our first goal was to optimize a protocol allowing combined Immunostaining & RNA-

FISH on all 4 cell types involved on our *in vitro* PGC-LC X-reactivation model: ESCs, Epi-LCs, PGC-LCs and MEFs. Additionally we aimed to obtain a protocol that would allow sufficient sample preservation to allow for routine analysis of the scarce & elusive *in vivo* PGCs prior to E10.5-12.5 gonad invasion in the mouse development (Sugimoto & Abe 2007; Hu, Peter K. Nicholls, et al. 2015).

While we initially assumed that simultaneous Immunostaining & RNA-FISH protocols developed for ESC & MEFs cell suspensions (Satoshi H. Namekawa & Lee 2011) should be appropriate for use on Epi-LCs and PGC-LCs, the experiments with *in vitro* PGC-LCs & Epi-LCs in chapter1 showed us that this was not the case, and we found two major obstacles.

The first was that Epi-LCs, and particularly PGC-LCs, were too fragile and suffered grievous morphological damage, as well as the loss of most RNA-FISH signal. Immunostaining signal was, however, adequate.

The second was that PGC-LCs in suspension were very hard to keep attached to the substrate, experiencing massive detachment rates. In our experience, as few as 2% of the original PGC-LC input at the start of the protocol remained attached at the end of the initial Immunostaining, and even less after the RNA-FISH step. We noticed that the detachment rate was caused by poor attachment to the substrate, and that it increased proportionally to the number of washing steps.

When our initial steps to solve the problem with moderate changes in our initial protocol failed, we became aware that a drastic development strategy was required. In order we tried to define a panel of elements present in all FISH sampling protocols, and tried to explore a fair representation of them all.

From a simplified view, all Immunostaining & FISH steps can be described in 4 experimental decisions: Attachment support, Fixation step, Permeabilization step, and the order between fixation & permeabilization steps.

Attachment support: There are broadly 3 common ways to attach and manipulate the sample of interest: Whole-mount tissue or histological slice, Cell suspension attachment to an adherent imaging vessel, or Centrifugal cell suspension attachment to an imaging

vessel.

In whole-mount strategies, a dissected piece of tissue, organ or even whole embryo is treated in an inclusion media that rigidifies it, then subject either the whole structures or histological slices are attached to a substrate and subject to Immunofluorescence & FISH steps. It offers the best protection of germ cells and less detachment, since the fragile germ cells are protected inside a structure that attaches and protects them. Most reports on PGC research have used this approach (Sugimoto & Abe 2007; Shiura et al. 2014; Irie et al. 2015). Sadly, we could not follow it, since we were obliged to work with FACs-sorted cell suspensions.

In cell suspension attachment to adherent imaging vessels, the cell suspension is applied to an imaging vessel that has been pre-treated to promote cell attachment. This attachment can be driven by active cell attachment to the surface by cell surface molecules such as integrins, or can be a passive attachment by electrostatic treatment or un-specific adhesive molecules present on the surface of the imaging vessel. This strategy is very popular, given its simplicity, throughput and low cost, but it usually relies on cell types that have very good active cell attachment properties, and fails otherwise. An example is the imaging of ESCs and MEFs in X-inactivation research (Chaumeil et al. 2008).

In Centrifugal cell suspension attachment strategies, the cell suspension is driven and physically stuck by centrifugal force into the imaging vessel, which is spun in a centrifuge. This strategy is usually combined with adhesive treatments of the imaging vessel and is the weapon of choice for non-adherent cell suspensions or application in which the input number of cells is very small; that is, troublemaker non-adherent cell types such as lymphocytes. All reports using *in vivo* germ cell suspensions to date have used this strategy (Nesterova et al. 2002; de Napoles et al. 2007)

Fixation step: The diversity in this step is much more limited. Since most classic fixatives increase background autofluorescence to unacceptable levels or threaten RNA integrity, with the exception of paraformaldehyde & methanol, the field uses mostly paraformaldehyde fixation in FISH protocols, generally used at [4% Weight/Volume]

concentrations (Johnson et al. 1991). The methanol has niche applications, such as increasing FISH speed in the Turbo-FISH protocol **(QUOTE)**.

Permeabilization step: The choice of the agent & exposure time is crucial, and heavily interdependent with the strength of the fixation step. The choice of permeabilization step is the most important decision to take when creating a protocol. A mild permeabilization agent used for a short period of time is going to preserve cell morphology better, but may lead to excessive background & FISH staining failure. On the other hand, strong permeabilization agents used for long periods of time will ensure FISH signal in the most complex samples, but are prone to destroy cell morphology. There are five main permeabilization agents, in order of increasing harshness to the sample: [0.5% Triton in PBS](Chaumeil et al. 2008), N2 Freeze-thawing & Saponin **(QUOTE)**, [0.5% Triton in CSK](Satoshi H. Namekawa & Lee 2011), Methanol & Xylenes (Nesterova et al. 2002). We explored all of them with the exception of Freeze-thawing in liquid Nitrogen (N2) & Saponin treatment.

The order of fixation & permeabilization steps: From our own experience, this is the most critical decision to take in any FISH protocol. This stems from the fact that the cytoplasm of any cell type is considered to be an obstacle to the penetration of antibodies & nucleic acid FISH probes. As such, the fixation & permeabilization steps are intertwined in a faustian bargain that aims to remove as many cytoplasmic components as possible to increase probe diffusion in the entire cell, but leave behind a faithful morphologic imprint of the cell and avoid the degradation of any mRNA, DNA, and protein epitopes for a reliable quantitative analysis.

If the cell is permeabilized first, the contents of the cytoplasm can be extracted more readily, maximizing probe & antibody diffusion afterwards. The signal tends to be cleaner, particularly if the FISH probe is large, but the cell morphology and attachment suffers as a consequence (Satoshi H. Namekawa & Lee 2011; Johnson et al. 1991).

If the cell is fixed first, the cell morphology and attachment are preserved. Protein epitopes and cell surface attachment molecules are cross-linked to the imaging vessel,

preserving the cell. In addition, the permeabilization times may be longer and harsher without damaging cell morphology. This approach increases background and diminishes cleanliness, but the better preserved morphology, inactivation of cellular nucleases and tolerance to harsh permeabilization make it ideal to find a protocol that works simultaneously in vastly different cell types (Chaumeil et al. 2008; Johnson et al. 1991).

In last instance, this left us with 2 attachment support strategies, 4 permeabilization agents and 2 decisions of fixation-permeabilization order for a 4 cell types to test. We decided to test 3 different permeabilization times for each agent, for a total of 200 different Immunostaining & RNA-FISH conditions tested **(data not shown)**.

In order to obtain sufficient PGC-LCs for routine testing, male PGC-LCs obtained through the overexpression of master germ cell fate transcription factors were used (Nakaki et al. 2013c).

Each condition was tested for Immunofluorescence against nuclear markers using the H3k27me3 histone mark target for ESCs, Epi-LCs & MEFs, and the AP2-Gamma master transcription factor for PGC fate in PGC-LCs (Nakaki et al. 2013c)**.** The logic behind this decision is that staining the nucleus is the shortest way to check if all of the cell is properly permeabilized and can be accessed by antibodies or FISH probes.

The same logic was followed for the FISH, choosing nuclear RNA targets alone.

For the RNA-FISH staining, the ESCs & PGC-LCs were stained against the *Tsix* LncRNA and the Epi-LCs & MEFs against *Xist* nuclear LncRNAs. Both LncRNAs were used because they have high expression in the targeted cell types and are routinely used as positive control in RNA-FISH studies. *Tsix* expression is driven by the naïve pluripotency network transcription factors, particularly *Prdm14*, shared between ESCs & PGC-LCs (Payer et al. 2013). *Prdm14* overexpression was also used for PGC-LC induction (Nakaki et al. 2013c). The *Xist* LncRNA accumulates in X-inactivating cells, and was the target of choice for Epi-LCs & MEFs.

For convenience, we only display the end result of this screening. Our final protocol consisted on passive attachment of a single cell suspension to an adhesive-coated imaging vessel as a liquid droplet. This was followed by careful addition of fixative to [4%Paraformaldehyde in PBS] concentration for 10 minutes at room temperature, followed by Centrifugal cell suspension attachment to the imaging vessel, and culminated by 8 minutes of permeabilization in [0.5% Triton in PBS].

We discovered that this strategy allows targeting all 4 cell types both for RNA-FISH signal **(Fig3.a)**, as well as for Immunofluorescence staining **(Fig.3b)**.

In addition, we found out the following:

The first key finding during this process was that, both for Epi-LCs and PGC-LCs, it is absolutely necessary to fix first before any kind of cytocentrifugal attachment or permeabilization treatment, since their morphology is too fragile to tolerate them otherwise. This is consistent with their reported mechanical fragility (Hayashi & Saitou 2013b; Hayashi & Saitou 2013c).

The second was that PGC-LCs do not attach actively to the standard cell culture surface coatings used for the cell suspension attachment strategy, or regular cell culture. The PGC-LCs did not visibly attach to imaging vessels coated with cell culture compatibility treatments, Gelatin, Fibronectin or other extracellular matrix substrates at different concentrations. Because of the former, the only way we managed to attach PGC-LC suspensions to the imaging vessel was to treat it with sequential Poly-L-Lysine & Cell-TAK treatments to promote un-specific cell adhesion. The cell suspension was provided in a [2% Wt/Vol. Gelatin] solution and let sediment atop of the coverslip, so that the Gelatin would form a polymer on top of the cells and over the imaging surface. The fixative was then carefully added to the cell solution, and the solution was subject to centrifugal attachment, because any other solution would result in cell detachment. The reasoning was that the attachment of PGC-LCs was so dim, that it was necessary to create a “net” of Gelatin polymer, cross-linked in place by the paraformaldehyde fixative, and stuck in place by centrifugation, in order to obtain any meaningful attachment.

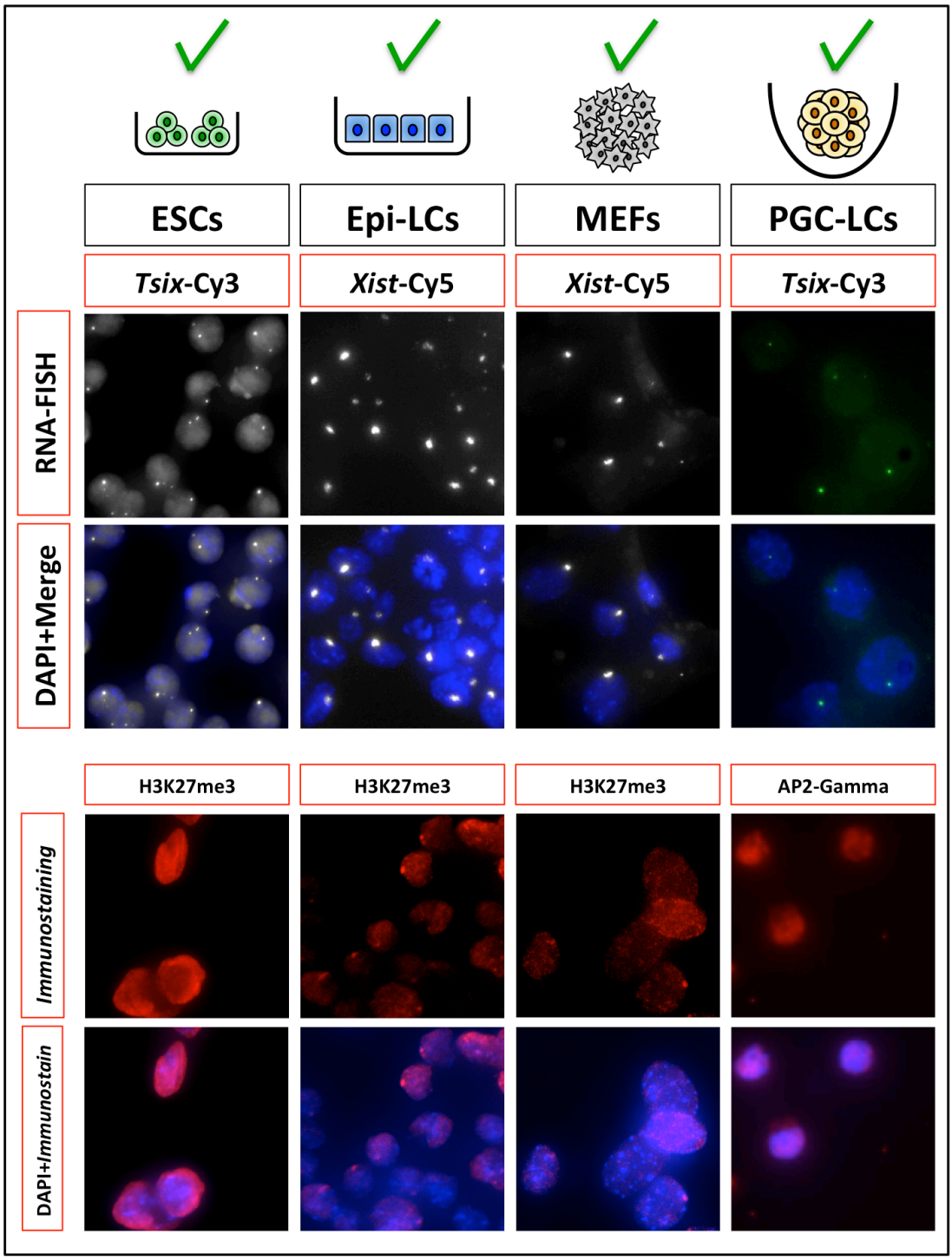

Figure 3: Optimized Immuno & RNA-FISH against the 4 cell types of interest:

a) .

b) .

c) .

The third is that, even with the precautions taken above, the amount of PGC-LCs available after combined Immunofluorescence & RNA-FISH protocol is typically less than 10% of the starting Input. This phenomenon is specific to PGC-LCs and does not affect any other cell type. Our interpretation is that PGC-LCs are resistant to most coatings for cell attachment, either passive or active, because most of them require at least some degree of active binding from cell surface receptors present in the cell. Since PGC-LCs have very poor attachment characteristics, the safest approach is to cross-link & fix a polymer net on top of the live PGC-LC cell suspension, and then stick it in place through centrifugation. Since detachment was still high, it would be convenient to find a more efficient polymer than [2% Gelatin]. It is likely that extracellular matrix component polymers with higher branching index and adhesiveness, such as laminin or matrigel, may provide better alternatives.

The above results led us to several conclusions.

First, we had a protocol that allowed us to target all 4 cell types used on our *In vitro* PGC-LC X-reactivation model (ESCs, Epi-LCs, PGC-LCs and MEFs) with Immunofluorescence & RNA-FISH analysis. As far as we are aware, it is the only protocol with the ability to combine Immunofluorescence & RNA-FISH in PGC cell suspensions. Another protocol combining Immunofluorescence & DNA-FISH was published after we discovered it, but it is performed mostly after significant *in vitro* expansion and proliferation of PGC-LCs (Ohta et al. 2017b), presumably due to propensity of PGC-LCs to detachment. In addition, as a consequence of the constraints of our experimental models, this protocol has proven to be convenient to work with exceedingly low cell number counts (as few as 10^4 cells per sample).

Second, we noticed that, due to the propensity of PGC-LCs to detach, we could target *in vitro* PGC-LCs (10^4-10^5 cells per experiment), but that the scarce number of *in vivo* PGCs prior to gonad invasion (10^3-10^4 cells per litter & dissection), was too low to be effectively targeted with this protocol, barring a disproportionate expense, or the use of somatic cells as a "carrier" solution. It is very likely that the replacement of gelatin in the protocol with stronger polymerizing agents, like matrigel, will offer the necessary improvement to target pure *in vivo* PGC suspensions.

As a consequence, we focused on the use of this protocol to characterize the kinetics of X-inactivation & reactivation on our *In vitro* PGC-LC system, as seen in chapters 1 & 2 of this thesis. The main contribution of the protocol to the results was to highlight that *Xist* & H3k27me3 spot signals in Epi-LCs & PGC-LCs and genic silencing were not automatically synonymous, as was erroneously assumed before, and to prove that d1 Embrioid bodies had undergone homogeneous X-inactivation& gene silencing, proving that the spontaneous X-reactivation seen in PGC-LCs was a phenotype caused by the signaling molecules present in the cytokine PGC induction media.

With the ability to perform Immunofluorescence & RNA-FISH on all cell types of our interest, we next focused on developing a pipeline to design and synthesize our own probes against X-linked genes & LncRNAs.

Testing the N-SH, Enzymatic & Commercial synthesis probe labeling methods:

Our next goal was to design & implement our own oligonucleotide probes against X-linked genes or LncRNAs of our choosing. Since we had access to 2 validated & published oligo probesets following the traditional 20bps pattern against X-linked genes, *Med14* & *Msn*, we decided to focus on the In-house labeling methods that relied on transferring fluorescent groups to un-labeled oligonucleotides ordered from a commercial provider: The N-SH & the Enzymatic probe labeling methods.

The major consideration was the need for powerful & accurate positive controls.

The first was a positive control for intronic probesets that were proven to detect nascent transcription from X-linked XCI marker genes, in order to have a reliable benchmark. For this, we used published oligo probesets against *Med14* (96 oligos) & *Msn* (48 oligos) which had been quantified for their ability to track nascent transcription in X-active ESCs & X-inactive MEFs (Yang et al. 2016).

The second was a positive control for positive probe labeling, both from in-house & commercial sources. Since any initial attempt at probe labeling was liable to obtain sub-

par results and only label a fraction of the oligonucleotide pool, we needed a positive control able to show visible results even at low labeling efficiencies. For this, we used repeat-based oligonucleotide probes targeting the LncRNAs *Tsix* & *Xist* (Del Rosario et al. 2017). The *Tsix* oligo probeset is comprised of 2 oligonucleotide probes that bind a total of **132 times** to a repeat sequence in the *Tsix* LncRNA. The *Xist* oligo probeset is comprised of 2 oligonucleotide probes that bind a total of **25 times** to a repeat sequence wholly specific to the *Xist* LncRNA.

Since only 4 oligonucleotide probes were necessary to target the *Tsix* & *Xist* LncRNAs, we could afford to order them with 3´ commercial labeling with Cy3 (Red) & Cy5 (Far red) fluorescent groups & HPLC purification. This is very important, since 3´ labeling is the only guarantee for the inclusion of a functional group in the oligonucleotide sequence from commercial providers (all oligo sequences must start synthesis from a fluorescently labeled nucleotide), while HPLC-grade purification ensures that any un-conjugated contaminant fluorescent dye is eliminated. We also did order the 4 oligonucleotide probes against *Tsix* & *Xist* LncRNAs unlabeled for testing.

As such, the labeling efficiency and performance of X-linked *Med14* & *Msn* and *Tsix* & *Xist* oligo probes was compared against the commercially labeled *Tsix* & *Xist* oligos.

The results were subject to the 3 exclusion principles applying for FISH (standard karyotype, detection efficiency & signal Intensity) and compared against the performance of the commercially labeled *Tsix* & *Xist* probes. In order to ensure maximal efficiency, all In-house probes were labeled using the Cy5 (Far-red) fluorophore to avoid cellular autofluorescence interfering with detection efficiency.

We first tested the N-SH labeling method and scored its performance on the unlabeled *Med14*, *Msn*, *Tsix* & *Xist* probesets **(Fig.4)**.

The first probe was *Med14* **(Fig.4a)**. We observed that, for X-active ESCs, **49%** of cells did not show any recognizable transcription spot, **26%** of them showed 1x single spot, and only **25%** of them showed the expected 2X nascent transcription spots **(Fig.4a)**, instead the desired > **80%.** In addition, the signal intensity was faint, and very hard to tease from background.

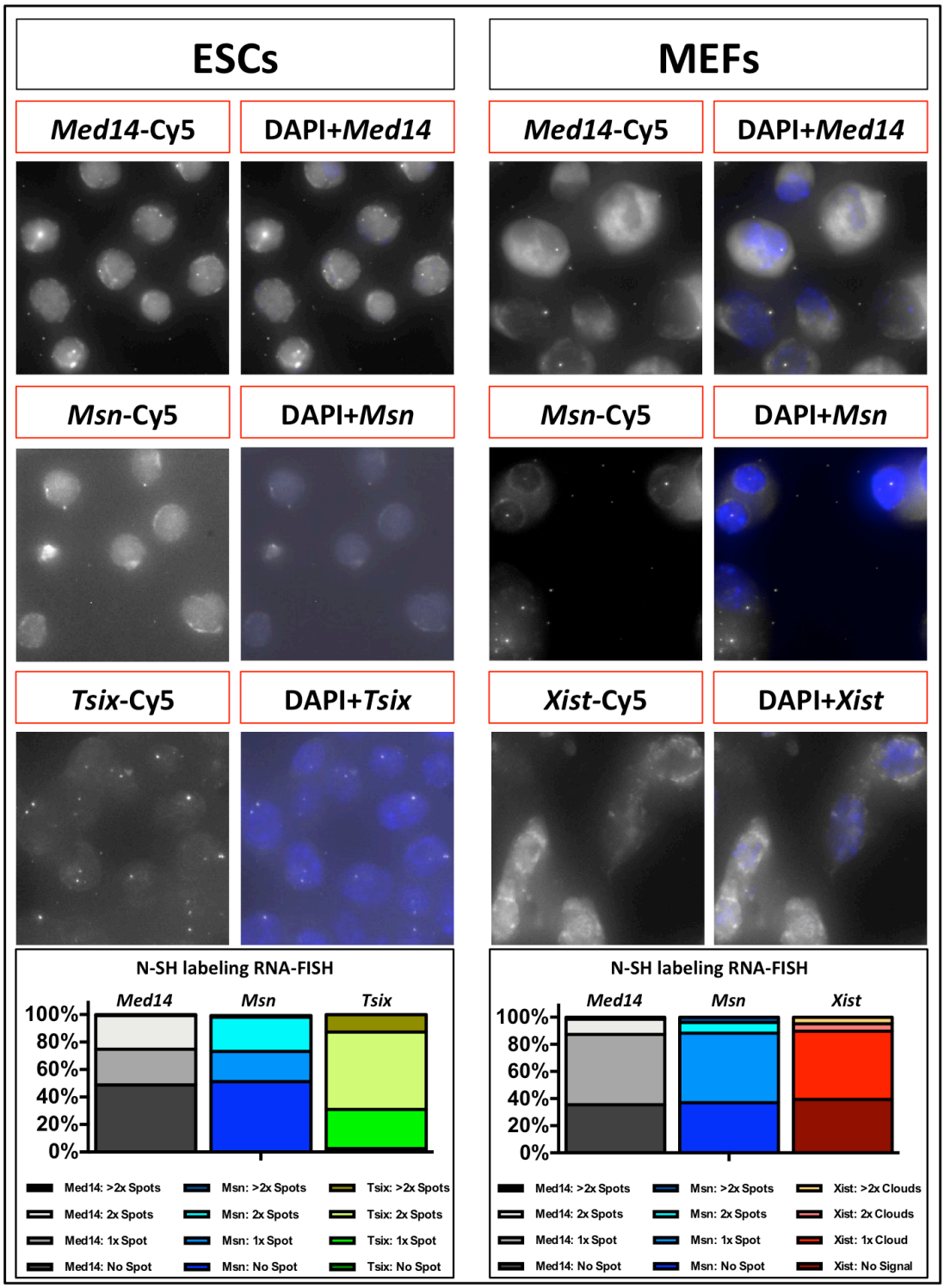

Figure 4: The N-SH labeling method:

a) The *Med14* Intron RNA-FISH probeset labeling.

b) The *Msn* Intron RNA-FISH probeset labeling.

c) The *Tsix* & *Xist* probeset labeling.

We then observed X-inactive MEFs, in which **36%** of cells did not show any recognizable transcription spot, **52%** of them showed the expected 1x single spot, and **13%** of them showed undesired 2X nascent transcription spots **(Fig.4a)**, instead the desired **0%.** While the percentages of cells with 2x nascent transcription spots was within bounds of spontaneous polyploidization and cell division in MEF cell cultures, the faint signal intensity was a concern.

This led us to conclude that *Med14* labeling was not performing adequately. True ability to reach allelic resolution required **80%** of ESCs showing 2x spots, and **80%** of MEFs showing a single nascent transcription spot.

The next probe was *Msn* **(Fig.4b)**. We observed that, for X-active ESCs, **51%** of cells did not show any recognizable transcription spot, **22%** of them showed 1x single spot, and only **25%** of them showed the expected 2X nascent transcription spots **(Fig.4b)**, instead the desired > **80%.**

We then observed X-inactive MEFs, in which **36%** of cells did not show any recognizable transcription spot, **53%** of them showed the expected 1x single spot, and **12%** of them showed undesired 2X nascent transcription spots **(Fig.4b)**, instead the desired **0%.** The percentage of cells with 2x nascent transcription spots was again within bounds of spontaneous polyploidization and cell division.

This led us to conclude that *Msn* labeling was not performing adequately either, and showed the same limitations of low signal intensity and quantification that the *Med14* probeset. The problem was global one, independent on the sequence set used.

At last, we tested the *Tsix* & *Xist* probes in ESCs & MEFs, respectively **(Fig.4c)**. We observed that in the X-active ESCs, *Tsix* probes generated a strong signal. Only **2%** of cells did not show any recognizable *Tsix* transcription spot, **28%** of them showed 1x single *Tsix* spot, and **56%** of them showed the expected 2X *Tsix* spots **(Fig.4c)**, still a distance from the desired > **80%** biallelic expression. The **12.6%** of cells with more than 2 *Tsix* spots are consistent with *Tsix* locus replication prior to cell division**.**

This led us to conclude that, while *Tsix* was detectable in virtually all X-active ESCs, as expected, only a fraction of the expected biallelic *Tsix* expression is seen. We credited this to inefficiencies in probe labeling, meaning a sizable fraction of the cells with monoallelic expression were probably expressing *Tsix* biallelically, but we couldn´t see it.

The *Xist* probes fared noticeably worse **(Fig.4c)**. A **39%** of cells lacked any recognizable *Xist* signal, with only **50%** of them showing the expected single *Xist* signal **(Fig.4c)**, still a distance from the desired > **90%** expected *Xist* clouds. The **10%** of cells with more than 2 *Xist* signal were again consistent with *Xist* locus replication prior to cell division.

This led us to conclude that, we were again seeing only a fraction of the expected *Xist* expression due to inefficiencies in probe labeling.

At the end of our experiments with N-SH probe labeling, we appreciated a common trend: The detection efficiencies were low, with an abnormally high amount of cells not showing *Med14* & *Msn* (Yang et al. 2016), or *Tsix* & *Xist* expression (Del Rosario et al. 2017), and compounded by lower signal intensity than expected from source publications.

One possible explanation was that only a fraction of the oligonucleotide probe was properly labeled. However, even repeated purification of the probe from un-bound Cy5 fluorophores turned out that, according to spectrometry measurements, 66% of *Med14*, 143% of *Msn*, 99% of *Tsix* & 87% of *Xist* probe molecules were labeled with the Cy5 dye **(data not shown)**. While these measurements showed some inefficiencies or slight contaminations with unbound dye, none of them were significant enough to explain the poor results. However, given that N-SH protocol has 2 separate steps for labeling (inclusion of the NH2-modified nucleotide with tdt transferase in the oligo sequence & conjugation with vast molar excess of SH-conjugated Cy5 dye) which were difficult to discriminate, the results of the purification and measurement were not necessarily that accurate.

At the end, the combined results led us to three conclusions.

First, there was an unexplained discrepancy between published detection efficiency & signal intensity from our results Vs the expected published reports, and it wasn´t explained from our labeling index measurements.

Second, we were unable to monitor the 2 labeling steps of our oligonucleotide pool, and couldn´t ascertain where the problem was located if we kept using the N-SH probe labeling protocol.

Third, we would need to perform repeated labeling attempts, which were not viable if each trial run consumed a full 150€ vial of fluorescent dye.

In order to bypass those inconveniences, we moved onto the Enzymatic probe labeling protocol (Gaspar et al. 2017), which had just recently been published. This protocol had the advantage that the SH-fluorescent dye could be conjugated with the did-deoxy nucleotide, and kept alicuoted for multiple labeling attempts. It also eased the recognition of problems in the labeling attempts, since the emphasis of the protocol was displaced to the inclusion of the fluorescent dye to the oligo by the tdt enzyme, which was the most likely point of failure in the protocol.

We also focused on the comparison against commercially labeled *Tsix* & *Xist* oligo probes, and their signal intensity compared with our attempts to label the *Med14* & *Msn* probesets and previous results with the N-SH probe labeling method.

We first labeled the *Med14* probeset **(Fig5.a)**. The results were similar to N-SH labeling. For X-active ESCs, **56%** of cells did not show transcription spot, **25%** of them showed 1x single spot, and only **20%** of them showed the expected 2X nascent transcription spots **(Fig.5a)**, instead the desired > **80%.**

For the X-inactive MEFs, **47%** of cells did not show any recognizable transcription spot, **42%** of them showed the expected 1x single spot, and **11%** of them showed undesired 2X nascent transcription spots **(Fig.5a)**.

We then labeled the *Msn* probeset **(Fig5.b)**, with similar results. For X-active ESCs, **39%** of cells did not show transcription spot, **26%** of them showed 1x single spot, and

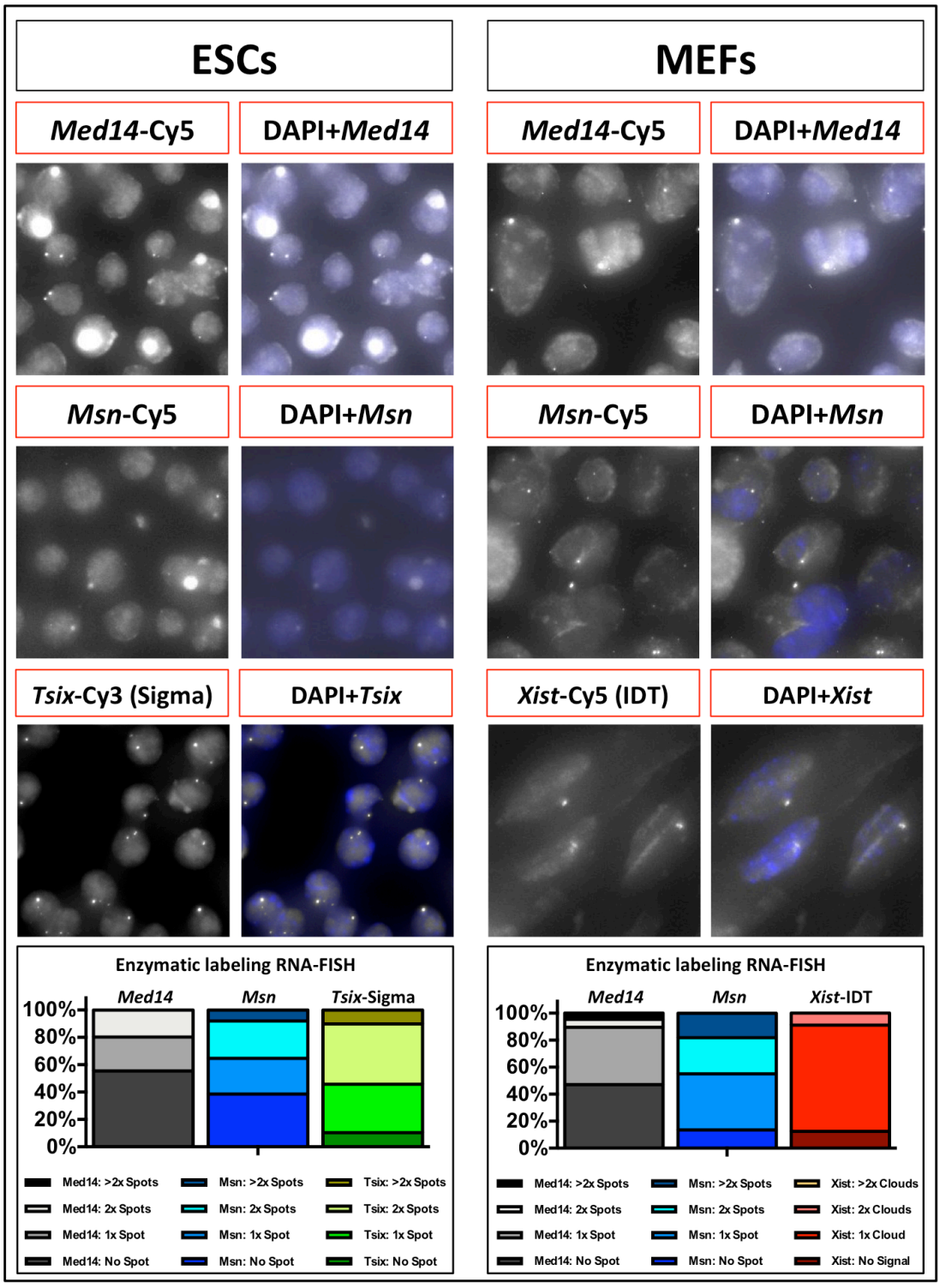

Figure 5: The Enzymatic labeling method:

a) The *Med14* Intron RNA-FISH probeset labeling.

b) The *Msn* Intron RNA-FISH probeset labeling.

c) The *Tsix* & *Xist* probes commercial labeling.

only **27%** of them showed the expected 2X nascent transcription spots **(Fig.5b)**, instead the desired > **80%.** For the X-inactive MEFs, **13%** of cells did not show any recognizable transcription spot, **42%** of them showed the expected 1x single spot, and an aberrant **45%** of them showed undesired 2X or more nascent transcription spots **(Fig.5b)**, instead the desired **0%.**

In conjunction, the results from the Enzymatic probe labeling method failed to show any sizeable improvement of the situation, suffering from the same defects as N-SH labeling (low signal intensity, high background). The results and signal intensity led us to the conclusion that Enzymatic probe labeling efficiencies must be performing as poorly as the N-SH probe labeling, and probably introducing a degree of un-specific fluorophore trapping in MEFs.

What brought valuable information to the light was the behavior of commercially labeled *Tsix* & *Xist* probesets **(Fig.5c)**. We observed that both *Tsix* & *Xist* commercial probes generated a far stronger signal than N-SH & Enzymatically-labeled probes. In the X-active ESCs, only **10%** of cells lacked *Tsix* spot, **35%** of them showed 1x single *Tsix* spot, and **44%** of them showed the expected 2x *Tsix* spots **(Fig.5c)**, still a distance from the desired > **80%** biallelic expression.

The *Xist* probes fared dramatically better **(Fig.5c)**. Only **12%** of cells lacked *Xist* signal, and **79%** of them showed the expected Xist cloud **(Fig.5c)**, fully consistent with benchmark results (Del Rosario et al. 2017). The **9%** of cells with 2 *Xist* signals were again consistent with *Xist* locus replication prior to cell division.

The results of those experiments led us to conclude that N-SH & Enzymatic probe labeling methods were labeling only one fraction of the probes, no matter what the results after ethanol probe purification were suggesting.

We next verified the degree of labeling of *Med14* & *Msn* probesets with the enzymatic labeling method. After repeated ethanol purification, we observed **14%** *Med14* & **16%** *Msn* degree of labeling with Enzymatic probe labeling, which was consistent with the poor results observed **(Fig.5a&b)**. Since the results from Enzymatic probe labeling

showed similar brightness as the ones from N-SH probe labeling, we suspected that the ethanol purification was incomplete in the N-SH protocol.

In order to verify it, we purified the probes subject to N-SH labeling using a size **GE Healthcare-50** size exclusion column. This column retains nucleic acid sequences above 10bps, and washes away efficiently unbound dyes.

When we did so, the degree of labeling of *Med14* changed from **66%** to **8%**; that of *Msn* from **143%** from **20%**; and the one of *Tsix* from **99%** to **22%**. The above combined results led us to the conclusion that the vast molar excess of unbound SH-dye in the N-SH probe labeling protocol cannot be cleared by the ethanol purification protocols, contrarily as claimed. The Enzymatic probe labeling protocol, on the other hand, does not seem to incur in this problem, but does not improve very significantly the degree of probe labeling or the results.

With the new results the combined N-SH & Enzymatic probe labeling protocols resulted in the following: *Med14* probeset provided a range of **8-14** dyes/target RNA; *Msn* probeset **8-10** dyes/target RNA; and *Tsix* probeset provided **29** dyes/target RNA.

Discussion and Conclusions:

The combined results from this section led us to 4 conclusions.

First, neither N-SH nor Enzymatic probe labeling were remotely close to providing the degree of probe labeling that we required, and the 5-fold increase in labeling efficiency that we aimed for was unlikely to be achieved.

Second, the In-house labeling approaches were unwieldy (3-5days long protocols before quantification) and the number of dyes per target RNA in these approaches was unlikely to get anywhere close to the focal dye concentration found in the *Tsix* locus, a well-known positive control known for easy biallelic expression targeting.

Third, the number of control steps required to evaluate proper performance at each step of N-SH & Enzymatic probe labeling were excessively expensive and time-intensive to be worth the effort.

Fourth, only careful 3´ dye labeling from a reputed manufacturer (we recommend to use IDT and to avoid Sigma-Aldrich industries), followed by HPLC purification, was a guarantee for deterministic, 100% labeling efficiency that we seeked.

As such, we decided to focus on strategies that relied on the signal amplification of unlabeled oligonucleotide probe with commercially labeled fluorescent imager oligos. We aimed for strategies guaranteeing at least one order of magnitude of signal amplification, and abandoned protocols that require to conjugate fluorescent dyes in-house.

Hairpin Chain Reaction RNA-FISH method testing:

Motivation:

As a consequence of the shortcomings of N-SH & Enzymatic probe labeling, we looked for a different technology. I decided to focus on the recently published V2.0 hairpin chain FISH protocols, for long 100bps oligos (Choi et al. 2014), and short oligos with 20bps target recognition modules (Shah, Lubeck, Schwarzkopf, T.-F. He, et al. 2016). The use of hairpin chain reaction technology offered several key advantages to us.

First, since each primary probe could generate a minimum of 100 fluorescent groups on target, the cost of the probeset and signal intensity increased dramatically. A single primary probe could recruit more fluorescent signal than an entire N-SH or Enzymatic labeling probeset could.

Second, since both the primary probe and the fluorescently labeled hairpins could be bought separately, commercial labeling chemistry for the few fluorescent imager hairpin oligos could be purchased. The only factor that we needed to optimize would be the quality of our probe design.

Third, since primary probe and fluorescent imager hairpin oligo were separate, the fluorophore used could be changed from one experiment to the next, without the need to synthesize again an entire fluorescence-conjugated probeset.

We were however facing a disadvantage. Since the failure of the N-SH & Enzymatic labeling protocols, and the associated monetary losses, the skepticism of the lab against

Oligo-FISH probe technology was high. Due to this, I initially had to use Alexa488 fluorescent imager hairpin oligos in these experiments, kindly provided by the James Sharpe laboratory, in order to justify the expense. Since the entirety of our cell lines used *X-eGFP* & *X-tdTomato* transgenes to ensure that all female cells had an XX female karyotype, the V2.0 smHCR RNA-FISH had to punch through preserved fluorescent protein background signal to be seen. While usually no oligo RNA-FISH technology is able to perform that, I banked that the signal amplification of V2.0 smHCR RNA-FISH would be able to punch through the background and overcome those unfavourable circumstances.

We had two goals in mind.

The first was to see if V2.0 smHCR RNA-FISH performance was enough to justify further reagent expenditure and ensure the continuity of the oligo-FISH project.

The second was to see if we could adapt existing oligonucleotide probesets from different techniques to work with V2.0 smHCR and efficiently target X-linked genes & LncRNAs with them.

Methods and results:

To achieve our goals, we needed to test the protocol with a limited number of positive control oligo-FISH probesets. In order to do so, we followed two approaches.

The first was to use the original control probe for the V2.0 smHCR, a set of 6x oligonucleotides of 100bps targeted against the eGFP mRNA sequence. Since each primary probe had 2 initiation sites and each fluorescent hairpin carried 1 fluorescent dye, the entire probeset could recruit as much as 1.200 fluorescent dyes/target RNA molecule. The *eGFP* exonic RNA-FISH probeset and the Alexa488-labeled fluorescent hairpins were kindly provided by the James Sharpe laboratory.

The second was to adapt the proven *Tsix* & *Xist* oligo-FISH sets we had (Del Rosario et al. 2017) to the short V2.0 smHCR technology by adding a single HCR initiator sequence in their 3´ end (Shah, Lubeck, Schwarzkopf, T.-F. He, et al. 2016). Since the

Tsix LncRNA is located to the nascent transcription site, we reasoned that it would provide a good starting point for the ability of the technique to target nascent transcription. The *Xist* LncRNA accumulates multiple copies when it coats the X chromosome, and this would make it a forgiving positive control.

For the *Tsix* LncRNA, this resulted in 2x primary oligo probes with 132 binding sites, for a theoretical maximum of 13.200 dyes/target *Tsix* RNA molecule. For the *Xist* LncRNA, this resulted in 2x primary oligo probes with 25 binding sites, for a theoretical maximum of 2.500 dyes/target *Xist* RNA molecule.

We then tested the *eGFP*, *Tsix* & *Xist* probesets against X-active hybrid El16.7 TST A10 ESCs **(QUOTE)** and X-inactive MEFs that expressed the *X-eGFP*, and used conditions lacking the primary probes, but supplied the fluorescent HCR hairpins as a negative control. To maximize the signal intensity, we performed the V2.0 smHCR RNA-FISH with maximum incubation times, to ensure the maximal possible length of the fluorescent hairpin polymers and signal intensity.

Choi & Shah V2.0 smHCR method testing on *eGFP*, *Tsix* & *Xist* positive controls:

We first analyzed the results of *Tsix* V2.0 smHCR adaptation **(Fig.6a)**. The *Tsix* signal in X-active ESCs was exceedingly bright and surpassed entirely the existing *X-eGFP* background, while signal was negative **(0%)** in the X-inactive MEFs and (-) primary probe hairpin background controls, as expected. Only **1.8%** of ESCs lacked *Tsix* transcription spots, **18.6%** had a single *Tsix* transcription spot, and **59%** had the expected two *Tsix* transcription spots. The only discordant spot was the presence of **21.2%** of cells with more than two *Tsix* transcription spots, which was more than the expected near **10%** attributed to cell division observed with commercially labeled probes **(Fig5.c)**. We attributed this to the legitimate and verified existence of faint off-target binding sites in the original *Tsix* probeset (Del Rosario et al. 2017). Since the probeset is based on a repeat motif that is enriched a hundred-fold in the *Tsix* LncRNA compared to any other transcribed RNA, we considered that the un-specific signal had always existed and was only now visible due to the hairpin chain reaction signal amplification.

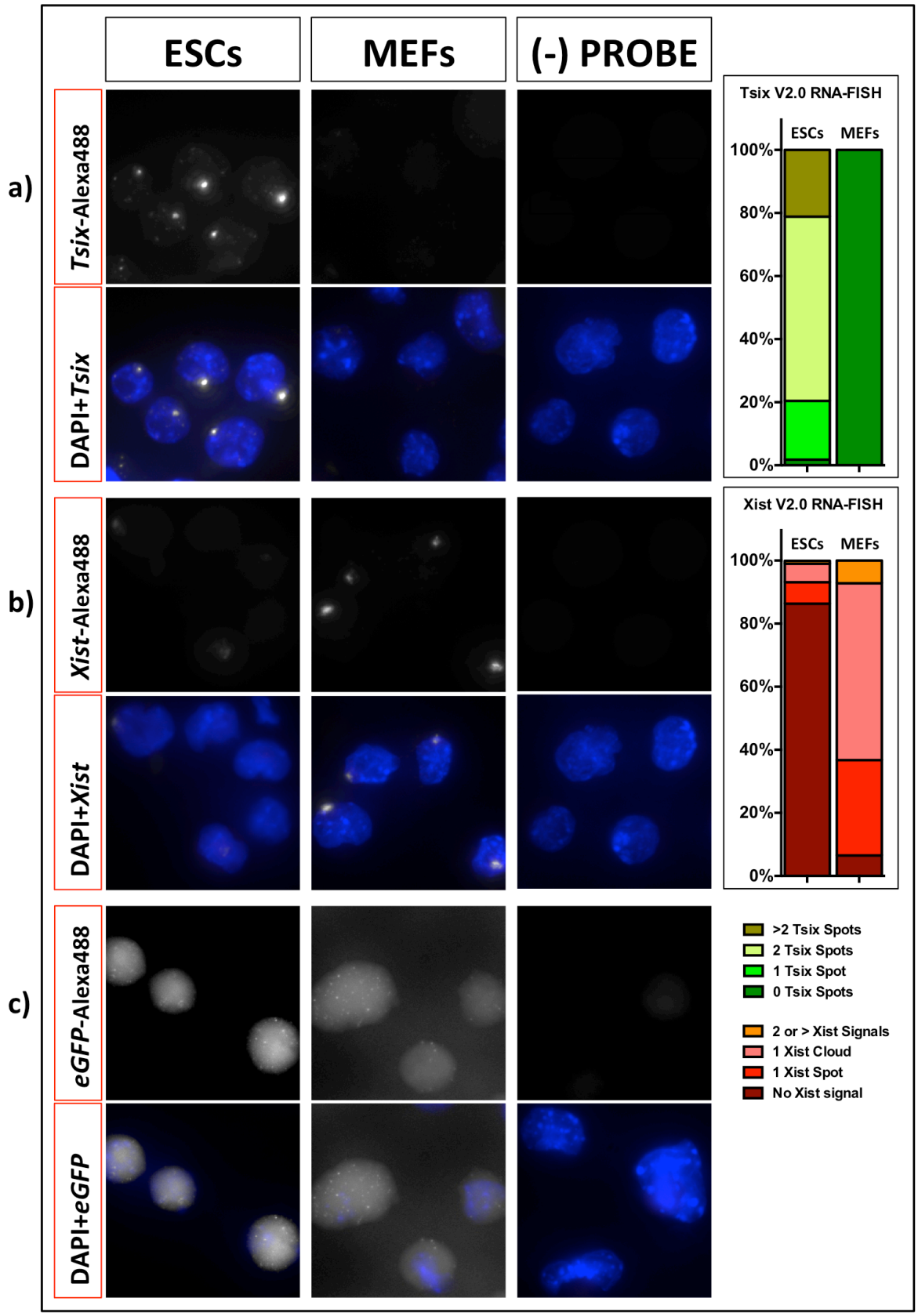

Figure 6: Testing the V2.0 smHCR with *Tsix, Xist* & *eGFP* exon RNA-FISH

We next analyzed the results of *Xist* V2.0 smHCR adaptation **(Fig.6b)**. The *Xist* signal in X-inactive MEFs was even brighter and surpassed entirely the *X-eGFP* background. While the faint amount of nascent *Xist* transcription related with the naïve pluripotent state prior to X-inactivation choice was visible in a large fraction of the ESC population, a feature that previously was only visible with large BAC-FISH probes or RT-PCR **(data not shown)**, only **13%** of the X-active ESCs showed any *Xist* levels that could be relevant for the X-inactivation process, and **87%** of them were negative. This low percentage was compatible with the spontaneous differentiation rates & concomitant X-inactivation rates seen in ESCs cultured in Serum+LIF media **(QUOTES)**.

In the X-inactivated MEFs, only **7%** of MEFs lacked *Xist* signal, **30%** had an accumulating *Xist* nascent transcription spot or expanding cloud, and **56%** had the expected full *Xist* cloud signal. The **7%** of cells with more than one *Xist* signal were attributed to cell division.

At last, we analyzed the results of the V2.0 smHCR control oligo set against the *X-eGFP* transgene. **(Fig.6c)**. While not as bright as *Tsix* & *Xist* signals, the signal was still able to entirely surpass the existing *X-eGFP* background, while signal was fully negative in the (-) primary probe hairpin background controls, as expected. Still, the signal intensity was sub-par, and any exonic mRNA-FISH with as few as 1.200 dyes per target mRNA should avoid fluorescent protein backgrounds if possible, or clear the background with the appropriate image analysis filters. Still, we considered these results to be another argument for hairpin chain reaction approaches, since nascent transcription of X-linked genes would cluster multiple target RNAs in the nascent transcription site, increasing the expected signal intensity against a single exonic mRNA molecule by at least one order of magnitude (Levesque & Raj 2013).

The former results led us to four conclusions.

First, V2.0 smHCR approach allowed us to target effectively target nascent transcription sites, as demonstrated by *Tsix* signal, as well as fully spliced LncRNAs, as *Xist* analysis had shown. Since we had been able to target the *Tsix* & *Xist* LncRNAs, the only factor

left for the V2.0smHCR FISH to fulfill our requirements was to demonstrate ability to target the nascent transcription of X-linked XCI marker & escapee genes with an efficiency comparable to traditional BAC-FISH probes.

Second, the increased V2.0 smHCR signal intensity allowed us to gain more information from FISH analysis than previous technologies. The ability to detect exceedingly low copy numbers of *Tsix* and *Xist* LncRNAs increased the detection efficiency, and hence the amount of information we could obtain. In particular, *Xist* accumulation as a nascent transcription spot is very hard to follow otherwise, and would have figured as a "false negative" in an important fraction of the X-inactivated cells if we didn´t use V2.0smHCR.

Third, both V2.0 smHCR approaches, either with long (Choi et al. 2014) or short (Shah, Lubeck, Schwarzkopf, T.-F. He, et al. 2016) oligonucleotide probes had proven to be able to target RNAs very satisfactorily. Faced to the question of which of the two approaches to use, we decided to focus on the approach using the short **50bps** oligonucleotides (Shah, Lubeck, Schwarzkopf, T.-F. He, et al. 2016) for two reasons. The first was that this approach used **20bps** sequence to recognize the target RNA, allowing us to use the preexisting documentation on probe design used in traditional single-molecule Stellaris oligo-FISH (Levesque & Raj 2013). The second was that the short **50bps** oligonucleotides could be synthesized reliably by most commercial providers, while **100bps** oligonucleotide length and above require expensive purification to ensure full-length synthesis, or are otherwise truncated (Sinnamon & Czaplinski 2014). The third was that we could buy more short **50bps** primary probes for the same price, ensuring redundancy and the ability to target more X-linked loci.

Fourth, the good V2.0 smHCR experimental results **(Fig.6)** and the experience with commercially labeled probes **(Fig.5)** had convinced us that the main factor for success was signal intensity per primary probe, and that as few as 5-10 primary probes could be enough to target effectively X-linked nascent transcription. Since each **50bps** primary

probe costed approximately **7.5€** and recruited 100 fluorescent dyes, we thought that with 5-10 primary probes alone we could obtain 5-10.000 dyes/target RNA at a cost of **40-75€** per target locus, an attractive price.

Driven by these considerations and the good performance of hairpin chain reaction, we set to design V2.0 smHCR primary probes against the XCI marker genes *Atrx* & *Ndufb11*, as well as the XCI escapee gene *Ddx3x*, and test their ability to monitor the X chromosome transcriptional activity.

Performance of Shah V2.0 smHCR probes against X-linked nascent transcription:

Our goal was to design specific HCR probesets targeting XCI marker & escapee genes that could accurately monitor the X transcriptional activity and demonstrate their specificity.

We first designed a V2.0 smHCR FISH probeset against the XCI marker gene *Atrx*. We designed the primary probes so that their **20bps** target sequence recognition module would have a single, full length binding site on the target RNA, and that all off-target binding sites on any predicted transcript on the genome would be of **16bps** length or less. The primary probe sequences were targeted against intron sequences that were not included in any existing exon of a mRNA, be it experimentally tested or bioinformatically predicted. All of those precautions follow the design recommendations for classic Intronic Oligo-FISH probes (Levesque & Raj 2013).

We designed a main probeset using the B2 HCR initiator site, and a smaller probeset using the B1 HCR initiator site. Our purpose was to validate the specificity of our FISH signal by doing two-color colocalization analysis, using Alexa-647 far-red fluorescence for B2 hairpins & Alexa-488 green fluorescence for B1 hairpins. If our designs were accurate, we would find a single nascent transcription spot in X-inactive cells, and two on X-active cells. The spot would be the same in the two fluorescence channels.

When we tested our probesets against the *Atrx* XCI marker gene, the results did not

match our expectations **(Fig.7a&b)**. When targeted against the same *Atrx* nascent transcripts, both B2 & B1 *Atrx* probesets failed to show a number of spots restricted to the karyotype in both X-active ESCs **(Fig.7a)** and X-inactive MEFs **(Fig.7b)**.

While the biggest fluorescent spots were nuclear, and consistent with nascent transcription spots, the great amount of fainter fluorescent spots did not allow performing counts with any degree of confidence. In addition, many of the supernumerary fluorescent spots did not seem to co-localize in the slightest between the *Atrx* B2 & *Atrx* B1 probesets. These results led us to conclude that, either the *Atrx* probesets were un-specific, or the RNA-FISH protocol had been done improperly.

We wished to test that the results were not due to any defects in the execution of the RNA-FISH protocol. The *Atrx* B2 probeset was used with the *Tsix* B1 probes against X-active ESCs **(Fig.7c)** or *Xist* B1 probes against X-inactivated MEFs **(Fig.7d)** that had proved specificity and good performance before **(Fig.6)**.

In both cases, only the *Atrx* B2 showed supernumerary spots, while the *Tsix* & *Xist* B1 probes showed the same specific signal as before. In addition, the noise & un-specific spot signals in the *Atrx* probesets improved moderately when more stringent hybridization conditions, with increased temperature and formamide content were used **(data not shown)**.

The above led us to the conclusion that the results were due to un-specific binding of the *Atrx* probeset against off-target RNAs. The question was what was the cause.

I had two working hypotheses.

When designing the primary probes, I had assumed that the HCR initiator site could not interfere with probe specificity, since that sequence would be needed to hybridize at full length with the hairpin oligos for the HCR polymer to appear. But I noticed in a later publication from the creators of the short V2.0 smHCR protocol that the BLAST analysis later included the initial 10bps of the HCR initiator site in the calculation off-

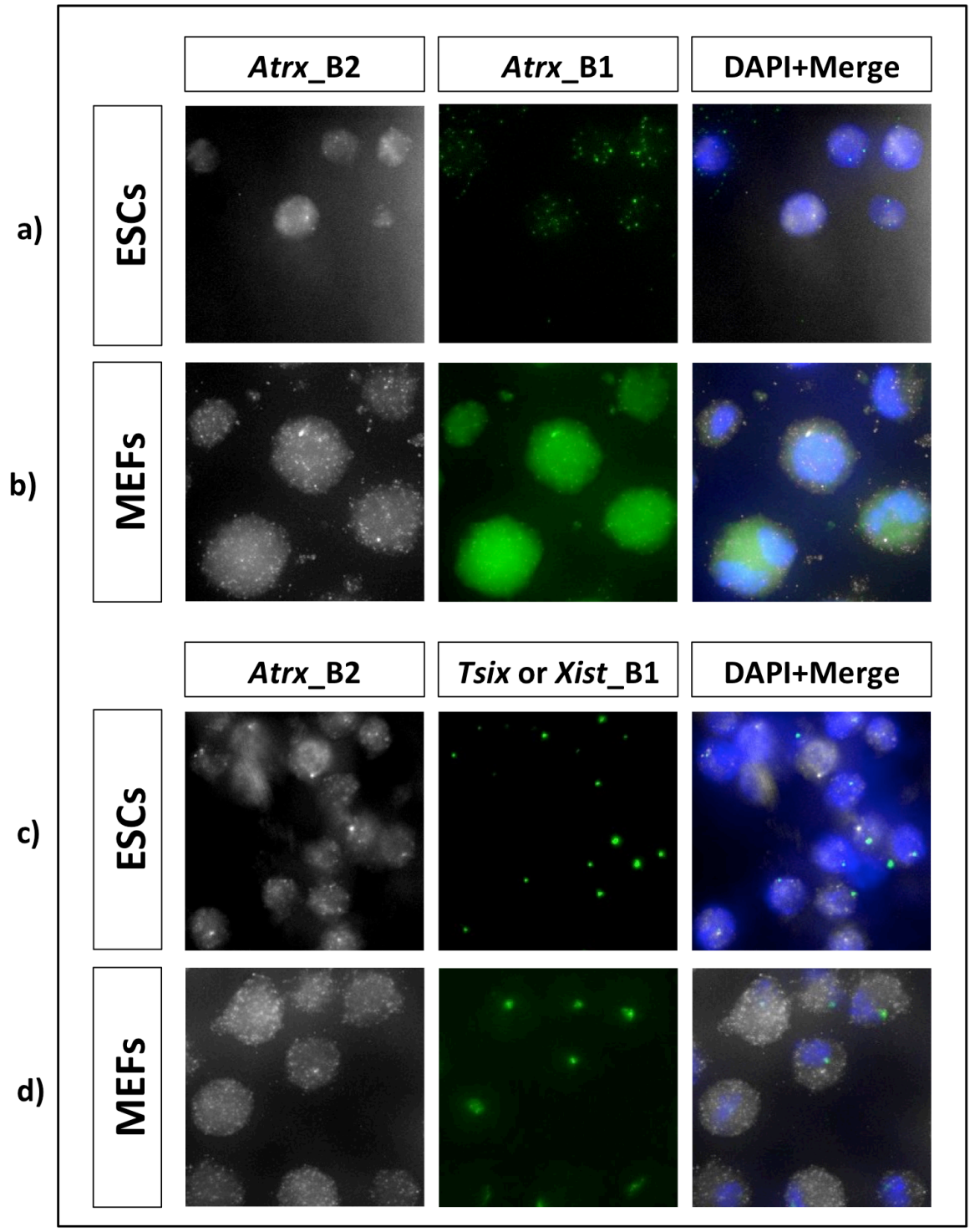

Figure 7: The *Atrx* smHCR V2.0 intron RNA-FISH probeset shows un-specificity:

a) .

b) .

c) .

d) .

target binding sites **(QUOTE Shah 2016 NEURON)**, creating a source of un-specificity we did not plan against.

The second hypothesis was that poor commercial oligo synthesis efficiency created a fraction of truncated oligonucleotide products, which were the ones binding un-specific off-target RNAs and creating noise. This stems from the fact that commercial oligonucleotide synthesis technology is 3´-5´, elongating nucleic acid sequence from a single 3´ terminus nucleotide, which is anchored to the synthesis substrate. As the synthesis proceeds, successive nucleotides are added, elongating the sequence until it reaches the 5´end. This process is not perfect, and since the addition of each base is a separate step with a given % efficiency, unless the synthesis efficiency is close to 100%, a significant fraction of the population (known as "shortmers") will have less than the intended 50bps length. While this can be offset, it only may be done with cost-prohibitive HPLC or PAGE purification, which would defeat the point of cost-effective oligo-FISH **(QUOTES)**.

The problem was that, in the traditional short V2.0 smHCR design (Shah, Lubeck, Schwarzkopf, T.-F. He, et al. 2016), the gene-specific targeting sequence was located in the 5´end, meaning that it was very likely to be truncated. I hypothesized that the un-specific signal was created by "shortmers" with truncated gene-specific targeting sequences, which instead of the full **20bps** length, had truncated sequences with degenerate binding properties, able to bind multiple RNAs within the cell.

Our goal was to correct the source of un-specificity, so we addressed both hypotheses.

We first accounted the first 10bps of the HCR initiator site in addition to the 20bps of the conventional gene-specific targeting sequence.

We then altered the probe design properties. For the X-linked XCI escapee *Ddx3x* and the XCI marker gene *Ndufb11*, as well as for *Tsix* probe sequences specific to the *castaneus* & *musculus* chromosomes, the probe design was the traditional arrangement, with a 5´gene-specific targeting sequence and a 3´HCR initiation site **(Fig.8a)**.

In a second set of probes, we adapted the V2.0 smHCR design. For the X-linked XCI escapee *Ddx3x* and the XCI marker genes *Ndufb11* & *Fmr1*, as well as for the

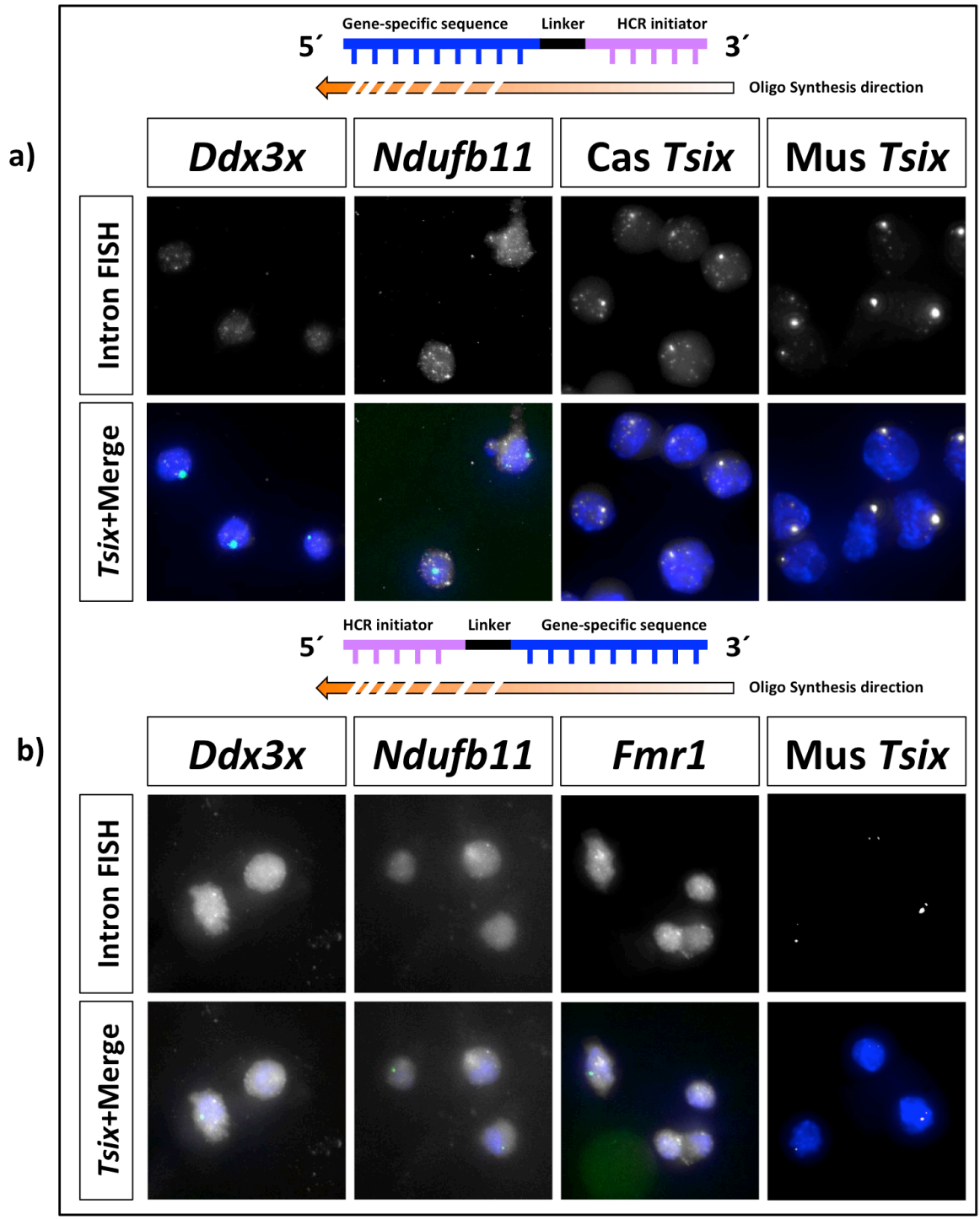

Figure 8: The synthesis direction does not reduce un-specificity in V2.0smHCR:

a) .

b) .

c) .

musculus-specific *Tsix* probe, we created a second, smaller set of probes in which the 3´gene-specific targeting sequence was followed by 5´HCR initiation site **(Fig.8b)**. We were able to perform this by adapting the second 5´ HCR site of the long oligosV2.0 smHCR technology (Choi et al. 2014).

In order to ensure that results were not being confused by karyotype abnormalities, all X-linked genes were co-stained with *Tsix* probes, providing an internal control.

We first tested the traditional 5´gene-specific sequence-Linker-3´HCR initiation site probesets in X-active hybrid ESCs **(Fig.8a)**. We observed that, for the *Ddx3x* & *Ndufb11* probesets, the situation had only moderately improved. While bright signals consistent with nascent transcription spots were observed, and the amount of un-specific signal had moderately improved, it was not enough to allow scoring X-activity confidently without using automated background subtraction tools. The performance of the probesets was strictly dependent on the number of primary probe binding sites on the target RNA. The repeat-based *Tsix* probes fared the best and the single legitimate nascent transcription spot could be easily tracked over the background noise, thanks to their **rough 60 binding sites each**. The XCI escapee *Ddx3x* fared worse, with **19 primary probes**, but better than the *Ndufb11*, with only **11 primary probes**.

This led us to conclude that the performance of probesets was strictly dependent on binding site number, and that taking into account the HCR initiation site sequence when calculating off-targets was not enough.

We next tested the 5´HCR initiation site-Linker-3´gene-specific sequence alternative probeset designs in X-active hybrid ESCs **(Fig.8b)**. When we observed the *musculus*-specific *Tsix* repeat probe, we could observe strong, scorable and specific signal, supporting that the re-design had not destroyed the ability of the primary probes to drive hairpin chain reaction or RNA-FISH. But when we analyzed the new designs for the X-linked genes *Ddx3x*, *Ndufb11* and *Fmr1*, all of them still showed the same problems with un-specific signal present in traditional V2.0 smHCR FISH designs.

We concluded that our un-specificity problem was a feature of the V2.0 smHCR

system, instead of being explainable by “shortmers” or probe design. Since we were using less primary probes than in the original report, which had focused on exonic mRNA-FISH and used 40 probes per target and automated background subtraction with dual-color colocalization analysis, we assumed that the original report achieved its results by a “brute force” approach we could not a sustain, due to the high cost of so many probes.

This view was later supported when the same authors published a report on a high-throughput derivative of this technique, called intron-seqFISH (Shah et al. 2018).

On it, the authors changed the probe design approach, increasing the gene-specific targeting sequence length to **35bps**, and using a sophisticated oligoprobe design pipeline with iterative optimization to ensure specificity. The fact that they used such an approach, reserved to dealing with DNA-FISH oligopaints against troublesome repeat-enriched sequences, lend credence to our view that the un-specificity was an original feature of the protocol, and could not be solved with the limited expertise and resources at our disposal.

Our final conclusion was that, while the hairpin chain reaction was definitively the way to go, the primary oligo probe technology had to change. In order to be able to use hairpin chain reaction, we needed a radically different approach that would dramatically increase the specificity of primary oligonucleotide probes.

Hairpin Chain Reaction RNA-FISH results & implications:

Motivation:

The results of the previous experiments had shown us that while HCR signal amplification performed adequately, we needed an improvement of the specificity of primary probes. The question was how this increase in specificity may be achieved.

The original *Stellaris* single-molecule FISH used multiple short 20bps oligos because

the on-target specific binding would overpower the stray off-targets of a minority of the probeset, either by increased signal intensity or by the fact that the faint off-target signal would be indistinguishable from the cell background autofluorescence. When reading between the lines, the idea behind it, and one of the key reasons why it replaced the previous single molecule Oligo-FISH approach by the Singer lab **(QUOTES)**, which used 5-10 oligos with 5 fluorescent groups each, was that the short 20bps oligo sequences had always allowed a degree of off-target binding, and that the *Stellaris* approach from the Raj lab solved this problem by a brute-force approach, distributing an equivalent amount of fluorescent dyes between many more probes. This sacrificed the cost-effectiveness for a gain in *perceived* specificity (Gaspar & Ephrussi 2015; van Gijtenbeek & Kok 2017)**(QUOTE)**.

I considered that the main parameters governing specificity that we could understand & manipulate more easily, were the hybridization length difference between probe on-target binding and off-target binding sites, and the use of split-paired primary probes vs traditional single primary probes.

The more intuitive parameter was the hybridization length difference. In the classic Stellaris oligo-FISH approach, the typical length difference achievable is 20bps on target and 16 bps to any transcribed off-target RNA: this means only a 20% of sequence divergence to exploit. An additional caution is that this kind of sequence divergence only applies to conserved RNA transcript sequence; when considering DNA as a target, the sequences are under less evolutionary pressure for specificity, and the ones who are tend to be bound by protein complexes that cross-link around the sequence after fixation and prevent probe binding to them **(QUOTES)**.

When dealing with problematic DNA sequences, the length of the primary probe was increased to 35bps in all the oligo-paint DNA-FISH protocols to date, such as MER-FISH and others (Nora et al. 2014; Beliveau et al. 2015)**(QUOTE DNA-FISH Beliveau & Ting Wu)**. In our experience, typical intron DNA sequence offered at best 17bps off-targets to a 20bps on-target with Stellaris Oligos; that is, only 15% sequence divergence. If the probe length increased to 35bps, the theoretical gain of a 35bps on-target to 17bps off-targets would be a 49% of sequence divergence to exploit. If all off-

targets have a sequence divergence of almost half of the primary probe length, it is easier for stringent hybridization conditions (high temperature, salt & formamide content) to prevent off-target binding events while preserving the specific on-target probe binding. Interestingly enough, the original V2.0 smHCR approach had used a 50bps sequence length, which would press sequence divergence even further (Choi et al. 2014).

This 35bps probe length increase sounded promising, but it had been originally developed for DNA-FISH without any kind of signal amplification, and only adopted as an afterthought for HCR methods (Shah et al. 2018)**(QUOTE NEURON)**.

The other option was the use of split-paired probes. The best-documented cases on sequence-driven signal amplification present in the literature were the branched DNA (bDNA) approaches. Since they were first developed at the end of the nineties & beginning of the new millennia (Player et al. 2001)**(QUOTES)**, they moved on from initial single primary probes for academic research purposes (Sinnamon & Czaplinski 2014; Player et al. 2001) towards the use of split-paired probes. Intriguingly, the leading commercial bDNA technologies available nowadays, RNAscope (Wang et al. 2012) & ViewRNA (Battich et al. 2013) use the same split-paired probe design. On it, the two probes with 25bps gene-specific sequence have to bind to the same target RNA at a specific distance from each other. Under these very specific circumstances, the split-paired probes generate a hybridization platform that a readout oligonucleotide can bind. It contains multiple repeats that shorter probes can bind. After multiple hybridization steps, a docking platform for the fluorescent readout oligos is created, yielding 10^4 fluorescent dyes per split probe pair. This approach had the advantage that an effective 50bps on-target sequence length was created, and the specific binding distance further helped specificity.

Sadly enough, two major inconveniences precluded the use of RNAscope & ViewRNA approaches. The first was that the cost was out of our budgetary limit of 200€ per targeted RNA. The second was that the approach required a total of 4 hybridization

steps & consecutive sets of washes. Since we intended to apply the technique to PGC-LCs, which suffered serious detachment issues with as few as 2 hybridization/HCR amplification steps, commercial RNAscope & ViewRNA were unlikely to preserve enough sample for analysis.

We did nonetheless extract a lesson from this. Those two commercial platforms were able to show specificity for 10^4 fluorescent dyes per single probe, even more when single-probe miRNA detection with alkaline phosphatase was needed, and never used more than 25 probe pairs. This meant that these approaches could not rely on brute force to overcome background signal; consequently, the split-paired probe design should necessarily guarantee specificity for the few 10^2 dyes per single probe pair that the HCR signal amplification would yield.

I deduced that, since the HCR FISH approach had been continued steady development, with a publication every 2-4 years (Choi et al. 2016; Choi et al. 2014; Shah, Lubeck, Schwarzkopf, T. He, et al. 2016; Shah et al. 2018) **(QUOTE V1.0)**, the split-paired probe technology for HCR RNA-FISH would be close to publication. The patents from the Niles A. Pierce laboratory suggested as much.

We contacted the personnel from Molecular Technologies, the spin-off that managed the distribution of HCR commercial kits, and were kindly offered the use of the split-paired probe V3.0 smHCR technology several months prior to the publication of the seminal report (Choi et al. 2018) and its application to whole-mount embryos (Trivedi et al. 2018).

Our goal was to use the reported improvement in signal specificity for V3.0 smHCR primary probes to create specific probesets to monitor the transcriptional status of X-linked genes fulfilling the 3 exclusion principles outlined at the beginning of the chapter: standard karyotype, detection efficiency & signal Intensity.

Methods and results:

The split-paired V3.0 smHCR works by dividing the HCR initiator site between two primary probes, which each have a target-specific hybridization site of 25bps length each. When two of them bind to the intended target at a distance of exactly 2bps between them, the HCR initiation site is reconstituted and a 10^2 copies-long polymer of fluorescent hairpin oligonucleotides is formed. This offers two key advantages. The first is to increase probe specificity, since off-target binding events need to include the 2 probes at a set distance. The second is that this approach performs better in whole-mount embryos, tissue slices or other applications that have poor permeabilization & probe diffusion. In those instances, single primary probes can get un-specifically trapped within the tissue, contributing to the background. Since the HCR initiator site is reconstituted only when the probes are bound at a certain orientation & distance, split-paired probes create far less background signal.

The end results is that the V3.0 smHCR probesets scale linear & efficiently the signal intensity depending on the number of probes and perform much better in whole-mount embryo settings (Choi et al. 2018).

We decided to test the method by creating two new probesets targeting the intron sequence of the XCI escapee *Eif2s3x* and the XCI marker gene *Prdx4*. In order to maximize signal intensity & detection efficiency, we used 25 split-paired probes per gene, focusing on maximal probe concentration in the first intron of the gene, then covering all possible introns excepting the last. This approach was intended to maximize signal intensity by targeting the intron most shared between all nascent transcripts at the nascent transcription site, and boost detection efficiency by ensuring the representation of all possible intron sequence. The last intron was purposefully avoided, since its splicing and degradation sometimes happens after the transcript is detached from the nascent transcription site **(QUOTE)**.

In order to ensure specificity, we strived to maximize the on-target to off-target binding sequence divergence of the primary probes. The primary probe sequences were designed by the personnel of Molecular Technologies to saturate the available intron sequence; we then tested the specificity by focusing on the effective binding span: 52bps binding interval, for two 25bps individual probes and 2bps un-bound spacing

between the two primary probes. We only took the primary probes that had a unique on-target effective binding site of 52bps and whose off-target bindings on all predicted transcripts were 28bps length or less. In effective terms, this is a 54% sequence divergence limit, with most of the probes yielding 50% divergence.

The 25 split-paired primary probes could recruit a maximum of 2.500 dyes/nascent RNA transcript, at a cost of **200€** per target locus.

We only faced a problem. Since we were limited by budget, we were forced to use a suboptimal Alexa555-labeled hairpin for the RNA-FISH experiments. Since the entirety of our cell lines used *X-eGFP* & *X-tdTomato* transgenes to ensure that all female cells had an XX female karyotype, the V3.0 smHCR RNA-FISH would have to punch through preserved red fluorescent protein background signal to be seen.

Choi V3.0 smHCR method testing on *eGFP*, *Eif2s3x* & *Prdx4* X-linked loci:

In order to test the performance of the V3.0 smHCR FISH, we assayed the nascent transcription of XCI escapee gene *Eif2s3x* **(Fig.9a)**, the XCI marker gene *Prdx4* **(Fig.9b)** and the X-linked *X-eGFP* reporter mRNA **(Fig.9c)** in EL16.7 TST dual color ESCS. To guarantee the normal karyotype and transcriptional status of the ESCs, each cell was co-stained for *Tsix* expression with the V2.0 smHCR probeset used in earlier experiments **(Fig.6a)**.

For the XCI escapee *Eif2s3x*, only **27%** of cells lacked a nascent transcription spot, **13%** of them had a single nascent transcription spot, and **60%** of the cells had two nascent transcription spot **(Fig.9a)**. This **60%** biallelic expression was close to our professed objective of **80%** of biallelic expression, but did not reach it.

For the XCI marker gene *Prdx4*, **46%** of cells lacked a nascent transcription spot, **18%** of them had a single nascent transcription spot, and **36%** of the cells had two nascent transcription spot **(Fig.9b)**. This **36%** biallelic expression was still far from the **80%** biallelic expression objective.

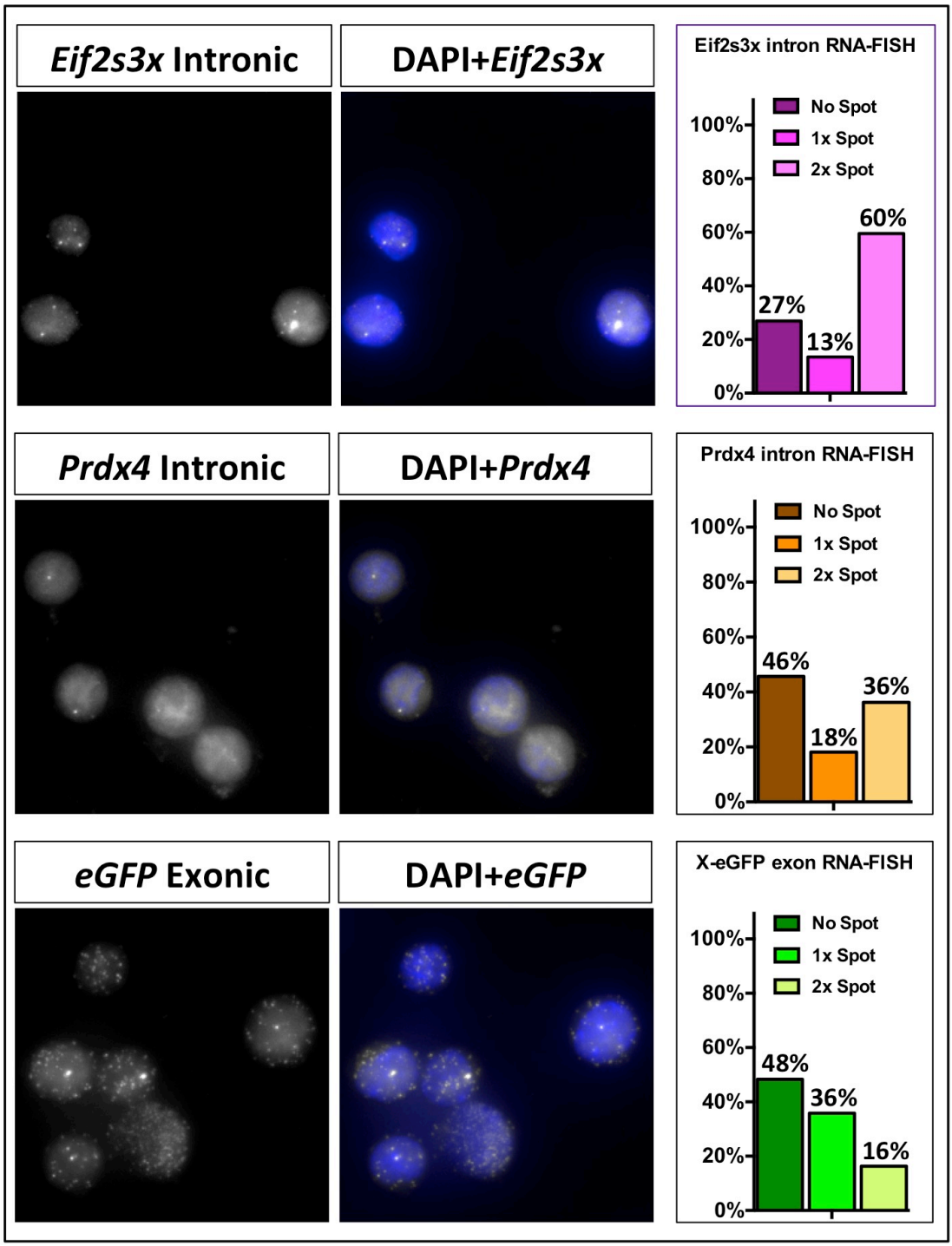

Figure 9: The smHCR V3.0 provides specific & simple Intron RNA-FISH scoring:

a) .

b) .

c) .

We concluded from the results from the two X-linked probesets that we had achieved our goal to design specific intron RNA-FISH probesets able to monitor accurately the expression of the X-Linked genes. However, the percentage of biallelic expression was still too low to fulfill our goal of **80%** or superior biallelic detection in X-active cells. Still, the **60%** biallelic detection rate for the *Eif2s3x* probeset is an encouraging result, opening the possibility of fulfilling the **80%** detection rate objective if the experiment was repeated in a channel without fluorescent protein background.

Intriguingly enough, *Eif2s3x* is one of the "pedigree" XCI escapee genes that are very frequently targeted in FISH studies; conversely *Prdx4* is a reliable RT-PCR XCI marker gene, but has been slightly underused for FISH analysis. While we selected the *Prdx4* gene for its high expression in all 4 cell types of interest, it may be possible that using another XCI marker gene with more "pedigree", such as *Atrx*, may yield better detection efficiency.

The X-linked *X-eGFP* marker gene is a special case, since it is targeted against the exons of the *eGFP* mRNA **(Fig.9c)**; it was originally not intended to score nascent transcription, but as a positive control for the V3.0 smHCR. However, we reasoned that it should be possible to score the single nascent transcription for the transgene, since the *eGFP* mRNAs should cluster around the single *X-eGFP* transgene in the *mus musculus* X chromosome of the hybrid cell line.

We scored nascent transcription sites targeting the single brightest nuclear spot in the *eGFP* staining, and scored it negative if there was no visibly stronger fluorescence spot. While **48%** of the cells had no clear nascent transcription spot, **36%** of the cells had the expected single nascent transcription spot, and **16%** of the cells had two nascent transcription spots. While there is a single copy of the *X-eGFP* transgene, the **16%** of cells that score two nascent transcription spots are likely to be explained by cell division; the number of ES cells with more than two *Tsix* spots detected with commercial probes was in the range of **13%** of the population **(Fig.5c)**.

This result led us to two conclusions. First, the V3.0 smHCR had the ability to perform exonic RNA-FISH, and had a qualitatively cleaner signal than its old V2.0 smHCR

counterpart at similar probe counts **(See Fig.9c Vs Fig.6c)**. Second, the use of exonic probesets may be used to supplement the intronic probesets to enhance the detection of nascent transcription spots.

The combined results from V3.0 smHCR probesets led us to six conclusions.

First, we could design specific intronic RNA-FISH probesets that could be directly scored to interrogate the transcriptional status of the X chromosome, no image analysis pipeline required, fulfilling our initial goals of signal intensity & specificity.

Second, we were able to predict the specificity of the probeset *in silico* without complex bioinformatics expertise. By using maximizing the sequence divergence between on-target and off-target binding sites, the arbitrary simple cutoff of discarding probes with more than 28bps length off-target binding sites from the total effective 52bps binding span seemed sufficient to ensure specificity of the probeset.

The BLAST analysis used for probe validation is simple enough that any user may ensure the specificity of their probeset without any specific training.

While ensuring full specificity is not possible until co-localization experiment with another probeset directed to the same target RNA is done, the fact that all probesets give results constrained to the tested XX karyotype of female ESCs is a very strong indicator.

Third, while we did not yet reach our goal of 80% or superior detection efficiency, the V3.0smHCR intron FISH approach looks able to reach it, and our current *Eif2s3x* & *Prdx4* probesets may already be able to reach it. It is very likely that a fraction of the faint nascent transcription sites are buried under the red fluorescent protein background, and using a channel with null autofluorescence background, like if Alexa647-labeled fluorescent hairpins were used for HCR amplification, would certainly result in increased detection rates.

The only way this advantage could be offset would be if un-specific signal was also buried under the red fluorescent protein background.

Fourth, the “pedigree” of the XCI escapee or marker gene hinted to predict a better

detection efficiency, to some degree. While concluding this merely from the compared results of *Eif2s3x* Vs *Prdx4* may seem hasty, in the failed V2.0 smHCR attempts for X-linked intron-FISH, the *Ddx3x* & the *Atrx* "pedigree" genes performed better than the *Fmr1* & *Ndufb11* ones.

It is however likely than any future attempts to expand the number of intron-FISH probesets will fare better if classic X-linked genes such as *Atrx, Chic1* & *Ddx3x* are tested first.

Fifth, the use of exonic targets can be used to score nascent transcription to some degree. While this is suboptimal compared to intron RNA-FISH, it is very possible that it could be used to supplement it. For an example, co-localization experiments to validate the intronic RNA-FISH specificity you could use an additional probeset targeted against the exons of the X-linked gene. Not only would you have an additional way to score its nascent transcription, but if any number of supernumerary spots is detected in your intron set, you can double-check if they co-localize with mRNA spots outside the nascent transcription site. If this is the case, your intron probeset is simply targeting intron sequence that is used as an alternative exon, or spliced out away from the nascent transcription site.

All the former results led us to conclude that the V3.0 smHCR oligo-FISH technology is the technology that can fulfill our goals. From the 3 original exclusion principles applying to FISH technology, (Standard karyotype, Signal intensity, noise and visual scoring, and Detection efficiency), the only requirement that is not yet met is the 80% biallelic detection efficiency. The latter is likely to change with the materials already at hand in the lab and experimental repetitions. From the 10 desirable traits of the oligo-FISH technology, it has met 8 of them in our hands (Simple bioinformatic design, short oligos, less than 200€/target cost, non-commercial, switchable fluorophores, exonic & intronic targets, scorable by naked eye), and only 2 remain to test: Its ability for oligo DNA-FISH below a 200€ pricetag, and the ability to be scorable by Flow cytometry (FACs).

One of the main desirable traits for HCR technology is its ability to generate comparable theoretical signal intensities to the oligo-paint DNA-FISH approaches under a 200€ pricetag if directed against DNA loci (Nora et al. 2014; Deng et al. 2015)**(QUOTE BELIVEAU)**. This has already been experimentally proven for V2.0 smHCR approaches (Shah et al. 2018)**(VERIFY QUOTES!)** and it only remains to be tested in V3.0 smHCR. Given that V3.0 is an improvement of the technology, it is not a big leap to assume it is going to perform at least equally well.

The ability of the V3.0 smHCR to generate enough signal intensity to separate mammalian cell populations based on their transcriptional heterogeneities by FACs analysis is a proven feature present in the original V3.0 smHCR publication (Choi et al. 2018). While we did not have a chance to test it personally, it is one of the best arguments for the technology. One of the big limitations of the classic Stellaris oligo-FISH technology is that the transcriptional heterogeneities in a cell population could be recognized and their functional impact ascertained, but how to sort & purify this fraction of the population for more detailed functional analysis and testing? With the use of a flow cytometer, it is not only possible to purify the desired cell population for detailed analysis with "omics" approaches such as transcriptomics, epigenomics & proteomics; it is also possible to sort cell populations for the expression of any cell fate RNA marker of interest.

This FACs analysis feature opens an interesting niche, in which any transcribed RNA can be used for sorting instead cell surface antibody markers. Given that it is much faster and easier to design specific V3.0 probesets than to brew a new specific antibody against the desired epitope, the use of V3.0 smHCR RNA-FISH probes instead of antibodies may drastically accelerate the work in non-mammalian or model organisms that have fewer commercially available antibodies. Examples that come to mind are the fields of microbiology, non-vertebrate eumethazoa and botany.

The last interesting feature of RNA-FISH FACs analysis is that it may well be amenable to system biology approaches. If V3.0 smHCR specificity is combined with well expressed exonic mRNA targets that accumulate hundreds of copies and the innate ability of modern flow cytometers to score even low amount of fluorescence with ease, the cost for an exonic probeset may well lower to 50-100€. Since flow cytometers have

been shown able to quantify the number of transcripts at single-cell resolution, this opens up an scenario in which many MRNA targets may be quantitated at the high speeds and low cost necessary for the high throughput analysis typically seen in systems biology approaches. This was already a published feature of commercial RNAscope & ViewRNA platforms (Wang et al. 2012; Battich et al. 2013), but this was offset by fluorescence kit costs in the thousand of euros, 150-350€/target primary probesets and significant cell losses in the multiple washing steps needed. Nowadays, with the increasing interest in FACs analysis of RNA-FISH and advances that offset cell loss during washes **(QUOTES)**, now may well be the time in which FACs analysis of RNA-FISH assays becomes commonplace.

The last argument for HCR FISH approaches is its great potential for gains in signal intensity in the near future. One recently explored avenue is the branched HCR, in which the primary probe is recognized by a first unlabeled hairpin chain reaction set. This primary set generates a 100-copy long HCR polymer, but it is one that instead of fluorescence generates a set of 100 HCR initiation sites. Those 100 HCR sites are, in time, recognized by a fluorescently labeled Hairpin chain reaction set.

The end result is a tree of 10^4 fluorescent dyes per primary probe (Liu et al. 2018). Interestingly enough, this approach is scalable; if instead of 2 branched HCR sets, 3 sets were used, the end result would be 10^6 fluorescent dyes per primary probe, and there is no current theoretical limit on how much this approach can be upscaled, excepting convenience and desired size of the HCR polymer.

This feature is particularly interesting when working in whole-mount embryos or other challenging samples. While V3.0 smHCR in whole-mount embryos (Trivedi et al. 2018) allows analysis that were previously reserved to genomic amplicon probes (BACs, PCR fragments) amplified by enzymatic activities such as tyramide deposition or alkaline phosphatase, it is still mostly restricted to highly expressed mRNAs, good image processing and lacks the sheer numbers of fluorescent molecules per target that traditional enzymatic signal amplification in whole-mount embryos uses to muster (Hauptmann et al. 2016). An important consideration is that all that enhanced signal intensity is only useful if the primary probe is completely specific, or you will amplify

unspecific off-target bindings too, partly defeating the point; the branched HCR method used a special approach to ensure that their primary probe would be fully specific (Liu et al. 2018) for a reason.

Given the interest of the Niles A. Pierce lab on whole-mount FISH in embryos, it is likely that the adaptation of the branched HCR approach to the split-paired V3.0 smHCR probes is currently in development; once this is done, the degree of signal will likely reach or exceed 10^4 fluorescent dyes per primary split-paired probe, and scaled up further in this hypothetical future "V4.0 branched HCR approach".

This would have important consequences for DNA-FISH, FACs analysis of RNA & DNA-FISH, and whole-mount embryo FISH; fields in which the signal intensity per primary probe heavily matters, and constraints for low cost per primary probeset limit how much the number of primary probes per target may be increased. In these approaches, the cost per target would dramatically decrease, and the increased signal intensity would lift many of the complex image analysis and bioinformatics requirements needed to discriminate signal from noise, leading those approaches to high throughput status.

In conclusion, our results support that V3.0 smHCR is the technology that can fulfill our goals to monitor the transcriptional activity of the X chromosome. With it, we managed generate specific probesets for all the 4 classes of X-linked targets we were interested in: the *Tsix* & *Xist* LncRNAs **(Fig6a&b)**; the XCI escapee genes, represented by *Eif2s3x* **(Fig.9a)**; and the XCI marker genes, represented by *Prdx4* **(Fig.9b)**.

The only strict requirement we are currently missing is the 80% biallelic detection efficiency of XCI marker and escapee genes in X-active cells, and we stand a good chances of overcoming this limitation with the materials currently present in the lab.

In addition, we have argumented the ability of V3.0 smHCR and future developments of it to fulfill 8 out of 10 desirable features in an oligo-FISH assay and to address the remaining frontiers of the oligo-FISH field: oligo DNA-FISH, FISH FACs analysis, whole-mount embryo FISH and increased signal by branched HCR.

While there were still experiments to be done to fully reach our original goals, we did

not have any more time or funding left to pursue them. As such, we focused on reviewing previous results and reinterpreting them in light of the new developments, in order to offer a review of the project results to anyone interested in future exploitation of it.

Performance between In-house labeling, V2.0 & V3.0 smHCR methods:

Our next goal was to offer a comprehensive review of all the results obtained in this chapter. We focused on the visual comparison of signal intensity & noise and the quantitative differences when scoring the transcriptional status of the X chromosome.

For this, we show representative pictures of RNA-FISH of the relevant X-linked targets imaged under the optimal settings and circumstances to ensure the most effective scoring of the signal, and compare the results of their quantitations.

Our first focus was the markers of the X-active ESCs. Our first concern was the *Tsix* LncRNA, marker of the X-active chromosome status **(Fig.10a)**. We compared the performance differences when labeled with the N-SH probe labeling method (Sunwoo et al. 2015), a commercial probe labeling by Sigma-Aldrich, and the results obtained by the same probes adapted to V2.0 smHCR (Shah, Lubeck, Schwarzkopf, T. He, et al. 2016).

We first compared the total detection efficiency, that is, the amount of cells that score any number of recognizable *Tsix* signals. In N-SH probe labeling, it was **98%**; in commercial probe labeling, it was **90%**, and in V2.0 smHCR probes it was **98.2%**.

The detection efficiency was fairly similar, consistent with the high number of probe binding sites to the target LncRNA and no great performance differences crop up when analyzing the percentages of cells with the desired biallelic expression. In N-SH probe labeling, it was **56%**; in commercial probe labeling, it was **44%**, and in V2.0 smHCR probes it was **60%**. The comparatively worse performance than expected from the commercially labeled probe stems from the use of a red Cy3 fluorophore over a preserved red fluorescent protein background, due to experimental constraints **(Fig.10a)**.

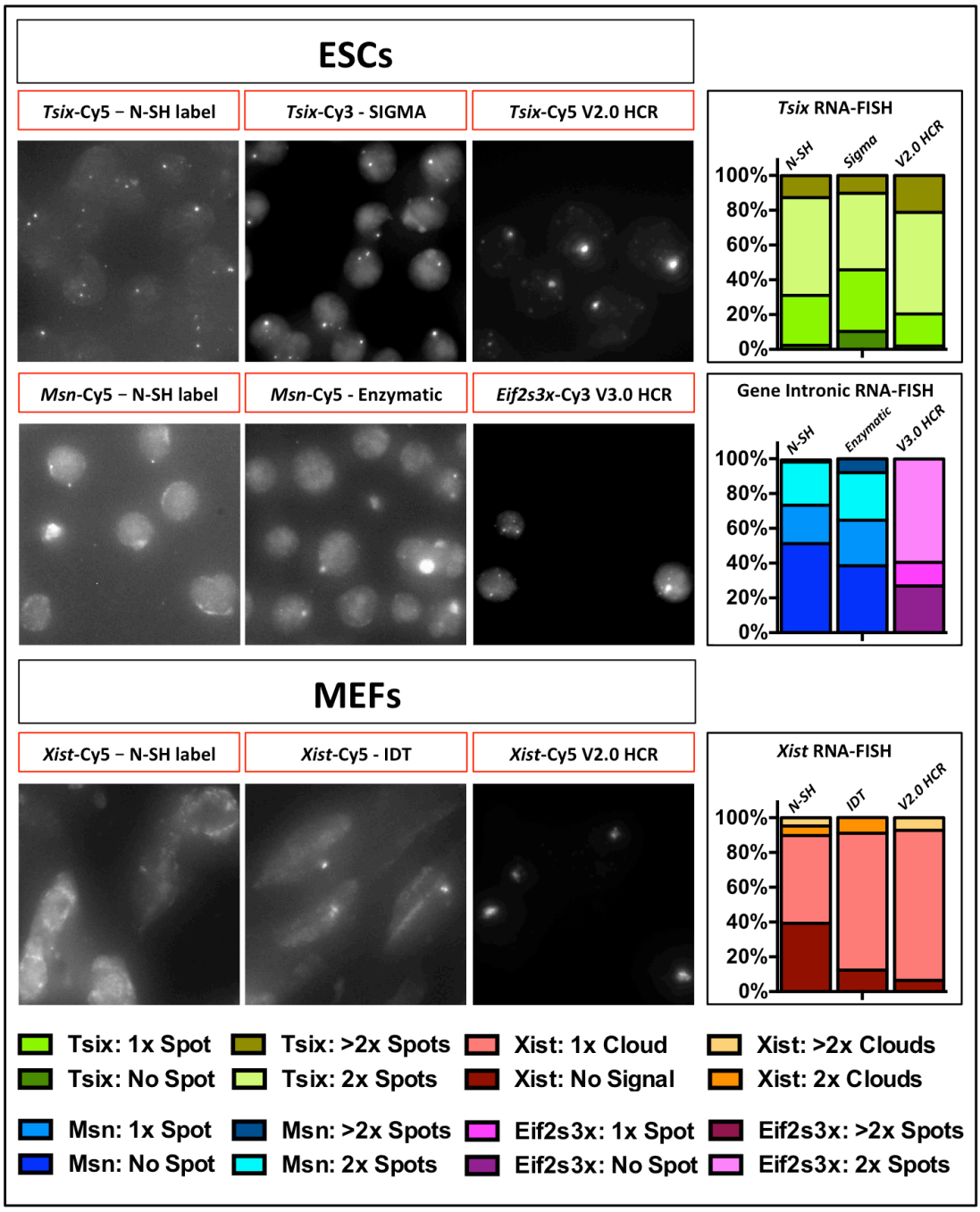

Figure 10: Gain of detection efficiency Vs tradeoffs between methods tested:

a) .

b) .

c) .

The major benefit comes in signal intensity gains, which steadily increases from N-SH to commercial probe labeling and then to V2.0 smHCR. The increased signal intensity of V2.0 smHCR is paid in terms of added un-specific background, and is only offset because of the 132 repeats on-target the probe binds vs the proven individual off-targets of this repeat motif elsewhere in the genome. Still, it is clear that the brute-force multiple bindings of the probe to the target overcome many of the un-specificity problems we found in the V2.0 smHCR, and play an important part into making its functionality tolerable.

The conclusion is that in case of well-expressed targets with probe designs based on multiple specific repeat bindings on-target, even inefficiencies in probe labeling, specificity and suboptimal setups may be negated to some extent. However, these target sequences, often included in methods papers and commercial providers as positive controls, are rather the misleading positive exception than the norm when it comes to evaluate a technique shortcomings.

When next moved to compare the performance of N-SH probe labeling, Enzymatic probe labeling and V3.0 smHCR to score the expression of X-linked genes **(Fig.10b)**. Only the best probeset of each class is compared. We first compared the total detection efficiency, as the amount of cells that score any number of recognizable nascent transcription signals. In *Msn* N-SH probe labeling, it was **49%**; in *Msn* Enzymatic probe labeling, it was **61%**, and in the *Eif2s3x* V3.0 smHCR probeset it increased to **73%**.

The differences in detection efficiency had severe repercussion in the ability of the probesets to score the desired biallelic expression in the X-active ESCs. In *Msn* N-SH probe labeling, it was **25%**; in *Msn* Enzymatic probe labeling, it was **27%**; and in the *Eif2s3x* V3.0 smHCR probeset, where the total detection efficiency was far larger, biallelic expression scoring increased to a hefty **60%**.

The improved performance of V3.0 smHCR comes from the increased signal intensity and specificity of the probeset, even when employed over a preserved red fluorescent protein background **(Fig.10b)**. We hypothesized that the increased signal intensity and total detection efficiency affects the biallelic detection efficiency through two main

ways. First, it lowers the number of nascent transcripts that need to be clustered in a nascent transcription site to generate enough signal intensity to be scored and signaled; with the signal intensity involved in V3.0 smHCR, one single transcript may be enough to see. This means that the nascent transcription site would be visible at the beginning and the end of its transcriptional activation, instead of a narrow timeframe in which a maximum number of nascent transcripts is accumulated for N-SH & Enzymatic labeling.

Second, each of the two alleles in each X chromosome has a similar random chance to be activated when the cell needs the mRNAs produced by the X-linked gene. If the chance for the allele to trigger a transcriptional burst is an independent probability, the chance that simultaneous biallelic expression is detected is the product of the individual probabilities of the two alleles being activated, and is consequently lower.

The working hypothesis would be that V3.0 smHCR yields improved detection efficiency because it has the added signal intensity to detect more of the time window of the nascent transcription burst, making more likely that the transcriptional activation of the two X-linked alleles is captured at the same time, even if they are expected to be asynchronic. This explanation comes from the known behavior and widely accepted model of nascent transcription in mammalian cells. (Levesque & Raj 2013; Shah et al. 2018; van Gijtenbeek & Kok 2017; Gaspar & Ephrussi 2015)

Our last goal was to compare the performance of N-SH probe labeling, Commercial probe labeling and V2.0 smHCR to monitor the *Xist* LncRNA in MEFs **(Fig.10c)**. The *Xist* LncRNA is chosen because, besides its functional relevance in the X-inactivation field, is a prime example of a LncRNA which function involves accumulating far way from its transcription site and its localization pattern in *trans* is vital to its function.

In cells committed to X-inactivation, the *Xist* LncRNA starts as a nascent transcription spot in the inactivating X chromosome and then expands to a whole cloud covering the entire X chromosome. In stably X-inactivated cells such as MEFs, the *Xist* cloud pattern is still disrupted with cell division and needs to be formed again; this means that nascent transcription spots and expanding clouds will be seen alongside the fully formed *Xist*

cloud **(QUOTE)**.

We first measured the total detection efficiency. In N-SH probe labeling, it was **61%**; in commercial probe labeling, it was **88%**; and with the V2.0 smHCR probeset adaptation, with 100x brighter signal per probe, total detection efficiency increased to **93%**. The specificity of the probe is demonstrated because in all probe labeling methods, the number of MEFs with more than the single expected *Xist* signal is under **10%**. The main benefit of the V2.0 smHCR *Xist* probe is instead the visible gain of signal over background and its ability to detect the nascent *Xist* transcription spot, which accounts for the gain in detection efficiency over the N-SH & commercial labeling methods.

The combined results lead us to the following conclusions.

First, the disadvantages associated with any in-house probe labeling method that chemically or enzymatically conjugates fluorescent dyes to unlabeled oligonucleotides can tolerate inefficiencies to some extent only if three extenuating circumstances are present:

The target is highly expressed and accumulates multiple copies in a very narrow region of the cell (such as *Tsix* for the nascent transcription site or *Xist* for the X chromosome); the probeset binds a highly specific & accessible repeat motif multiple times in the target RNA (132 repeats for *Tsix* and 25 repeats for *Xist*); and the far-red channel is available for imaging, as it almost lacks autofluorescence in mouse cells.

If not, such as in the case of the X-linked gene intronic FISH, you will need to ensure absolute labeling efficiency, and to control separately every single labeling step of the protocol. While this is theoretically possible, in practice this requires a major commitment from the researcher, and it only should be performed if the probe labeling is the only technique to optimize for the research project to succeed and deliver reliable results. If the oligo-FISH is intended as a relatively minor control readout, or a requirement of the field, but does not deliver the main findings needed for the project, it is much more efficient to obtain it via collaboration or purchase a tested commercial probeset once the project is near completion. Given the reagent costs alone, without considering man-hours and the multiple probeset designs before success, it is a far more

cost-effective approach.

Second, while multiple sequence-dependent signal amplification methods have become available in the last years, if not using split-paired primary oligo probes, all of them require sophisticated image processing, fastidious informatic or wetlab optimization of every single primary oligo probe, or brute-force increase to the number of primary probes to obtain a completely clean and specific signal over background. While this may be a bold claim, all recent papers that followed this approach, such as V2.0 smHCR (Shah, Lubeck, Schwarzkopf, T. He, et al. 2016) or CLAMP-FISH **(QUOTE)** more or less explicitly report the need to carefully cut out the un-specific background that can be seen once the signal is amplified. We have argued that the increase in primary probe length is a common designer response to fight against this issue, and the newer follow-up methods such as intronSeq, SABER and MER-FISH unanimously increase the primary probe sequence length to at least 35bps length, a standard response against embryo imaging, problematic DNA or RNA sequences, and other environments inimical to FISH (Shah et al. 2018; Kishi et al. 2018; Chen et al. 2015)

Third, as a consequence of the above, methods for sequence-dependent signal amplification usually need the same number of primary oligo probes as the Classic Stellaris 20bps-long oligo-FISH technology, bar a single exception. It is very important to factor this when the approach is budgeted. While it may be possible to reduce the probeset size, it may only happen after primary oligos are experimentally tested to find fully specific ones.

The one exception may be when the method uses split-paired primary probes. Such methods, such as V3.0 smHCR FISH (Choi et al. 2018) and commercial platforms RNAscope (Wang et al. 2012) & ViewRNA (Battich et al. 2013), report enough background suppression and have a simple enough informatics prediction of their specificity that the number of primary probes per RNA target could be greatly reduced to lower the cost.

Our own V3.0 smHCR experience with the exonic *eGFP* probeset (12 primary probe

pairs) and X-linked *Eif2s3x* & *Prdx4* (25 primary probe pairs) support this. Still, the cost involved is roughly 100€ for the exonic targets and 200€ for the intronic ones: A sizable reduction from the 1.000$ Stellaris standard, but not high-troughput standards as often claimed.

Fourth, of all the approaches tested, only V3.0 smHCR is close to the original ideals that started the project: non-commercial, simple-to-design, fast and inexpensive oligo-FISH technology for routine single-cell analysis of the X chromosome transcriptional activity; and it is more justified for benefits unrelated to the original purpose of a cheap single-cell transcriptional readout.

For its Intron RNA-FISH purpose, more experiments are warranted and the detection efficiency is still below our objective of 80% biallelic detection in X-active ESCs.

When compared to other alternatives to gain single-cell resolution for our X-reactivation model in PGC-LCs, such as single-cell RT-PCR or RNA-SEQ, our intron RNA-FISH with V3.0 smHCR does offer a relatively moderate cost benefit, but did take more man-hours to optimize that single-cell RT-PCR or RNA-SEQ would have needed.

Its main benefit lies in its flexibility: In the X-inactivation and reactivation field, it allows us to target known and new X-linked LncRNA candidates at a relatively low cost; also can give allelic resolution of X chromosome status by Intron-FISH; stands a high chance to allow inexpensive oligo DNA-FISH; can be used for FACs analysis of RNA expression; and is liable to gain enough signal intensity and become inexpensive enough in the near future to be upscaled as a systems biology scale readout soon.

While it is still a more invested technique than expected, and requires far more knowledge on the part of the user than we would like, its benefits still warrant its use.

However, anyone whishing to use this technique should focus more on it as a foundation for some research project rather than a simple “fire and forget” readout such as routine immunofluorescence of a well-known protein epitope.

Global Discussion and Conclusions:

The experiments of this chapter were articulated around 2 main goals.

The first was the development of a universal Immuno & RNA-FISH protocol for all 4 cell types of interest of our *in vitro* X reactivation model, with an additional focus for low cell population sizes (10^3 input cells) to allow routine analysis of *in vivo* PGCs.

The second was the implementation of a non-commercial, inexpensive oligo-FISH technology for routine analysis of the 4 main readout transcripts groups for the X chromosome activity: the LncRNAs *Tsix* & *Xist*, and the nascent transcription of the XCI marker & escapee genes, with an eye on publication of a set of validated Oligo-FISH probes against those targets to offer an alternative to the traditional BAC-FISH. To ensure that workflows remained simple enough for routine use, a number of stipulations were implemented.

The Oligo-FISH technology had to follow 3 main restrictions: to check in each experiment that cells preserved their standard XX female karyotype, that the probeset design was simple & the signal intensity strong enough for routine analysis without any informatics expertise needed, and that the detection efficiency was high enough to score X-activity at single-cell resolution (80% or above Biallelic expression in X-active naïve pluripotent stem cells). In addition, we strived to follow a set of 10 desirable features for the Oligo-FISH to select the optimal solution for our workflows.

We succeeded in our first goal of developing a universal Immuno & RNA-FISH protocol for all the 4 cell types of interest in our X-reactivation model: ESCs, Epi-LCs, PGC-LCs and MEFs. However, because only a fraction of the input PGC-LCs (roughly 10%) remains attached to the imaging vessel after combined Immuno & RNA-FISH, we can currently analyze *in vitro* PGC-LCs (10^4-10^5 input cells per experiment) but not *in vivo* PGCs, as their input cell sizes are too low (10^3 input cells per experiment).

We extracted two other important conclusions from our experiments.

The first was that Epi-LCs and PGC-LCs need fixation prior to permeabilization & attachment by centrifugation to the imaging vessel for Immuno & RNA-FISH, while PGC-LCs seemingly lacked the ability for active binding to standard adhesion treatments such as gelatin or fibronectin coating of imaging vessels. These results are

unusual, but consistent with the literature on the reported mechanical fragility of Epi-LCs & PGC-LCs (Hayashi & Saitou 2013b; Hayashi & Saitou 2013c), and that all current state of the art *in vitro* germ cell protocols expand the PGC-LCs as 3D organoids (Hayashi et al. 2017b) or attached to a feeder cell monolayer (Ohta et al. 2017b; Hidetaka Miyauchi et al. 2017).

The second was that in such unfavorable circumstances for sample preservation, the best approach was to combine successive coatings of the imaging vessel with passive adhesives (Poly-L-Lysine & Cell-TAK), followed by depositing the sample as a single cell suspension droplet in a polymerizing agent and *in situ* fixation and centrifugation to the imaging vessel without removing fluids. The rationale was to favor the formation and fixation of a cross-linked "polymer net" that binds the cells to the imaging vessel. We hypothesize that testing the use of extracellular matrix protein polymers with increasing cross-linking index (such as fibronectin, laminin and matrigel) and in a range of concentrations will yield protocols with low enough input cell size to ensure analysis of *in vivo* PGCs (10^3 cells per sample).

The strategy for Immuno & RNA-FISH we used allows to target an unusual amount of cell types and low input cell size, and to target both cytoplasmic and nuclear RNAs. In addition, it was implemented with scalability and high throughput in mind, and to be compatible with very heterogeneous FISH targets in mind (MEFs boast high cytoplasm to nucleus ratio & high permeabilization resistance, while PGC-LCs are unusually fragile and have large nuclei). For this reason, we recommend to use our strategy as a universal starting point when it is necessary to develop an Immuno & RNA-FISH protocol against cell suspension targets.

For the second goal of implementing an inexpensive oligo-FISH technology to target the 4 main classes of X-linked transcripts of interest, while respecting the 3 main restrictions, we managed most of our objectives thanks to the implementation of V3.0 smHCR oligo-FISH (Choi et al. 2018).

We managed to target the 4 classes of X-linked transcripts *(Tsix*, *Xist*, and X-linked XCI marker and escapee genes), and to fulfill two of our three restrictions: internal control of

standard XX karyotype at each experiment, and probeset design & RNA-FISH scoring without informatics expertise.

However, we did not achieve the single-cell resolution detection efficiency restriction, since our X-linked intron RNA-FISH probesets lacked biallelic detection efficiency in X-active cells (60% for *Eif2s3x* & 46% for *Prdx4*, instead the required 80% mark).

While we suspect that the repetition of the experiment with the same *Eif2s3x* & *Prdx4* probesets currently present in the laboratory would reach the single-cell resolution detection efficiency required, now that optimal far-red fluorophores and setup for HCR are available, but we did not have the time to perform those experiments before the end of the Phd. In addition, in order to reach our goal of publication, 3-4 X-linked intron probesets and 2 other exonic LncRNA RNA-FISH probesets would need to be designed and tested. This would likely take an additional 3-4 months, and hence the project would need to be finished by another researcher from the lab.

We extracted important conclusions from the experiments in this chapter.

From our experiments with in-house fluorophore probe labeling with the N-SH & Enzymatic probe labeling protocols, we extracted three conclusions.

First, the only practical guarantee for routine & deterministic fluorophore labeling of oligonucleotide probes is 3′-labeling modification during 3′-5′ oligo synthesis by a commercial provider, followed by HPLC or PAGE purification. The choice of a reputable manufacturer with high synthesis efficiencies is critical, with IDT being the best trade-off for price and reliability in our hands.

Second, the N-SH & Enzymatic probe labeling protocols yield probesets with relatively low signal intensities, require extensive experimental control steps and are very time-consuming, making them unsuitable for our goals of routine RNA-FISH analysis of X-linked intron nascent transcription & LncRNAs at high throughputs.

Third, any attempt at routine high-throughput RNA-FISH analysis should rely on unlabeled primary oligonucleotide probes that are recognized by fluorescent dyes coming from commercially guaranteed kits or sources. From our understanding of the

current state of the art, routine deterministic fluorescence labeling of oligonucleotide probes in-house at high-throughput is unrealistic & expensive for most laboratories.

From our experiments with V2.0 smHCR RNA-FISH, we extracted six conclusions.

First, FISH protocols using unlabeled primary oligonucleotide probes that undergo sequence-dependent signal amplification with commercially labeled fluorescent oligonucleotides yield fast and conclusive results. Compared with in-house labeling protocols, the only controls needed and challenges involved are related to primary oligonucleotide probe design. Since multiple hypothesis and design philosophies can be tested per order and the synthesis of oligonucleotides is fully done by commercial provider, the pace of experiments is very fast. All the hairpin chain reaction experiments, both for V2.0 & V3.0 smHCR were performed in less than 4 months.

Second, V2.0 smHCR, as all known protocols using sequence-dependent signal amplification, will amplify a correspondent un-specific background signal in addition to the legitimate signal, unless specific measures are taken, such as the use of split-paired primary probes, or sophisticated informatic design of single primary probes with on-target hybridization lengths of 35bps or above. In order to ensure discrimination of on-target specific signal against background, these protocols need primary oligonucleotide probeset sizes similar to classic Stellaris oligo-FISH probesets, two-color co-localization controls or sophisticated image analysis and background subtraction pipelines. This should be taken into account, as it is a substantial expertise and monetary investment, and we discourage using those protocols.

Third, in our hands, V2.0 smHCR can target exonic mRNA & LncRNA targets by visual inspection, but only if the probeset is large enough to discriminate against unspecific background, and not against intron targets for nascent transcription FISH.

V2.0 smHCR should not be used to target single-copy targets such as nascent transcription sites, or DNA sequences. Since the nascent transcription site has very variable numbers of target transcripts and spans of intron sequence to bind across the cell population, image analysis & background subtraction pipelines that rely on expected signal intensity are liable to perform very poorly, and DNA targets share some

of those features. Against DNA & Intron targets, we recommend to use V3.0 smHCR (Choi et al. 2018) or, at worst, the refined primary oligo-FISH design of intron SEQ-FISH (Shah et al. 2018), an limited attempt of solving the problems that V2.0 smHCR suffers to address those targets, and always double-check the specificity of the results with two-color co-localization controls.

Fourth, it should be assumed that the minimum primary oligonucleotide probeset size is going to oscillate at the standard 25-50 probes per nucleic acid target in all oligo-FISH protocols. The main reason is that even in protocols with sequence-specific signal amplification at levels that allow RNA or DNA detection with a single probe (10^2 to 10^4 fluorescent dyes per probe), a degree of unspecific off-target probe binding happens, generating a background that is only discriminated by the use of multiple on-target bindings. The secondary reason is that in protocols that ensure full primary probe specificity (split-paired probes, or single probes with careful design with on-target hybridization lengths above 35bps), there is no guarantee that the nucleic acid region targeted by the probe will be available for binding, be it obscured by RNA, protein binding or other causes. The resulting requirement for a redundant probeset size is a key consideration when budgeting oligo FISH-based projects.

Fifth, the increased signal intensities per target nucleic acid (10^3 to 10^4 fluorophores) yielded by signal amplification methods such as V2.0 smHCR are beneficial for LncRNA-FISH analysis. The fact that we were able to routinely observe the trace nascent transcription amounts of the *Xist* LncRNA from the XIC locus of X-active ESCs or follow different stages of *Xist* spreading in the X-inactive MEF population that usually need more optimized setups are examples of those benefits. This is particularly relevant because most LncRNAs are noted to be transcribed at very low copy number levels and need to be discriminated from *cis* to *trans* effectors, depending if their effects stem from clustering in their transcription site or not (Bassett et al. 2014). The increased signal intensity helps in those circumstances.

Sixth, we recommend the use oligo-FISH technologies with split-paired probes, like V3.0 smHCR (Choi et al. 2018), RNAscope (Wang et al. 2012) or ViewRNA (Battich et al. 2013) instead V2.0smHCR, due to their higher specificity and design simplicity.

From our experiments with V3.0smHCR, we extracted seven conclusions.

The first was that the academic V3.0 smHCR oligo RNA-FISH technology (Choi et al. 2018) is the only technology that we tested that can reliably perform intron RNA-FISH, thanks to the extra specificity granted by the split-paired primary probe design.

For the reasons discussed above, we also recommend V3.0 smHCR for DNA-FISH.

The second was that V3.0 smHCR FISH allows us to target specifically and score reliably all 4 classes of X-linked transcripts we aim to study: LncRNAs, exons of mRNAs and intronic sequences of X-linked XCI marker & escapee genes. While the necessary two-color co-localization experiments for intron RNA-FISH probesets are still pending, the lack of un-specific signal observed and the fact that all results are consistent with standard XX karyotype and X-activity status support specificity.

The third was that the principles governing V3.0 smHCR probe specificity are simple enough for in-house primary probe design with standard user-level programs used for RT-PCR primer design (such as Primer3) and informatics probe specificity prediction with routine BLAST analysis (such as with the ENSEMBL database).

This fact is what allowed us to do in-house probeset design against Intron RNA-FISH targets, in which even a single probe with off-target unspecific binding can prevent the obtention of conclusive results if scoring by eye as we did.

The fourth was that we did not reach the intended single-cell resolution ability for our XCI marker & escapee probesets, since we did not reach the 80% biallelic detection requirement in X-active cells. The detection efficiency requirement for the allele and probeset guarantees that visualization is guaranteed in any single-cell of the population. While our current XCI marker & escapee probesets do not reach this threshold, we think that if the experiments were repeated with the optimal far-red fluorophore and no fluorescent protein background, they are liable to reach the desired detection efficiency, particularly the *Eif2s3x* probeset. While single-cell resolution is not necessary *per se* to discriminate if the cell population is fully X-active or inactive, it avoids any reliable quantitation of the percentage of X-active & inactive cells if there is any heterogeneity in the sample population. Consequently, only intron RNA-FISH results and probesets with the requisite single-cell resolution & 80% biallelic detection efficiency are

considered reliable and publishable.

The fifth was that the detection efficiency of an X-linked gene seems to be explained by its "pedigree" rather than its expression levels alone. When we selected the genes for probe design in this chapter, we selected only target genes that had high expression levels in all 4 cell types of the *in vitro* X-reactivation model. However, at least judging from nascent transcription site signal intensities, certain genes frequently targeted in the X-inactivation field, such as *Eif2s3x, Atrx* or *Ddx3x* fared better than X-linked genes such as *Prdx4* or *Ndufb11*, seemingly without explanation pertaining to their supposed expression levels. For this reason, we recommend to target by intron RNA-FISH genes well used in the field, such as XCI escapees *Eif2s3x* & *Ddx3x*, and XCI marker genes *Atrx*, *Chic1, Hprt* & *Fmr1* for future probeset designs.

The sixth was that two-color validation of the specificity of an intron RNA-FISH probeset would benefit from exonic RNA-FISH targeting the mRNA of the same gene. This brings several added benefits to the experimental control. First, nascent transcription spots also can be discerned to some extent by exonic RNA-FISH as a brighter nuclear RNA cluster. Second, some introns may be spliced away from the nascent transcription site; the co-localization control with an exonic probeset is the only way to known if this extra spot is a specificity problem or the result of some of the targeted introns being spliced way from the nascent transcription site. Third, cells which show anomalies in the exonic RNA-FISH are compromised, and any concurrent anomalies in the intron RNA-FISH can be ascertained as such.

The seventh is that split-paired primary probe approaches, such as V3.0 smHCR (Choi et al. 2018), RNAscope (Wang et al. 2012) & ViewRNA (Battich et al. 2013) are the only approaches which we believe able to guarantee routine oligo-FISH analysis at high throughputs. This is motivated because the ability to fully predict absolute specificity of the probeset at user level expertise, followed by the use of short unlabeled primary oligonucleotides and subsequent fluorescent dye localization with commercially guaranteed solutions are much more important than high fluorescent signal levels thanks to any signal amplification. It is the specificity of the primary probeset and the commercial guarantee over the finicky fluorescent dye chemistry & location that yields the reproducible success & accurate budgeting for day-to day use.

Contrarily to what is frequently advertised, the multiple signal amplification methods that exist nowadays actually have the role of allowing additional applications (FACs-FISH analysis, DNA-FISH, whole-mount embryo FISH, lower probeset sizes), but are enslaved to the primary probeset specificity, with older technologies often performing better than new ones that have bright signal but fail this key requirement.

As a conclusion, I would like to point that oligo-FISH approaches have been unfairly lionized over the years. While the prevailing view is that FISH staining, be it traditional BAC-FISH or sophisticated oligo-FISH is "just a staining" and expected to be a fairly simple and fast readout, my experience is that it is an involved and time-consuming technique that relies too much on a very specialized expertise and insider knowledge of the "good regions to target" or "which oligo-FISH technology is actually reaching the standards that the company claims it does". It is not helpful that virtually all research publication the author got its hands on never published the unmodified raw images, but always subject the images to background subtraction filter, or arbitrarily cut out the unspecific background using the two-color co-localization controls, not giving the reader an accurate assessment of what are the real signal-to-noise ratios and image one should expect when checking your FISH staining on the microscope.

When one considers the necessary amount of trial and error and the expense of the commercial labeling kits and reagents, one should never expect less than 3-5.000€ expense to implement successfully the technique in the lab, even for a handful of genes, unless collaboration with a specialized researcher or a reliable commercial FISH provider is collaborating in the project.

With the former point raised and the fact that cell population heterogeneity can usually be addressed with strategies such as live fluorescent protein FACs-sorting, it is probably more cost-effective to use methods for single-cell amplification, followed by RT-PCR or sequencing. Given that the presence of cell population transcriptional heterogeneities is generally addressed once the project is near completion, the experiment will stand a consequently high chance of success. The expense of a single-cell amplification kit and sequencing is definitively justified in those circumstances. In addition, given the relative complication of addressing this problem, single-cell transcription heterogeneity should

be addressed at last, instead of holding back the completion of the research project and casting a veil of doubt over it the whole time.

At the end of the project, we recommend the use of oligo-FISH either as a validation technique that should be obtained through collaboration or from a commercial source, and only be used sparingly unless absolutely required, or the foundation of the research project. However, we also think V3.0 smHCR and future developments may change this. If the signal intensity is increased by one order of magnitude, such as 10^3 or 10^4 dyes per split-paired primary probe, while maintaining the signal specificity, routine design of 50-100€ probesets against any RNA or DNA target and purification of cell populations of interest FACs-sorting of FISH stainings are a real possibility. The commercial RNAscope & ViewRNA technologies already allow this, and remain under-used due to commercial kit cost in the 1.000€ range and 350€ or above per new target. It is likely that the next development of the smHCR in the next two years will include branched HCR signal amplification, bringing 10^4 or more dyes per primary probe at costs compatible with systems biology approaches to the common laboratory.

We hope that the laboratory will continue on the very real possibility of publishing a methods paper with a set of V3.0 smHCR intron RNA-FISH probesets against the X-linked genes and LncRNAs of major interest in the X-reactivation field. We also recommend to any researcher to use commercial split-paired probe approaches if targeting 3 or less nucleic acids of interest, but to consider V3.0 smHCR and successor techniques if targeting larger amounts of nucleic acids. The initial investment of time & expertise in setting up the technique will be worth it in those circumstances.

Global Conclusions:

Conclusions 1: Model of the *in vitro* PGC-LCs XCR phenotype:

In conclusion, our own results and the reinterpretation of multiple overlapping reports support that the same signaling mechanisms are reused amongst the epiblast and PGC X-reactivation phenotypes. I would like to propose a model for the signaling pathways enforcing the X-reactivation and inactivation phenotypes in the epiblast and in PGCs *in vivo*, how they cause the X-reactivation phenotype during *in vitro* PGC-LC induction, and the experiments required to characterize them.

The combination of previous experimental reports has shown that LIF, BMP4, as well as Wnt3 & Hedgehog, actively signal in the inner cell mass (ICM) of the blastocyst, where they drive pluripotency of the epiblast and its associated naïve X-chromosome reactivation from its sperm-imprinted X-inactivation starting state. These same BMP4 signal will later specify PGC fate, with the protection from pro-differentiation cues granted by local high BMP8, Nodal & Lefty levels in the posterior Epiblast, which negate differentiation cues coming from the visceral endoderm.

The epiblast, from which PGCs are later specified undergoes differentiation and X-inactivation due to Wnt3 signaling, ActivinA, FGF signaling & Integrins, Patched and other cell-to-cell attachment signaling cues. The short pulse of cytokine signaling (PGC specification occurs from E6.5-7.25) and the fact that specified PGC-LCs migrate out of their specification niche towards the developing embryonic gonads allows for X-inactivation to be maintained initially as seen in the early *in vivo* E7.75 PGCs. As PGCs migrate to the differentiating female gonad, immersed in a pro-differentiation signaling environment, they are guided by increasing concentrations of LIF & SCF morphogens, which drive the initial stages of *in vivo* PGC reactivation, likely by expression of pluripotency factors like Prdm14, Nanog and Oct4, which are known repressors of the *Xist* gene, the master regulator of X-inactivation. This leads to a loss of the Xist-mediated repressive chromatin configuration by passive erosion during cell division like of the H3K27me3 mark and of DNA methylation. As the PGCs get close to and invade the female gonad from E10-11.5, they are exposed again to BMP & Retinoic acid signaling, which is synergized with Wnt4, LIF, SCF & Hedgehog family ligands to

ensure the entry into early meiotic prophase, and, combined with the erasure of DNA methylation marks and the euchromatin general context driven by the PGC epigenetic reprogramming, ensures X-chromosome reactivation. In both the epiblast & female meiotic PGCs, the X-reactivating signaling input from BMP ligands is routed by Alk3-6 receptors and SMADs 1, 5 & 8, while in X-inactivation, TGF-Beta superfamily signaling is driven through Alk1-2 receptors and SMADs 2 & 4. This X-inactivation cascade and receptor arrangement notably transduces ActivinA, but also BMP signaling input to drive random X-inactivation where appropriate. The PI3K/Akt pathway, which is essential for pluripotency maintenance, would be similarly rewired to be able to drive X-reactivation, or to enforce X-inactivation in cells in which the signaling input has already initiated random X-inactivation. This process is probably mediated to some extent by meiosis-associated cohesin complexes, which are also expressed in the epiblast to drive the open 3D conformation and chromatin accessibility required for the X-active chromosome (Serena Generoso, personal communication).

In addition, ligands such as Atx-produced LPA and Ascorbic Acid might be present both in the epiblast and upon female gonad invasion, where LPA may enhance expression of core naïve pluripotency effectors such as Klf2-Klf4-Prdm14 through ROCK signal transduction, while Ascorbic acid synergizes with Retinol & Retinoic Acid to ensure optimal TET2 & TET3 activity during DNA-demethylation. Those DNA demethylases help erasure of DNA methylation marks, one of the major epigenetic drivers of X-inactivation. It is likely that TET enzyme up-regulation is what drives the erasure of paternal imprints and the DNA-demethylated context that the meiosis & X-reactivator genes require to enter meiotic prophase and drive X-reactivation in PGCs.

It is further possible that multiple of those signaling outputs are in fact coordinated by the master transcriptional regulator GATA4, which is the major determiner of primitive/visceral endoderm & the female genital ridge, two structures which might produce some of the X-reactivating ligands (Chuva De Sousa Lopes et al. 2008; Hu, Peter K Nicholls, et al. 2015). This provides a common rationale of the shared expression and role of those signaling molecules in ICM & female meiotic gonad.

The signaling input and cues for X-reactivation would ultimately stimulate the activity of a shared core of naïve pluripotency and germ cell factors such as Prdm14, EsrrB and

Nanog(Schulz 2017). These transcription factors would ultimately inhibit master X-inactivator *Xist* lncRNA expression in epiblast and germ cells leading to erosion of the X-inactivation state. As such, a shared core of transcription factors can explain X-reactivation phenotypes across all *in vivo* cell types that naturally undergo it.

While the above paradigm explains why cells undergo X-reactivation, it doesn´t explain why the X-inactivation signaling is coincident with the male gonad differentiation pathways. The most likely option is that the female developmental pathway is proposed to be the default sex differentiation pathway in mammalian evolution (Jameson et al. 2012) and that the E10.5-12.5 male gonadal signaling is NOT an actual drive for meiosis initiation, but a stimulus for mitotic arrest . Indeed, meiosis initiation in the male mammal is dependent on Wnt4 & Retinoic Acid coincident signaling, instead of the ActivinA, FGF, Nodal & Lefty signaling, which actually inhibit meiosis onset and set the male germ cells to quiescence until postnatal development. Moreover, the role of Wnt signaling may seem counter-intuitive, as it is present in the Epiblast before PGC specification and in the female gonad, yet it drives X-inactivation, cell differentiation and pluripotency loss. However, it should be noted that Wnt3 & Wnt4 signaling has been linked to PGC competence (Ohinata et al. 2009) and BMP receptor expression in female meiotic, X-reactivated PGC-LCs (H. Miyauchi et al. 2017). As such Wnt ligands could serve both roles: they could enforce efficiently X-inactivation through Beta-catenin accumulation and disruption of naïve core pluripotency factor action (Schulz 2017), while enhancing competence for X-reactivating BMP signaling.

It makes sense to consider that the presence of female characteristics must predate the male developmental sexual differentiation pathways, and that a non-chromosomal sex determination pathway would be dependent on environment-driven switches with much less degree of specialization and functional redundancy that we see nowadays in modern mammals; in some modern examples for environment-driven sex determination such as teleosts and crocodiles, the elements involved in the sex determination switch may be argued to be much simpler, to allow environmental conditions to affect them **(QUOTE)**.

The naïve pluripotency & germ cell specification signaling must necessarily be kept in

check and restricted to small areas, due to the danger of teratomas that un-differentiated cells pose to the host. There are a scarce number of circumstances in which reactivating the X-chromosome and having double dosage in female vs the male may have a benefit. This includes enabling random X-inactivation mosaics as the epiblast enters eventual differentiation and to allow meiotic recombination between the 2 female X chromosomes, which repressive X-inactivation marks could inhibit. Otherwise it makes sense that signaling pathways intended to drive cell differentiation would be adapted to drive X-inactivation in all cells excepting these 3 female cell types: epiblast, PGCs & to some extent in naïve lymphocytes. As the somatic tissues need to have as small as a divergence in X-linked gene dosage as possible in order to simplify genic regulation and limit sexual differences in genetic regulation, it makes sense that those pro-differentiation pathways would gain a function in suppressing the extra X-chromosome dosage found in females, which is only allowed to break through in those aforementioned specific circumstances. As such, the signaling of somatic differentiation would enforce X-inactivation and male sexual differentiation characteristics; the original naïve pluripotency/germ cell signaling would gain the X-reactivating function as a side effect, but would more or less kept intact, while it would be the somatic /male sexual differentiation pathway which would have to evolve quickly to gain suppression of genic dosage differences.

Why are then pro-differentiation pathways needed to drive the male sexual differentiation? In the first place, ActivinA, FGF, Nodal & Lefty signaling actually suppresses meiosis in male germ cells. It would make sense to do so to avoid premature start of meiosis in male mammals, as the testicles have not been externalized, and male sperm development cannot take place properly at the 37ºC of homeotermal mammals. The male signaling would delay meiotic onset until the testicles have been properly externalized, the spermatocyte stem cells proliferated until the massive extents which can support the massive amounts of gametogenesis that will take place over all the life of the individual. As such, ActivinA, FGF, Nodal & Lefty could rather be a dosage control module bolted on top of the male germ sexual differentiation, and whose purpose would not be actual male germ cell development, but controlling the adverse effects of dosage imbalance and handling the necessary differences in germ cell behavior in the male sex, but not tasked with keeping germ cell identity *per se*. It should

be noted that, while ActivinA, FGF, Nodal & Lefty are comparatively overexpressed in the male gonad, LIF, SCF, Wnt4 & BMP signaling are still present and keep the germ cell identity (Windley & Wilhelm 2016). When later in development Wnt4 & Retinoic Acid cues are locally supplied, this triggers meiosis and spermatogenesis waves as they did in female germ cells (Mark et al. 2014). As the niche for germ cell specification cytokine role and the X-reactivation signaling were already occupied and functionally tied by necessity and evolutionary history, the only way to develop and evolve the dosage compensation was to recruit previously un-used signaling pathways to correct the dosage imbalances and discrepancies for male germ cell biology consequence of the switch to chromosomal cell determination from an ancestor which relied on stochastic or environmental sex determination cues.

The former can be resumed in my so-called "evil twin hypothesis": The TGF-Beta superfamily, and the BMP signaling pathway is the core determiner of the X-activity state of female cells. In the epiblast and during PGC specification, BMP signaling would enforce naïve/core pluripotency factor expression, and indirectly or through those it will enforce X-reactivation as a result, unless it is specifically opposed by other signaling cues. If other signaling pathways and sensors are provided in a pluripotency/germ cell niche, like PI3K/Akt pathway, LIF, SCF, HH ligands, Wnt4, RSP01 & FSH and Atx-produced LPA or low-dosage Retinoic Acid, the pathway is rewired for BMP signal transduction through Alk3-6 receptors and SMADs 1, 5 & 8 (H. Miyauchi et al. 2017), eventually impacting in core naïve pluripotency factors, impairing *Xist* expression and recruitment of X-inactivation factors to the X, as well as Histone & TET demethylase expression. When the general context is prone to somatic cell differentiation or E10.5-12.5 male gonad, however, Wnt, Integrin ActivinA, FGF, Nodal, Lefty and other cell-to-cell contact signaling rewire the BMP signaling output. Preferential signaling from Alk1-2 and SMADs 2 & 4 or BMP2r ensure that any BMP signaling will enforce X-inactivation, as it was discovered from pharmacologic screenings for XCI-factors (Sripathy et al. 2017b; Bhatnagar et al. 2014; Przanowski et al. 2018). As such, BMP can also enforce X-inactivation instead of activation – hence the "evil twin" designation.

If left at this stage, the model would not be able to explain the nature of the auxiliary cues that mediate the differential output of the BMP signaling pathway. Fortunately, the

results of recent loss of function and signaling screens in the XCI- enforcing factors (Bhatnagar et al. 2014; Przanowski et al. 2018; Sripathy et al. 2017b) have pointed out 2 common signaling rationales: Absence of cell polarity vs Cell polarization & Glycolytic anaerobic vs oxidative metabolism. The X-active, pluripotent state is defined by poor cell polarization & a glycolitic anaerobic metabolism, while the differentiating, X-inactivating cells are defined by high cell polarity & oxidative, aerobic mitochondrial metabolism with high rates of active oxygen radicals formation.

The cell polarity signaling can not only be driven by Integrin signaling and cell-to-cell contacts, but also non-canonical Integrin signaling results in accumulation of Beta-Catenin, the main effector of Wnt signaling. Beta-catenin accumulation acts as a mechanical sensor integrating cell-to-cell binding, cell polarity and substrate binding information able to speed up dramatically cell differentiation, but there is another signaling pathway critical for cell polarity and naïve pluripotency state: the PI3K/Akt pathway. This pathway is majorly involved in cell polarity, besides naïve pluripotency. It has been increasingly argued that cell polarity runs counter to pluripotency **(QUOTE)**, as the processes involved in cancer may show **(QUOTE)**, and naïve pluripotency (represented by ICM, ESCs & iPSC cells) & PGCs are distinctly lacking in cell polarization. Avoiding polarization cues to transit through the PI3K/Akt may well represent a common denominator of naïve pluripotency; this provides a rationale explaining how Wnt (Schulz 2017), Integrin **(QUOTE)** & the PI3k/Akt pathway signaling kinases Pi3kcb & PPDK1 (Bhatnagar et al. 2014; Sripathy et al. 2017b) have been identified as X-inactivation enforcers: Embryoid body aggregation provides a model for the *in vivo* Epiblast differentiation, in which starting morphogenetic movements and gastrulation convey a previously absent source of mechanical tension, which may stimulate the acquisition of cell polarity. It is interesting to consider that Pi3kcb is involved in transduction and integration of Integrin signaling, and that specific Integrin heterodimers are used as highly distinctive markers of pluripotent stem cells, offering a linchpin to coordinate multiple X-inactivating activities. This could be an attractive explanation for how embryoid body aggregation can induce X-inactivation on X-active day 2 Epi-LCs in only 12 hours, which, is very fast in the X-inactivation field.

The lipid and glycolytic metabolism may also be a key factor. It is interesting to consider that multiple X-reactivator signals or agonists identified in the last years are lipidic in nature: the X-linked, Atx-produced Lysophosphatidic Acid (LPA) ligand (Kime et al. 2016), low dosage of Retinoic Acid (Hore et al. 2016) signaling, and interestingly enough, Ascorbic acid, with its enhancing effect on DNA-demethylation comes from its ability to provide a pool of reduced Fe2+ ion to TET family DNA demethylases(Hore et al. 2016). A key of naïve pluripotency signaling might be that it has a large presence of autocrine lipidic signaling produced by the naïve epiblast: PI3K/Akt results in accumulation in cell membranes of activated phosphatidil-inositol-3-phosphate, LPA and Retinoic Acid are lipidic and can diffuse & accumulate in cell membranes. These lipidic molecules are steadily produced and accumulated in the cell membranes, where they may act as a reservoir of pluripotency-enforcing signaling. Curiously enough, one of the most surprising findings in the story of XCI-factor screening was the identification of Acss1 & Acaca enzymes as key factors for X-inactivation maintenance. If their function was suppressed in a shRNA screening, differentiated somatic cells would undergo X-linked gene reactivation. Now, they are key enzymes in the Trycarboxilic acid pathways, and Acss1 & Acaca knockdown bottlenecks both Acetyl-Coa & Malonyl-Coa synthesis steps, respectively. In general effects, those enzymes are needed for oxidative metabolism & fatty acid Beta-oxidation pathways, which are eminently tied to aerobic catabolic metabolism, and in general terms, oxidative catabolic metabolism. So how do those enzymes may be enforcing something seemingly as pinpointed as the X-inactivation phenotype?

I propose that the oxidative metabolism is key. In absence of those enzymes, the cells are favored to switch to anaerobic, glycolytic metabolism. The epiblast & naïve pluripotent stem cell cultures like ESCs & iPSCs have anaerobic glycolytic metabolism, and it has been known that the culture in conditions of low oxygen can stimulate naïve pluripotency and the associated X-reactivation processes **(QUOTE).** In these circumstances, and without access to fatty acid Beta-oxidation pathways, the naïve pluripotency autocrine lipid signaling ligands such as phosphatidil-inositol-3-phosphate & LPA are free to accumulate within the cell and are not degraded. In the epiblast, in combination with the input from other naïve pluripotency ligands such as LIF, this

would give the edge required to withstand the autocrine differentiation signaling such as Wnt3 & FGF4 produced by the same cells of the epiblast.

In the absence of additional naïve cues to the lipidic ligands, the pro-differentiation autocrine signaling would win and the cells undergo differentiation. An immediate consequence of differentiation is that cells switch to oxidative respiration & fatty acid Beta-oxidation pathways, which degrades the naïve pluripotency lipid signaling and switches further the autocrine signaling balance towards cell differentiation. Under those circumstances, the generation of active oxygen radicals is high, which in turn limits the longevity of the cell. As such, it is logical that stem cells and cell types which require a high longevity and replication fidelity use anaerobic instead of oxidative metabolism. Using the autocrine lipid signaling to enforce naïve and stem/germ cell status and tying it to the metabolic state of the cell would ensure redundancy and help to limit the reacquisition of pluripotency: while the loss of control of cell proliferation may lead to tumorigenic process, it may be far harder to switch the energy harvesting metabolism from aerobiosis to anaerobiosis. Moreover, the difference from naïve stem/germ cells relying in anaerobic metabolism means that the effect of lipidic pluripotency signaling may be much more restricted to its intended target cells than the surrounding somatic cells, since the lipidic ligands would be degraded in somatic cells before they could accumulate to functional levels.

At last, it should be reminded that estrogen signaling, lipidic &membrane-accumulative in its nature, has been shown to be an important component of naïve pluripotency culture media **(QUOTE)**, and that an important event in the increase of cancer malignancy is the switch to an anaerobic metabolism. Interestingly enough, the reactivation of the X-chromosome is an event that has been related to an significant increase in cancer malignancy and poor prognosis **(QUOTE).** Multiple tumors are known to be dependent in estrogen or androgen stimulation for their continued proliferation **(QUOTE)**, and as such, it makes sense that anaerobic metabolism may be an advantageous trait, conferring an increased signaling impact to those pluripotency-enhancing lipidic cues they may be accessing; moreover, the X-reactivation would likely follow as a side effect.

This part of the model gives an explanation to several well-known, but hitherto hard to

explain observations in the X-epigenetics field, such as the correlation between cancer malignancy and X-reactivation **(QUOTE)**, or why the culture in low-oxygen conditions ([5% O2]) can stimulate X-reactivation **(QUOTE)**. It also explains how the role of Ascorbic Acid, an enhancer of X-reactivation during iPSC-reprogramming, has been revealed as a reducing factor whose major impact was to provide reduced Fe2+ to TET enzyme DNA demethylases during DNA-demethylation (Hore et al. 2016): the anaerobic stem cell metabolism generates a microenvironment that synergizes at sensing and relating pluripotency status with low levels of active oxygen radicals, and the lack of oxidative catabolic metabolism.

The last set of observations I would like to explain is the disproportionate enrichment of mitotic kinases and DNA replication factors found in XCI-factor screenings (Bhatnagar et al. 2014; Sripathy et al. 2017b; Lessing et al. 2016). The emerging view that the chromatin mark balance laid upon the replicating chromatin depends of the timing at which the DNA is replicated offers a solution for this (Klosin et al. 2017). Late-replicating DNA is favored for heterochromatic & silencing epigenetic modifications, while recently transcribed DNA has a higher chance of gaining transcription-enhancer chromatin marks **(QUOTE)**. It is notable that the event that signals the stable, locked inactive status of the X chromosome during XCI is its transition to an inactive compartment and its assignment to have late DNA replication.

DNA replication timing may be used in this fashion to drive fast, sweeping X-inactivation in a relatively sequence-independent and coordinated fashion during X-inactivation. By the “replication and combined arms hypothesis”, I postulated that the fast embryoid body aggregation X-inactivation phenotype may actually be the effect of Wnt, FGF & ActivinA signaling cooperating with the Integrin and cell-to-cell attachment and polarization cues to generate the late replication timing of the Inactive X. This offers the chance to replace quickly euchromatic epigenetic marks with heterochromatic marks, and once the heterochromatinization has occurred, it enforces its own late replication, ensuring the X chromosome will remain stably inactivated.

However, this dynamic also offers the converse effect: that fast X-reactivation may take place by prioritizing the early DNA replication of the X-reactivating chromosome, and

inserting euchromatic marks and replacing heterochromatic ones in the space of a few cell divisions. Recently, experiments in C-elegans, have shown that disrupting DNA replication can derepress heterochromatic regions and enforce genome-wide euchromatin states in a few cell divisions. These epigenetic marks can then even be inherited transgenerationally (Klosin et al. 2017).

The mechanism of DNA demethylation in PGCs is a hotly debated topic. Some support that the main agent of euchromatin context is the gradual dilution of DNA methylation after downregulation of DNA-methyltransferase enzymes by non-renewal after cell division, which would lead to a passive dilution of X-inactivation marks over time. This has been offered as an explanation for the seeming absence of TET DNA demethylase knockout impact on genome-wide DNA methylation levels, and even imprint erasure (Kagiwada et al. 2012). This has been challenged by others, who observed an important role of Tet1 demethylase in genomic imprint erasure. On the other hand, this begs the question about the mechanism of X-reactivation in females when repressive X-inactivation marks are lost from the inactive X-chromosome, in particular, if this is driven by passive dilution or active removal mechanisms. Evidence supports X-reactivation as being a non-autonomous phenotype requiring signaling, and that fast X-reactivation phenotypes can be obtained upon gonadal co-culture after only 48H (Chuva De Sousa Lopes et al. 2008), something also supported by our own results (Emmanuela Greco 2016; Severino 2018).

If the X-reactivation phenotype must happen in the span of only 2-3 days, as our *in vivo* PGC co-culture and the female PGC-LC X-reactivation phenotype show, one of the best ways to achieve this is to coordinate the euchromatin mark acquisition with cell DNA replication in a similar mechanism as it has been shown in C. elegans (Klosin et al. 2017). It should be possible to discriminate if this is the case if synchronized PGC-LCs are exposed to X-reactivating cues and the measure of genic X-inactivation is measured through allele-specific RT-PCR or RNA-SEQ vs nascent transcripts; if this is the case, X-reactivation should progress in staged bursts after each cell division.

To summarize, I propose that the BMP signaling pathway is the cornerstone of X-dosage compensation and activity status. Active in the first place in the ICM, it

cooperates with protein signaling LIF, SCF & HH ligands and lipid LPA, PI3K & Retinoic Acid ligands, also produced in an autocrine fashion, to drive naïve pluripotency and X-reactivation through Alk3-6 receptors & SMADs 1,5 & 8. At the effector and transcriptional level, core naïve pluripotency factors & Prdm14 will form the main switch repressing *Xist* lncRNA expression and upregulating its X-activator counterpart, *Tsix*.

Moreover, this combined signaling will be protected from cell differentiation cues by BMP8, Nodal & Lefty signaling in the posterior epiblast to give rise to the PGCs, and it will give those cells memory and X-reactivation competence, so that if the female PGCs encounter BMP signaling ligands again, it will drive X-reactivation.

However, the ICM also has an X-inactivation autocrine signaling source in the shape of Wnt & FGF signals, which promote cell differentiation and X-inactivation. While initially overcome by BMP and naïve pluripotency pathways displayed above, when the Epiblast differentiates, increased Retinoic Acid levels and ActivinA, Wnt, FGF, Nodal & Lefty protein ligand converge with Integrin & other cell-to-cell attachment molecules to drive cell polarization and a switch towards oxidative aerobic metabolism. These factors will cooperate synergistically to enforce X-inactivation in all cells, including the precursors of PGCs, and will rewire the BMP signaling pathway, through preferential signaling by Alk1-2 and SMADs 2 & 4. This will, in ultimate instance, result in a stable memory in all somatic lineages that makes further BMP signaling stimulate and enforce X-inactivation instead. The only exception will be the germ lineage embodied by the PGCs, which are protected from this effect.

This X-inactivating pulse upon embryoid body differentiation will use several auxiliary dynamics beyond the X-inactivation ligand signaling.

The acquisition of cell polarity cues will be used as a proxy for stable somatic fate and allows to synergize signaling from Wnt & Integrin signaling pathways not only to enforce X-inactivation, but also to rewire the PI3K/Akt pathway to stimulate cell polarization and interpret further signaling cues to it as X-inactivation cues. Only the epiblast and PGCs , will escape this influence, further helped by the protective effect of their pluripotent signaling pathways.

The metabolism will also be used as a way to enforce and lock X-inactivation. The pluripotent, X-active ICM and PGCs will benefit of an anaerobic, glycolytic fermentative metabolism that increases the half-life of naïve pluripotency, X-reactivation signaling lipid ligands, helping their accumulation and autocrine signaling. This will ensure increased dosage of the lipid ligands in those cells, ensuring X-reactivating signaling will have the advantage and rewiring BMP to enforce X-reactivation.

In somatic cells, the energy obtention metabolism of choice will be oxidative and aerobic respiration. Helped by Beta-oxidation of fatty acids and increased levels of oxygen radicals, this will greatly reduce the half-lifes of X-reactivating lipid ligands, ensuring the differentiation and X-inactivation of somatic cells.

Finally, the timing of DNA replication might be critical in ensuring fast X-Inactivation and Reactivation. By enforcing early DNA replication of the whole reactivating X chromosome, euchromatin marks can be quickly gained across its whole span during epiblast X-reactivation, and later in female PGCs upon gonad invasion and exposure to X-reactivating cues. During epiblast differentiation, however, the inactivating X chromosome will have its DNA replication timing shifted to late replication, which will allow increased heterochromatin mark incorporation. When coordinated with enhanced recruitment of pre-assembled silencing complexes triggered by cell polarization, this might allow the X-inactivation burst as suggested by our *in vitro* embryoid body aggregation results.

While aforementioned factors will ensure stable X-inactivation in all somatic lineages, female PGCs and partially lymphocytes will eventually undergo X-reactivation. The combination of naïve pluripotency signaling pathways during germ cell specification and their expression of germ cell and naïve pluripotency core transcription factors will ensure that BMP & PI3K/Akt signaling pathways will be interpreted as X-reactivation signaling cues. Upon migration and invasion of the E10.5-12.5 female gonad, they will encounter protein signaling LIF, SCF & HH ligands and lipid LPA, PI3K & Retinoic Acid ligands –the very same signaling pool used for the epiblast X-reactivation in the ICM. In the female gonad, Wnt4 & RSPO1 will stimulate BMP receptor expression and

signaling competence in PGCs, while FSH will repress the pro-inactivation pathway ActivinA. The female PGCs will rely in the action of their core naïve pluripotency factors and *Prdm14* expression, combined with meiosis onset, to repress *Xist* expression and enforce an open, euchromatic environment on the reactivating X chromosome. This will also be possible thanks to the genome-wide epigenetic reprogramming that PGCs underwent during migration to the female gonad, which eliminated some of the most pervasive X-inactivating marks, such as DNA methylation, and rendered the X epigenetic substrate accessible for meiotic prophase transition.

In the male gonad, however, the naïve pluripotency ligands shared with the female gonad will be overridden by increased ActivinA, FGF, Nodal & Lefty signaling and the degradation of Retinoic Acid ligand. This will ensure the quiescence of male germ cells and suppress their entry in meiosis. It´s also their meiosis-suppressive effect and previous role during X-inactivation of the differentiating female epiblast that renders the male gonad environment unable to drive X-reactivation in female PGCs.

Only one more cell type besides female PGCs will be susceptible to undergo partial X-reactivation: naïve un-activated lymphocytes. Their X-reactivation is the result of the detachment of the Xist lncRNA from the inactive X-chromosome, which leads to partial reactivation of X-linked genes. This reactivation is only temporal and reversed during lymphocyte activation when YY1 and hnRNPU aid in relocalization of Xist RNA to the inactive X-chromosome.

Conclusions 2: Conclusions & Future Outlooks on Oligo-FISH:

When we started our work on the Immunofluorescence and RNA-FISH analysis of the X chromosome status, be it X-Reactivation or Inactivation, the original goal was conceptually quite simple: To develop a universal Immuno & RNA-FISH protocol for all 4 cell types of interest of our *in vitro* X reactivation model, and try to also enable routine analysis of *in vivo* PGCs. This original goal was set with the concept that the cytokine *in vitro* PGC-LC induction model was going to yield X-inactive PGC-LCs with a yield of at least 10^5-10^6 X-inactive PGC-LCs per experiment. In those circumstances, enough purified PGC-LC sample was expected to be available for routine analysis without having a particular emphasis on sample preservation, and all cell types were assumed to be amenable for Immuno & FISH analysis based on minor alterations of a pre-existing protocol (Satoshi H. Namekawa & Lee 2011).

In addition, the FISH analysis of X-linked genes was intended to be a routine control, which did not have particular exploratory value, but which needed nonetheless to be performed at a moderately large amount of X-linked genes in addition to standard LncRNAs. It was intended as a concession to the quintessential exigency of the field to always perform this kind of experiments, to have a readout at the single-cell resolution level of the X chromosome activity. This exigency had far less weight for us because we could use a pool of up to 13 allele-specific RT-PCR primers for a faster assessment of more of the X chromosome activity of any cell population during our experiments, and the X-linked *X*-eGFP reporter FACs-sorting ensured that this population was homogeneously X-reactivated or X-inactive.

When we faced the PGC-LC specific X-reactivation phenotype, which we credited on the cytokine media composition, this changed everything.

First, we could only obtain at most 10^4 X-active PGC-LCs per experiment, and multiple X-linked loci needed to be quick, routine assessment for each cell differentiation stage and experiment to confirm the extent of the supposedly anomalous phenotype at single cell resolution. This was a problem because most commercial fixtures & published protocols are adapted for magnitudes of 10^{4-5} cells per sample, instead of the 10^3 cells per sample we were supposed to spare per sample, if we wanted to have an adequate amount of coverslips to stain & analyze. For a practical example of commercial fixture

side, in our hands, commercial Shandon instruments cytospin centrifugation kits, which are very reliable in normal circumstances, incur in extremely severe cell losses if less than 10^4 cells per sample are used.

For a practical example of published protocol side, the Epi-LCs & PGC-LCs were very fragile to the standard Immuno & RNA-FISH protocols, which are based on two twin assumptions for cell resistance. The first is that all cell types are able of active attachment to an adhesive-coated imaging vessel, or if not, that they will remain attached after centrifugation to an imaging vessel. The second is that all cell types tolerate treatment with a detergent-mixed permeabilizer solution and the consequent extraction of their cytoplasm *prior* to any fixation treatment (Satoshi H. Namekawa & Lee 2011; Chaumeil et al. 2008; Johnson et al. 1991). While permeabilizing before fixation is supposed to help for FISH staining of nuclear nucleic acids (DNA or RNA), in our experience, this creates a very narrow and finicky tolerance window for each cell different cell type and introduces a vulnerability in the protocol, besides promoting cell detachment. Neither Epi-LCs nor PGC-LCs did conform to any of those two standards.

We faced three stringent requisites: a need for high throughput, high cell attachment & wide ranges of cell permeabilization tolerance. When we implemented a protocol compatible for all of our 4 cell types of interest, we did so by following a slightly unconventional route. The cells remained attached because we piled up together all 4 available resources for single-cell suspension attachment: 2 layers of adhesive in the imaging vessel for cell attachment, crosslinking a polymer net to trap the cell to the substrate, fixating & crosslinking the cell *in situ* without fluid removal, and centrifuging the sample to the imaging substrate. We could target a variety of cell types & RNAS with a single permeabilization condition because the cells were fixed first, and then used a mild permeabilizer that lacks aggressive osmotic cytoplasm extraction, but for a longer time than usual (8 minutes). The high throughput & scalability, a requirement for the number of different samplings & stainings we needed to perform in quick succession during the *in vitro* PGC differentiation protocol, are reached through the use of cell suspension droplets adhered to detachable coverslips in multi-well plates. The multi-well plates can be prepared in advance to the experiments, and stored for months at -20ºC, and the requisite number of coverslips per experiment used, while the rest remains stored.

The second objective, the implementation of a non-commercial, inexpensive oligo-FISH technology for routine analysis of the X chromosome activity, is whose planning was less straightforward, but may yield the most long-term benefits.

The initial reason why I personally pushed to test the in-house N-SH & Enzymatic probe labeling protocols because the traditional BAC-FISH probe labeling attempts were unproductive and were not liable to yield the amounts of probe needed for the routine labeling of at least 4 X-linked loci, as the project was originally envisioned.

It also was intended as a long term-investment on oligo-FISH as a technology that could target strand-specific LncRNAs, which are functionally relevant & well characterized in X chromosome dosage compensation. The testing of N-SH & Enzymatic probe labeling protocols occurred midway during the Phd, at the same time the Immuno & RNA-FISH protocol was optimized, and allelic resolution readouts seemed the last straw to adjust for a confirmation of the *in vitro* cytokine PGC-LC model suitability for X-reactivation research.

The main lesson from those experiments was fruitful: the only practical & cost-effective guarantee of deterministic oligonucleotide synthesis & fluorescent labeling was commercial 3´ fluorescent labeling & HPLC purification of oligonucleotides no longer than 50bps. As such, any protocol that did not use inexpensive, short & unlabeled primary oligonucleotide probes to call a source of commercial fluorescent imager oligonucleotides was going to be utterly unsuitable for routine use.

After allele-specific RT-PCR & X-linked X-eGFP reporter cell lines became available, the oligo-FISH project was first abandoned to focus into the unexpected X-reactivation phenotype shown by the *in vitro* cytokine PGC-LC induction model.

I immediately assumed that the worst scenario, that it was indeed the cytokine cocktail driving a *physiologic* X-reactivation phenotype in PGC-LCs, as a recently published report showed that Epiblast Stem Cells exposed to the same cytokine cocktail underwent X-reactivation (Kime et al. 2016), and those cytokines were expressed in the female E10.5-12.5 gonad (Spiller et al. 2017; Windley & Wilhelm 2016) and

throughout the ICM to epiblast differentiation as well, the two instances for *in vivo* X-reactivation (Ohinata et al. 2009).

After I managed to provide strong enough evidence of this interpretation through the experiments of the first two chapters of the thesis, I pushed for two reactions.

The first was to switch to transgene-based *in vitro* PGC-LC induction in my successor's experiments. While the initial consensus of the lab was against it, driven by the very legitimate concern that the *Prdm14* transgene in the cassette would be sufficient to drive X-reactivation when overexpressed (Payer et al. 2013), I managed to argue with my data that embryoid body formation without cytokines should convey enough X-inactivating influences for the transgene PGC-LCs to remain X-inactive. This gambit paid off, with the transgene *in vitro* PGC-LC induction model recently producing large amounts of X-inactive PGC-LCs that are driven to X-reactivation by a series of candidate factors the laboratory is currently quite busy testing (Severino 2018).

The second was to recover and expand the oligo-FISH implementation project. With only 4 months left before being forced into thesis writing, it was the only chance to leave lasting positive impact and obtain any publishable results or expertise before leaving the laboratory. I focused on the hairpin chain reaction as both its V2.0 smHCR published results at the time (Choi et al. 2014; Shah, Lubeck, Schwarzkopf, T.-F. He, et al. 2016) as well as its foreseeable future developments towards adaptation to MER-FISH-like libraries (Shah et al. 2018) and V3.0 smHCR split-paired primary probes (Choi et al. 2018; Trivedi et al. 2018) offered the most cost-effective and fast testing of different oligo-FISH design philosophies over a reliable commercial fluorescent signal intensity source. The original goal of this part of the project was to implement a flexible oligo-FISH technology for routine X-linked gene intron, LncRNA & exon RNA-FISH analysis of the X chromosome activity at single-cell & allelic resolution, and publish the resulting set of validated primary probesets as a methods paper alongside the Immuno & RNA-FISH protocol developed earlier in this chapter. While the 4 months left were scarce time, sufficiently good results with some optimized probesets may have been used as a bargaining chip for several months of lab residence after thesis publication.

When we set to implement the oligo-FISH technology, we put our sights on four main objectives: that probes were as inexpensive as possible, that probeset informatic design was simple & fully predictive of probe performance, that probe specificity was absolute, and to maximize signal intensity per probe as much as possible.

This stemmed from our understanding of introns as the most difficult FISH targets.

When targeting the introns of a nascent transcript, you have the problem that only a very small fraction of your probeset is available for binding, as the introns are spliced out nearly as soon as they are transcribed. Even if you have the advantage that several nascent transcripts cluster at the nascent transcription site, you still have only access to a fraction of the fluorescent signal intensity in your probeset.

In order to make most of your chances, you need as much signal intensity per probe as possible, but, more importantly, you need as many probes on-target as you can. This is where simple informatic design of probes & low price is important, as you need to input as many probes covering all available intron sequence of the transcript as possible, and this means you need to design many probes, often, and veto them conclusively for specificity before the attempt. In addition, the probes need to be utterly specific: because the number of probes binding the target is unlikely to ever be the same between cell and experiment, as few as a single off-target probe binding event may have the same signal intensity as your legitimate target. For this reason, you need absolute probe specificity & for it to be fully predicted at the informatic probe design stage. If not, all the benefits of the signal intensity gained by adding new probes on-target would be lost with the concomitant increase of background off-target signal, as each probe added brings the chance of off-target bindings. As such, you need the signal intensity to increase linearly, but the background off-target to be constant & closest to zero as possible.

This peculiar set of challenges possibly makes introns the hardest target for oligo-FISH, followed by DNA sequences and mRNAs & LncRNAs being the easiest targets. The reason is that DNA sequences pose the challenge of being single copies, but the entire probeset is available for binding the target; the exons in mRNAs & LncRNAs are the

easiest, because not only the entire probeset is available for binding, but also hundreds to thousands of target copies accumulate in the cell. While DNA target sequences are usually the hardest targets due to the low signal intensities per probeset available before, the signal intensity brought by the hairpin chain reaction makes the intron variable binding footprint far more relevant.

Due to this model, we favored the use of V3.0 smHCR, as it brought the split-paired golden standard of specificity only previously found in commercial approaches (Wang et al. 2012; Battich et al. 2013) in an academic and sufficiently simple approach for fast design, as well as inexpensive enough for sequence saturation.

The end result of this part of the project is bittersweet.

We did not manage our initial objective of multiple validated X-linked intron RNA-FISH probesets ready for publication, due to them still lacking enough detection efficiency for guaranteed single-cell resolution of the X-chromosome activity in every cell of the population. We did, however, achieve proof of concept for the X-linked Intron RNA-FISH probesets, with a detection efficiency up to 4 times to what was previously detectable with classic computer-assisted Stellaris oligo-FISH technology (Levesque & Raj 2013). The detection efficiency is bound to rise even with our existing V3.0 probesets, now that optimal fluorophores are available, and excepting the 80% biallelic detection efficiency needed for single-cell resolution, the key properties of high specificity, simple bioinformatics design and signal intensity are fulfilled. As such, while the optimal X-linked Intron RNA-FISH experiment was not performed during this thesis, I conclude that the path to generate the X-linked probesets for the methods paper is open.

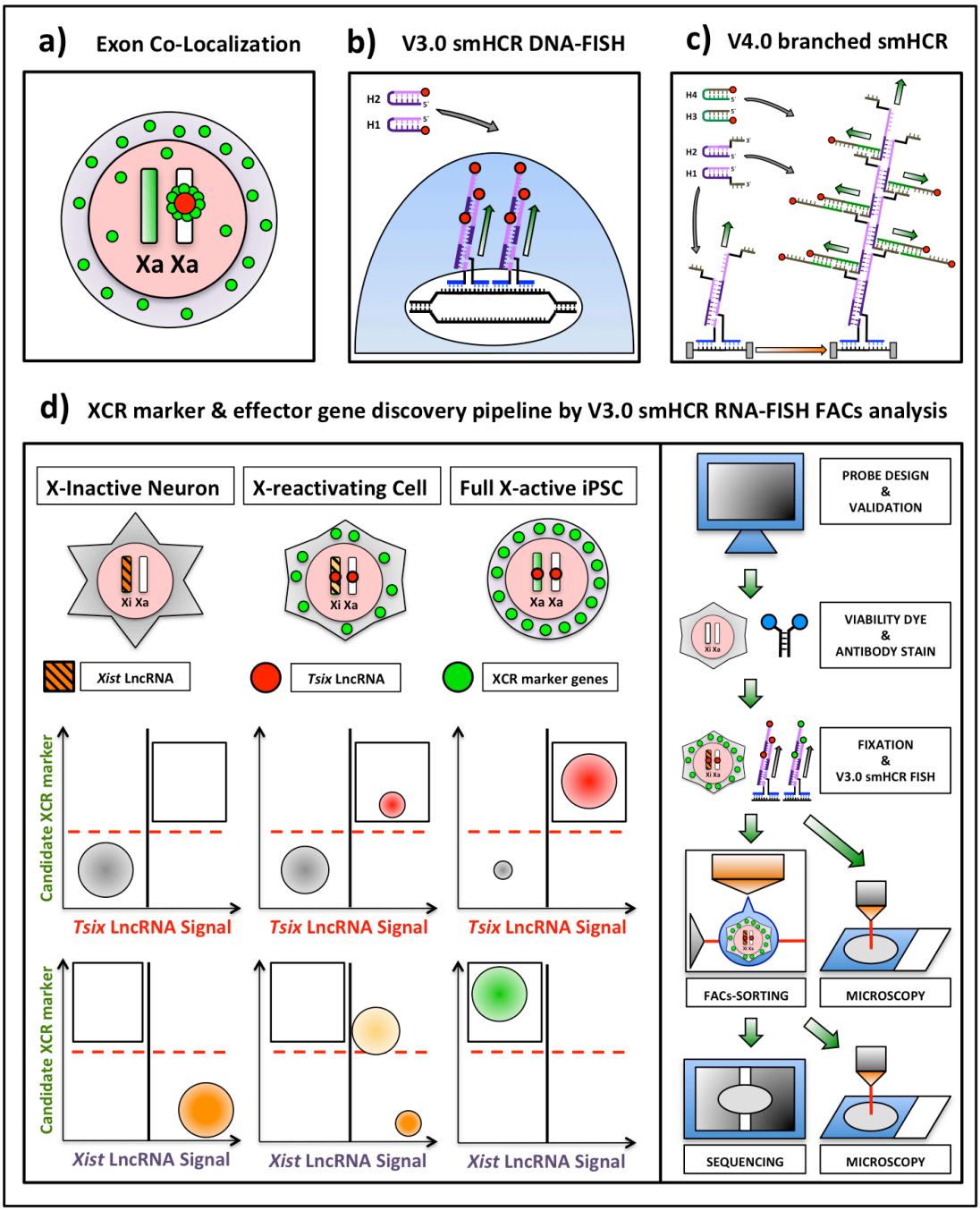

Figure 2: Future perspectives on V3.0 smHCR RNA-FISH method applications:

a) Two-color co-localization experiment. Exon-FISH in Green, Intron-FISH in red

b) DNA-FISH experiment with V3.0 smHCR probes against DNA locus.

c) Schematic of a hypothetic V4.0 branched HCR setup.

d) Workflow schematic of a FACs-FISH based XCR marker & effector gene discovery pipeline. The dual *Tsix* & *Xist* RNA-FISH staining is used to FACs-Sort X-reactivating iPSCs for sequencing and co-staining with candidate factors allows to stratify XCR and locate markers for the XCR process.

The next priority is to define what experiments should be performed next **(Fig.2)**. Four main particularly profitable avenues remain: the pending validation experiments for developing the intron-FISH probesets **(Fig.2a)**, the adaptation of V3.0 smHCR for DNA-FISH **(Fig.2b)**, the adaption of branched HCR to split-paired probes **(Fig.2c)**, and the use of FACs-sorting for stratification of the XCR process & discovery of X-reactivation effectors **(Fig.2d)**.

The first priority is the validation & optimization of the intron RNA-FISH probesets against XCI marker & escapee genes. While achieving an increase in detection efficiency is relatively straightforward, either by experimental repetition or by adding new primary oligo probes to the probeset, the main priority is to ensure & validate absolute probeset specificity for each intron probeset.

For this, a two-color colocalization experiment is the gold standard in the field **(Fig2.a)**. Two probesets in two different colors are targeted against the same target RNA, and every single fluorescent spot must coincide between the two channels. Otherwise, it is the result of an off-target unspecific binding event (Levesque & Raj 2013; Gaspar & Ephrussi 2015; Kwon 2013; Raj & Tyagi 2010).

This approach clashes with three practical problems. First, the most specific and valuable sequence along the intron span are going to be occupied by the main intron-FISH probeset, giving the validation probeset only the sequences most prone to unspecific binding. Second, in order to fully check all the intron sequence length, the control probeset would have to be near as large in probe number as the primary intron probeset. Third, if spots are found outside of the nascent transcription site, it would be hard to know if the cause is unreported intron alternative splicing or a shared sequence span was unspecific enough to cause off-targeting in both probesets.

In order to solve those problems, we suggest the secondary color validation probeset to be targeted against the mRNA exon sequence of the same gene **(Fig.2a)**. Because the exons are present in un-spliced & mature mRNA, even 5-10 probes will generate a sizable signal, making the control probeset inexpensive. The mRNA sequence tends to be very conserved, further helping the specificity of the control. The only co-localization that should happen is the one in the nascent transcription spot, which will be the brightest in both intron & exon probeset due to transcript clustering. If any other

spot is detected for the intron probeset, it will be either visible only in the intron probeset, indicating off-target binding, or visible in the intron & exon probesets both, indicating that some of the introns are spliced away from the transcription site. This covers the two main obstacles to intron RNA-FISH probeset optimization in an effective fashion.

One of our secondary priorities to compensate for the expertise & time investment was to flexibilize the application of the FISH technology. One of the key features that we aimed for was to reach the 10^4-10^5 fluorophores per target RNA range. When this level of signal intensity is reached, it opens the use of the technology for DNA-FISH, FISH FACs-Sorting of cells & whole-mount embryo FISH applications. Those applications are guaranteed for the RNAscope (Wang et al. 2012) & ViewRNA (Battich et al. 2013) commercial methods, which lie in the same signal intensity & probe specificity range, and the V3.0 smHCR already has published reports for its suitability for all those applications (Choi et al. 2018; Trivedi et al. 2018), with DNA-FISH being the only exception.

The second priority for the laboratory is to perform DNA-FISH for X-linked loci **(Fig.2b)**. One of the most interesting features of the X chromosome is that changes in the X-activity are mirrored by drastic changes in the 3D structure of the X chromosome, forming and disassembling megadomains that can be readily studied by oligo DNA-FISH (Nora et al. 2014; Deng et al. 2015). One of the projects in the laboratory yielded a series of candidates needed for the X-reactivation process. In order to demonstrate functional relevance, DNA-FISH experiments needed to be performed against multiple loci in the X chromosome, to monitor alterations in 3D structure of the X chromosome and to see recruitment of the X-reactivation effectors to the X-reactivating chromosome (Generoso 2018).

The usual method for oligo-paint DNA-FISH needs the perfect labeling of multiple hundreds of primary oligonucleotides, raising an excessive cost issue that was first addressed with the use of MERFISH-like amplification libraries that amplify hundreds of single fluorescent oligos by PCR (Chen et al. 2015; Deng et al. 2015). Sadly enough, this requires the (difficult) simultaneous perfect labeling of hundreds of oligos to

generate faint signal and reduces cost to the “mere” 2-3.000€ of the library.

In comparison, 5 probes for V3.0smHCR alone generate the same signal intensity at 50€ cost. Even if the advanced design pipelines for DNA-FISH oligo-Paint probes probably ensure higher binding rates, it should be very simple to scale up the number of V3.0 smHCR probes against the DNA-FISH target until it binds, at a very low price.

As such, we recommend the testing of V3.0 smHCR for DNA-FISH **(Fig.2b)**. Even if not all the primary probes find sequence available for binding, $2{,}5*10^3$ potential dyes per DNA target for 200€ with simple design and no labeling should guarantee success.

The last capability that should definitively be acquired is to expand the V3.0 smHCR design by adapting a branched HCR module on top of it, for a hypothetical “V4.0 branched HCR” **(Fig.2c)**. The key benefit is that it provides fully scalable signal intensity. Currently, a single smHCR circuit provides 10^2 fluorescent dyes per probe; two enslaved HCR circuits will generate 10^4 dyes, and three HCR circuits 10^6 dyes, with no known theoretical limit in mind. Since the single primary probe can generate enough signal for all desired applications, as long as the split-paired probes of V3.0 smHCR maintain full specificity, using 5 primary probes for a measure of redundancy should ensure successful visualization of any target for the cost of 50€ alone.

This would allow for a systems biology approach, in which very few probes are ordered against many targets of interest, evaluated for specificity, and any failures are simply discarded, designed and ordered anew from the commercial provider.

The applications that would benefit the most would be DNA-FISH, FACs-FISH analysis at systems biology levels, and whole-mount FISH, in which the FISH signal could reach the degrees of labeling only previously seen for enzymatic amplification.

We have discussed that this approach is probably in development in the Niles A. Pierce lab, as well as already being published with a suboptimal primary probe technology (Liu et al. 2018). As such, either this technology can be obtained through collaboration with the Nile A. Pierce laboratory, or by introducing an intermediate hybridization step, in which an adaptor oligo binding the split-paired probe pair and containing a motif for the published branched HCR approach is used.

The most promising application of the V3.0 smHCR FISH with the materials present in the lab, however, is its use as a pipeline for the discovery of markers & effectors of the X-Reactivation process **(Fig.2d)**. One of the problems commonly found in most discovery projects in multi-step cell differentiation or reprogramming processes is that the research is based on the knowledge of the transcriptional profiles of the initial cell type and desired target end cell fate, for which transgenic fluorescent reporter cell lines are built. The fully differentiated desired cell type can then be enriched and analyzed for the cell fate effectors.

The problem with this kind of approach is that the fluorescent reporters are tuned only to the end of the differentiation process, so that once the fluorescent protein finally accumulates enough to purify the desired population from the contaminants, the reprogramming is already fully complete. As such, the information of which *intermediate* reprogramming factors & effectors, and in which *sequence* they drive the process, is lost.

This is particularly true for X Chromosome reactivation & iPSC reprogramming. The current superficial description of the iPSC X reactivation is based on staining procedures, but it conveys the view that it is a long two weeks, multi-step process that involves intermediate cell populations arising during the reprogramming until full XCR is reached (Pasque et al. 2014). Two of our laboratory projects lie in studying iPSC X-reactivation and sequencing the X chromosome-wide kinetics of X-reactivation. While the project has been initially successful, the problem is that the X-eGFP reporter used only recognizes the population in which X-reactivation is fully completed, and the pluripotency markers tested to coax an earlier X-reactivating population face the same issue (Bauer 2017). The only information available from the sequencing experiments is that *Xist* downregulation happens first, followed by *Tsix* expression (Bauer 2017), consistent with the only preexisting publication (Pasque et al. 2014).

There is then a pressing need to discover the markers that define the early X-reactivating cell population from its somatic neighbors. The approach to perform a screen with different fluorescent transgene reporters would take too long. We propose instead to screen for X-reactivation markers & effectors with the FISH FACs-analysis

of V3.0smHCR probesets **(Fig.2d)**.

In this approach, we use the *Xist* & *Tsix* LncRNAs as a positive population marker of the

Materials & Methods

Chapter 1: Cytospin RNA-FISH sample preparation

When we performed Immunostaining and RNA-FISH, a major consideration was that we used multiple different cell types: Embryonic Stem Cells (ESCs), Mouse Embryonic Fibroblasts (MEFs), Epiblast-Like Cells (Epi-LCs) and Primordial-Like Cells (PGC-LCs). Because published RNA-FISH protocols are focused on preserving the specific target cell type they were designed against, we needed to use different RNA-FISH protocols against the different cell types mentioned above. Later optimization yielded a single RNA-FISH protocol able to work satisfactorily on all cell types mentioned before, but it wasn´t available at the time the data of this chapter were acquired.

For the ESCs, MEFs & PGC-LCs, we used a previous Immuno-RNA-FISH method optimized for ESCs (Satoshi H Namekawa & Lee 2011). While it yielded satisfactory results for ESCs & MEFs, it damaged both Epi-LC & PGC-LC nuclear morphology, and required a minimum of 10.000 cells per sampling for reliable results. Given the limited amount of *In vitro* PGC-LCs, generated per induction, this protocol was later discontinued and replaced by our own.

Briefly, all cells were fed fresh cell culture media 30 minutes to 1 Hour before sampling to promote transcription and subject to trypsinization for 9-12 minutes at 37ºC in [0.05% Wt/vol.] Trypsin-EDTA (Life Technologies, 25300054).

Afterwards, all solutions and steps of the protocol were carried at 4ºC temperature, unless specified otherwise.

Cell suspensions were quenched in 10% fetal-bovine serum containing media (Life Technologies, 10270106) and filtered through 70micron cell strainers (Corning, 352350) to ensure single-cell suspensions, and spun at 250 RCFs for 5 minutes. Cell pellets were then resuspended & washed in [0.1% RNAse-free BSA] Dulbecco PBS (VWR, 0332-25G), then spun again as above.

The cell pellet was resuspended in [0.1% RNAse-free BSA] Dulbecco PBS and an aliquot used for cell number measurement with the Countess assay (Life Technologies, C10228).

A total of 60.000 cells were loaded within 200uL volume into a cytospin funnel (Tharmac, JC306). The Cytospin funnels were assembled with a filtercard adaptor (Tharmac, 307-500) over an electrostatic adsorption microscopy glass slide (VWR, MENZJ1800AMNZ). These assemblies were then loaded into a Cytospin4 centrifuge (Thermoscientific, 3120110), and spun at 113 RCFs for 10 minutes.

All solutions in following steps and sample storage were performed by the use of 5-slot slidemailers (Heathrow Scientific, HS15986).

Slides were air-dried for 2 minutes and then equilibrated in Dulbecco PBS for 5 minutes.

Posteriorly, the slides were exposed to CSK buffer for 30 seconds, [CSK+0.5% Triton X-100] buffer for 1 minute, and then again to CSK buffer for 1 minute.

The slides were then fixed in electron microscopy grade [4% PFA] (Electron Microscopy Sciences, 15713) in Dulbecco PBS for 10 minutes at room temperature.

The slides were then subject to 2 washes in [70% ETOH] for 2 minutes each at 4ºC, and then stored in [70% ETOH] at -20ºC for a minimum of 24 hours and a maximum of 3

months before staining.

Chapter 1: Adherent Coverslip RNA-FISH sample preparation for Epi-LCs

While the first Immunostaining & RNA-FISH data were obtained by using the aforementioned protocol (Satoshi H Namekawa & Lee 2011), it induced excessive damage to the Epi-LC nuclear morphology to yield reliable results.

The constraints of cytospin use also made it excessively time-consuming for high throughput sampling.

As such, a new protocol was developed for Epi-LC, MEF & ESC Immunostaining & RNA-FISH.

Briefly, a single 12-mm round coverslip (VWR, MARI0111520) was placed per well of a 12-well cell culture plate (VWR, 734-2324) and coated overnight in a [0.05% Wt/Vol.] Poly-Lysine solution (Sigma-Aldrich, P8920-100ML).

Coverslips were washed 3X times with Ultrapure-Mili-Q water, then dried, and a hydrophobic barrier was drawn around each individual coverslip with a Pap-pen (Sigma-Aldrich, Z672548-1EA) for attachment to the carrier cell culture plate & containment of cell suspensions. All coverslips were stored at RT & used within the 48H of their elaboration.

All cell types and lines analyzed (ESCs, MEFs & Epi-LCs) were fed fresh cell culture media 30 minutes to 1 Hour before sampling to promote transcription and subjected to trypsinization for 9-12 minutes at 37ºC in [0.05% Wt/vol.] Trypsin-EDTA (Life Technologies, 25300054).

All the solution in the following steps were supplied with [0.2 miliMolar

Ribonucleoside-Vanadyl-Complex (RVC)](New England Biolabs, S1402S) RNAse inhibitor unless specified otherwise. All the subsequent steps were performed at 4ºC unless specified.

Cell suspensions were quenched in 10% fetal-bovine serum containing media (Life Technologies, 10270106), filtered through 70micron cell strainers (Corning, 352350) to ensure single-cell suspensions, and spun at 250 RCFs for 5 minutes. Cell pellets were then resuspended & washed in [0.1% RNAse-free BSA] Dulbecco PBS (VWR, 0332-25G), then spun again as above.

Cell pellets were resuspended in [2% RNAse-free BSA]-supplemented DMEM/F12 (ThermoFisher Scientific, 11320074) and an aliquot was used for cell number measurement with the Countess assay (Life Technologies, C10228). A single 50uL droplet of 10.000 cells in [2% RNAse-free BSA] DMEM/F12 was seeded per coverslip, and the cells were allowed to attach for 30 minutes in a 37ºC normal oxygen incubator.

After this step, another 100uL droplet of [0.2% Wt/Vol. Gelatin in PBS](Sigma-Aldrich, G1890-100G) per coverslip was seeded on top of the cells and incubated 30 minutes in a 37ºC normal oxygen incubator to form a polymer layer.

After incubation, 1mL of [4% Wt/Vol. PFA in PBS, pH 7.4] fixative (Electron Microcopy Sciences, 15713) was added & sample was fixed for 12 minutes at room temperature.

All the following steps were performed at 4ºC.

Fixative was withdrawn, and washed with dulbecco PBS for 5 minutes, then permeabilized in [0.5% Vol/Vol. Triton X-100 in PBS](Sigma-Aldrich, T8787-250ML) permeabilization solution for 8 minutes for ESCs & Epi-LCs; MEFs were permeabilized for 10minutes to account for their bulkier cytoplasm. Permeabilization solution was discarded, and washed 2 times for 5 minutes with PBS.

At last, all plate wells were filled with 70% Ethanol (Panreac AppliChem, 131086.1214), sealed with parafilm (VWR, BRND701611) and stored at -20ºC from 16

Hours to 3 months before RNA-FISH procedure.

Chapter1: Immunostaining & RNA-FISH procedure and signal scoring

Immunostaining , as well as RNA-FISH procedure, alone or in combination, were performed as in (Satoshi H Namekawa & Lee 2011), with some modifications.

All tools were previously cleaned from RNAses with RNAse Xterminator Spray (GRiSP, GB43.500S).

All solutions except washes were supplemented with [2 miliMolar RVC] (New England Biolabs, S1402S) and prepared as sterile single-use aliquots. Washing solutions were supplemented with [0.1 miliMolar RVC].

All reagents excepting antibodies, including bovine serum albumina (BSA)(VWR, 0332-25G), and dulbecco PBS were manufactured as being RNAse-free. Dulbecco PBS was elaborated in-house from nuclease-free certified H20 from a MiliQ A10 distiller (Millipore, Z00Q0V0WW).

In immunostaining procedure, the samples were retrieved from -20ºC [70% ETOH] storage and rinsed in dulbecco PBS for 3 minutes. A droplet of 100uL of blocking solution [1% BSA, 0.1% Triton X-100 in Dulbecco PBS], hence known as (PBT), was applied on a parafilm-lined, nuclease-free tipbox chamber and the sample overlaid to it. Incubation with the blocking solution was performed for 40 minutes at room temperature.

The rabbit anti-H3K27me3 polyclonal antibody (EMD Millipore, ABE44) at [1:500] dilution in PBT was used. Primary antibody solution was supplemented with RVC, incubated for 20 minutes at room temperature to neutralize RNAses, then spun at 2350 RCFs. 100uL of solution were provided per sample and incubated overnight at 4ºC. Three PBT washes of 7 minutes at room temperature were performed prior to secondary antibody exposure.

The donkey anti-rabbitt (ThermoFisher, A31573) at [1:500] dilution in PBT was used. Secondary antibody solution was supplemented with RVC, incubated for 20 minutes at room temperature to neutralize RNAses, then spun at 2350 RCFs. 100uL of solution were provided per sample and incubated for 1 hour at room temperature., followed by three PBT washes of 7 minutes at room temperature.

If only an Immunostaining procedure was performed, coverslips were mounted in Vectashield+DAPI antifade mounting media (Vector laboratories, H1200) onto microscopy slides (VWR, MENZJ1800AMNZ), and imaged within the 24H of the procedure in a Zeiss Observer Inverted microscope, with a 63xOil Immersion objective.

If a RNA-FISH was to be performed in combination to immunostaining, instead of a mounting step, the RNA-FISH procedure would proceed immediately after the secondary antibody washes.

The RNA-FISH procedure was performed as in (Satoshi H Namekawa & Lee 2011), with modifications stated when applicable. All solutions & reagent composition are the same, except when explicitly stated otherwise.

The hybridization & amplification solutions were supplemented with [20 miliMolar RVC] (New England Biolabs, S1402S).

All of remainder non-Ethanol solutions are supplemented with [0.2 miliMolar RVC].

The Hybridization solution was [**2xSSC**+**10%** Vol.Vol. **Dextran Sulfate** (Sigma-Aldrich, D6001-10G) +**25%** Vol./Vol. **deionized Formamide** (VWR, 1.09684.1000), pH7.4].

RNA-FISH Oligonucleotide probe sequences targeting the *Xist* & *Tsix* lncRNAs (Del Rosario et al. 2017) were ordered from IDT technologies. *Xist* probes were fitted with two Cy5 dyes, one on each terminus, while *Tsix* probes were fitted with two Cy3 dyes, one on each terminus**.**

All Oligonucleotide sequences are listed in **table 2.4.5.2.**

FISH Hybridization solution was supplemented with [3nanograms/mL] of each Oligonucleotide FISH probe against target lncRNAs, [20milimolar RVC] & [1microgram/uL yeast t-RNA](Life Technologies, 15401029), and incubated in a thermocycler at 80ºC for 10 minutes, then at 37ºC for 30 minutes.

Stored coverslip samples were transferred with forceps to a new 12-well cell culture plate, and subject to a 70-80-90-100% Ethanol dehydration procedure, 3 minutes each at room temperature.

Coverslips were allowed to dry for 3minutes at room temperature, then transferred into a 30uL droplet in a tipbox hybridization chamber, as described in (Satoshi H. Namekawa & Lee 2011), and incubated overnight at room temperature.

The washing procedures were performed as described in (Satoshi H Namekawa & Lee 2011). After this, coverslips were mounted in Vectashield+DAPI antifade mounting media (Vector laboratories, H1200) onto microscopy slides (VWR, MENZJ1800AMNZ), and imaged within the 24H of the procedure in a Zeiss Observer Inverted microscope, with a 63xOil Immersion objective.

An Orca Hamamatsu 2000 camera was used for image acquisition, and 400 & 500miliseconds exposure times were used for *Xist* and *Tsix* RNA-FISH signal imaging, respectively. Z-stacks encompassing the entirety of cell volume with a 0.7micron z-step were acquired, and pseudocoloring, channel level optimization, channel merging & maximal intensity z-projection performed with ImageJ (FIJI) V.2.0.0-2017 software.

Signals were manually scored & quantified. Due to H3K27me3 epigenetic mark, as well as *Tsix* & *Xist* lncRNAs being restricted to nuclear locations, signals were verified to co-localize with DAPI staining before scoring to guarantee the absence of artifacts.

The plots were elaborated in Microsoft Excel for mac 2011, V14.7.1, and figure panels assembled on Microsoft Power Point for mac 2011, V14.7.1.

Chapter1: RNA extraction & Real time PCR (RT-PCR)

A challenge for assessing germ cell differentiation quality & proper *In vitro* PGC induction and fate is that *In vitro* PGC-LC cells can number as few as 6% of the PGC induction body and as few as 20.000 live Germ cells per induction run. This is further complicated by the fact that PGCs are characterized for having particularly low transcription rates before they colonize the gonad and start sexual differentiation (Kagiwada et al. 2012)**.**

The end result is that we obtained very low yields of PGC RNA, precluding the use of most column-based RNA purification commercial kits, such as Thermofisher Scientific Qiagen kits.

Sadly, upscaling *In Vitro* PGC inductions for increased RNA yield is simply not viable at the optimization runs stage due to the prohibitive cost of the cytokines used for PGC Induction.

As such, all PGC & PGC-LC RNA extractions were performed from entire, unsorted PGC Induction bodies, which also contained differentiated populations in addition to our target *In vitro* PGC-LCs.

It was our assumption that the expression of PGC-specific marker genes was only expected from the PGC-LC subpopulation, and that the remaining differentiated somatic cells acted as a carrier medium, allowing us to isolate the PGC RNA within unsorted PGC induction bodies, but not from FACS-sorted, isolated PGC-LCs.

While we later optimized an RNA-extraction protocol able to yield sufficient RNA from FACs-sorted, pure PGC-LC populations, the PGC-LC RT-PCR results described in this section were performed with the abovementioned setup and limitations.

As such, we used 2 different protocols.

The purification of EpiLC RNA for the allele-specific RT-PCR during X-inactivation timelines was performed with the commercial column-based Qiagen RNeasy Plus Mini kit (Thermofisher Scientific, 50974136), as per manufacturer instructions.

The purification of Embrioid bodies, PGC Induction bodies, and their ESC & Epi-LC precursor cells during *In Vitro* PGC Induction, was carried out with the column-less protocol described below.

In order to avoid loss of RNA from low cell numbers, we used a column-free RNA purification protocol based on a propietary monophasic lysis reagent and acidified phenol for RNA extraction: TripleXtractor (GRISP, GB23.0100). Protocol was performed as per manufacturer instructions. All steps used appropriate filter tips.

Briefly, Embryoid bodies & PGC Induction bodies were collected with a P1000 pipette with appropriate filter tips (LabClinics, LAB1000ULFNL) in a 1.5ml eppendorf (Sigma Aldrich, T9661-1000EA), and spun for 250 RCFs for 1 minute at 4ºC. The cell culture media was replaced with cell culture grade Dulbecco PBS (VWR, 0332-25G) at 4ºC, and for 250 RCFs for 1 minute at 4ºC. The procedure was repeated for a total of 2 washing steps.

The PBS was discarded and the bodies were resuspended in 1mL of TripleXtractor (GRISP, GB23.0100). The bodies were forcibly resuspended with a P1000 pipette until no macroscopic remains were observed, then vortexed for 30 seconds at maximum speed.

Eppendorfs with the sample were immediately flash-frozen in ETOH-treated dry Ice, and stored at -80ºC until processing.

Upon use, eppendorfs containing the sample were thawn and incubated for 5 minutes at room temperature to fully release RNA from ribonucleoprotein complexes.

A 1:5 proportion of acid chloroform (pH 4.0) (Panreac AppliChem, A3691.0500) was added and mixed by pipetting & inversion for 30 seconds, then incubated for 2-3 minutes at room temperature.

The tubes were then centrifugated at 16.000 RCFs for 10 minutes at 4ºC. The aqueous

phase was pipetted out to a new eppendorf, and mixed at 1:1 volume proportion with Isopropanol (Merck Chemicals and Life Science, 109634) and 2uL of Pellet paint (VWR, 690493) at room temperature.

The mixture was incubated 10 minutes at room temperature, then centrifugated at 16.000 RCFs for 10 minutes at 4ºC.

The supernatant was discarded, and 1mL of nuclease-free 70%ETOH at 4ºC was added. The tube was mixed by inversion and spun at 16.000 RCFs for 10 minutes at 4ºC.

The entire procedure was repeated 2 times more for a total of 3 washing steps.

The ETOH supernatant was fully discarded and the RNA pellet was air-dried for 5-10 minutes at room temperature. It was then resuspended in 20-50uL of nuclease-free H20 (Life Technologies, 10977035), and heated at 55ºC for 10 minutes before additional resuspension.

The RNA concentration was measured with a Nanodrop 1000 (Thermofisher Scientific), and 100ng of pure RNA per sample were used for CDNA synthesis with the "high capacity RNA-to-cDNA kit" from Life technologies (Life Technologies, 4387406) as per manufacturer instructions in a 96-well PCR plate (Attendbio Research (Niborlab), NL 6078).

Both reactions (+) & (-) for reverse transcriptase (RT) enzyme were done for each biologic sample.

Each CDNA synthesis reaction was afterwards diluted to [0.5ng/uL] in nuclease-free H20 prior to its use in RT-PCR procedure.

The primer set sequences for germ cell fate assessment were obtained from (Hayashi et al. 2011b). The primer set sequences for allele-specific RT-PCR were kindly provided by the Lee lab (Lee 2016)**.** The primer set sequences for *Xist* lncRNA detection were obtained from (Shibata & Lee 2003)**.**

Each RT-PCR reaction was supplied 1ng of template CDNA, and 3 replicates

performed for each biological sample. Both (+) & (-) RT reactions were performed, and experiments which evidenced genomic DNA contamination discarded. Reaction composition & primer concentration were set as per RT_PCR mix manufacturer instructions (Thermofisher Scientific, 4367659).

The RT-PCR reactions were performed on a 384 well optical plate (Life Technologies, 4309849), sealed with optical quality seals (Biorad, MSB1001), and amplified in a Viia7 RealTime PCR machine **(Thermofisher Scientific)**.

The following RT-PCR amplification program was used:

1. First denaturation step (**1x**): 50ºC for 2 minutes, then 95ºC for 3 minutes.
2. Amplification cycles (**49x**): 95ºC for 30seconds; 60ºC for 30seconds; 72ºC for 30seconds(readout step)
3. Melting curve (**1x**): 95ºC for 10seconds; 65ºC for 10seconds; melting curve to 95ºC (readout step)

Only results from reactions in which standard deviation (STD) was below 1 were considered. Wherever possible, outlier picking was performed to ensure a STD value below 0.5. The house-keeping gene Arbp was selected for its constant expression rate across all cell fates involved in Germ cell Induction procedure.

The germ cell fate marker and *Xist* gene expression was calculated by using the ΔΔCT method (Green & Sambrook 2014).

The allele-specific expression ratios were obtained by calculating gene expression fold change for each of the 2 alleles of the gene with allele-specific primers using the formula described below:

$$\frac{FGeneI = A^{\Delta CT=(CTMean\ HouseKeeping\ gene - CTMean\ Gene\ of Interest)}}{FGeneN.ESCs = A^{\Delta CT=(CTMean\ HouseKeeping\ gene\ ESCs - CTMean\ Gene\ of Interest\ ESCs)}}$$

$F.GeneI = Fold\ change\ gene\ of\ interest$
$F.GeneN.ESCs = Fold\ change\ gene\ of\ Interest\ for\ the\ normalization\ cell\ type\ sample\ (ESCs)$
$A = Amplification\ Efficiency\ Gene\ of\ Interest$

Then calculating the ratio of *Musculus* to *Castaneus* allelic expression by the following formula:

$$Musculus\ to\ Castaneus\ ratio = \frac{Fold\ change\ Musculus\ allele}{Fold\ change\ Castaneus\ allele}$$

The values were then plotted using Microsoft Excel for mac 2011, V14.7.1, and figure panels assembled on Microsoft Power Point for mac 2011, V14.7.1.

Chapter1: *In Vitro* Epi-Lc Induction for X-inactivation kinetics assessment

The Epi-LC cell Induction procedure was performed as in (Hayashi & Saitou 2013b)**,** with some modifications.

5 different naïve pluripotent ESC lines were screened for their X-inactivation kinetics as they were differentiated from naïve pluripotency to epiblast-like cells.

3 induced pluripotent stem cell lines (iPSCs) of *Mus musculus/Mus spretus* hybrid background carrying an X-linked *eGFP* reporter array (A. K. Hadjantonakis et al. 2001) on their *Mus musculus*-inherited X chromosome and reprogrammed from somatic cell lines by the use of a STEMCCA lentiviral cassette (Sommer et al. 2016) were FACs-sorted and tested for XX genotype integrity.

Two of them, iPSC line 76.6 & 30, were devoid of additional alterations. The iPSC line 77-1D2, on the other hand, carried an additional deletion of the CPG island driving transcription of the *musculus*-linked *Tsix* lncRNA locus, and, as such, the X-inactivated chromosome will always be the *musculus* X chromosome bearing the *eGFP* reporter array **(QUOTE)**.

After confirmation, the ES cell lines were seeded at 2.7*10^4 viable cells/cm2 on 6-well

cell culture plates (Thermofisher Scientific, 140675) over an irradiated male embryonic fibroblast feeder layer, fed fresh 2i+LIF media daily, and split each 48H at above-mentioned density for 4 passages in order to select cells growing robustly in 2i+LIF media.

In preparation for *In Vitro* Epi-LC induction procedure, ESCs split and seeded at 2.7*10^4 viable cells/cm2 in a 6-well cell culture plate well on 2i+LIF cell culture media. Media was changed daily, and cells were split at 48H onto 2i+LIF media at same confluence and vessel as above.

After 2 passages on 2i+LIF, the ES cells were split & Epi-LC Induction with ActivinA (Peprotech, 120-14E-50ug) & bFGF (Life Technologies, 13256-029) cytokines was performed as described in (Hayashi & Saitou 2013a), but the following alterations were introduced:

Instead the 36H Epi-LC Induction timing prior to PGC Induction, the cells were induced for up to 216H (9 days). The cells were not split in this experiment, but let grow in the same vessel for fear that splitting would favor the increased cell death phase observed after 4 days of Epi-LC culture (Hayashi et al. 2011b).

2 hybrid ESCs lines, carrying one *Mus musculus*-inherited & one *Mus castaneus*-inherited X chromosomes **(QUOTES)** were obtained & expanded on ES+LIF cell culture media **[QUOTE & REAGENT REFs]** over an irradiated male embryonic fibroblast feeder layer.

A selection procedure for pluripotency maintenance on gelatin-coated surface and 2i+LIF media was carried out.

The EL16.7 TST A10 dual color cell line results from the targeted insertion of *eGFP* & *Td-tomato* in the *Hprt* gene locus for both the *Mus musculus* & *Mus castaneus*-inherited X chromosomes.

The EL16.7 TST A4 Single Color cell line results from the targeted insertion of *eGFP* in the *Hprt* gene locus of the *Mus musculus*-inherited X chromosome.

All procedures were performed by fellow phd student Moritz Bauer (Bauer 2017).

After cell line establishment, all cell lines were adapted for growth in naïve pluripotency-enhancing 2i+LIF media (Nichols & Ying 2006b). The ES cells were seeded at 2.7*10^4 viable cells/cm2 on 6-well cell culture plates (Thermofisher Scientific, 140675), fed fresh 2i+LIF media daily, and split each 48H at above-mentioned density for 4 passages, whereupon they were stored in [ESmedia+**10%Fetal Bovine serum (FBS)**(Life technologies, 10270106)+10%Dimethyl sulfoxide (DMSO)(Sigma-Aldrich, D5879-500ML)] freezing solution.

In preparation for *In Vitro* Epi-LC induction procedure, the two hybrid ESC lines were split and seeded at 2.7*10^4 viable cells/cm2 in a 6-well cell culture plate well on 2i+LIF cell culture media. Media was changed daily, and cells were split at 48H onto 2i+LIF media at same confluence and vessel as above.

After 2 passages on 2i+LIF, the ES cells were split & Epi-LC Induction with ActivinA (Peprotech, 120-14E-50ug) & bFGF (Life Technologies, 13256-029) cytokines was performed as described in (Hayashi & Saitou 2013a), but the following alterations were introduced:

Instead the 36H Epi-LC Induction timing prior to PGC Induction, the cells were induced for up to 168H (7 days). In contrast with the previous experiment with iPSC cell line differentiation, the Epi-LCs were trypsinized by exposure to Tryple-express enzyme (Life Technologies, 12604-021) for 3 minutes at room temperature and split every 48H upon cell confluence. This procedure was repeated until the end of the experiment.

Chapter1: *In Vitro* Germ cell Induction protocols

The In Vitro Germ cell Induction procedure was performed as in (Hayashi & Saitou 2013b)**,** with some modifications.

Embryonic stem cell Lines hybrid Embryonic stem cell lines (ESCs), carrying one *Mus musculus*-inherited & one *Mus castaneus*-inherited X chromosomes **(QUOTES)** were

obtained & expanded on ES+LIF cell culture media **[QUOTE & REAGENT REFERENCES]** on a male embryonic feeder layer.

A procedure for pluripotency maintenance on gelatin-coated surface and the insertion of *eGFP* & *Td-tomato* in the *Hprt* gene locus for both the *Mus musculus* & *Mus castaneus*-inherited X chromosomes was performed by fellow phd student Moritz Bauer (Bauer 2017)

After cell line establishment, cell lines were adapted for growth in naïve pluripotency-enhancing 2i+LIF media (Nichols & Ying 2006b) and Gelatin-coated surfaces. The ES cells were seeded at 2.7*10^4 viable cells/cm2 on 6-well cell culture plates (Thermofisher Scientific, 140675), fed fresh 2i+LIF media daily, and split each 48H at above-mentioned density for 4 passages, whereupon they were stored in [ESmedia+**10%Fetal Bovine serum** (FBS)(Life technologies, 10270106)+**10%Dimethyl sulfoxide** (DMSO)(Sigma-Aldrich, D5879-500ML)] freezing solution.

Upon *In Vitro* PGC induction procedure, vials of EL16.7 TST hybrid ESCs were thawn and seeded at 2.7*10^4 viable cells/cm2 in a 6-well cell culture plate well on ES+LIF cell culture media. Media was changed daily, and cells were split at 48H onto 2i+LIF media at same confluence and vessel as above.

After 2 passages on 2i+LIF, the ES cells were split & Epi-LC Induction with ActivinA (Peprotech, 120-14E-50ug) & bFGF (Life Technologies, 13256-029) cytokines was performed as described in (Hayashi & Saitou 2013a), but the following alterations were introduced:

Instead the 36H Epi-LC Induction timing prior to PGC Induction, those were carried out at 48H (day2), 72H (day3) & 96H (day4) of Epi-LC development.

Epi-LCs were left to grow without splitting in the same induction culture vessel up to 72H (day3) of Epi-LC development. For PGC induction from 96H (day4) Epi-LCs, Epi-LCs were split after 48H of culture and 3*10^5 viable Epi-LCs were seeded per well of a 12-well plate, in same conditions used for Epi-LC induction, and let grow until 96H since Epi-LC Induction.

PGC Induction was performed as described in (Hayashi & Saitou 2013b) with some modifications.

A total of 5.000 viable Epi-LCs cells were seeded per body, and 2 conditions were performed:

- PGC Induction (BMP4(+) conditions), in which the full cytokine complement for PGC induction & expansion was provided.
- Negative Control conditions were seeded in base GK15 cell culture media for PGCs, but no cytokines were provided. This led to the formation of Embrioid bodies, known to proceed to fast random cell differentiation and x-inactivation **(QUOTE)**, acting as a positive control for X-inactivation and a negative control for X-reactivation.

The cells were cultured without media change for 96H (day4), 144H (day6) or 168H (day7) of development, before FACs analysis & processing for RNA extraction.

Chapter 1: ESCs & Epi-LCs FACs analysis

The FACs analysis procedure was adapted from (Hayashi & Saitou 2013b), with some modifications. ESCs were trypsinized for 8 minutes at 37ºC with [0.05% Trypsin-EDTA], while Epi-LCs were trypsinized for 3 minutes at room temperature with the Tryple-express enzyme (Life Technologies, 12604-021), accounting for their increased mechanosensitivity and general fragility.

Upon trypsinization, single-cell resuspension and 40 micron mesh (LabClinics, PLC93040) filtering for single-cell suspension, each FACs condition cell pellet was resuspended in 200uL of an antibody staining solution in a 1.5mL eppendorf tube (Sigma Aldrich, T9661-1000EA).

All remaining steps and solutions below are maintained at 4ºC temperature.

The antibody staining solution was comprised of [DMEM/F12+1%BSA-Cell culture grade](Life technologies, 15260-037), which was supplemented with the antibodies SSEA1-Alexa660 (eBioscience, 50-8813-42) at [1:50=0.6uG/mL] dilution, and CD61-

PE-Vio770 (Miltenyi Biotech, 130-102-627) at [1:20=1uG/mL] dilution.

The increased 1% BSA and use of DMEM/F12 media as solvent were included to favor antibody specificity & increase viability of the PGCs for FACs procedure, respectively.

The antibody cell suspensions were incubated for 1H at 4ºC with continuous rotation in an orbitator platform, whereupon they were transferred to a 15mL Falcon tube per condition (Falcon, 352096), and the original eppendorf was rinsed twice to ensure full transfer of cell suspension.

A 10mL of [PBS+0.1%BSA , cell-culture grade] were added to each condition, and the cells spun at 250 RCFs for 5 minutes in a 4ºC centrifuge. The solution was discarded, the cell pellet resuspended, and the same washing procedure was performed again 2X times.

Prior to FACs-analysis procedure, cell pellets were resuspended to single-cell solution in [DMEM/F12+0.1%BSA-RNAse-free] supplemented with DAPI (Biogen Cientifica, BT-40043) at [1uG/mL] as viability marker.

Cells were incubated for a minimum of 15 minutes before filtering through a 70micron cell strainer and run through an LSRII or Fortessa FACs-analyzer, using a 100micron nozzle and as few psi as possible without negatively impacting analysis ability.

The change to a higher nozzle diameter allows for reduced hydrostatic pressure. Hydrostatic pressure has been found to be particularly deleterious for mechanosensitive cells such as Epi-LCs and Primordial germ cells (PGCs) (Hayashi & Saitou 2013b).

After data acquisition, the gates were fine-tuned and FACs plots edited in Flowjo V10.5.0 software.

Image panels were assembled on Microsoft Power Point for mac 2011, V14.7.1.

Chapter 1: PGC-LC & Embrioid body FACs analysis

The FACs analysis procedure was performed as in (Hayashi & Saitou 2013b), with

some modifications. The day4 bodies were trypsinized for 8 minutes at 37ºC with [0.05% Trypsin-EDTA], while the day 6 & 7 bodies were trypsinized for 10 minutes at 37ºC, in order to account for increased cell adhesion and body size upon longer culture.

Upon trypsinization, single-cell resuspension and 70 micron mesh (Corning, 352350) filtering for single-cell suspension, each FACs condition cell pellet was resuspended in 200uL of an antibody staining solution in a 1.5mL eppendorf tube (Sigma Aldrich, T9661-1000EA).

All remaining steps and solutions below are maintained at 4ºC temperature.

The antibody staining solution was comprised of [DMEM/F12+1%BSA-Cell culture grade](Life technologies, 15260-037), which was supplemented with the antibodies SSEA1-Alexa660 (eBioscience, 50-8813-42) at [1:50=0.6uG/mL] dilution, and CD61-PE-Vio770 (Miltenyi Biotech, 130-102-627) at [1:20=1uG/mL] dilution.

The increased 1% BSA and use of DMEM/F12 media as solvent were included to favor antibody specificity & increase viability of the PGCs for FACs procedure, respectively.

The antibody cell suspensions were incubated for 1H at 4ºC with continuous rotation in an orbitator platform, whereupon they were transferred to a 15mL Falcon tube per condition (Falcon, 352096), and the original eppendorf was rinsed twice to ensure full transfer of cell suspension.

A 10mL of [PBS+0.1%BSA , cell-culture grade] were added to each condition, and the cells spun at 250 RCFs for 5 minutes in a 4ºC centrifuge. The solution was discarded, the cell pellet resuspended, and the same washing procedure was performed again 2X times.

Prior to FACs-sorting procedure, cell pellets were resuspended to single-cell solution in [DMEM/F12+0.1%BSA-RNAse-free] supplemented with DAPI (Biogen Cientifica, BT-40043) at [1uG/mL] as viability marker.

Cells were incubated for a minimum of 15 minutes before filtering through a 70micron cell strainer and run either through a BD Influx cell sorter, or a LSRII or Fortessa FACs-analyzer.

FACs-sorting procedures used using a 140micron nozzle, while FACs-analyzers used a

100micron nozzle.

In both cases, as few psi as possible were used, as long as they did not negatively impacting sorting ability.

The change to a higher nozzle diameter allows for reduced hydrostatic pressure. Hydrostatic pressure has been found to be particularly deleterious for Primordial germ cells (PGCs) (Hayashi & Saitou 2013b), and they also have an increased cell size (Yamaji et al. 2010)**,** meaning the use of 100micron nozzle diameter or below usually results in very poor PGC viability and cell losses during sorting.

The increased cell size means that the use of cell strainers below 70micron size results in a selective Germ cell depletion.

After data acquisition, the gates were fine-tuned and FACs plots edited in Flowjo V10.5.0 software.

Image panels were assembled on Microsoft Power Point for mac 2011, V14.7.1.

Chapter 2: Cytospin RNA-FISH sample preparation

When we performed Immunostaining and RNA-FISH, a major consideration was that we used multiple different cell types: Embryonic Stem Cells (ESCs), Mouse Embryonic Fibroblasts (MEFs), Epiblast-Like Cells (Epi-LCs) and Primordial-Like Cells (PGC-LCs). Because published RNA-FISH protocols are focused on preserving the specific target cell type they were designed against, we needed to use different RNA-FISH protocols against the different cell types mentioned above. Later optimization yielded a single RNA-FISH protocol able to work satisfactorily on all cell types mentioned before, but it wasn´t available at the time the data of this chapter were acquired.

For the ESCs, MEFs & PGC-LCs, we used a previous Immuno-RNA-FISH method optimized for ESCs (Satoshi H Namekawa & Lee 2011). While it yielded satisfactory results for ESCs & MEFs, it damaged both Epi-LC & PGC-LC nuclear morphology,

and required a minimum of 10.000 cells per sampling for reliable results. Given the limited amount of *In vitro* PGC-LCs, generated per induction, this protocol was later discontinued and replaced by our own.

Briefly, all cells were fed fresh cell culture media 30 minutes to 1 Hour before sampling to promote transcription and subject to trypsinization for 9-12 minutes at 37ºC in [0.05% Wt/vol.] Trypsin-EDTA (Life Technologies, 25300054).

Afterwards, all solutions and steps of the protocol were carried at 4ºC temperature, unless specified otherwise.

Cell suspensions were quenched in 10% fetal-bovine serum containing media (Life Technologies, 10270106) and filtered through 70micron cell strainers (Corning, 352350) to ensure single-cell suspensions, and spun at 250 RCFs for 5 minutes. Cell pellets were then resuspended & washed in [0.1% RNAse-free BSA] Dulbecco PBS (VWR, 0332-25G), then spun again as above.

The cell pellet was resuspended in [0.1% RNAse-free BSA] Dulbecco PBS and an aliquot used for cell number measurement with the Countess assay (Life Technologies, C10228).

A total of 60.000 cells were loaded within 200uL volume into a cytospin funnel (Tharmac, JC306). The Cytospin funnels were assembled with a filtercard adaptor (Tharmac, 307-500) over an electrostatic adsorption microscopy glass slide (VWR, MENZJ1800AMNZ). These assemblies were then loaded into a Cytospin4 centrifuge (Thermoscientific, 3120110), and spun at 113 RCFs for 10 minutes.

All solutions in following steps and sample storage were performed by the use of 5-slot slidemailers (Heathrow Scientific, HS15986).

Slides were air-dried for 2 minutes and then equilibrated in Dulbecco PBS for 5

minutes.

Posteriorly, the slides were exposed to CSK buffer for 30 seconds, [CSK+0.5% Triton X-100] buffer for 1 minute, and then again to CSK buffer for 1 minute.

The slides were then fixed in electron microscopy grade [4% PFA] (Electron Microscopy Sciences, 15713) in Dulbecco PBS for 10 minutes at room temperature.

The slides were then subject to 2 washes in [70% ETOH] for 2 minutes each at 4ºC, and then stored in [70% ETOH] at -20ºC for a minimum of 24 hours and a maximum of 3 months before staining.

Chapter2: Adherent Coverslip RNA-FISH sample preparation for Epi-LCs

While the first Immunostaining & RNA-FISH data were obtained by using the aforementioned protocol (Satoshi H Namekawa & Lee 2011), it induced excessive damage to the Epi-LC nuclear morphology to yield reliable results.

The constraints of cytospin use also made it excessively time-consuming for high throughput sampling.

As such, a new protocol was developed for Epi-LC, MEF & ESC Immunostaining & RNA-FISH.

Briefly, a single 12-mm round coverslip (VWR, MARI0111520) was placed per well of a 12-well cell culture plate (VWR, 734-2324) and coated overnight in a [0.05% Wt/Vol.] Poly-Lysine solution (Sigma-Aldrich, P8920-100ML).

Coverslips were washed 3X times with Ultrapure-Mili-Q water, then dried, and a hydrophobic barrier was drawn around each individual coverslip with a Pap-pen (Sigma-Aldrich, Z672548-1EA) for attachment to the carrier cell culture plate & containment of cell suspensions. All coverslips were stored at RT & used within the 48H of their elaboration.

All cell types and lines analyzed (ESCs, MEFs & Epi-LCs) were fed fresh cell culture media 30 minutes to 1 Hour before sampling to promote transcription and subjected to trypsinization for 9-12 minutes at 37ºC in [0.05% Wt/vol.] Trypsin-EDTA (Life Technologies, 25300054).

All the solution in the following steps were supplied with [0.2 miliMolar Ribonucleoside-Vanadyl-Complex (RVC)](New England Biolabs, S1402S) RNAse inhibitor unless specified otherwise. All the subsequent steps were performed at 4ºC unless specified.

Cell suspensions were quenched in 10% fetal-bovine serum containing media (Life Technologies, 10270106), filtered through 70micron cell strainers (Corning, 352350) to ensure single-cell suspensions, and spun at 250 RCFs for 5 minutes. Cell pellets were then resuspended & washed in [0.1% RNAse-free BSA] Dulbecco PBS (VWR, 0332-25G), then spun again as above.

Cell pellets were resuspended in [2% RNAse-free BSA]-supplemented DMEM/F12 (ThermoFisher Scientific, 11320074) and an aliquot was used for cell number measurement with the Countess assay (Life Technologies, C10228). A single 50uL droplet of 10.000 cells in [2% RNAse-free BSA] DMEM/F12 was seeded per coverslip, and the cells were allowed to attach for 30 minutes in a 37ºC normal oxygen incubator.

After this step, another 100uL droplet of [0.2% Wt/Vol. Gelatin in PBS](Sigma-Aldrich, G1890-100G) per coverslip was seeded on top of the cells and incubated 30 minutes in a 37ºC normal oxygen incubator to form a polymer layer.

After incubation, 1mL of [4% Wt/Vol. PFA in PBS, pH 7.4] fixative (Electron Microcopy Sciences, 15713) was added & sample was fixed for 12 minutes at room temperature.

All the following steps were performed at 4ºC.

Fixative was withdrawn, and washed with dulbecco PBS for 5 minutes, then permeabilized in [0.5% Vol/Vol. Triton X-100 in PBS](Sigma-Aldrich, T8787-250ML) permeabilization solution for 8 minutes for ESCs & Epi-LCs; MEFs were permeabilized for 10minutes to account for their bulkier cytoplasm. Permeabilization solution was discarded, and washed 2 times for 5 minutes with PBS.

At last, all plate wells were filled with 70% Ethanol (Panreac AppliChem, 131086.1214), sealed with parafilm (VWR, BRND701611) and stored at -20ºC from 16 Hours to 3 months before RNA-FISH procedure.

Chapter 2: Immunostaining & RNA-FISH procedure and signal scoring

Immunostaining , as well as RNA-FISH procedure, alone or in combination, were performed as in (Satoshi H Namekawa & Lee 2011), with some modifications.

All tools were previously cleaned from RNAses with RNAse Xterminator Spray (GRiSP, GB43.500S).

All solutions except washes were supplemented with [2 miliMolar RVC] (New England Biolabs, S1402S) and prepared as sterile single-use aliquots. Washing solutions were supplemented with [0.1 miliMolar RVC].

All reagents excepting antibodies, including bovine serum albumina (BSA)(VWR, 0332-25G), and dulbecco PBS were manufactured as being RNAse-free. Dulbecco PBS was elaborated in-house from nuclease-free certified H20 from a MiliQ A10 distiller (Millipore, Z00Q0V0WW).

In immunostaining procedure, the samples were retrieved from -20ºC [70% ETOH] storage and rinsed in dulbecco PBS for 3 minutes. A droplet of 100uL of blocking solution [1% BSA, 0.1% Triton X-100 in Dulbecco PBS], hence known as (PBT), was applied on a parafilm-lined, nuclease-free tipbox chamber and the sample overlaid to it.

Incubation with the blocking solution was performed for 40 minutes at room temperature.

The rabbit anti-H3K27me3 polyclonal antibody (EMD Millipore, ABE44) at [1:500] dilution in PBT was used. Primary antibody solution was supplemented with RVC, incubated for 20 minutes at room temperature to neutralize RNAses, then spun at 2350 RCFs. 100uL of solution were provided per sample and incubated overnight at 4ºC. Three PBT washes of 7 minutes at room temperature were performed prior to secondary antibody exposure.

The donkey anti-rabbitt (ThermoFisher, A31573) at [1:500] dilution in PBT was used. Secondary antibody solution was supplemented with RVC, incubated for 20 minutes at room temperature to neutralize RNAses, then spun at 2350 RCFs. 100uL of solution were provided per sample and incubated for 1 hour at room temperature., followed by three PBT washes of 7 minutes at room temperature.

If only an Immunostaining procedure was performed, coverslips were mounted in Vectashield+DAPI antifade mounting media (Vector laboratories, H1200) onto microscopy slides (VWR, MENZJ1800AMNZ), and imaged within the 24H of the procedure in a Zeiss Observer Inverted microscope, with a 63xOil Immersion objective.

If a RNA-FISH was to be performed in combination to immunostaining, instead of a mounting step, the RNA-FISH procedure would proceed immediately after the secondary antibody washes.

The RNA-FISH procedure was performed as in (Satoshi H Namekawa & Lee 2011), with modifications stated when applicable. All solutions & reagent composition are the same, except when explicitly stated otherwise.

The hybridization & amplification solutions were supplemented with [20 miliMolar RVC] (New England Biolabs, S1402S).

All of remainder non-Ethanol solutions are supplemented with [0.2 miliMolar RVC].

The Hybridization solution was [**2xSSC**+**10%** Vol.Vol. **Dextran Sulfate** (Sigma-Aldrich, D6001-10G) +**25%** Vol./Vol. **deionized Formamide** (VWR, 1.09684.1000), pH7.4].

RNA-FISH Oligonucleotide probe sequences targeting the *Xist* & *Tsix* lncRNAs (Del Rosario et al. 2017) were ordered from IDT technologies. *Xist* probes were fitted with two Cy5 dyes, one on each terminus, while *Tsix* probes were fitted with two Cy3 dyes, one on each terminus**.**

All Oligonucleotide sequences are listed in **table 2.4.5.2.**

FISH Hybridization solution was supplemented with [3nanograms/mL] of each Oligonucleotide FISH probe against target lncRNAs, [20milimolar RVC] & [1microgram/uL yeast t-RNA](Life Technologies, 15401029), and incubated in a thermocycler at 80ºC for 10 minutes, then at 37ºC for 30 minutes.

Stored coverslip samples were transferred with forceps to a new 12-well cell culture plate, and subject to a 70-80-90-100% Ethanol dehydration procedure, 3 minutes each at room temperature.

Coverslips were allowed to dry for 3minutes at room temperature, then transferred into a 30uL droplet in a tipbox hybridization chamber, as described in (Satoshi H. Namekawa & Lee 2011), and incubated overnight at room temperature.

The washing procedures were performed as described in (Satoshi H Namekawa & Lee 2011)**.** After this, coverslips were mounted in Vectashield+DAPI antifade mounting media (Vector laboratories, H1200) onto microscopy slides (VWR, MENZJ1800AMNZ), and imaged within the 24H of the procedure in a Zeiss Observer Inverted microscope, with a 63xOil Immersion objective.

An Orca Hamamatsu 2000 camera was used for image acquisition, and 400 & 500miliseconds exposure times were used for *Xist* and *Tsix* RNA-FISH signal imaging, respectively. Z-stacks encompassing the entirety of cell volume with a 0.7micron z-step were acquired, and pseudocoloring, channel level optimization, channel merging &

maximal intensity z-projection performed with ImageJ (FIJI) V.2.0.0-2017 software.

Signals were manually scored & quantified. Due to H3K27me3 epigenetic mark, as well as *Tsix* & *Xist* lncRNAs being restricted to nuclear locations, signals were verified to co-localize with DAPI staining before scoring to guarantee the absence of artifacts.

The plots were elaborated in Microsoft Excel for mac 2011, V14.7.1, and figure panels assembled on Microsoft Power Point for mac 2011, V14.7.1.

Chapter 2: *In Vitro* Epi-Lc Induction for X-inactivation kinetics assessment

The Epi-LC cell Induction procedure was performed as in (Hayashi & Saitou 2013b)**,** with some modifications.

5 different naïve pluripotent ESC lines were screened for their X-inactivation kinetics as they were differentiated from naïve pluripotency to epiblast-like cells.

3 induced pluripotent stem cell lines (iPSCs) of *Mus musculus/Mus spretus* hybrid background carrying an X-linked *eGFP* reporter array (A. K. Hadjantonakis et al. 2001) on their *Mus musculus*-inherited X chromosome and reprogrammed from somatic cell lines by the use of a STEMCCA lentiviral cassette (Sommer et al. 2016) were FACs-sorted and tested for XX genotype integrity.

Two of them, iPSC line 76.6 & 30, were devoid of additional alterations. The iPSC line 77-1D2, on the other hand, carried an additional deletion of the CPG island driving transcription of the *musculus*-linked *Tsix* lncRNA locus, and, as such, the X-inactivated chromosome will always be the *musculus* X chromosome bearing the *eGFP* reporter array **(QUOTE)**.

After confirmation, the ES cell lines were seeded at 2.7*10^4 viable cells/cm2 on 6-well cell culture plates (Thermofisher Scientific, 140675) over an irradiated male embryonic fibroblast feeder layer, fed fresh 2i+LIF media daily, and split each 48H at above-mentioned density for 4 passages in order to select cells growing robustly in 2i+LIF media.

In preparation for *In Vitro* Epi-LC induction procedure, ESCs split and seeded at 2.7*10^4 viable cells/cm2 in a 6-well cell culture plate well on 2i+LIF cell culture media. Media was changed daily, and cells were split at 48H onto 2i+LIF media at same confluence and vessel as above.

After 2 passages on 2i+LIF, the ES cells were split & Epi-LC Induction with ActivinA (Peprotech, 120-14E-50ug) & bFGF (Life Technologies, 13256-029) cytokines was performed as described in (Hayashi & Saitou 2013a), but the following alterations were introduced:

Instead the 36H Epi-LC Induction timing prior to PGC Induction, the cells were induced for up to 216H (9 days). The cells were not split in this experiment, but let grow in the same vessel for fear that splitting would favor the increased cell death phase observed after 4 days of Epi-LC culture (Hayashi et al. 2011b).

2 hybrid ESCs lines, carrying one *Mus musculus*-inherited & one *Mus castaneus*-inherited X chromosomes **(QUOTES)** were obtained & expanded on ES+LIF cell culture media **[QUOTE & REAGENT REFs]** over an irradiated male embryonic fibroblast feeder layer.

A selection procedure for pluripotency maintenance on gelatin-coated surface and 2i+LIF media was carried out.

The EL16.7 TST A10 Dual Color cell line results from the targeted insertion of *eGFP* & *Td-tomato* in the *Hprt* gene locus for both the *Mus musculus* & *Mus castaneus*-inherited X chromosomes.

The EL16.7 TST A4 Single Color cell line results from the targeted insertion of *eGFP* in the *Hprt* gene locus of the *Mus musculus*-inherited X chromosome.

All procedures were performed by fellow phd student Moritz Bauer (Bauer 2017).

After cell line establishment, all cell lines were adapted for growth in naïve pluripotency-enhancing 2i+LIF media (Nichols & Ying 2006b). The ES cells were

seeded at 2.7*10^4 viable cells/cm2 on 6-well cell culture plates (Thermofisher Scientific, 140675), fed fresh 2i+LIF media daily, and split each 48H at above-mentioned density for 4 passages, whereupon they were stored in [ESmedia+**10%Fetal Bovine serum (FBS)**(Life technologies, 10270106)+10%Dimethyl sulfoxide (DMSO)(Sigma-Aldrich, D5879-500ML)] freezing solution.

In preparation for *In Vitro* Epi-LC induction procedure, the two hybrid ESC lines were split and seeded at 2.7*10^4 viable cells/cm2 in a 6-well cell culture plate well on 2i+LIF cell culture media. Media was changed daily, and cells were split at 48H onto 2i+LIF media at same confluence and vessel as above.

After 2 passages on 2i+LIF, the ES cells were split & Epi-LC Induction with ActivinA (Peprotech, 120-14E-50ug) & bFGF (Life Technologies, 13256-029) cytokines was performed as described in (Hayashi & Saitou 2013a), but the following alterations were introduced:

Instead the 36H Epi-LC Induction timing prior to PGC Induction, the cells were induced for up to 168H (7 days). In contrast with the previous experiment with iPSC cell line differentiation, the Epi-LCs were trypsinized by exposure to Tryple-express enzyme (Life Technologies, 12604-021) for 3 minutes at room temperature and split every 48H upon cell confluence. This procedure was repeated until the end of the experiment.

Chapter 2: *In Vitro* Germ cell Induction protocols

The In Vitro Germ cell Induction procedure was performed as in (Hayashi & Saitou 2013b)**,** with some modifications.

Embryonic stem cell Lines hybrid Embryonic stem cell lines (ESCs), carrying one *Mus musculus*-inherited & one *Mus castaneus*-inherited X chromosomes **(QUOTES)** were obtained & expanded on ES+LIF cell culture media **[QUOTE & REAGENT REFERENCES]** on a male embryonic feeder layer.

A procedure for pluripotency maintenance on gelatin-coated surface and the insertion of

eGFP & *Td-tomato* in the *Hprt* gene locus for both the *Mus musculus* & *Mus castaneus*-inherited X chromosomes was performed by fellow phd student Moritz Bauer (Bauer 2017)

After cell line establishment, cell lines were adapted for growth in naïve pluripotency-enhancing 2i+LIF media (Nichols & Ying 2006b) and Gelatin-coated surfaces. The ES cells were seeded at 2.7*10^4 viable cells/cm2 on 6-well cell culture plates (Thermofisher Scientific, 140675), fed fresh 2i+LIF media daily, and split each 48H at above-mentioned density for 4 passages, whereupon they were stored in [ESmedia+**10%Fetal Bovine serum** (FBS)(Life technologies, 10270106)+**10%Dimethyl sulfoxide** (DMSO)(Sigma-Aldrich, D5879-500ML)] freezing solution.

Upon *In Vitro* PGC induction procedure, vials of EL16.7 TST hybrid ESCs were thawn and seeded at 2.7*10^4 viable cells/cm2 in a 6-well cell culture plate well on ES+LIF cell culture media. Media was changed daily, and cells were split at 48H onto 2i+LIF media at same confluence and vessel as above.

After 2 passages on 2i+LIF, the ES cells were split & Epi-LC Induction with ActivinA (Peprotech, 120-14E-50ug) & bFGF (Life Technologies, 13256-029) cytokines was performed as described in (Hayashi & Saitou 2013a), but the following alterations were introduced:

Instead the 36H Epi-LC Induction timing prior to PGC Induction, those were carried out at 48H (day2), 72H (day3) & 96H (day4) of Epi-LC development.

Epi-LCs were left to grow without splitting in the same induction culture vessel up to 72H (day3) of Epi-LC development. For PGC induction from 96H (day4) Epi-LCs, Epi-LCs were split after 48H of culture and 3*10^5 viable Epi-LCs were seeded per well of a 12-well plate, in same conditions used for Epi-LC induction, and let grow until 96H since Epi-LC Induction.

PGC Induction was performed as described in (Hayashi & Saitou 2013b) with some

modifications.

A total of 5.000 viable Epi-LCs cells were seeded per body, and 2 conditions were performed:

- PGC Induction (BMP4(+) conditions), in which the full cytokine complement for PGC induction & expansion was provided.
- Negative Control conditions were seeded in base GK15 cell culture media for PGCs, but no cytokines were provided. This led to the formation of Embrioid bodies, known to proceed to fast random cell differentiation and x-inactivation **(QUOTE)**, acting as a positive control for X-inactivation and a negative control for X-reactivation.

The cells were cultured without media change for 96H (day4), 144H (day6) or 168H (day7) of development, before FACs analysis & processing for RNA extraction.

Chapter 2: ESCs & Epi-LCs FACs analysis

The FACs analysis procedure was adapted from (Hayashi & Saitou 2013b), with some modifications. ESCs were trypsinized for 8 minutes at 37ºC with [0.05% Trypsin-EDTA], while Epi-LCs were trypsinized for 3 minutes at room temperature with the Tryple-express enzyme (Life Technologies, 12604-021), accounting for their increased mechanosensitivity and general fragility.

Upon trypsinization, single-cell resuspension and 40 micron mesh (LabClinics, PLC93040) filtering for single-cell suspension, each FACs condition cell pellet was resuspended in 200uL of an antibody staining solution in a 1.5mL eppendorf tube (Sigma Aldrich, T9661-1000EA).

All remaining steps and solutions below are maintained at 4ºC temperature.

The antibody staining solution was comprised of [DMEM/F12+1%BSA-Cell culture grade](Life technologies, 15260-037), which was supplemented with the antibodies SSEA1-Alexa660 (eBioscience, 50-8813-42) at [1:50=0.6uG/mL] dilution, and CD61-PE-Vio770 (Miltenyi Biotech, 130-102-627) at [1:20=1uG/mL] dilution.

The increased 1% BSA and use of DMEM/F12 media as solvent were included to favor

antibody specificity & increase viability of the PGCs for FACs procedure, respectively.

The antibody cell suspensions were incubated for 1H at 4ºC with continuous rotation in an orbitator platform, whereupon they were transferred to a 15mL Falcon tube per condition (Falcon, 352096), and the original eppendorf was rinsed twice to ensure full transfer of cell suspension.

A 10mL of [PBS+0.1%BSA , cell-culture grade] were added to each condition, and the cells spun at 250 RCFs for 5 minutes in a 4ºC centrifuge. The solution was discarded, the cell pellet resuspended, and the same washing procedure was performed again 2X times.

Prior to FACs-analysis procedure, cell pellets were resuspended to single-cell solution in [DMEM/F12+0.1%BSA-RNAse-free] supplemented with DAPI (Biogen Cientifica, BT-40043) at [1uG/mL] as viability marker.

Cells were incubated for a minimum of 15 minutes before filtering through a 70micron cell strainer and run through an LSRII or Fortessa FACs-analyzer, using a 100micron nozzle and as few psi as possible without negatively impacting analysis ability.

The change to a higher nozzle diameter allows for reduced hydrostatic pressure. Hydrostatic pressure has been found to be particularly deleterious for mechanosensitive cells such as Epi-LCs and Primordial germ cells (PGCs) (Hayashi & Saitou 2013b).

After data acquisition, the gates were fine-tuned and FACs plots edited in Flowjo V10.5.0 software.

Image panels were assembled on Microsoft Power Point for mac 2011, V14.7.1.

Chapter 2: PGC-LC & Embrioid body FACs analysis

The FACs analysis procedure was performed as in (Hayashi & Saitou 2013b), with some modifications. The day4 bodies were trypsinized for 8 minutes at 37ºC with [0.05% Trypsin-EDTA], while the day 6 & 7 bodies were trypsinized for 10 minutes at 37ºC, in order to account for increased cell adhesion and body size upon longer culture.

Upon trypsinization, single-cell resuspension and 70 micron mesh (Corning, 352350) filtering for single-cell suspension, each FACs condition cell pellet was resuspended in 200uL of an antibody staining solution in a 1.5mL eppendorf tube (Sigma Aldrich, T9661-1000EA).

All remaining steps and solutions below are maintained at 4ºC temperature.

The antibody staining solution was comprised of [DMEM/F12+1%BSA-Cell culture grade](Life technologies, 15260-037), which was supplemented with the antibodies SSEA1-Alexa660 (eBioscience, 50-8813-42) at [1:50=0.6uG/mL] dilution, and CD61-PE-Vio770 (Miltenyi Biotech, 130-102-627) at [1:20=1uG/mL] dilution.

The increased 1% BSA and use of DMEM/F12 media as solvent were included to favor antibody specificity & increase viability of the PGCs for FACs procedure, respectively.

The antibody cell suspensions were incubated for 1H at 4ºC with continuous rotation in an orbitator platform, whereupon they were transferred to a 15mL Falcon tube per condition (Falcon, 352096), and the original eppendorf was rinsed twice to ensure full transfer of cell suspension.

A 10mL of [PBS+0.1%BSA , cell-culture grade] were added to each condition, and the cells spun at 250 RCFs for 5 minutes in a 4ºC centrifuge. The solution was discarded, the cell pellet resuspended, and the same washing procedure was performed again 2X times.

Prior to FACs-sorting procedure, cell pellets were resuspended to single-cell solution in [DMEM/F12+0.1%BSA-RNAse-free] supplemented with DAPI (Biogen Cientifica, BT-40043) at [1uG/mL] as viability marker.

Cells were incubated for a minimum of 15 minutes before filtering through a 70micron cell strainer and run either through a BD Influx cell sorter, or a LSRII or Fortessa FACs-analyzer.

FACs-sorting procedures used using a 140micron nozzle, while FACs-analyzers used a 100micron nozzle.

In both cases, as few psi as possible were used, as long as they did not negatively impacting sorting ability.

The change to a higher nozzle diameter allows for reduced hydrostatic pressure. Hydrostatic pressure has been found to be particularly deleterious for Primordial germ cells (PGCs) (Hayashi & Saitou 2013b), and they also have an increased cell size (Yamaji et al. 2010)**,** meaning the use of 100micron nozzle diameter or below usually results in very poor PGC viability and cell losses during sorting.

The increased cell size means that the use of cell strainers below 70micron size results in a selective Germ cell depletion.

After data acquisition, the gates were fine-tuned and FACs plots edited in Flowjo V10.5.0 software.

Image panels were assembled on Microsoft Power Point for mac 2011, V14.7.1

Bibliographic References:

Ahn, J.Y. & Lee, J.T., 2010. Retinoic acid accelerates downregulation of the Xist repressor, Oct4, and increases the likelihood of Xist activation when Tsix is deficient. *BMC Developmental Biology*, 10.

Babak, T. et al., 2008. Global survey of genomic imprinting by transcriptome sequencing. *Current biology : CB*, 18(22), pp.1735–41. Available at: http://dx.doi.org/10.1016/j.cub.2008.09.044.

Bassett, A.R. et al., 2014. Considerations when investigating lncRNA function in vivo. *eLife*, 3(August2014), pp.1–14.

Battich, N., Stoeger, T. & Pelkmans, L., 2013. Image-based transcriptomics in thousands of single human cells at single-molecule resolution. *Nature Methods*, (october), pp.1–10. Available at: http://dx.doi.org/10.1038/nmeth.2657.

Bauer, M., 2017. private communication. *personal comunication*.

Beliveau, B.J. et al., 2015. Single-molecule super-resolution imaging of chromosomes and in situ haplotype visualization using Oligopaint FISH probes. *Nature Communications*, 6(May).

Berletch, J.B. et al., 2015. Escape from X Inactivation Varies in Mouse Tissues. *PLoS Genetics*, 11(3), pp.1–26. Available at: http://dx.doi.org/10.1371/journal.pgen.1005079.

Bhatnagar, S. et al., 2014. Genetic and pharmacological reactivation of the mammalian inactive X chromosome. *Proceedings of the National Academy of Sciences*, 111(35), pp.12591–12598. Available at: http://www.pnas.org/cgi/doi/10.1073/pnas.1413620111.

Borensztein, M., Okamoto, I., et al., 2017. Contribution of epigenetic landscapes and transcription factors to X-chromosome reactivation in the inner cell mass. *Nature Communications*, 8(1). Available at: http://dx.doi.org/10.1038/s41467-017-01415-5.

Borensztein, M., Syx, L., et al., 2017. Xist-dependent imprinted X inactivation and the early developmental consequences of its failure. *Nature Structural and Molecular Biology*, 24(3), pp.226–233.

Cattanach, B.M. & Papworth, D., 1981. Controlling elements in the mouse. V. Linkage tests with X-linked genes. *Genetical research*, 38(1), pp.57–70. Available at: http://www.ncbi.nlm.nih.gov/pubmed/7024043.

Chaumeil, J. et al., 2008. Combined immunofluorescence, RNA fluorescent in situ hybridization, and DNA fluorescent in situ hybridization to study chromatin changes, transcriptional activity, nuclear organization, and X-chromosome inactivation. *Methods in molecular biology (Clifton, N.J.)*, 463, pp.297–308.

Chen, K.H. et al., 2015. Spatially resolved, highly multiplexed RNA profiling in single cells. *Science*, 348(6233), pp.1360–1363.

Choi, H.M.T. et al., 2016. Mapping a multiplexed zoo of mRNA expression. *Development*, 143(19), pp.3632–3637. Available at:

http://dev.biologists.org/lookup/doi/10.1242/dev.140137.

Choi, H.M.T. et al., 2018. Third-generation in situ hybridization chain reaction : multiplexed , quantitative , sensitive , versatile , robust. , 1.

Choi, H.M.T., Beck, V.A. & Pierce, N.A., 2014. Terms of Use Next-Generation in Situ Hybridization Chain Reaction : Higher Gain , Lower Cost , Greater Durability. , (5), pp.4284–4294.

Chuva De Sousa Lopes, S.M. et al., 2008. X chromosome activity in mouse XX primordial germ cells. *PLoS Genetics*, 4(2).

Chuva de Sousa Lopes, S.M. & Roelen, B.A.J., 2008. Primordial germ cell specification: the importance of being "blimped". *Histology and histopathology*, 23(12), pp.1553–61. Available at: http://www.ncbi.nlm.nih.gov/pubmed/18830940 [Accessed May 22, 2015].

Costanzi, C. & Pehrson, J.R., 1998. of Female Mammals. *Nature*, 628(1997), pp.1997–1999.

Deng, Q. et al., 2014. Single-cell RNA-seq reveals dynamic, random monoallelic gene expression in mammalian cells. *Science*, 343(6167), pp.193–196.

Deng, X. et al., 2015. Bipartite structure of the inactive mouse X chromosome. , pp.1–21.

Deuve, J.L. et al., 2015. Antagonist *Xist* and *Tsix* co-transcription during mouse oogenesis and maternal *Xist* expression during pre-implantation development calls into question the nature of the maternal imprint on the X chromosome. *Epigenetics*, 10(10), pp.931–942. Available at: http://www.tandfonline.com/doi/full/10.1080/15592294.2015.1081327.

Durcova-Hills, G. et al., 2008. Reprogramming Primordial Germ Cells into Pluripotent Stem Cells J.-N. Volff, ed. *PLoS ONE*, 3(10), p.e3531. Available at: http://dx.plos.org/10.1371/journal.pone.0003531.

Durcova-Hills G, M.A., 2006. Isolation and maintenance of murine embryonic germ cell lines. In L. R, ed. *Isolation and maintenance of murine embryonic germ cell lines*. Elsevier Academic Press, pp. 299–304.

Emmanuela Greco, 2016. private communication. *personal comunication*.

Gaspar, I. & Ephrussi, A., 2015. Strength in numbers: Quantitative single-molecule RNA detection assays. *Wiley Interdisciplinary Reviews: Developmental Biology*, 4(2), pp.135–150.

Gaspar, I., Wippich, F. & Ephrussi, A., 2017. Enzymatic production of single-molecule FISH and RNA capture probes. *Rna*, 23(10), pp.1582–1591.

Geijsen, N. et al., 2004. Derivation of embryonic germ cells and male gametes from embryonic stem cells. *Nature*, 427(6970), pp.148–154. Available at: http://www.nature.com/doifinder/10.1038/nature02247.

Generoso, S., 2018. private communication. *personal communication*.

van Gijtenbeek, L.A. & Kok, J., 2017. Illuminating messengers: An update and outlook on RNA visualization in bacteria. *Frontiers in Microbiology*, 8(JUN).

Green, M.R. & Sambrook, J., 2014. Molecular Cloning: A Laboratory Manual (Fourth edition). In *Molecular Cloning: A Laboratory Manual(Fourth edition).* Cold Spring Harbor Laboratory

Press, p. 2028. Available at: https://www.cshlpress.com/default.tpl?cart=153337963498445831 8&fromlink=T&linkaction=full&linksortby=oop_title&--eqSKUdatarq=934.

Hadjantonakis, a K. et al., 2001. An X-linked GFP transgene reveals unexpected paternal X-chromosome activity in trophoblastic giant cells of the mouse placenta. *Genesis (New York, N.Y. : 2000)*, 29(3), pp.133–40. Available at: http://www.ncbi.nlm.nih.gov/pubmed/11252054 [Accessed December 19, 2014].

Hadjantonakis, A.K. et al., 2001. An X-linked GFP transgene reveals unexpected paternal X-chromosome activity in trophoblastic giant cells of the mouse placenta. *Genesis*, 29, pp.133–140.

Hauptmann, G., Lauter, G. & Söll, I., 2016. Detection and signal amplification in zebrafish RNA FISH. *Methods*, 98, pp.50–59.

Hayashi, K. et al., 2012. Offspring from oocytes derived from in vitro primordial germ cell-like cells in mice. *Science (New York, N.Y.)*, 338(6109), pp.971–5. Available at: http://www.ncbi.nlm.nih.gov/pubmed/23042295 [Accessed November 14, 2014].

Hayashi, K. et al., 2012. Offspring from Oocytes Derived from in Vitro Primordial Germ Cell-Like Cells in Mice. *Science*, 338(6109), pp.971–5. Available at: http://www.ncbi.nlm.nih.gov/pubmed/23042295 [Accessed November 14, 2014].

Hayashi, K. et al., 2017a. Reconstitution of mouse oogenesis in a dish from pluripotent stem cells. *Nature Protocols*, 12(9), pp.1733–1744.

Hayashi, K. et al., 2017b. Reconstitution of mouse oogenesis in a dish from pluripotent stem cells. *Nature Protocols*, 12(9), pp.1733–1744. Available at: http://www.nature.com/doifinder/10.1038/nprot.2017.070.

Hayashi, K. et al., 2011a. Reconstitution of the mouse germ cell specification pathway in culture by pluripotent stem cells. *Cell*, 146(4), pp.519–532. Available at: http://www.ncbi.nlm.nih.gov/pubmed/21820164 [Accessed July 12, 2014].

Hayashi, K. et al., 2011b. Reconstitution of the mouse germ cell specification pathway in culture by pluripotent stem cells. *Cell*, 146(4), pp.519–532. Available at: http://dx.doi.org/10.1016/j.cell.2011.06.052.

Hayashi, K. & Saitou, M., 2013a. Generation of eggs from mouse embryonic stem cells and induced pluripotent stem cells. *Nature protocols*, 8(8), pp.1513–24. Available at: http://www.ncbi.nlm.nih.gov/pubmed/23845963 [Accessed November 14, 2014].

Hayashi, K. & Saitou, M., 2013b. Generation of eggs from mouse embryonic stem cells and induced pluripotent stem cells. *Nature protocols*, 8(8), pp.1513–24. Available at: http://www.ncbi.nlm.nih.gov/pubmed/23845963.

Hayashi, K. & Saitou, M., 2013c. Stepwise Differentiation From Naïve State Pluripotent Stem Cells to Functional Primordial Germ Cells Through an Epiblast-Like State R. Alberio, ed. , 1074, pp.1–13. Available at: http://link.springer.com/10.1007/978-1-62703-628-3 [Accessed December 16, 2014].

Hore, T.A. et al., 2016. Retinol and ascorbate drive erasure of epigenetic memory and enhance reprogramming to naïve pluripotency by complementary mechanisms. *Proceedings of the National Academy of Sciences of the United States of America*, 113(43), pp.12202–12207.

Available at: http://www.ncbi.nlm.nih.gov/pubmed/27729528%5Cnhttp://www.pubmedcentral.nih.gov/articlerender.fcgi?artid=PMC5086989.

Hu, Y.-C., Nicholls, P.K., et al., 2015. Licensing of primordial germ cells for gametogenesis depends on genital ridge signaling. *PLoS genetics*, 11(3), p.e1005019. Available at: http://journals.plos.org/plosgenetics/article?id=10.1371/journal.pgen.1005019 [Accessed May 22, 2015].

Hu, Y.-C., Nicholls, P.K., et al., 2015. Licensing of Primordial Germ Cells for Gametogenesis Depends on Genital Ridge Signaling. *PLOS Genetics*, 11(3), p.e1005019. Available at: http://dx.plos.org/10.1371/journal.pgen.1005019.

Irie, N. et al., 2015. Article SOX17 Is a Critical Specifier of Human Primordial Germ Cell Fate. *Cell*, 160(1–2), pp.253–268. Available at: http://dx.doi.org/10.1016/j.cell.2014.12.013.

Jameson, S.A. et al., 2012. Temporal transcriptional profiling of somatic and germ cells reveals biased lineage priming of sexual fate in the fetal mouse gonad. *PLoS Genetics*, 8(3).

Johnson, C. V, Singer, R.H. & Lawrence, J.B., 1991. Fluorescent detection of nuclear RNA and DNA implication for genome organization. *Meth. Cell Biol.*, 35, pp.73–99.

Kagiwada, S. et al., 2012. Replication-coupled passive DNA demethylation for the erasure of genome imprints in mice. *The EMBO journal*, 32(3), pp.340–53. Available at: http://www.pubmedcentral.nih.gov/articlerender.fcgi?artid=3567490&tool=pmcentrez&rendertype=abstract [Accessed December 7, 2014].

Kalantry, S. et al., 2010. HHS Public Access. , 460(7255), pp.647–651.

Keane, T.M. et al., 2011. Mouse genomic variation and its effect on phenotypes and gene regulation. *Nature*, 477(7364), pp.289–94. Available at: http://www.ncbi.nlm.nih.gov/pubmed/21921910.

Kime, C. et al., 2016. Autotaxin-mediated lipid signaling intersects with LIF and BMP signaling to promote the naive pluripotency transcription factor program. *Proceedings of the National Academy of Sciences of the United States of America*, p.201608564. Available at: http://www.ncbi.nlm.nih.gov/pubmed/27738243.

Kishi, J.Y., Wang, Y. & Cepko, C.L., 2018. SABER enables highly multiplexed and amplified detection of DNA and RNA in cells and tissues.

Klosin, A. et al., 2017. Impaired DNA replication derepresses chromatin and generates a transgenerationally inherited epigenetic memory. *Science Advances*, 3(8).

Kurimoto, K. et al., 2015. Quantitative Dynamics of Chromatin Remodeling during Germ Cell Specification from Mouse Embryonic Stem Cells. *Cell Stem Cell*, pp.1–16. Available at: http://linkinghub.elsevier.com/retrieve/pii/S1934590915001137.

Kwon, S., 2013. Single-molecule fluorescence in situ hybridization: Quantitative imaging of single RNA molecules. *Bmb Reports*, 46(2), pp.65–72.

Lee, J., 2016. private communication. *personal comunication*.

Lee, J.T. & Lu, N., 1999. Targeted mutagenesis of Tsix leads to nonrandom X inactivation. *Cell*, 99(1), pp.47–57.

Leitch, H.G., Tang, W.W.C. & Surani, M.A., 2013. Primordial Germ-Cell Development and Epigenetic Reprogramming in Mammals. *Current Topics in Developmental Biology*, 104, pp.149–187. Available at: http://dx.doi.org/10.1016/B978-0-12-416027-9.00005-X.

Lessing, D. et al., 2016. A high-throughput small molecule screen identifies synergism between DNA methylation and Aurora kinase pathways for X reactivation. *Proceedings of the National Academy of Sciences*, p.201617597. Available at: http://www.pnas.org/lookup/doi/10.1073/pnas.1617597113.

Levesque, M.J. & Raj, A., 2013. Single-chromosome transcriptional profiling reveals chromosomal gene expression regulation. *Nature Methods*, 10(3), pp.246–248. Available at: http://www.nature.com/doifinder/10.1038/nmeth.2372.

Liu, L. et al., 2018. Branched Hybridization Chain Reaction Circuit for Ultrasensitive Localizable Imaging of mRNA in Living Cells. *Analytical Chemistry*, 90(3), pp.1502–1505.

Mak, W., Nesterova, T.B., et al., 2004. Reactivation of the paternal X chromosome in early mouse embryos. *Science (New York, N.Y.)*, 303(5658), pp.666–9. Available at: http://www.ncbi.nlm.nih.gov/pubmed/14752160 [Accessed May 26, 2015].

Mak, W., Nesterova, T.B., et al., 2004. Reactivation of the Paternal X Chromosome in Early Mouse Embryos. *Science*, 303(5658), pp.666–669.

Mark, M. et al., 2014. Role of retinoic acid receptor (RAR) signaling in post-natal male germ cell differentiation. *Biochimica et Biophysica Acta - Gene Regulatory Mechanisms*, 1849(2), pp.84–93. Available at: http://dx.doi.org/10.1016/j.bbagrm.2014.05.019.

Marks, H. et al., 2015. Dynamics of gene silencing during X inactivation using allele-specific RNA-seq. *Genome Biology*, 16(1), p.149. Available at: http://genomebiology.com/2015/16/1/149.

Miyauchi, H. et al., 2017. Bone morphogenetic protein and retinoic acid synergistically specify female germ-cell fate in mice. *The EMBO Journal*, p.e201796875. Available at: http://emboj.embopress.org/lookup/doi/10.15252/embj.201796875.

Miyauchi, H. et al., 2017. Bone morphogenetic protein and retinoic acid synergistically specify female germ cell fate in mice. *Embo*, in press, pp.1–20.

Mohammed, H. et al., 2017. Single-Cell Landscape of Transcriptional Heterogeneity and Cell Fate Decisions during Mouse Early Gastrulation. *Cell Reports*, 20(5), pp.1215–1228.

Nakaki, F. et al., 2013a. Induction of mouse germ-cell fate by transcription factors in vitro. *Nature*, 501, pp.222–6. Available at: http://www.ncbi.nlm.nih.gov/pubmed/23913270.

Nakaki, F. et al., 2013b. Induction of mouse germ-cell fate by transcription factors in vitro. *Nature*, 501(7466), pp.222–6. Available at: http://www.ncbi.nlm.nih.gov/pubmed/23913270.

Nakaki, F. et al., 2013c. Induction of mouse germ-cell fate by transcription factors in vitro. *Nature*, 501(7466), pp.222–6. Available at: http://www.ncbi.nlm.nih.gov/pubmed/23913270 [Accessed July 23, 2014].

Nakaki, F., 2017. private communication. *personal communication*.

Namekawa, S.H. et al., 2010. Two-Step Imprinted X Inactivation: Repeat versus Genic Silencing in the Mouse. *Molecular and Cellular Biology*, 30(13), pp.3187–3205. Available at:

http://mcb.asm.org/cgi/doi/10.1128/MCB.00227-10.

Namekawa, S.H. & Lee, J.T., 2011. Detection of nascent RNA, single-copy DNA and protein localization by immunoFISH in mouse germ cells and preimplantation embryos. *Nature protocols*, 6(3), pp.270–284. Available at: http://dx.doi.org/10.1038/nprot.2010.195.

Namekawa, S.H. & Lee, J.T., 2011. Detection of nascent RNA, single-copy DNA and protein localization by immunoFISH in mouse germ cells and preimplantation embryos. *Nature Protocols*, 6(3), pp.270–284. Available at: http://dx.doi.org/10.1038/nprot.2010.195.

de Napoles, M., Nesterova, T. & Brockdorff, N., 2007. Early loss of Xist RNA expression and inactive X chromosome associated chromatin modification in developing primordial germ cells. *PLoS ONE*, 2(9), pp.9–14.

Nef, S. et al., 2005. Gene expression during sex determination reveals a robust female genetic program at the onset of ovarian development. *Developmental Biology*, 287(2), pp.361–377.

Nesterova, T.B. et al., 2002. Xist expression and macroH2A1.2 localisation in mouse primordial and pluripotent embryonic germ cells. *Differentiation*, 69(4–5), pp.216–225.

Nichols, J. & Ying, Q.-L., 2006a. Derivation and propagation of embryonic stem cells in serum- and feeder-free culture. *Methods in molecular biology (Clifton, N.J.)*, 329, pp.91–98.

Nichols, J. & Ying, Q.-L., 2006b. Derivation and propagation of embryonic stem cells in serum- and feeder-free culture. *Methods in molecular biology (Clifton, N.J.)*, 329, pp.91–8. Available at: http://www.ncbi.nlm.nih.gov/pubmed/16845986.

Nora, P. et al., 2014. Predictive Polymer Modeling Reveals Coupled Fluctuations in Chromosome Conformation and Transcription.

Ogawa, Y. & Lee, J.T., 2003. Xite, X-inactivation intergenic transcription elements that regulate the probability of choice. *Molecular cell*, 11(3), pp.731–43. Available at: http://www.ncbi.nlm.nih.gov/pubmed/12667455.

Ogawa, Y., Sun, B.K. & Lee, J.T., 2008. Intersection of the RNAi and X-inactivation pathways. *Science*, 320(5881), pp.1336–1341.

Ohinata, Y. et al., 2008. A comprehensive, non-invasive visualization of primordial germ cell development in mice by the Prdm1-mVenus and Dppa3-ECFP double transgenic reporter. *Reproduction*, 136, pp.503–514.

Ohinata, Y. et al., 2009. A Signaling Principle for the Specification of the Germ Cell Lineage in Mice. *Cell*, 137(3), pp.571–584. Available at: http://dx.doi.org/10.1016/j.cell.2009.03.014.

Ohinata, Y. et al., 2005. Blimp1 is a critical determinant of the germ cell lineage in mice. *Nature*, 436(7048), pp.207–213. Available at: http://www.ncbi.nlm.nih.gov/pubmed/15937476 [Accessed December 16, 2014].

Ohta, H. et al., 2017a. In vitro expansion of mouse primordial germ cell- like cells recapitulates an epigenetic blank slate. , pp.1–20.

Ohta, H. et al., 2017b. In vitro expansion of mouse primordial germ cell-like cells recapitulates an epigenetic blank slate. *The EMBO journal*, 36(13), pp.1888–1907. Available at: http://www.ncbi.nlm.nih.gov/pubmed/28559416.

Okamoto, I., Otte, A.P., et al., 2004. Epigenetic dynamics of imprinted X inactivation during early mouse development. *Science (New York, N.Y.)*, 303(5658), pp.644–9. Available at: http://www.ncbi.nlm.nih.gov/pubmed/14671313 [Accessed May 26, 2015].

Okamoto, I., Otte, A.P., et al., 2004. Epigenetic Dynamics of Imprinted X Inactivation during Early Mouse Development. *Science*, 303(5658), pp.644–649.

Pasque, V. et al., 2011. Histone variant macroH2A confers resistance to nuclear reprogramming. *The EMBO journal*, 30(12), pp.2373–2387. Available at: http://dx.doi.org/10.1038/emboj.2011.144.

Pasque, V. et al., 2012. Histone variant macroH2A marks embryonic differentiation in vivo and acts as an epigenetic barrier to induced pluripotency. *Journal of Cell Science*, 2, pp.6094–6104.

Pasque, V. et al., 2014. X Chromosome Reactivation Dynamics Reveal Stages of Reprogramming to Pluripotency. *Cell*, 159(7), pp.1681–1697. Available at: http://linkinghub.elsevier.com/retrieve/pii/S0092867414015177 [Accessed December 19, 2014].

Patrat, C. et al., 2009. Dynamic changes in paternal X-chromosome activity during imprinted X-chromosome inactivation in mice. *Proceedings of the National Academy of Sciences*, 106(13), pp.5198–5203. Available at: http://www.pnas.org/cgi/doi/10.1073/pnas.0810683106.

Payer, B. et al., 2013. Tsix RNA and the germline factor, PRDM14, link X reactivation and stem cell reprogramming. *Molecular Cell*, 52(6), pp.805–818. Available at: http://www.pubmedcentral.nih.gov/articlerender.fcgi?artid=3950835&tool=pmcentrez&rendertype=abstract [Accessed December 16, 2014].

Payer, B., Lee, J.T. & Namekawa, S.H., 2011. X-inactivation and X-reactivation: Epigenetic hallmarks of mammalian reproduction and pluripotent stem cells. *Human Genetics*, 130(2), pp.265–280.

Pinter, S.F. et al., 2015. Allelic Imbalance Is a Prevalent and Tissue-Specific Feature of the Mouse Transcriptome. *Genetics*, 200(2), pp.537–49. Available at: http://www.ncbi.nlm.nih.gov/pubmed/25858912.

Pitetti, J.-L. et al., 2013. Insulin and IGF1 receptors are essential for XX and XY gonadal differentiation and adrenal development in mice. *PLoS genetics*, 9(1), p.e1003160. Available at: http://journals.plos.org/plosgenetics/article?id=10.1371/journal.pgen.1003160#s3 [Accessed April 6, 2016].

Player, A.N. et al., 2001. Single-copy gene detection using branched DNA (bDNA) in situ hybridization. *Journal of Histochemistry and Cytochemistry*, 49(5), pp.603–611.

Przanowski, P. et al., 2018. Pharmacological reactivation of inactive X-linked *Mecp2* in cerebral cortical neurons of living mice. *Proceedings of the National Academy of Sciences*, p.201803792. Available at: http://www.pnas.org/lookup/doi/10.1073/pnas.1803792115.

Raj, A. & Tyagi, S., 2010. *Detection of Individual Endogenous RNA Transcripts In Situ Using Multiple Singly Labeled Probes* 1st ed., Elsevier Inc. Available at: http://dx.doi.org/10.1016/S0076-6879(10)72004-8.

Reis, K., 2016. Epigenetic inheritance and DNA replication in Caenorhabditis elegans.

Del Rosario, B., 2016. private communication. *personal comunication*.

Del Rosario, B.C. et al., 2017. Genetic Intersection of Tsix and Hedgehog Signaling during the Initiation of X-Chromosome Inactivation. *Developmental Cell*, 43(3), p.359–371.e6. Available at: https://doi.org/10.1016/j.devcel.2017.09.027.

Sakashita, A. et al., 2015. Sex Specification and Heterogeneity of Primordial Germ Cells in Mice. *PloS one*, 10(12), p.e0144836. Available at: http://journals.plos.org/plosone/article?id=10.1371/journal.pone.0144836 [Accessed April 15, 2016].

Sangrithi, M.N. et al., 2017. Non-Canonical and Sexually Dimorphic X Dosage Compensation States in the Mouse and Human Germline. *Developmental Cell*, 40(3), p.289–301.e3.

Schulz, E.G., 2017. X-chromosome dosage as a modulator of pluripotency, signalling and differentiation? *Philosophical Transactions of the Royal Society B: Biological Sciences*, 372(1733), p.20160366. Available at: http://rstb.royalsocietypublishing.org/lookup/doi/10.1098/rstb.2016.0366.

Severino, J., 2018. private communication. *personal comunication*.

Shah, S. et al., 2018. Dynamics and Spatial Genomics of the Nascent Transcriptome by Intron seqFISH Article Dynamics and Spatial Genomics of the Nascent Transcriptome by Intron seqFISH. , pp.363–376.

Shah, S., Lubeck, E., Schwarzkopf, M., He, T.-F., et al., 2016. *Single-molecule RNA detection at depth by hybridization chain reaction and tissue hydrogel embedding and clearing*, Available at: http://dev.biologists.org/lookup/doi/10.1242/dev.138560.

Shah, S., Lubeck, E., Schwarzkopf, M., He, T., et al., 2016. *Single-molecule RNA detection at depth by hybridization chain reaction and tissue hydrogel embedding and clearing*,

Shibata, S. & Lee, J.T., 2003. Characterization and quantitation of differential Tsix transcripts: Implications for Tsix function. *Human Molecular Genetics*, 12(2), pp.125–136.

Shiura, H. et al., 2014. Whole-mount MeFISH: A novel technique for simultaneous visualization of specific DNA methylation and protein/RNA expression. *PLoS ONE*, 9(4).

Sinnamon, J.R. & Czaplinski, K., 2014. Locating RNAs In Situ with FISH-STIC Probes. *Regulatory Non-Coding RNAs: Methods and Protocols*, 1206, pp.1–178.

Sommer, C.A. et al., 2016. iPS Cell Generation Using a Single Lentiviral Stem Cell Cassette. , 27(3), pp.543–549.

Spiller, C., Koopman, P. & Bowles, J., 2017. Sex Determination in the Mammalian Germline. *Annual review of genetics*, (August), pp.265–285. Available at: https://doi.org/10.1146/annurev-genet-120215-035449:265-285.%0Awww.annualreviews.org%0Ahttp://www.ncbi.nlm.nih.gov/pubmed/28853925%0Ahttps://doi.org/10.1146/annurev-genet-120215-035449.

Sripathy, S. et al., 2017a. Screen for reactivation of MeCP2 on the inactive X chromosome identifies the BMP/TGF-β superfamily as a regulator of XIST expression. *Proceedings of the National Academy of Sciences*, 114(7), pp.1619–1624. Available at: http://www.pnas.org/lookup/doi/10.1073/pnas.1621356114.

Sripathy, S. et al., 2017b. Screen for reactivation of MeCP2 on the inactive X chromosome identifies the BMP/TGF-β superfamily as a regulator of XIST expression. *Proceedings of the National Academy of Sciences*, 114(7), pp.1619–1624. Available at: http://www.pnas.org/lookup/doi/10.1073/pnas.1621356114.

Sugimoto, M. & Abe, K., 2007. X chromosome reactivation initiates in nascent primordial germ cells in mice. *PLoS Genetics*, 3(7), pp.1309–1317.

Sunwoo, H., Wu, J.Y. & Lee, J.T., 2015. The Xist RNA-PRC2 complex at 20-nm resolution reveals a low Xist stoichiometry and suggests a hit-and-run mechanism in mouse cells.

Suzuki, A. et al., 2016. Loss of MAX results in meiotic entry in mouse embryonic and germline stem cells. *Nature Communications*, 7, p.11056. Available at: http://www.nature.com/doifinder/10.1038/ncomms11056.

Syrett, C.M. et al., 2017. Loss of Xist RNA from the inactive X during B cell development is restored in a dynamic YY1-dependent two-step process in activated B cells. *PLoS Genetics*, 13(10), pp.1–28.

Tan, K. et al., 2016. Impaired imprinted X chromosome inactivation is responsible for the skewed sex ratio following in vitro fertilization. *Proceedings of the National Academy of Sciences*, 113(12), p.201523538. Available at: http://www.pnas.org/lookup/doi/10.1073/pnas.1523538113.

Thorvaldsen, J.L. et al., 2012. Nonrandom X chromosome inactivation is influenced by multiple regions on the murine X chromosome. *Genetics*, 192(3), pp.1095–107. Available at: http://www.ncbi.nlm.nih.gov/pubmed/22887817.

Trivedi, V. et al., 2018. *Multidimensional quantitative analysis of mRNA expression within intact vertebrate embryos*, Available at: http://dev.biologists.org/lookup/doi/10.1242/dev.156869.

Tsanov, N. et al., 2017. smiFISH and FISH-quant – a flexible single RNA detection approach with super-resolution capability. , 44(22).

Wang, F. et al., 2012. RNAscope: A novel in situ RNA analysis platform for formalin-fixed, paraffin-embedded tissues. *Journal of Molecular Diagnostics*, 14(1), pp.22–29.

Wang, J. et al., 2016. Unusual maintenance of X chromosome inactivation predisposes female lymphocytes for increased expression from the inactive X. *Proceedings of the National Academy of Sciences*, 113(14), pp.E2029–E2038. Available at: http://www.pnas.org/lookup/doi/10.1073/pnas.1520113113.

Wangkumhang, P. et al., 2007. WASP: a Web-based Allele-Specific PCR assay designing tool for detecting SNPs and mutations. *BMC genomics*, 8(1), p.275. Available at: http://bmcgenomics.biomedcentral.com/articles/10.1186/1471-2164-8-275 [Accessed May 12, 2016].

Williams, L.H. et al., 2011. Transcription precedes loss of Xist coating and depletion of H3K27me3 during X-chromosome reprogramming in the mouse inner cell mass. *Development*, 138(10), pp.2049–2057. Available at: http://dev.biologists.org/cgi/doi/10.1242/dev.061176 [Accessed May 26, 2015].

Windley, S.P. & Wilhelm, D., 2016. Signaling Pathways Involved in Mammalian Sex Determination and Gonad Development. *Sexual Development*. Available at:

http://www.karger.com/?doi=10.1159/000444065.

Wutz, A., 2011. Gene silencing in X-chromosome inactivation: advances in understanding facultative heterochromatin formation. *Nature reviews. Genetics*, 12(8), pp.542–553. Available at: http://dx.doi.org/10.1038/nrg3035.

Yamaji, M. et al., 2010. Functional reconstruction of NANOS3 expression in the germ cell lineage by a novel transgenic reporter reveals distinct subcellular localizations of NANOS3. *Reproduction*, 139(2), pp.381–393.

Yang, F., Babak, T., Shendure, J. & Disteche, C.M., 2010. Global survey of escape from X inactivation by RNA-sequencing in mouse. *Genome research*, 20(5), pp.614–22. Available at: http://www.ncbi.nlm.nih.gov/pubmed/26235224%5Cnhttp://www.pubmedcentral.nih.gov/articlerender.fcgi?artid=PMC4546214.

Yang, F., Babak, T., Shendure, J., Yang, F., et al., 2010. Global survey of escape from X inactivation by RNA-sequencing in mouse Global survey of escape from X inactivation by RNA-sequencing in mouse. *Genome Research*, (206), pp.614–622.

Yang, L. et al., 2016. Female mice lacking Xist RNA show partial dosage compensation and survive to term. *Genes and Development*, 30(15), pp.1747–1760.